TU Delft

Delft University of Technology

Document Version
Final published version

Citation (APA)
Heidary, A. (2026). *Transformer Protection Against Resonance Overvoltages in Power Systems*. [Dissertation (TU Delft), Delft University of Technology]. https://doi.org/10.4233/uuid:69ab5b2b-b611-488a-9ae4-d3121834749c

Important note
To cite this publication, please use the final published version (if applicable).
Please check the document version above.

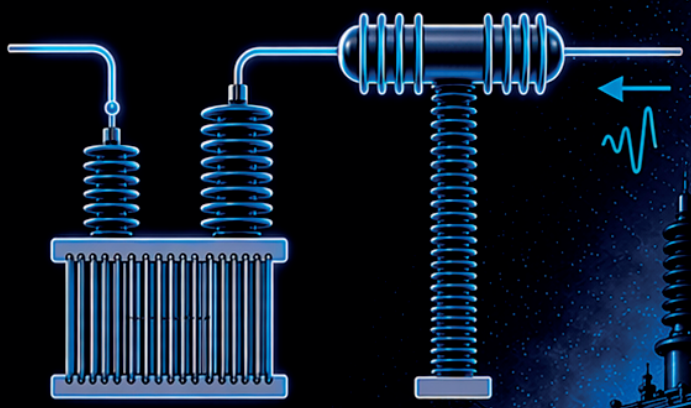
Copyright
In case the licence states “Dutch Copyright Act (Article 25fa)”, this publication was made available Green Open Access via the TU Delft Institutional Repository pursuant to Dutch Copyright Act (Article 25fa, the Taverne amendment). This provision does not affect copyright ownership.
Unless copyright is transferred by contract or statute, it remains with the copyright holder.

Sharing and reuse
Other than for strictly personal use, it is not permitted to download, forward or distribute the text or part of it, without the consent of the author(s) and/or copyright holder(s), unless the work is under an open content license such as Creative Commons.

Takedown policy
Please contact us and provide details if you believe this document breaches copyrights.
We will remove access to the work immediately and investigate your claim.

This work is downloaded from Delft University of Technology.

TRANSFORMER PROTECTION AGAINST RESONANCE OVERVOLTAGES IN POWER SYSTEMS



Amir HEIDARY

TU Delft

Transformer Protection Against Resonance Overvoltages in Power Systems

Transformer Protection Against Resonance Overvoltages in Power Systems

Dissertation

for the purpose of obtaining the degree of doctor
at Delft University of Technology,
by the authority of the Rector Magnificus, Prof.dr.ir. H. Bijl,
Chair of the Board for Doctorates,
to be defended publicly on
Monday 15 June 2026 at 17:30
by

Amir HEIDARY

This dissertation has been approved by the promotors.

Composition of the doctoral Committee:	
Reactor Magnificus	Chairperson
Prof.dr.ir. M. Popov	Delft University of Technology, promotor
Dr.ir M. Ghaffarian Niasar	Delft University of Technology, promotor
Independent member:	
Prof.dr. P. Palensky	Delft University of Technology
Prof.ir. P.T.M. Vaessen	Delft University of Technology
Prof.dr. E. Rahimpour	Technical University of Applied Sciences Würzburg-Schweinfurt, Germany
Prof.dr. A.J.M. Pemen	Eindhoven University of Technology
Ir. K. Velitsikakis	TenneT TSO B.V., the Netherlands
Prof.dr.ir. O. Isabella	Delft University of Technology, reserve member

This research is financially supported by the Nederlandse Organisatie voor Wetenschappelijk Onderzoek (NWO) in collaboration with TenneT TSO B.V., Alliander N.V., Royal SMIT Transformers, and TSO National Grid, UK, in the framework of the NWO-TTW project "Protection of Future Crucial Power System Components, No.18.699.

Keywords: Transformer, Protection, Transient, Resonance, Overvoltage

Printed by: Gildeprint proefschrift

Cover by: Amir Heidary (assisted by GPT4)

Copyright © by Amir Heidary
ISBN: 978-94-6496-574-2
An electronic copy of this dissertation is available at
http://repository.tudelft.nl/.

Life is not about how far we can advance science and technology;
it is about how deeply we can be kind and spread love.

CONTENT

Chapter 1 Introduction 1
1.1 Power System Definition and Transition 1
1.2 The Role of Transformers in Electrical Systems 3
1.3 Background on Transformer Protection 6
1.4 Problem Definition 8
1.5 Thesis Objectives 9
1.6 Research Questions 11
1.7 Approach 12
1.8 Thesis Outline 13
1.9 Thesis contribution 14
References 16

Chapter 2 Transformer Resonance 21
2.1 Abstract 21
2.2 Overview of Existing Protection Methods 22
2.3 Reasons for Transformer Resonance 23
2.4 Methods for measuring and modeling transformer resonance 29
2.5 Solutions for Transformer Resonance 34
2.6 Study of applicable protection against transmission transformer resonance 40
2.7 Conclusion 44
References 44

Chapter 3 Choke protection for transformer windings 51
3.1 Abstract 51
3.2 An overview of transformer modeling and protection by choke 52
3.3 Transformer admittance matrix 58
3.4 Verification of the studied winding model 59
3.5 Performance evaluation of an R-L protection circuit (known as a choke) 61
3.6 Conclusion 64
References 65

Chapter 4 Transformer protection using a parallel air-core reactor and resistor 67
4.1 Abstract 67
4.2 An overview of the transformer protection against transient phenomena 68
4.3 Addressing the problem of series reactor saturation 69
4.4 High-frequency model of transformer winding 73
4.5 Transformer model for protection studies 75
4.6 Protection device evaluation 80
4.7 Experimental validation 81
4.8 Comparison analysis 83
4.9 Conclusion 84
References 84

Chapter 5 Ring-core parallel inductor and resistor for transformer protection against transients 87
5.1 Abstract 87

5.2 An overview of transformer protection devices against transient overvoltage..... 88
5.3 R-PIR configuration and operation..... 89
5.4 R-PIR modeling..... 90
5.5 FEM analysis of R-PIR..... 99
5.6 EMTP simulation of R-PIR..... 104
5.7 Experimental evaluation of R-PIR..... 105
5.8 Conclusion..... 112
References..... 113

Chapter 6 Multi-module series suppressor for transformer resonance overvoltage protection..... 115
6.1 Abstract..... 115
6.2 An overview of transformer resonance overvoltage and protection..... 116
6.3 MSTS configuration, description, and analysis..... 117
6.4 MSTS simulation in EMT software..... 123
6.5 MSTS magnetic flux field study..... 126
6.6 MSTS experimental validation..... 130
6.7 MSTS advantages discussion based on comparison..... 134
6.8 Conclusion..... 135
References..... 136

Chapter 7 Introduction of future grids' transformer protection transient suppressors..... 139
7.1 Abstract on future protection devices..... 139
7.2 An overview of the cable-integrated transformer protection against transient phenomena and future power system protection devices..... 141
7.3 Cable shield connected grounding ferrite core reactor for protection of cable-connected transformers against transient overvoltage..... 142
7.4 SCGR configuration and operation rationale..... 143
7.5 EMTP simulation SCGR in a case study..... 147
7.6 Definition and design of a series-parallel transient suppressor..... 149
7.7 Simulation of the designed SPTS..... 153
7.8 Design, configuration, and analysis of the PMTS..... 153
7.9 FEM simulation of the PMTS during normal and transient conditions..... 157
7.10 Comparison of designed transient suppressor protection devices..... 159
7.11 Conclusion..... 160
References..... 161

Chapter 8 Discussion of the results and conclusion..... 163
8.1 Thesis summary..... 163
8.2 Comparison of the studied protection solutions..... 164
8.3 Key achieved results..... 169
8.4 Practical guidelines and methodological insights..... 170
8.5 Scientific and industrial contributions..... 172
8.6 Limitations and challenges..... 173
8.7 Response to the research questions..... 175
8.8 Future work and next steps..... 176
8.9 Concluding remarks..... 178

List of the publications..... 179
Acknowledgment..... 181
Biography..... 183

LIST OF ABBREVIATIONS

Abbreviation	Description
AC	Alternating Current
DC	Direct Current
CB	Circuit Breaker
IEEE	Institute of Electrical And Electronics Engineers
FT	Fast Transient
VFTs	Very Fast Transients
PAFT	Protection Against Fast Transients
PAIR	Parallel Air-Core Inductor And Resistor
R-PIR	Parallel Inductor And Resistor Circuit
FDD	Frequency Dependent Device
MSTS	Multimodular Series Transient Suppressor
SCGR	Shield Connected Grounding Reactor
SPTS	Series Parallel Connected Transient Suppressor
PMTS	Permanent Magnet-Based Transient Suppressor
RES	Renewable Energy Source
VNA	Vector Network Analyzer
FRA	Frequency Response Analyzer
IFRA	Impulse Source Frequency Response Analyzer
SFRA	Sinusoidal Sweep Frequency Response Analyzer
HV	High Voltage
LV	Low Voltage
EHV	Extra-High Voltage
UHV	Ultra-High Voltage
HVAC	High Voltage Alternating Current
HVDC	High Voltage Direct Current
GIT	Gas Insulated Transformer
FEM	Finite Element Method
EMT	Electromagnetic Transient
EMTP	Electromagnetic Transients Program
FS	Frequency Sweep
FTSC	Fast Frequency Suppressing Circuits
STLM	Single-Transmission Line Model
THD	Total Harmonic Distortion
VSC	Voltage Source Converter
SA	Surge Arrester
ZnO	Zinc Oxide
PIR	Pre-Inserted Resistors
DCRS	DC Reactor Suppressor
OVs	Overvoltages
SRs	Series Reactors
KCL	Kirchhoff's Current Law
KVL	Kirchhoff's Voltage Law
RRV	Rate Of Rise Of The Voltage
FFT	Fast Fourier Transform
PMs	Permanent Magnets
TSOs	Transmission System Operators
IEDs	Intelligent Electronic Devices
BESS	Battery Energy Storage System
DG	Distributed Generation
PRoteuS	Protection of Future Power System Crucial Components

SUMMARY

Transformers are a vital component of power systems. As well-established electromagnetic devices, they change voltage levels and enable efficient power transfer while preserving the system's frequency. Ensuring the reliable operation of these critical units is essential for the continuous transmission of electrical energy. Consequently, safeguarding transformers against various faults has always been a significant concern in power systems.

One phenomenon that threatens transformer performance is transient voltage in the power system. These transient voltages, containing a range of harmonic frequencies, propagate as electromagnetic waves through power lines and interact with transformers. Transients often result from lightning strikes or switching operations. Upon receiving these signals, transformers respond differently to various frequency components, necessitating precise modeling and frequency response analysis to predict their behavior under such conditions.

A key impact of transient voltage on transformers is resonance, which arises from transformer windings' inductive and capacitive characteristics and their connection to the power system. Resonance can appear in several forms, including terminal resonance, internal resonance, or resonance between the transformer and external components. These resonances often lead to overvoltage conditions that can partially or entirely damage the transformer.

The currently available protection devices have limitations in fully safeguarding transformers against transients. These shortcomings include constraints in voltage handling, inadequate harmonic filtering capabilities, susceptibility to protection device core saturation, and the inability to protect against internal transformer resonance.

Protecting transformers from the effects of transient signals, resonance, and overvoltage is the primary objective of this research. The thesis explores the following objectives:

- Investigating possible resonance and overvoltage scenarios in transformers subjected to transients
- Evaluating existing transformer protection technologies and their practical applications
- Identifying limitations and advantages of current protection methods to enhance future designs
- Developing a black-box transformer model and implementing a circuit model in a laboratory test setup

- Analyzing, simulating, and experimentally validating choke models for transformer protection against fast transients
- Designing and prototyping a tuned ring-core protection device through analysis, simulation, and experimentation
- Prototyping a PAIR protection device using analysis, simulation, and experimental methods
- Designing a shield-connected reactor to suppress the transient signal from the cable toward the transformer
- Study of the permanent integrated core effect on the suppression of the transient signal passing through the core
- Creating and testing an MSTS protection device with resistors based on analysis, simulation, and experimental validation

All the mentioned objectives aim to develop a practical and innovative method to protect transformers in increasingly complex future power systems. This Ph.D. project employs a comprehensive approach, incorporating analytical studies, MATLAB/Simulink, EMTP-RV, ANSYS Maxwell simulations, scaled-down prototyping, testing, and high-voltage experimental setups to achieve the goals.

SAMENVATTING

Transformatoren vormen een essentieel onderdeel van elektrische energiesystemen. Als gevestigde elektromagnetische apparaten veranderen zij spanningsniveaus en maken zij een efficiënte vermogensoverdracht mogelijk, terwijl de frequentie van het systeem behouden blijft. Het waarborgen van een betrouwbare werking van deze kritieke eenheden is essentieel voor de continue transmissie van elektrische energie. Daarom is de bescherming van transformatoren tegen verschillende soorten storingen altijd een belangrijk aandachtspunt geweest in energiesystemen.

Een verschijnsel dat de prestaties van transformatoren kan bedreigen, is transiënte spanning in het elektriciteitssysteem. Deze transiënte spanningen, die een reeks harmonische frequenties bevatten, planten zich voort als elektromagnetische golven langs hoogspanningslijnen en interageren met transformatoren. Transiënten ontstaan vaak als gevolg van blikseminslagen of schakelhandelingen. Wanneer transformatoren deze signalen ontvangen, reageren zij verschillend op de diverse frequentiecomponenten. Daarom zijn nauwkeurige modellering en frequentieresponsanalyse noodzakelijk om hun gedrag onder dergelijke omstandigheden te kunnen voorspellen.

Een belangrijk effect van transiënte spanningen op transformatoren is resonantie. Deze ontstaat door de inductieve en capacitieve eigenschappen van transformatorwikkelingen en hun koppeling met het elektriciteitssysteem. Resonantie kan zich in verschillende vormen voordoen, waaronder klemresonantie, interne resonantie of resonantie tussen de transformator en externe componenten. Dergelijke resonanties leiden vaak tot overspanningscondities die de transformator gedeeltelijk of zelfs volledig kunnen beschadigen.

De momenteel beschikbare beveiligingsapparaten vertonen beperkingen bij het volledig beschermen van transformatoren tegen transiënten. Deze tekortkomingen omvatten onder andere beperkingen in spanningsverwerking, onvoldoende mogelijkheden voor harmonische filtering, gevoeligheid voor kernverzadiging van beveiligingsapparaten en het onvermogen om bescherming te bieden tegen interne transformatorresonantie.

Het beschermen van transformatoren tegen de effecten van transiënte signalen, resonantie en overspanning vormt het primaire doel van dit onderzoek. In dit proefschrift worden de volgende doelstellingen onderzocht:

- Het onderzoeken van mogelijke resonantie- en overspanningsscenario's in transformatoren die worden blootgesteld aan transiënten
  Het evalueren van bestaande transformatorbeschermingstechnologieën en hun praktische toepassingen

- Het identificeren van beperkingen en voordelen van huidige beschermingsmethoden om toekomstige ontwerpen te verbeteren
- Het ontwikkelen van een black-box transformormodel en het implementeren van een circuitmodel in een laboratoriumtestopstelling
- Het analyseren, simuleren en experimenteel valideren van smoorspoelmodellen voor de bescherming van transformatoren tegen snelle transiënten
- Het ontwerpen en prototypen van een afgestemd ringkern-beveiligingsapparaat op basis van analyse, simulatie en experiment
- Het prototypen van een PIAR-beveiligingsapparaat met behulp van analyse, simulatie en experimentele methoden
- Het ontwerpen van een afschermingsgekoppelde reactor om het transiënte signaal van de kabel richting de transformator te onderdrukken
- Het bestuderen van het effect van een permanent geïntegreerde kern op de onderdrukking van transiënte signalen die door de kern worden geleid
- Het ontwikkelen en testen van een MSTS-beveiligingsapparaat met weerstanden, gebaseerd op analyse, simulatie en experimentele validatie

Alle bovengenoemde doelstellingen zijn gericht op het ontwikkelen van een praktische en innovatieve methode om transformatoren te beschermen in steeds complexere toekomstige energiesystemen. Dit promotieonderzoek maakt gebruik van een geïntegreerde aanpak, bestaande uit analytische studies, simulaties in MATLAB/Simulink, EMTP-RV en ANSYS Maxwell, het bouwen van schaalmodellen, testen en hoogspanningslaboratoriumexperimenten om de gestelde doelen te bereiken.

1

INTRODUCTION

1.1. POWER SYSTEM DEFINITION AND TRANSITION

The history of electrical systems dates back to the late eighteenth century, when scientists such as Benjamin Franklin and Alessandro Volta explored electricity's fundamental properties [1], [2]. Volta's invention of the electric battery in the early nineteenth century marked the first practical source of continuous electric current [2]. By the mid-1800s, Michael Faraday's experiments with electromagnetic induction paved the way for the development of generators and transformers, laying the foundation for modern power systems [3].

In the late nineteenth century, pioneers like Thomas Edison and Nikola Tesla revolutionized electrical power systems by introducing practical power generation and distribution applications. Edison pioneered DC systems [4]. At the same time, Tesla and George Westinghouse promoted AC, which eventually became the dominant method due to its efficiency over long distances [5]. Fig. 1.1 depicts the early forms of electrical components, such as a generator, transformer, AC motor, and lamp, showing the overall structure of an early electrical power system. By the early twentieth century, electrical grids expanded massively worldwide, and by powering homes, industries, and transportation, they became irreplaceable assets for modern life [6], [7].

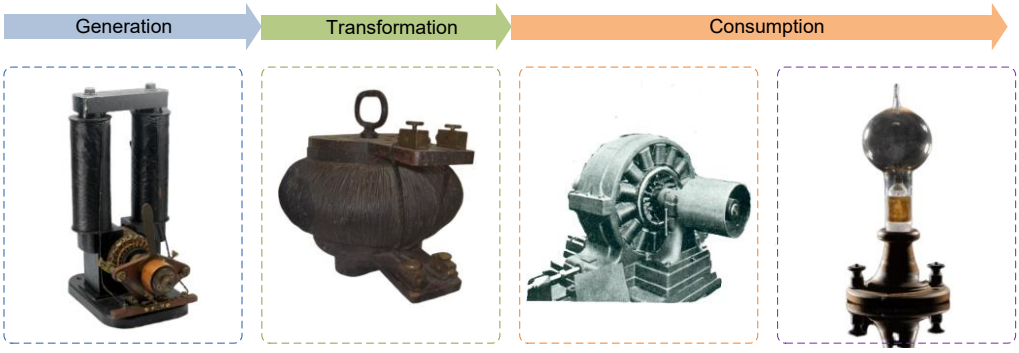


Fig. 1.1. Early electrical equipment forming the initial electrical system

1

The traditional power system follows a centralized model where large power plants, such as coal, gas, nuclear, or hydroelectric power plants, generate and transmit electricity over long distances through high-voltage transmission lines [8]. Electricity is distributed to consumers through substations and local distribution networks [9]. The system is mostly one-directional, with energy flowing from the generators to the end-users [10]. Control and monitoring are limited, making the system vulnerable to faults and inefficiencies, especially during peak demands [11]. The simplified diagram of the traditional power system is illustrated in Fig. 1.2.

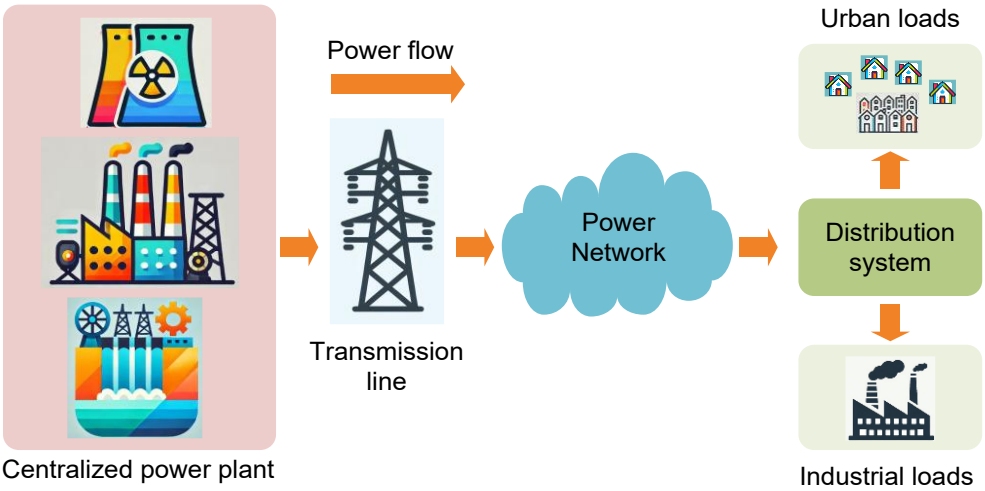


Fig. 1.2. Simplified diagram of the traditional power system

The modern grid is transitioning to a decentralized, intelligent network integrating renewable energy sources such as solar and wind, energy storage, and electric vehicles [12]. Smart grids use advanced sensors, communication technologies, and automation to enhance reliability, efficiency, and sustainability [13]. Energy can flow bidirectionally, allowing consumers to return electricity to the grid [14]. This shift improves resilience, reduces carbon emissions, and supports the growing demand for clean energy, ultimately creating a more dynamic and flexible power system [15]. In Fig. 1.3, a modern power system is illustrated, which indicates power system transition goals compared to Fig. 1.2 [16].

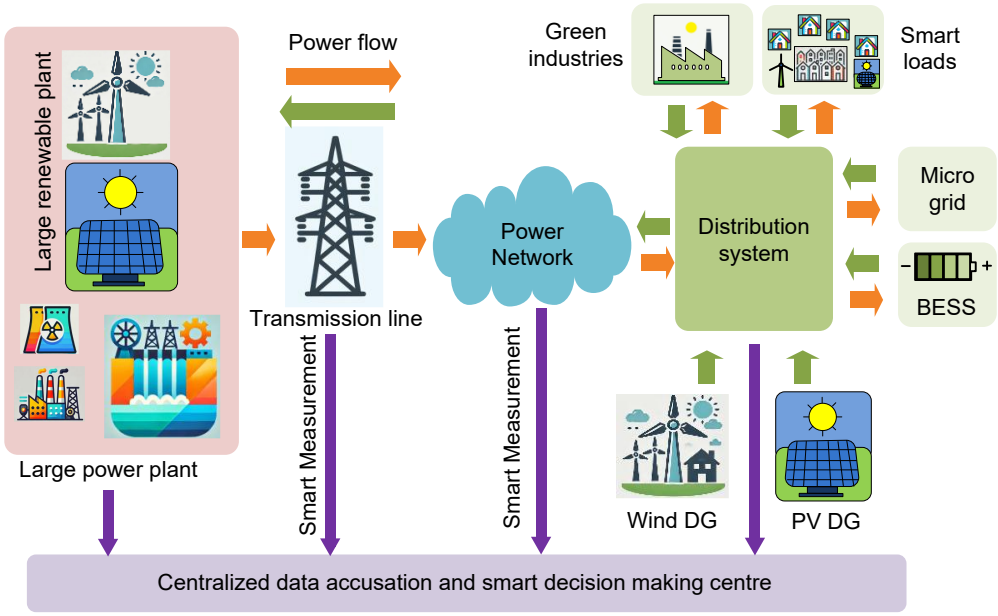


Fig. 1.3. Simplified diagram of the modern power system

1.2. THE ROLE OF TRANSFORMERS IN ELECTRICAL SYSTEMS AND THEIR DEVELOPMENT OVER TIME

The concept of transformers was initially demonstrated by Michael Faraday in 1831 upon discovering the electromagnetic induction phenomenon [17]. However, early devices were inefficient and impractical. In 1885, William Stanley, who worked for Westinghouse, built the first reliable and commercially viable transformer in Great Barrington, Massachusetts. His design used laminated cores to reduce eddy currents and separate primary and secondary windings to enhance performance [18]. Following this, by 1886, Westinghouse Electric began with a massive transformer production for use in AC power distribution, laying the foundation for modern electrical grids [19].

The main feature of the transformer that contributed to the initial power system was its ability to enable long-distance HVAC transmission, revolutionizing power distribution and making electricity easily accessible to consumers [20]. The technological advancements of power transformers over time are illustrated in Fig. 1.4.

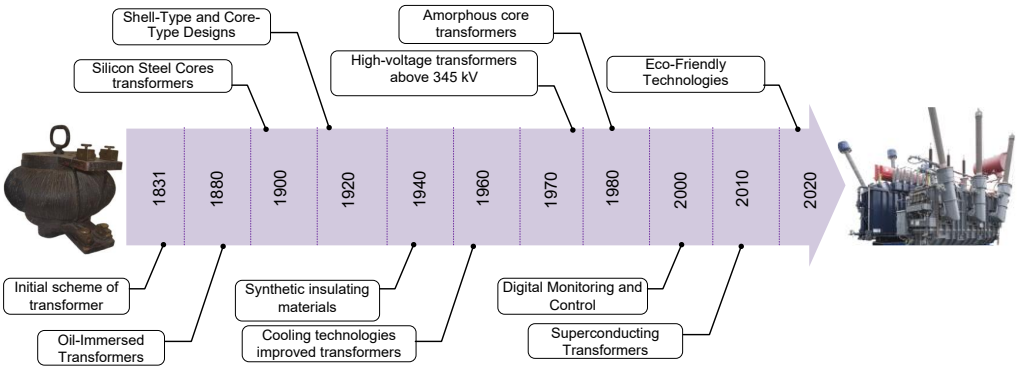


Fig.1.4. Transformer technological development trends over time

The main technologies that have affected the transformer over time are described as follows:

Oil-Immersed Transformers (Late 19th Century - 1880s): Early transformers used air for insulation and cooling; however, oil immersion significantly enhanced insulation and cooling capacity. It contributed to the voltage level increase and power handling capacity, allowing the use of more powerful and efficient transformers [21].

Silicon Steel Cores (1900s): The use of laminated silicon steel cores reduced eddy current losses, improving efficiency, minimizing energy losses, and enabling the development of more compact and efficient transformers [22].

Shell-Type and Core-Type Designs (the 1910s-1920s): The development of different winding and core configurations, such as shell-type and core-type designs, optimized flux paths, and reduced leakage reactance. Its effect has improved the short-circuit strength and efficiency [23].

Cooling Technologies (1930s-1940s): The introduction of forced oil circulation, radiators, and air-blast cooling systems to handle higher loads and prevent overheating. In this period, transformers were enabled to operate at higher ratings without risk of thermal failure [24].

Synthetic Insulating Materials (1950s-1960s): The use of synthetic materials like Nomex for insulation improved dielectric strength and thermal endurance. Its impact was to enhance reliability and lifespan, reducing maintenance needs [25].

High-Voltage Transformers (1970s): Development of EHV and UHV transformers (above 345 kV). This approach has facilitated long-distance power transmission with minimal losses, supporting grid expansion [26].

Amorphous Core Transformers (1980s): The introduction of amorphous metal cores reduced core losses by about 70% compared to silicon steel. This technology enhanced the energy efficiency, particularly for distribution transformers [27].

Digital Monitoring and Control (1990s-2000s): Sensors and digital relay systems allowed real-time monitoring of transformer health, detecting faults early. This technology improved preventive maintenance and extended operational life [28].

Superconducting Transformers (2010s): The use of superconducting materials for windings minimized resistive losses and improved power density. This technology has the potential to significantly reduce energy losses, although it is still in the experimental phase with a limited deployment [29].

Eco-Friendly Technologies (the 2020s): The development of biodegradable ester oils and GITs reduces environmental impact and enhances fire safety. This resulted in an alignment of transformer technology with sustainability goals and improved system resilience [30].

From a grid perspective, the number of components in a power system increases rapidly due to the ongoing power system transition. This transition focuses on integrating numerous renewable energy generators and energy storage systems into the grid. Transformers play a crucial role in this process, as they are essential for managing the varying voltage levels between renewable generators, energy storage units, and the power system. The comparison of Fig. 1.5 and Fig. 1.6 clearly shows the increase in transformer usage in traditional and modern power systems.

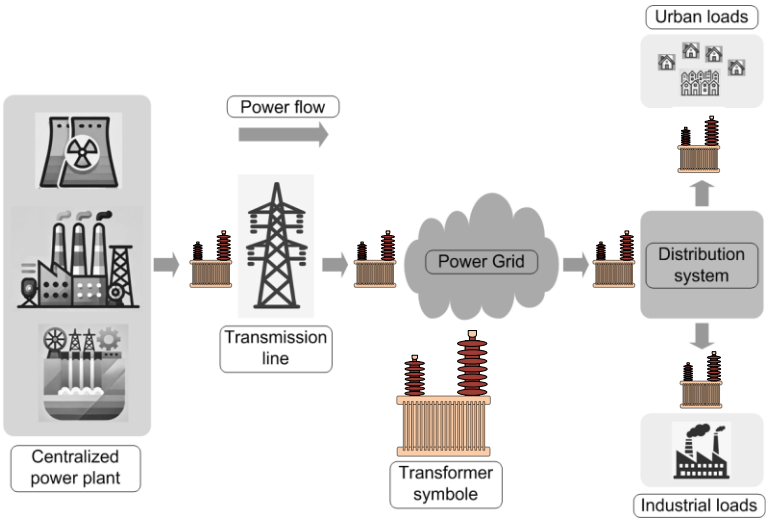


Fig. 1.5. The use of transformers in a traditional power system

As shown in Fig. 1.5, the number of transformers in traditional power systems is relatively low, primarily connecting generators to transmission lines, transmission and distribution systems, and end-users. In contrast, modern power systems require a significantly larger number of transformers to facilitate connections with renewable energy generators, energy storage systems, microgrids, and large-scale renewable power plants. An example of transformer integration in modern power systems is illustrated in Fig. 1.6.

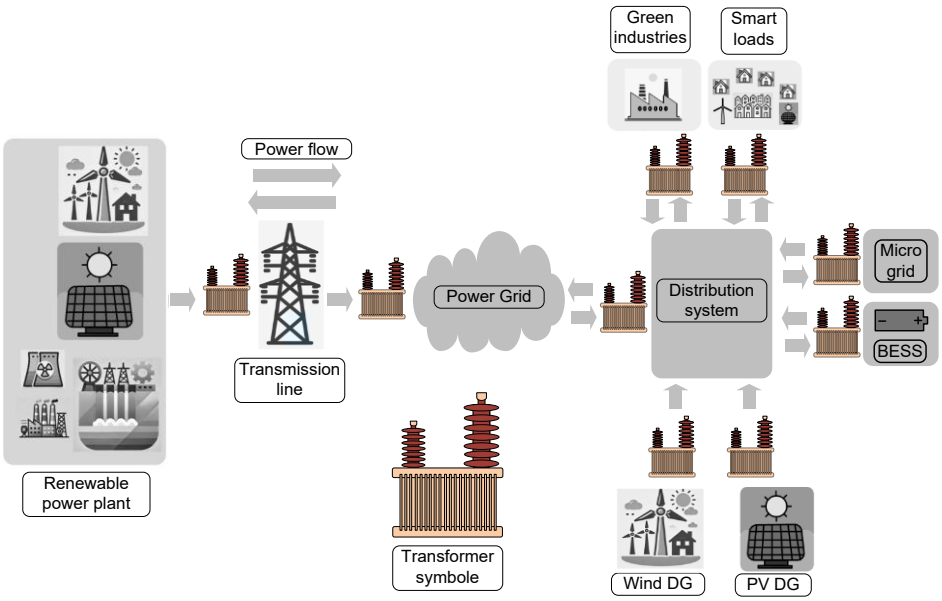


Fig. 1.6. The use of transformers in a modern power system

1.3. BACKGROUND ON TRANSFORMER PROTECTION

The future power system will integrate numerous renewable energy sources, power management devices, extended cable networks, overhead lines, and transformers. This power system expansion increases the risk of lightning strikes. Additionally, managing power in a large-scale power system requires frequent switching to ensure economic and reliable power transfer from generation to consumers.

A lightning strike occurs when a large current from ionized clouds hits a power system conductor. This energy injection into the power system generates high voltage stress. Lightning is a fast event, typically characterized by a signal lasting tens of microseconds with a very high rate of voltage change. This transient waveform propagates through the power system as an electromagnetic traveling wave, causing overvoltage, insulation breakdown, and damage to electrical equipment [31].

Switching operations in power systems are typically performed for two purposes. Firstly, it is used to control power flows, including busbar coupling, renewable generator arrangements, and overall system balancing. Secondly, switches interrupt fault currents and reclose faulty lines. These operations generate transient phenomena during the connection or disconnection of HV lines or connected equipment, like capacitor banks or reactors. Such transients propagate through the system and may cause power equipment overvoltage, resonance, or stress [32].

Transient signals caused by lightning and switching can be classified based on current or voltage parameters. Another classification approach is based on the variation rate, which determines their harmonic content. Depending on harmonic content, transients are categorized as FTs or VFTs. They are the reason for unwanted phenomena affecting various sections of the power system. From a protection perspective, they require different mitigation strategies [33].

The transformer is one of the vital devices of the power system, and transient phenomena seriously influence it. The equivalent circuit of the transformer includes a variety of inductors and capacitors, which may resonate with the harmonic content of the transient signals. An example of transformer failure due to the transient overvoltage in reality is illustrated in Fig. 1.7 [34].

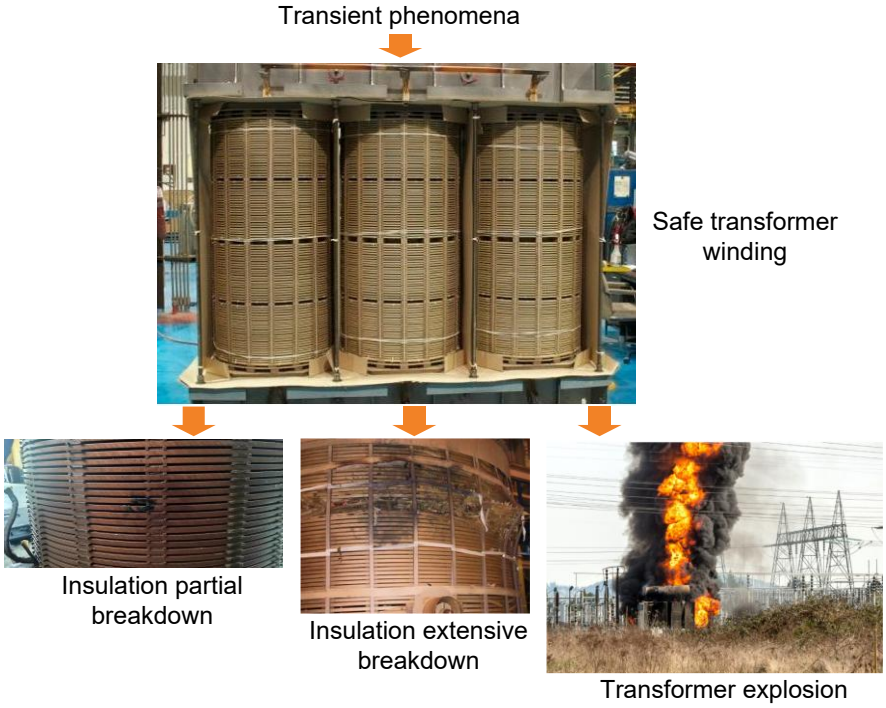


Fig. 1.7. Transformer breakdown resulting from transient phenomena

Currently, transformer protection solutions include parallel filters [35], surge arresters [36], and series inductive suppressors [37]. Each of these methods offers specific advantages and comes with inherent limitations. The primary objective of this Ph.D. research is to develop a new method for protecting transformers against transient phenomena.

1.4. PROBLEM DEFINITION

Worldwide, there are many reports of transformer failures due to circuit breaker operations. Understanding this phenomenon through accurate modeling and proposing implementable solutions are the main achievements of the "PRoteuS" project [38]-[41]. This thesis particularly focuses on the development of protection solutions for the transformer against transient phenomena.

Current solutions focus on mitigating fast transient effects in transformers to address the reported failures. These strategies involve the use of series [42] or parallel [43] components, incorporating resistive, capacitive, or inductive elements as a part of PAFT. A review of the state-of-the-art reveals that existing protection equipment for PAFT is not yet mature enough for widespread application. Many solutions face limitations or introduce additional concerns for other parts of the network.

Transient signals consist of various harmonic frequencies. The harmonic content of these signals can excite resonance frequencies within the power system. When a transient signal interacts with a transformer, two scenarios may occur.

1. **External Resonance:**

   The transformer may exhibit resonance frequencies when interacting with external components, such as cables or connected equipment. This interaction may lead to a transformer terminal voltage increase [44].

2. **Internal Resonance:**
   The harmonic content of the transient signal may excite internal resonance modes within the transformer, potentially increasing the voltage between the transformer's winding disks [45].

Two approaches have been proposed to mitigate the effects of transient signals on transformers:

1. **Voltage Suppression:**
   This method protects the transformer from terminal overvoltage by reducing the magnitude of the transient signal's overvoltage [46].

2. **Harmonics Filtering:**

This approach filters the harmonic content of transient signals. Targeting and mitigating critical harmonics through specialized filters prevents resonance-induced overvoltages and protects the transformer and associated equipment [46].

1.5. THESIS OBJECTIVES

The primary objective of this research is to develop a method that provides comprehensive protection for transformers in transmission systems against transient phenomena and resonance overvoltage. To achieve this, the transformer's resonance frequency will be identified and considered, followed by the design of a suppressor device to safeguard the transformer from internal and external resonance overvoltages. According to the primary objectives of the project (Protection of Future Crucial Power System Components), the sub-objectives of this thesis are listed and detailed as follows:

First objective:

The starting objective is to review the presently used protection devices applied to the transformers against transient phenomena and resonance overvoltage, and explore their positive and negative aspects. Next, it is evaluated to determine which method can benefit to protect HV transformers operating above distribution voltage levels. The main focus is to classify parallel and series protection devices and determine which method can be applied to HV transformers. An example of a high-risk transformer, which is extensively used in Dutch power systems, is a transmission transformer integrated with wind farm substations, which is damaged by switching and lightning transients.

Second objective:

The second objective is to propose a viable solution and to apply it as an extended protection for HV transformers. The solution is supposed to follow these steps:

- Designing of the protection device for HV transmission system voltage levels
- Meager power consumption in the normal condition of the power system
- Analysis of voltage and magnetic field distribution
- Evaluation of voltage suppression and filtering of the harmonic content of the transient wave

Using the assessment results, some viable innovative methods for transformer protection can be identified.

Third objective:

The objective is to design innovative protection devices that incorporate the advantages of existing schemes from the state of the art and enhance their performance and viability for transmission transformers. These advancements include the following technologies:

- Designing a series air-core reactor to protect transformers against transient resonance overvoltages.
- Evaluating a parallel RL circuit connected in series with the transformer to mitigate transient resonance overvoltages.
- Proposing a tuned choke to protect transformers against transient resonance overvoltages.
- Developing a modular series transient suppressor to safeguard transformers from transient resonance overvoltages.
- Designing a permanent magnet-based transient suppressor to provide protection against transient resonance overvoltages.
- Investigating the effects of a shunt reactor connected to the transformer cable shield and its role in mitigating transient resonance overvoltages.
- Assessing the superconducting reactor transient suppressor for its effectiveness in addressing transient resonance overvoltages.

Fourth objective:

During this objective, the specifications of each innovative component are thoroughly analyzed. These analyses are primarily conducted by applying mathematical modeling and simulation. The components are implemented in laboratory setups when the practical feasibility is demonstrated. The following stages are undertaken to achieve this objective:

- Analysing the innovative schemes' logic, focusing on their operation and impact on transformer protection against transient resonance overvoltage.
- Deriving equations to define the fundamental operation of each scheme.
- Simulating the designed schemes using various simulation platforms.
- Evaluating the designs, considering size, simplicity, and cost-effectiveness.
- Implementing laboratory test setups for both low-voltage and high-voltage validation.

Fifth objective:

The ultimate objective of this research is to develop a comprehensive model that demonstrates the impact of the protection scheme on the interaction between the transformer, cable, and grounding system within a simulation platform. The model aims to validate that the proposed protection device can deliver robust protection for the transformer, in conjunction with other power system components, against resonance overvoltages caused by transient phenomena.

1.6. RESEARCH QUESTIONS

The research questions formulated for this thesis address critical challenges, including transformer resonances, transformer-cable interactions, overvoltages caused by transient resonance, and transformer protection against phenomena. These questions aim to explore effective strategies for mitigating transient overvoltages in transformers. The research questions are summarized as follows:

1. Which transient signal frequencies cause transformer resonances?

This question focuses on identifying how transformers respond to transient signals, particularly determining the frequencies that cause resonance.

2. What types of transformer resonances in transformers lead to overvoltage, and how does the cable connected to the transformer influence the resonances and associated overvoltages?

These questions investigate the underlying causes of resonance-induced overvoltages and the role of transformer-cable interactions in exacerbating these phenomena.

3. What is the most viable solution for protecting transformers against fast transients, considering the high-frequency model of the transformer connected to the grounding and cable system?

This question aims to identify a protection method as a solution to address transformer resonance overvoltages caused by transient phenomena.

4. How does the innovative protection component operate to suppress fast transients and their effects on transformers?

This question explores the interaction between the protection device and the transformer, emphasizing the device's role in mitigating the impact of transient phenomena, resonance, and overvoltage.

5. Why does the innovative protection component outperform existing solutions?

This question highlights the unique features of the proposed protection device, explaining how it surpasses currently utilized protection methods.

1.7. Approach

The analysis of the transformer is based on the disk model and frequency-domain calculations. This analytical study identifies the critical resonance points of a simplified transformer model. To validate these findings, the model is implemented in MATLAB/Simulink, EMTP-RV, and ANSYS Maxwell FEM software for further evaluation.

Additionally, the analytical study of the innovative protection devices is conducted using two approaches:

1. Parameter Calculation:

   Key component parameters, such as inductance, capacitance, and resistance, are calculated based on the electrical and magnetic field distributions and the geometry of the sections.

2. Frequency-Domain Analysis:

   Using the most precise model, frequency-domain calculations are performed to characterize the behavior of the protection device.

The resulting protection device model is implemented in EMTP-RV and FEM software and connected to the transformer model. Time-domain simulations are then carried out to assess the protection device's performance during impulse testing.

The final phase involves implementing the protection device and transformer model in laboratory tests for validation, which are conducted using three approaches:

1. Frequency Sweep Test:

   This test confirms the frequency-domain behavior of the prototype by performing a frequency sweep using a VNA Bode 100 measurement device. The device is excited with signals sweeping across the studied frequency range.

2. Low-Voltage Testing:

   To evaluate their performance, devices are tested with sinusoidal signals at critical resonance frequencies or low-voltage transient impulses.

3. High-Voltage Impulse Testing:

   Conducted in a high-voltage laboratory, this test uses an impulse generator to apply impulses ranging from 10 kV to 60 kV, assessing the protection

device's capability for transient voltage suppression under high-voltage conditions.

1.8. THESIS OUTLINE

Chapter 2 provides an overview of the thesis objectives based on a detailed literature review. This section focuses primarily on the phenomenon of transformer resonance, including its causes, modeling approaches for the transformer wide-frequency model, and current protection methods used to mitigate resonance overvoltages caused by transient phenomena.

Chapter 3 presents an introduction to transformer wide-frequency modeling using the grey-box approach. It explores the first protection solution, which involves a parallel RL circuit for protecting transformers from transient resonance and the resulting overvoltages. This chapter includes analyses of real transformer windings, the prototype of the protection device, and results from low-voltage laboratory testing.

Chapter 4 describes a method for deriving a transformer model from frequency response data and its implementation in the laboratory. This chapter also examines the second innovative protection scheme, a series of air-core reactors with parallel resistors. The design and performance of this topology are thoroughly studied through analysis, simulation, frequency sweep tests, high-voltage impulse tests, and a transformer setup.

Chapter 5 highlights the features of innovative protection devices based on chokes, a well-known type of equipment. The novelty of the proposed scheme lies in its tunability, which enhances choke performance and enables it to protect transformers at critical resonance frequencies. This chapter covers the geometry design, frequency-domain analysis, EMTP simulation, frequency sweep tests, and high-voltage testing of the proposed device.

Chapter 6 details the development of a protection device for transmission-level transformers, referred to as the MSTS. Analytical details of the MSTS design are provided and validated comprehensively through FEM analysis, EMTP-RV simulation, frequency sweep tests, and high-voltage impulse tests.

Chapter 7 focuses on the novel and future grid protection devices like cable shield connected grounding reactor, series-parallel connected transient suppressor, and permanent magnet-based transient suppressor. This chapter aims to introduce a

novel method based on future technologies and take a step forward by overall analysis and evaluation of the mentioned methods.

Chapter 8 concludes the thesis by summarizing the overall findings and addressing the research questions. It compares the protection devices studied comprehensively and recommends future research directions.

1.9. THESIS CONTRIBUTION TO THE "PROTEUS" PROJECT IN THE NETHERLANDS

From a project perspective, the primary objective is to develop innovative solutions to address the challenges associated with mysterious power equipment failures. These solutions will be based on the electromagnetic field theory, emphasizing the critical role of grounding, especially at high frequencies, to facilitate the study of various resonances and overvoltages in transformers. Key system components, including cables, transformers, and surrounding elements such as busbars and surge arresters, will be modeled with frequency-dependent impedance characteristics. The proposed topology will be designed and practically tested for the PAFT case, drawing on insights from these studies.

Building on results introduced by other researchers in the project, an accurate model of the studied transformer is developed, extending its interaction with the cable and grounding grid. This modeling enables a deeper understanding of transient effects on transformers.

Aligned with the research goals, this thesis aims to propose solutions for transformer failures in the Netherlands, which are sometimes caused by transient phenomena. The main contributions of the conducted research are as follows:

Analysis of Current Protection Methods:

The study examines the strengths and weaknesses of existing protection equipment to identify improvements needed to safeguard transmission system transformers against transient phenomena.

Development of Seven Novel Protection Devices:

A significant contribution of this thesis is the proposal of new protection methods that propose comprehensive protection for transmission system transformers. These include:

- Ring core Parallel RL circuit (R-PIR)
- Parallel Air-core Inductor and resistor (PAIR)
- Tuned choke
- Modular series transient suppressor (MSTS)
- Shiled-connected grounding reactor (SCGR)
- Series parallel transient suppressor (SPTS)
- Permanent magnet transient suppressor (PMTS)

Simulation of Designed Protection Devices and Systems:

The research employs MATLAB/Simulink, EMTP-RV, and ANSYS Maxwell FEM software for simulations. These simulations serve two purposes:

- To model and design the proposed protection devices accurately.
- To analyze the interaction of protection devices with other power system components, such as transformers, cables, and grounding systems.

Prototyping and Laboratory Testing:

Five protection devices are prototyped and tested in the laboratory to validate analytical and simulation findings. Tests include:

- Frequency sweep tests to verify prototype models.
- Impulse high-voltage tests to assess performance under transient conditions and ensure effective transformer protection.

This research is primarily conducted to protect Royal Smit Transformer against transient phenomena and resonance-induced overvoltage, and the results can be applied to other transformers, for example, the transformer illustrated in Fig. 1.8.



Fig. 1.8. An example of a transformer used in the power system of the Netherlands [47].

REFERENCES

[1] B. Franklin, "Franklin's Kite Experiment and the Lightning Rod," *Just Energy*, [Online]. Available: https://justenergy.com/blog/history-of-electricity-electric-power/.

[2] A. Volta, "Volta and the Electric Battery," *Just Energy*, [Online]. Available: https://justenergy.com/blog/history-of-electricity-electric-power/.

[3] M. Faraday, "Electromagnetic Induction and Early Generators," *Wikipedia*, [Online]. Available: https://en.wikipedia.org/wiki/Electric_generator.

[4] T. A. Edison, "Direct Current Systems and Commercial Electric Utility," *Wikipedia*, [Online]. Available: https://en.wikipedia.org/wiki/Electric_power_industry.

[5] N. Tesla, "Polyphase AC Systems and Power Transmission," *U.S. Energy Information Administration*, [Online]. Available: https://www.eia.gov/kids/history-of-energy/timelines/electricity.php.

[6] R. Whyte, "Technological Developments in Electricity," *Gale Research*, [Online]. Available: https://www.gale.com/intl/essays/rebecca-whyte-technological-developments-electricity.

[7] "The Expansion of Electric Grids," *Wikipedia*, [Online]. Available: https://en.wikipedia.org/wiki/Electric_power_industry.

[8] "Centralized Power System," *Cence Power*, [Online]. Available: https://cencepower.com/blog-posts/centralized-power-system.

[9] "Electric Power Systems," *Electrical Engineering Portal*, [Online]. Available: https://electrical-engineering-portal.com/electric-power-systems.

[10] “Centralized vs Decentralized Electricity Generation,” *American Security Project*, [Online]. Available: https://www.americansecurityproject.org/centralized-decenteralized-electricity-generation/

[11] A. Shahid, "Smart Grid Integration of Renewable Energy Systems," 2018 7th International Conference on Renewable Energy Research and Applications (ICRERA), Paris, France, 2018, pp. 944-948.

[12] S. Sarker, M. A. Rakib, S. Islam and S. S. Shafin, "An IoT-based Smart Grid Technology: Bidirectional Power Flow, Smart Energy Metering, and Home Automation," 2021 International Conference on Maintenance and Intelligent Asset Management (ICMIAM), Ballarat, Australia, 2021.

[13] “Bi-Directional Power Flow: The New World Order and What That Means for the Grid,” *IEEE Smart Grid*, [Online]. Available: https://smartgrid.ieee.org/bulletins/november-2017/two-way-power-flow-the-new-world-order-and-what-that-means-for-the-grid.

[14] S. S. Bhalshankar and C. S. Thorat, "Integration of smart grid with renewable energy for energy demand management: Puducherry case study," 2016 International Conference on Signal Processing, Communication, Power and Embedded System (SCOPES), Paralakhemundi, India, 2016.

[15] “The Smart Grid and Renewable Energy,” *IEEE Innovation at Work*, [Online]. Available: https://innovationatwork.ieee.org/smart-grid-transforming-renewable-energy/.

[16] “The U.S. Electric Power System Infrastructure and Its Vulnerabilities,” *National Academy of Engineering*, [Online]. Available: https://www.nae.edu/183133/The-US-Electric-Power-System-Infrastructure-and-Its-Vulnerabilities.

[17] “The Shocking History and Physics of Electric Transformers,” *Kathy Loves Physics*, [Online]. Available: https://kathylovesphysics.com/the-shocking-history-physics-of-electric-transformers/.

[18] “Transformers,” *Edison Tech Center*, [Online]. Available: https://edisontechcenter.org/Transformers.html.

[19] “Stanley Transformer 1886,” *National High Magnetic Field Laboratory*, [Online]. Available: https://nationalmaglab.org/magnet-academy/history-of-electricity-magnetism/museum/stanley-transformer-1886/.

[20] G. Frimpong, J. Hajek, and K. Kulasek, “Eco-friendly ester liquid transformer designs,” *ABB Review*, vol. 1, pp. 33–39, 2018.

[21] S. Khan, “Ester oil transformers: Another step towards greener energy,” *PTR Insights*, 2019.

[22] “Natural Ester Oil Transformer,” *Meidensha Corporation*, [Online]. Available: https://www.meidensha.com/products/energy/prod_01/prod_01_05/prod_01_05_14/.

[23] “Environmentally Friendly Power Transformer with Ester Oil,” *Transformers Magazine*, 2018.

[24] “CHINT’s Revolutionary 750 kV Ester Oil-Immersed Power Transformer Offers Significant Environmental Benefits,” *CHINT Global*, 2020.

[25] “Eco Power Products,” *Hyosung Heavy Industries*, [Online]. Available: https://www.hyosungheavyindustries.com/en/business/eco-solutions/S010100

[26] T. Nogueira, J. Carvalho, and J. Magano, "Eco-friendly ester fluid for power transformers versus mineral oil: Design considerations," Energies, vol. 15, no. 15, p. 5418, 2022.
[27] "MIDEL Natural and Synthetic Ester Transformer Fluids," *MIDEL*, 2021.
[28] "Superconducting Transformer Materials," *MIDEL*, 2021.
[29] "Eco-Friendly Transformer Oils," *Wikipedia*, [Online]. Available: https://en.wikipedia.org/wiki/Transformer_oil.
[30] F. A. R. Iqbal, M. S. Hossain, and A. J. B. S. Nahar, "Effects of lightning and switching transients on power system components and equipment," *IEEE Trans. Power Syst.*, vol. 28, no. 1, pp. 165–173, Feb. 2013.
[31] M. J. N. S. Samantaray and A. K. Pradhan, "Impact of lightning strikes and switching surges on transformer insulation systems," *IEEE Trans. Dielectr. Electr. Insul.*, vol. 22, no. 3, pp. 1224–1232, Jun. 2015.
[32] M. T. Jones and R. L. Hadley, "Lightning-induced transients in power systems: Analysis and protection strategies," *IEEE Trans. Power Delivery*, vol. 34, no. 4, pp. 1395–1404, Aug. 2019.
[33] M. A. S. R. T. Shukla and P. V. S. R. Kumar, "Mitigation strategies for fast and very fast transients in power systems," *IEEE Trans. Power Delivery*, vol. 33, no. 2, pp. 892–900, Apr. 2018.
[34] P. E. Sutherland and M. E. Valdes, "Snubber design for transformer protection," in *Proc. IEEE PCIC Conf.*, 2014, pp. 343–351.
[35] Y. Zhang, Q. Yang, S. Xie and C. Zhang, "Mechanism and application of arrester block voltage division to lightning transient voltage monitoring in substation transformers," *IEEE Trans. Electromagn. Compat.*, vol. 61, no. 3, pp. 689–696, Jun. 2019.
[36] D. Smugała, W. Piasecki, M. Ostrogorska, M. Florkowski, M. Fulczyk, P. Kłys, "Very fast transient suppressing device," *U.S. Patent* 8,929,048B2, 2015.
[37] S. M. Ghafourian, I. Arana, J. Holbøll, T. Sørensen, M. Popov, and V. Terzija, "General analysis of vacuum circuit breaker switching overvoltages in offshore wind farms," *IEEE Trans. Power Delivery*, vol. 31, no. 5, pp. 2351–2359, Oct. 2016.
[38] CIGRÉ JWG A2/C4.39, *Electrical Transient Interaction Between Transformers and the Power System – Expertise and Case Studies*, Brochure 577A/B, Apr. 2014.
[39] L. van der Sluis, *Electrical Transients in Power Systems*, John Wiley & Sons, 2001.
[40] G. Paap, A. Alkema, and L. van der Sluis, "Overvoltages in power transformers caused by no-load switching," *IEEE Trans. Power Delivery*, vol. 10, no. 1, pp. 301–307, Jan. 1995.
[41] D. Smugała, W. Piasecki, M. Ostrogorska, M. Florkowski, M. Fulczyk, P. Kłys, "New approach to protecting transformers against high-frequency transients – wind turbine case study," *Przegląd Elektrotechniczny*, vol. 89, pp. 186–190, 2013.
[42] T. Dionise and S. Johnston, "Surge protection for ladle melt furnaces," *IEEE Ind. Appl. Mag.*, vol. 21, no. 5, pp. 43–52, Sept.–Oct. 2015.
[43] S. Wei, "Analysis and study of resonance monitoring and suppression strategies of EHV main transformer," in *Proc. ICISCE*, 2016, pp. 848–852.
[44] T. Abdulahović and T. Thiringer, "Voltage stress in a transformer winding during very fast transients caused by breaker closing event," *IEEE Trans. Power Delivery*, vol. 29, no. 4, pp. 1946–1954, Aug. 2014.

[45] M. A. Atefi, M. Sanaye-Pasand and S. Bahari, "Preventing Transformer Energizing Resonant Overvoltages Using Surge Arrester Temperature Rise Index and Controlled Closing Method," in IEEE Transactions on Power Delivery, vol. 28, no. 2, pp. 998-1006, April 2013.

[46] A. Heidary, K. Rouzbehi, H. Radmanesh and J. Pou, "Voltage Transformer Ferroresonance: An Inhibitor Device," *IEEE Transactions on Power Delivery*, vol. 35, no. 6, pp. 2731-2733, Dec. 2020.

[47] Royal SMIT Transformers, [Online]. Available: https://www.tradecloud1.com/en/royal-smit-transformers-chooses-tradecloud/.

2

TRANSFORMER RESONANCE

2.1. ABSTRACT

Due to the expansion of power grids and the increasing complexity and compactness of power equipment, transformers become more vulnerable to transient phenomena caused by lightning strikes and switching operations. Transformer resonance can lead to severe overvoltages in internal winding components, potentially resulting in insulation failure and transformer outages. Although the causes of resonance, measurement techniques, and mitigation strategies have been explored in scientific reports over the past few decades, the literature lacks a comprehensive review of these studies. This review outlines the objectives and main steps of the thesis.

This thesis section aims to fill that gap by reviewing the primary causes of transformer resonance, discussing modeling methods, and elaborating on effective solutions for suppressing resonance. Additionally, it suggests potential protection strategies for future research and development.

The chapter explores the causes of transformer resonance by paying attention to recent scientific research. It also explains the details of various methods for measuring transformer resonance and resonance suppression techniques and extracts each method's key features. Furthermore, an overview of the existing protection technologies is presented.

This chapter of the thesis is published in the article:
A. Heidary, M. G. Niasar, M. Popov, and A. Lekić, "Transformer Resonance: Reasons, Modeling Approaches, Solutions," IEEE Access, vol. 11, pp. 58692-58704, 2023.

2.2. OVERVIEW OF THE EXISTING PROTECTION METHODS

The transformer, a fundamental element in power systems, is an electromagnetic device that alters voltage levels while maintaining the same power transfer and frequency within the electrical network [1]. Transformers are broadly classified into two types: power transformers, which facilitate energy transfer, and instrument transformers, which measure power system signals [2]. Ensuring the protection of these critical devices, particularly power transformers, is vital to the reliable operation of the entire system [3].

One of the most critical phenomena impacting transformer performance is resonance [4]. Different types of resonance can affect transformers in various ways [5]. Transformer resonance occurs due to the inductive and capacitive characteristics of the windings and the connected power system, potentially occurring at frequencies different than the grid frequency [6]. Resonance often poses detrimental effects that necessitate the implementation of protective measures [7]. The diverse nature of transformer resonance is classified in [8] according to its impact on the system.

Comprehensive transformer measurement and modeling for a wide frequency spectrum is crucial for the transformer design and provides valuable insights into the resonance risks during operation [9]-[10]. Numerous protective solutions have been explored to mitigate resonance-related faults in transformers [11]. These solutions generally fall into three categories: parallel damper circuits [12], series components [13], and solid-state protection devices [14].

Parallel damper circuits, including nonlinear resistors (such as SAs) and R-C circuits, are well-established solutions for mitigating transformer overvoltage [15]. Series components, such as FTSC [16] and FDDs [17], contribute additionally to resonance suppression. Furthermore, solid-state devices featuring controllable switches, capacitor banks, or reactors offer dynamic solutions for eliminating overvoltages resulting from transformer resonance [18]-[19].

This section of the thesis aims to comprehensively review the key concerns associated with transformer resonance, highlighting its causes, modeling techniques, and industrial mitigation strategies. The primary objective is to outline the main factors contributing to transformer resonance, present advanced modeling approaches, and discuss practical methods for suppressing resonance-induced overvoltage.

2.3. REASONS FOR TRANSFORMERS' RESONANCE

Two main reasons for the resonance occurrence are the high voltage multiple restrikes or the power line switching because of either the fault and protection equipment operation or renewable resources management [20]. When the system's topology changes, the predominantly inductive circuit changes to capacitive, and the other way around. Consequently, the system is exposed to oscillations with different frequencies and amplitudes [21], and therefore, components like transformers may experience resonances during the system transient [22]. The reasons for resonance occurrence are presented in the following subsections.

Transformer resonance occurring due to the lightning effect:
Lightning overvoltages are the crucial source of transformer resonance when lightning occurs in the vicinity of a power transformer [23]. Lightning modeling is explained in [24]-[27]. These models include electromagnetic models, distributed-circuit models, and engineering models. For electrical system studies, the engineering model comprises a dual nature, with lightning striking tall objects and ground-truth testing employed [24]. As shown in Fig. 2.1, there are four important cases of lightning strikes in power systems: lightning strike to a ground wire, phase conductor, ground near towers [24], as well as to a wind generator tower, which causes a surge that proceeds toward the transformer [28]. Generally, lightning strikes occur due to their height and installation location. Under these circumstances, several tens of kilo amperes may flow from the tower, which can induce a high overvoltage near the power transformers [28]. The lightning current usually includes a current with a high rate of rise, around 10 kA/μs, and a slower rate of fall, in the order of 0.6 kA/μs [29], demonstrating a variety of harmonic contents.
Transient voltage can induce a voltage with different harmonics and stimulate the transformer's resonance frequency after the lightning strike takes place [30]. This phenomenon can easily affect transformers with resonance overvoltage, partially or totally damaging the transformer's isolation [30]. Therefore, the best approach is to examine the transformer using the lightning impulse test before finalizing the manufacturing process [31] and protect transformers against lightning effects [32]; this is standardized in IEEE Std 998™-2012. This standard explains the details of charge formation in the cloud, showing various charge distributions in lightning. Then, the shield wire design is defined in detail, showing how to protect the transformer against lightning strikes [32]. The standard test of the induced voltage during the transformer lightning test is shown in Fig. 2.2 [33], considering that this voltage waveform is similar to a lightning impulse [34].

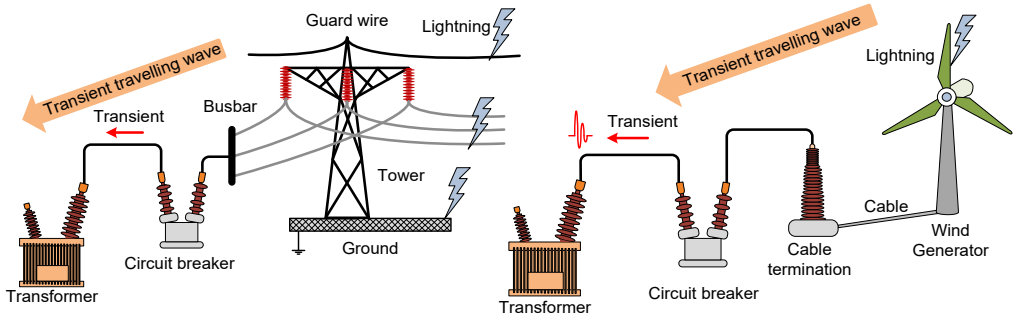


Fig. 2.1. a) Lightning strike on the overhead line, b) Lightning strike on the wind generators' tower

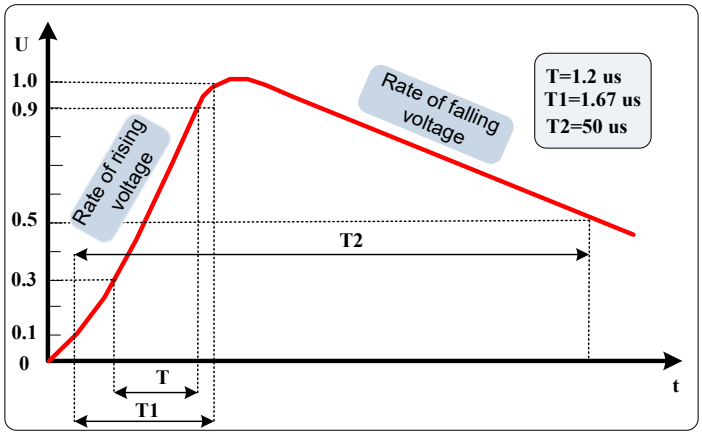


Fig. 2.2. Transformer lightning impulse

Transformer resonance occurred due to breaker switching:
CBs are a crucial part of the power system, which generally either operate to protect the power system from fault current damage or disconnect different parts of the network [35]. Fig. 2.3 depicts the configuration of the CB and transformer.

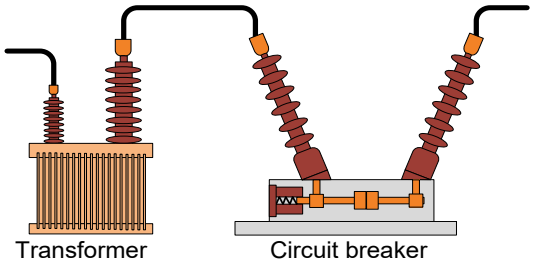


Fig. 2.3. An illustration of a transformer and circuit breaker connection

By opening the circuit of the unloaded transformer, overvoltage occurs on both the CB and transformer due to the magnetic energy stored in the transformer [36]. Equations (2-1) and (2-2) define the transformer and CB voltages, respectively, after the CB opening by ignoring the damping effect [36].

$$U_t = I_{ch}\sqrt{L_m / C_t} \tag{2-1}$$

$$U_{cb} = E_{kr}.v.t \tag{2-2}$$

Here, U_t and U_{cb} are the voltages of the transformer and CB, respectively. I_{ch} is the chopping current magnitude when the CB interrupts, L_m and C_t are the magnetization inductance and the transformer capacitor, E_{kr} is the electric field between the contacts, v is the speed of contact separation, and t refers to the time.

Fig. 2.4(a)-(e) depicts the operation sequence of the CB. It clarifies that during the operation of the CB, the electric arc will be formed and interrupted several times. Finally, the breaker reaches the end of the cycle, where maximum isolation is applied, and the arc interrupts permanently [37]. The no-load transformer can easily face resonance overvoltage, considering harmonically polluted voltage during the breaker's operation [38]-[39].

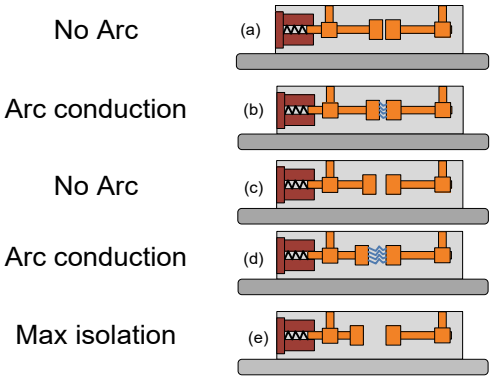


Fig. 2.4. Operation procedure of the CB

Fig. 2.5 illustrates an example of the open no-load transformer voltage during the vacuum CB operation to open the no-load transformer. Reference [38] provides analytical and experimental tests of CB prestrike and restrike effects on the winding of the transformer. The transformer's resonance overvoltage was studied by performing a three-phase CB switching test setup, applying different cable lengths at different loading conditions. The obtained results clarify the effect of vacuum CB operation on the transformer overvoltage, and this operation may cause a resonance effect.

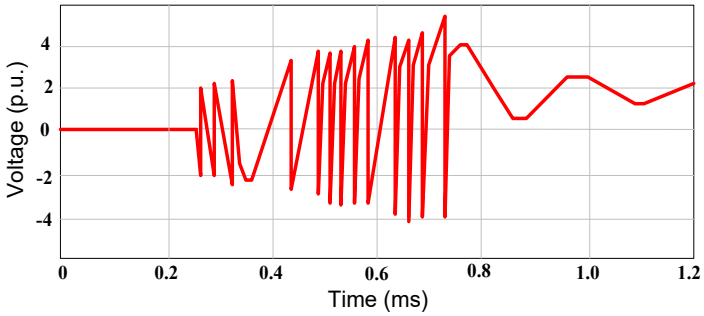


Fig. 2.5. The voltage of the transformer during CB operation

Another reason that may cause resonance is the unloaded transformer energization. By closing CB and energizing a transformer, the fast transient phenomenon may excite resonance in the internal transformer windings, causing high voltage overvoltages [40].

Transformer resonance occurred due to the open breaker effects:
After a power line interruption, the unloaded transformer is always connected in series with the CB, considering there is no transient phenomenon in the power system. In this state, the CB behaves as a series capacitor, and the transformer (power or voltage transformer) is a large reactor [41]. This situation is illustrated in Fig. 2.6.
A series resonance [42] may occur, considering an open CB capacitive model. However, by increasing the transformer current, the core will reach the saturation region, and ferroresonance may happen [43].
In addition, the harmonic content of the voltage during the ferroresonance can also affect the nearby transformers [44]-[45]. An example of the voltage signal of the transformer in a ferroresonance state is presented in Fig. 2.7 [19].

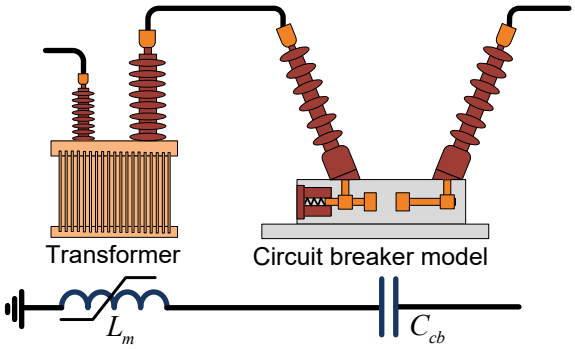


Fig. 2.6. An equivalent circuit of the transformer and open CB

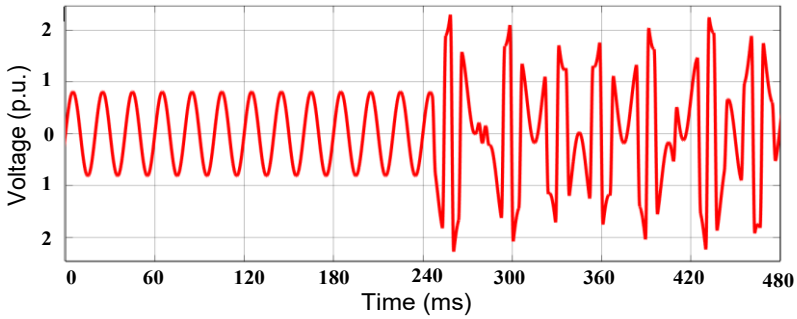


Fig. 2.7. Transformer ferroresonance overvoltage

Fig. 2.7 shows that the nonlinear ferroresonance voltage of the transformer causes overvoltages higher than 2 p.u. To study transformer ferroresonance, the transformer can be represented by equations (2-4) and (2-5). Equation (2-4) presents the nonlinear characteristic of the transformer as a generic *n*-order polynomial. The nature of the transformer core defines the order *n*. Then, by applying the derivative to (4), the transformer voltage can be expressed by (2-5) [19].

$$\lambda(t)+\lambda^{n}(t)=L\,i_{t}(t) \tag{2-4}$$

$$u_{t}(t)=N\,d\left(\varphi(t)+\varphi^{n}(t)\right)/dt \tag{2-5}$$

Here, φ refers to the transformer core flux and L, which are the transformer winding inductance and current, respectively. λ is the linked magnetic flux of the transformer.

Transformer resonance due to nonlinear loads:

The introduction of DC systems and DC nonlinear loads contributes to the increase of power system harmonic content [46]. Some harmonics may be close to the resonance frequency of large transformers [47]. Considering the power quality standard for power systems, IEC 61000, the magnitude of these harmonics should not exceed the values defined by the standard. However, the harmonics' magnitude might increase because of a power system malfunction, faults, or heavy nonlinear load switching [48]-[49], resulting in transformer resonance and overvoltage occurring due to the injection of harmonics in the transformer [50], as depicted in Fig. 2.8.

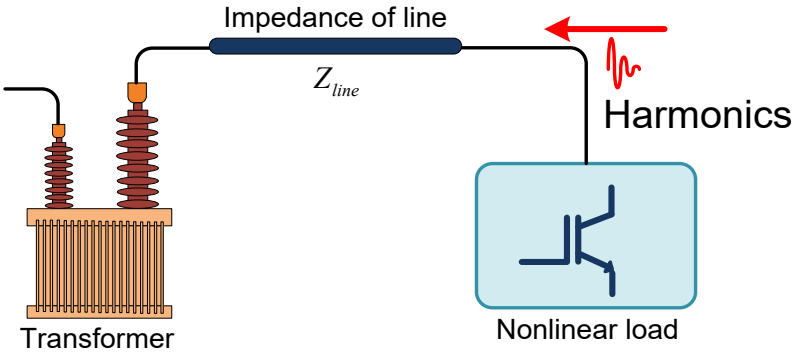


Fig. 2.8. Nonlinear load effects on the transformer

According to IEEE Std 1159-1995, the amplitude of the harmonics and the Total THD should be below the permissible values [51]. However, the harmonic content can be increased for system dynamics and power equipment interactions and induce transformer resonance [52]. An example of resonance occurrence due to the generated harmonics of the HVDC VSC in the HVDC power system is shown in Fig. 2.9 [53]. It can be seen that the transformer can be exposed to a risk of resonance caused by nonlinear power electronic devices, mainly triggered by the harmonics of the 30th-60th order.

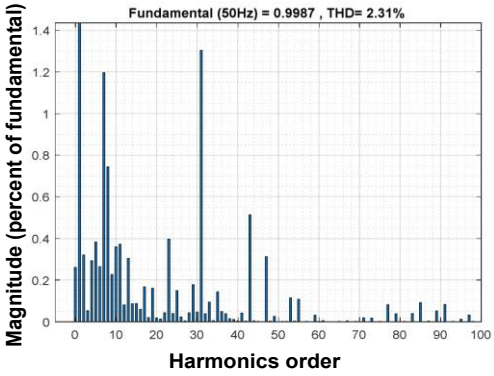


Fig. 2.9. Harmonic pollution of the transformer connected to VSC

Transformer resonance caused by the cable model:
In power systems, the high-voltage cable is used for power transmission or distribution between substations around urban areas. Accurate cable modeling is needed to investigate the interaction between the cable and transformer [54]. The theoretical formulation of the cable, considering bundle-shielded cable as the most common cable, shows the capacitive cable's impedance for various harmonic domains [55], which may interact with the inductive transformer impedance.

The cable's analysis conducted in power system transient studies [56] proves its influence on the overvoltage and resonance [57], as is illustrated in Fig. 2.10.
Considering the R-L-C models of the transformer and cable, many resonance points may appear, which can be stimulated by the harmonic content of fast transients and cause transformer overvoltage. The critical length of the connected cables for the primary and secondary sides of the transformer is determined by the travel time, the cable's resonance frequency, and the transformer's resonance frequency, which can be the main reason for transformer damage by overvoltage [58]. Mostly, cables have been modeled using frequency-dependent models designed based on the cable geometry [59]. One of the cases in which resonance overvoltage occurs is where the transformer's secondary side is not loaded, and its primary winding is connected to the grid by a cable [60].

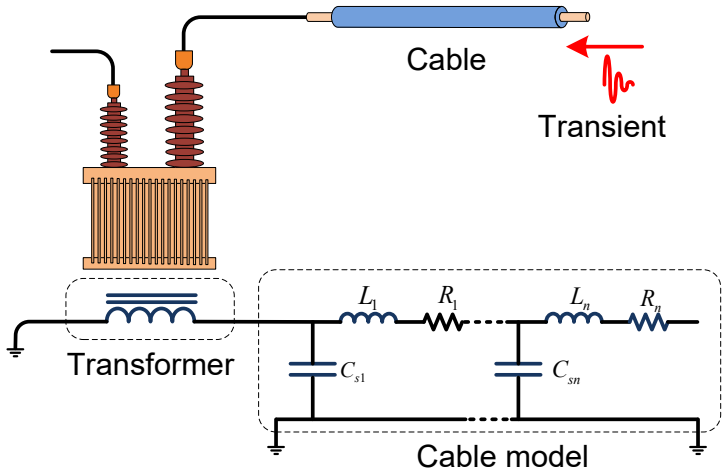


Fig. 2.10. Cable-transformer model

2.4. METHODS FOR MEASURING AND MODELING TRANSFORMER RESONANCE

This section presents the method that is currently used for transformer frequency-dependent modeling and measurement. The following methods are based on transformer resonance, and their wide frequency range model can be obtained.

1. **Frequency-dependent modeling of the transformer**

The possibility of resonance between the transformer and the rest of the power system equipment is a concern for transformer designers and system operators. Thus, transformer transient analyses and their accurate modeling are vital for protecting

transformers against resonance overvoltage [61]. The most commonly used transformer modeling approaches are:

- Black box model [62]-[65],
- White box model (physical model) [66]-[69],
- Gray box model (hybrid model) [70]-[74].

Black box model:
In this model, the transformer is considered a black box, and then the electrical behavior of internal circuits is studied based on measurements [62]. The back box model is the standard and traditional method proposed in 1988, which helps to understand power transformers' behavior within a high-frequency range [62].
As a black box, the three-phase transformer is connected to the source and the measurement device [63]. In this model, the source can be considered as a sinusoidal variable frequency [63] or an impulse generator [64], while the oscilloscope records measured signals from the terminal of the black-boxed transformer [63]-[64].
Different configurations are applied to this black box (short circuit or open circuit connection) in a way that specific terminals are connected to the source, and currents and/or voltages are measured to approximate admittance matrix elements [65]. An example of a black box model setup for the single- and zero-phase injection test for the black box model of the transformer is illustrated in Fig. 2.11 [63].

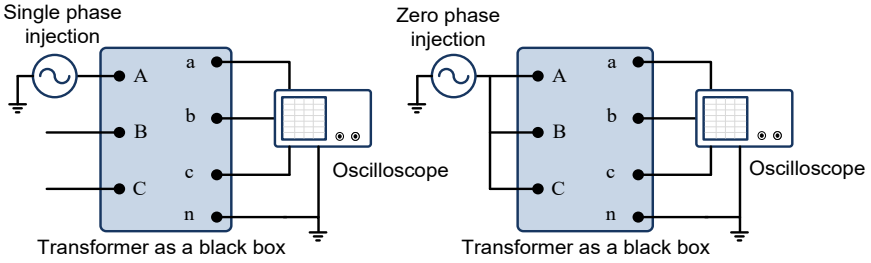


Fig. 2.11. A measurement example for the development of a black box model of a transformer

White box model:
White box models, also known as physical models, are based on either FEM or analytical analysis of R-L-C elements that define the transformer characteristic (also called a detailed model). The white box is a model that considers the geometry of all layers in the transformer, such as conductors, isolators, and core, as well as their mutual interactions. The extraction of the results by these models requires a long computational processing time due to the large matrices, with elements that should be computed for each frequency of the selected bandwidth [66].
The geometrical position of winding turns, the cross-section of the core, and the cross-section of the windings' wire are considered in a FEM transformer model [67]. Moreover, the capacitor calculation method between winding disks can be

implemented using series-parallel capacitors, which improves the accuracy of the transformer white box model [68]. A 3D design and a 2D scheme can focus on a simplified simulated model of a section of the transformer to increase the accuracy of the transformer FEM model. According to the procedure of the white box model, the self-inductance of each turn or disk can be calculated, and then the mutual inductance of windings (between the disks of windings or between (HV-LV) is studied. In addition, the capacitance of each disk to the transformer tank and the capacitance between disks and between HV to LV winding are needed to create a comprehensive model [69]. An illustration of the inductance and capacitances to be computed and used in a transformer coil is illustrated based on geometrical features in Fig. 2.12.

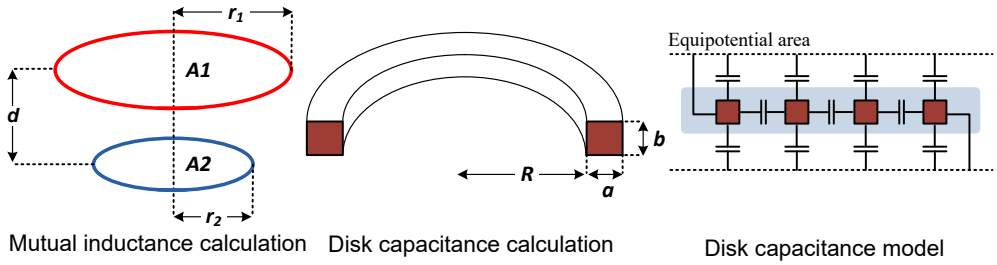


Fig. 2.12. An example of configurations for the white box model of the transformer

Gray box model:

The gray box model (so-called hybrid model) is comprised of a combination of black box and white box models, which is the method that provides faster and more accurate analysis [70].

In this method, firstly, a signal is applied as input to the transformer, and the output as a system response, is measured. Then, the transfer function is calculated using the transformer input and output. This model is improved by considering the winding geometry and FEM to calculate self- and mutual inductance [71]. In [72], the R-L-C model of the transformer is described, and it shows that the most critical issue of the gray box model is its ability to identify the model parameters when no information about the geometry of the transformer is available. Therefore, it is a practical method to model transformers with unidentified geometry or an old transformer (referred to as dielectric aging) and to diagnose the problem of the power system-connected transformer [73]. In addition, by simplifying the gray box model, it will be possible to improve the analysis and parameter estimation of the model faster and more accurately [74]. By developing a Simplified Transient Model (STM) in [74], the advantages of the method are presented as follows:

- The simulation is adequately fast
- Using STM with the other models of power network elements for power system studies and analysis is possible.

- The parameter identification of STM does not need any costly and time-consuming measurements.
- Considering the effects of faults on STM is possible.

2. Transformer resonance study based on transformer modeling

One of the vital goals of studying transformer models based on the wideband frequency domain is the detection of the resonance frequencies of the transformer [75]. The resonance frequencies closely depend on the type of transformer and its design conditions, which can be estimated by the nodal admittance measurement [75]. Transformer frequency-dependent impedance is a crucial parameter to determine the extreme impedance points that show the resonance frequency points and transformer phase changes [76]. Resonance overvoltages can occur at different resonance frequencies, and the overvoltage magnitudes may reach high values, even higher than 5 p.u [77].

To study power transformer resonance, the use of suitable algorithms to determine the resonance class is suggested in [78]:

For the transformer resonance determination and voltage distribution in each coil, it is investigated that a sinusoidal impulse with a period of 250 ns is applied to the transformer winding. Then, in [79], it is recommended that, before applying the STLM method to calculate transformer overvoltage, the actual measurement of the frequency characteristic of the inter-turn voltage distribution, the resonant frequencies, and the amplitude of the inter-turn overvoltage should be considered. Fig. 2.13 depicts an example of the magnitude of the transformer's impedance as a function of frequency and points out two resonance frequencies.

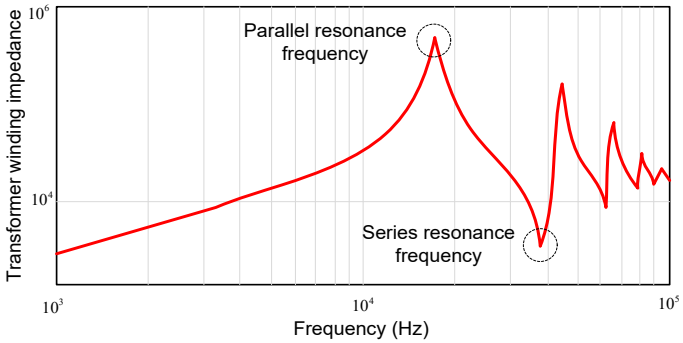


Fig. 2.13. Extracting transformer resonance frequencies from a measured frequency sweep characteristic

3. *Transformer resonance measurement methods*

In this subsection, the methods of transformer measurement are introduced. These methods are widely used to extract the resonance frequency of transformers in

practice. These methods provide appropriate protection of the transformer around the resonance frequency points [80].

The FRA test is based on the transformer response measuring for a wide frequency bandwidth, which is known as a vital method to diagnose resonance frequencies of the transformer [81]. This method is presented in IEC 60076-18. The FRA device consists of three channels. The first channel is for the source connected in series with a resistor. The second channel provides a reference value using a voltage drop on a 50 Ω resistor, and the third channel is the measurement port [82]. There are two types of FRA, depending on their internal source. The first type is designed based on an IFRA, and the second one is designed using an SFRA [82]. SFRA is the most commonly used device.

The FRA test is a method to test the terminal or internal resonance for various types of transformers as complex electrical circuits [83]. In addition, it is an appropriate test method to study wideband analysis of transformer admittance and modeling of the transformer [84]-[86]. Omicron SFRA is a commonly utilized device to test power transformers to diagnose their internal faults or resonance overvoltage [87]. Fig. 2.14 depicts the interface of the Omicron device for frequency sweep recording [88].

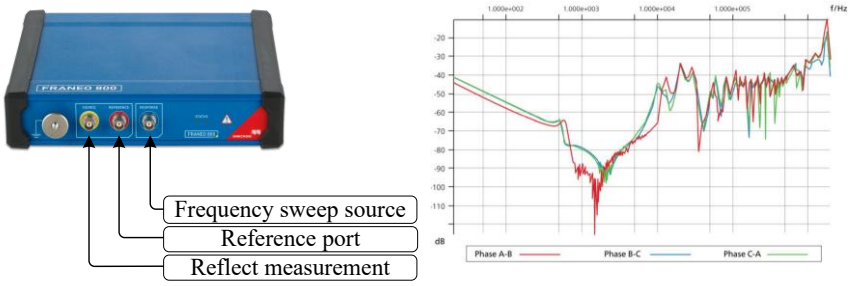


Fig. 2.14. Example of transformer measurement using Omicron SFRA

The second wideband measurement method uses a vector VNA device [89]. The crucial difference between VNA and SFRA is the different types of connection to the transformer, and only SFRA passes the requirement of the standard for transformer measurement [89]-[90]. In [90], transformer measurements were compared for black-box modeling by employing two different methods and measurement equipment (SFRA and VNA). These two methods show good agreement for different ranges of frequencies (up to several MHz). For the frequencies higher than those in the MHz range, the results obtained by the VNA device were shifted to higher frequencies compared with the results measured by the SFRA. Fig. 2.15 shows the VNA (Bode 100) and its measurement interface.

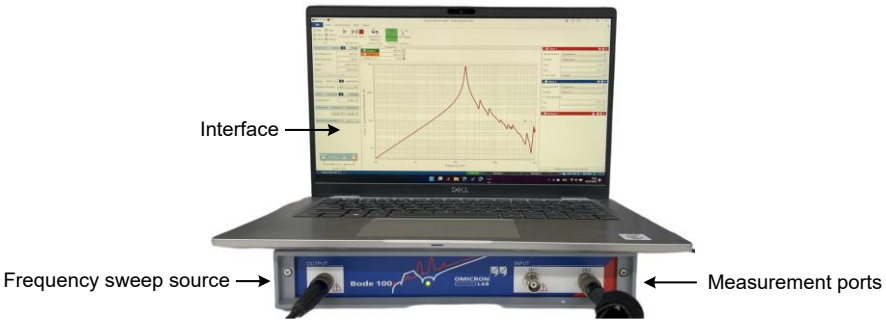


Fig. 2.15. Example of transformer measurement using a Bode 100 VNA

2.5. SOLUTIONS FOR TRANSFORMER RESONANCE

By taking into account the transformer's state-of-the-art protection against resonance overvoltage, several solutions have been introduced to suppress transient effects in power transformers. These structures are series or parallel protection devices acting as filters to reduce and suppress transient resonance overvoltage [91]. Due to the operation, the content of harmonics causes the transformer's resonance frequency to decrease to the acceptable value (which doesn't result in transformer overvoltage). The parallel protection equipment imposes mainly the capacitive-resistive model in parallel with the transformer, and series protection components impose the inductive-resistive model in series with the transformer; their operation is based on magnetic effects [92]-[105].

1. **The parallel-circuit solution against transformer resonance**

Surge arrester (SA) protection:
The most practical Protection Device Against Resonance, which only limits the overvoltage amplitude of a transformer, is the use of SA connected in parallel to the transformer terminals. SAs are known as overvoltage protection and are developed mainly from ZnO material [92]. Nevertheless, they can only chop the generated overvoltage by conducting the transient voltage to ground. Moreover, it cannot behave as a harmonic filter [93]-[94]. SAs are categorized based on the voltage level, particularly between 24-800 kV (RMS) [94]. The location and connection of the SA are illustrated in Fig. 2.16 [95].

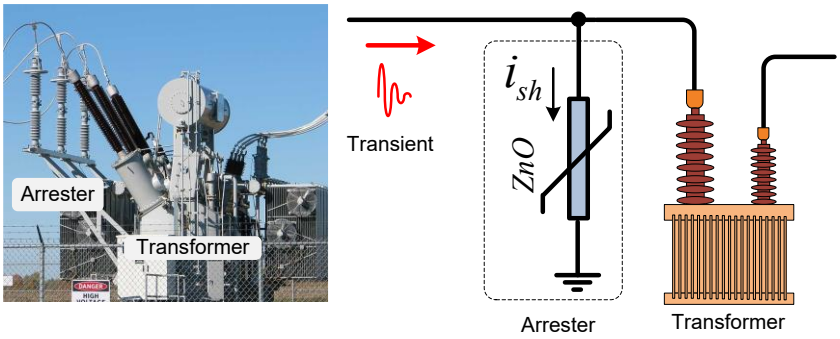


Fig. 2.16. Configuration of an SA to protect transformer resonance

Surge capacitor protection:
The protection against transformer resonance by a surge capacitor is very similar to the SA protection. Here, a surge capacitor is able to tolerate high dU/dt values in parallel with the transformer to suppress the transient voltage of the system as a low-pass filter. In contrast with the SA, the surge capacitor damps the magnitude of high-frequency overvoltage and decreases the transient's harmonic content, which may stimulate transformer inter-disk or terminal resonance [96]. Fig. 2.17 [97] shows an in-market surge capacitor and its configuration to protect the transformer. The conventional surge capacitors are designed for a 7.2-36 kV (medium voltage) range, and their capacity is between 0.05-0.8 µF [97].

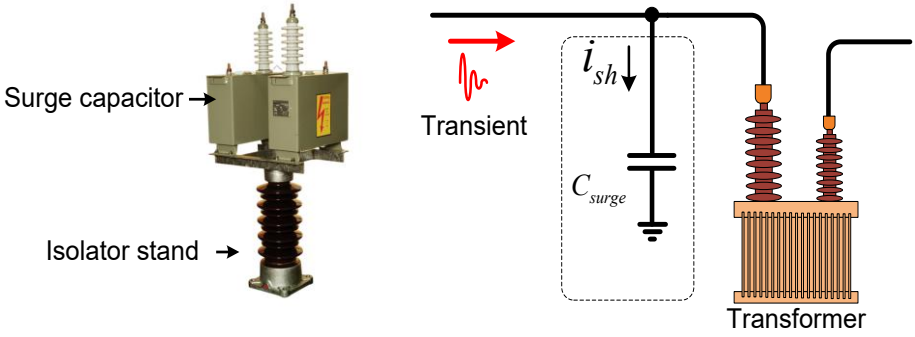


Fig. 2.17. Configuration of a surge capacitor to prevent transformer resonance

R-C Snubber:
Using a shunt R-C circuit as a snubber is a standard method to protect transformers from transients and resonance. This method connects a high-impedance R-C in parallel to the transformer [98]. The operation of R-C acts as a low-pass filter and absorbs the energy of the transient signal in the resistor. The voltage range of the conventional R-C snubber of the power system is between 7 and 34.5 kV, and the range of the resistor values is 20-500 Ω (300-750 W). The snubber's capacitance varies

between 0.08-0.75 μF [99]. Fig. 2.18 shows a configuration of an RC snubber connected to a transformer [99].

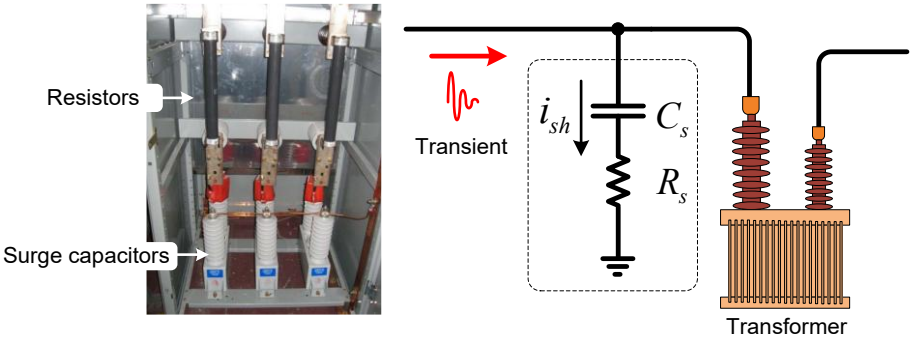


Fig. 2.18. Configuration of RC snubber to protect the transformer

ZnO-RC protection:
A modified structure of the R-C snubber, known as ZORC, has been developed as a solution to prevent transformer resonance. This structure comprises ZnO SAs, resistors, and capacitors, which are very effective devices for suppressing transient oscillations and protecting the transformer against resonance. Its operation is very similar to that of an RC snubber; however, it includes a nonlinear resistor, which can improve its operation [100]-[101]. A conventional ZORC is designed for a 3-40 kV voltage level. Fig. 2.19 illustrates a ZORC to protect the transformer [101].

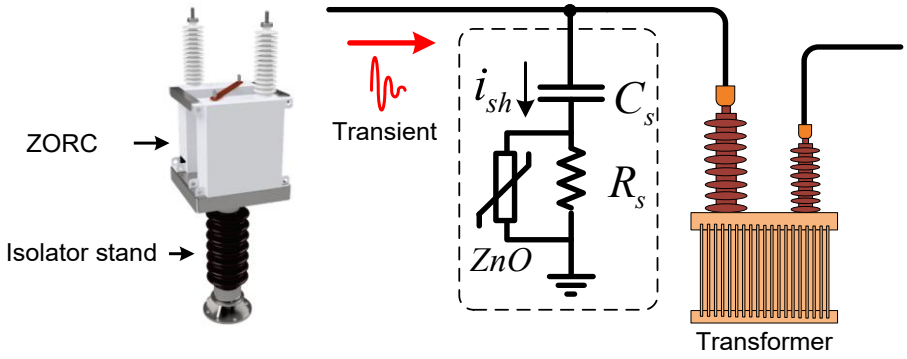


Fig. 2.19. Configuration of a ZORC to protect the transformer

2. Series-circuit solution against transformer resonance

Pre-insertion resistor (PIR) protection
A practical way to mitigate the high rate of transient variations in a power system is by using PIR before switching [102]. Two types of PIRs exist: series switches PIR or parallel switches connection PIR. Both can protect the transformer against resonance. This method's advantage is that it applies to high voltage transformers up to 400 kV, and its challenge is the very high power loss during power switching. Also, this method

suppresses only the transients that occur by switching [103]. Fig. 2.20 shows the configuration of PIR with a transformer [104].

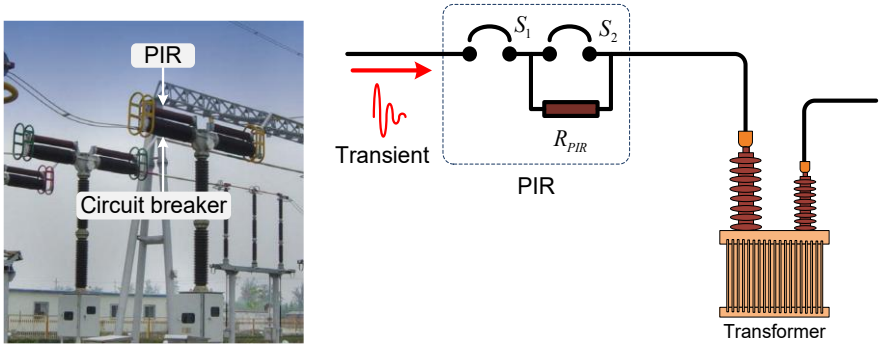


Fig. 2.20. Configuration of a pre-inserted resistor to protect the transformer

Frequency-dependent device (FDD) protection device

The series R-L circuit is a recently presented solution for protecting the transformer against transient phenomena and resonance. This circuit can be realized by using ferromagnetic shielded wire as an FDD [105]. This device comprises a multilayer wire using aluminum and ferromagnetic material, which are used as a reactor and connected to a power substation's input cables. FDD provides meager resistance for grid frequency (50 or 60 Hz) and imposes a high resistance of nearly 200 Ω for frequencies around 200 kHz [106]. In [106], it is obtained that FDD protects well from short pulses and imposes little effect on long pulses. The designed device parameters must be developed or integrated with devices like the SA to protect the transformer fully. The variable resistor of FDD is created based on the skin effect of composite ferromagnetic material [107]. Fig. 2.21 depicts the equivalent circuit of FDD and in-practice configuration [106].

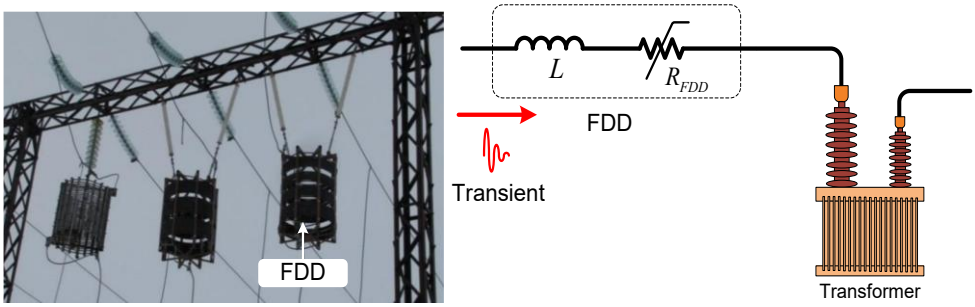


Fig. 2.21. Configuration of an FDD to protect the transformer

Choke protection:

The choke is a series device that can protect medium voltage power transformers against transients and resonance. The R-L choke model can mitigate transient harmonic content appropriately and drastically reduce transformer resonance

overvoltages [16]. During steady-state operation, the impedance of this component (power network 50/60Hz frequency) is nearly zero. During high-frequency transients, these devices behave as a parallel R-L and suppress the high-frequency oscillation by using the effect of a ferromagnetic core [108]-[109]. Fig. 2.22 shows the choke configuration [11].

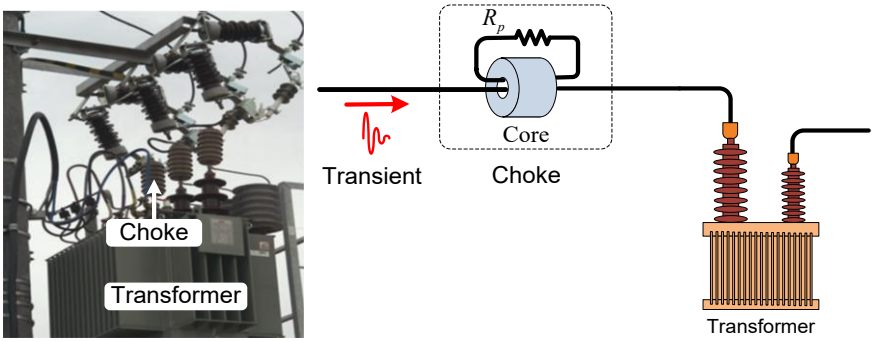


Fig. 2.22. Choke configuration to protect the transformer

Power electronic-based protection:
The solid-state DC reactors (DCRs) component is normally applied to protect transformers against transient and transformer resonance. With this practical method, the transformer can be protected against nonlinear resonance, which consists of a solid-state bridge (including four diodes) and parallel R-L. The transformer can appropriately protect itself by suppressing nonlinear oscillations of voltage transformer ferroresonance and mitigating harmonic overvoltage on the transformer terminal [110]. The topology of this power electronic-based transient suppressor device is presented in Fig. 2.23.

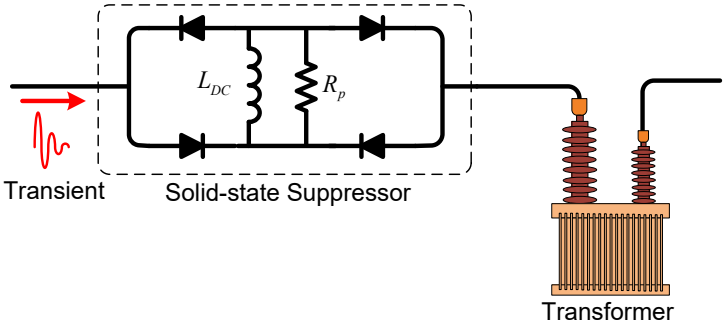


Fig. 2.23. Configuration of a solid-state suppressor to protect the transformer

Table 1.1 summarizes the essential data concerning reasons, measurement, and associated protection methods. Considering the transformer resonance issue, it is

crucial to determine the reason for transformer resonance and then provide an accurate model for the studied transformer. In the final stage, providing the appropriate compound solution for the resonance occurrence of the studied transformer should be considered.

Table 1.1. Transformer models and protection solutions against resonance

Transformer resonance reasons				
Lightning strike	Switching arc	Open CBs	Nonlinear loads	Cable effects
Modeling of a Transformer		**employed method**		
Black box model		The input is an excitation, and the output measurement.		
White box model		Finite element method by physical detail		
Gray box model		Using both measurement and FEM		
Transformer resonance measurement methods				
IFRA		SFRA	VNA	
Transformer protection		**Protection features**		
Resistive	Arrester	LV to HV protection, resonance overvoltage protection of the transformer terminal		
	PIR	MV to HV protection, resonance protection of the transformer in the switching case		
Capacitive	Surge capacitor	MV protection, harmonic content filter, resonance protection of transformer terminal, and inter-disk		
	R-C snubber	MV protection, harmonic content filter, resonance protection of transformer terminal, and inter-disk		
	ZORC	MV protection, harmonic content filter, resonance protection of transformer terminal, and inter-disk		
Inductive	FDD	MV to HV protection, harmonic content filter, resonance protection of transformer terminal, and inter-disk		
	Choke	MV protection, harmonic content filter, resonance protection of transformer terminal, and inter disk		
	DCRS	MV protection, resonance protection of transformer terminal, and inter-disc		

By observing the summary shown in Table 1.1, it is obvious that there is no universal solution to protect HV level transformers for transmission systems against power system transients and resonance overvoltage.
Considering the circumstances, the applicability of the available solution in the next section is briefly studied to obtain the next step of the research in this field.

2.6. STUDY OF APPLICABLE PROTECTION AGAINST TRANSMISSION TRANSFORMER RESONANCE

This section provides a brief overview of the limitations of the already used protection methods for the protection of high-voltage transmission transformers. The evaluation of the available protection solutions at a 200 kV voltage level has been considered, which is an example of a transmission system voltage level.

1. Parallel protection methods evaluation

Surge arrester:
This device is connected in parallel with the transformer to protect it against overvoltage. There are two operating concerns: The transformer model is inductive and dependent on the voltage magnitude. An equivalent model of the SA is illustrated in Fig. 2.24 [93].

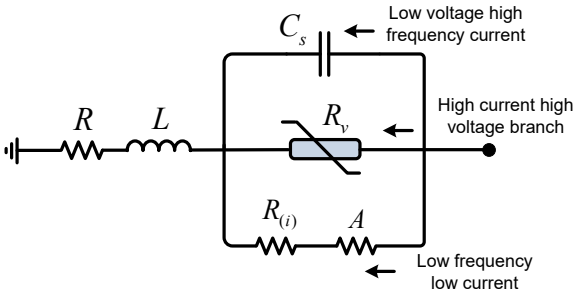


Fig. 2.24. An equivalent circuit of the SA

When transients do not exceed the SA continuous operation voltage, the equivalent of the SA circuit is a series RLC. The circuit depicted in Fig. 2.25 (a) is a band-pass filter around its resonance frequency. However, the remaining frequency content can cause the transformer inter-disk resonance, while the transformer terminal voltage never experiences an overvoltage due to SA voltage suppression.
The low voltage and high-frequency transients cause the next concern about SA protection. In this case, the SA behaves as an R-L circuit, as shown in Fig. 2.25 (b). This circuit can cause an operational delay against very fast transients, resulting in transformer resonance before the arrester operates.

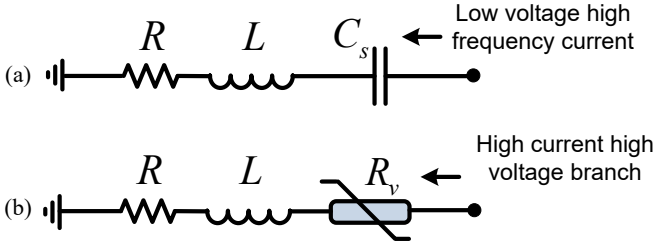


Fig. 2.25. An equivalent circuit of an SA for transient analysis

These two reasons show that SAs cannot provide comprehensive protection for transformer resonance:

- SA cannot protect the transformer against LV high-frequency transients.
- Operational delay considering its inductive circuit against LV high-frequency transients

Parallel surge capacitor protection:
There are three types of capacitive transformer protection: surge capacitors, R-C snubber, and ZORC [96], [99], [100]. Considering the industrial datasheets, to protect a 200 kV transformer, using 0.1 μF, 200 Ω (for R-C snubber and ZORC), and at least A capacitor bank with nominal voltage 360 kV (considering that a transient impulse adds 50-100 kV to the standard voltage of the system) is needed. Considering that in the steady-state condition, the impedance of the capacitor is much higher than the resistance (2-6); therefore, its effect can be ignored when calculating the reactive power produced by the protection branch.

$$R << \frac{1}{\omega C_s} \tag{2-6}$$

In addition, the nominal voltage of each industrial capacitor module (existing in the market) is 36 kV. Hence, to reach a voltage level of 360 kV, a 0.1 μF series-parallel connection of 100 capacitors is needed. This number is estimated under the assumption of linear voltage distribution. The leakage capacitor affects the high-frequency content when it is not distributed linearly. Thus, the number of capacitors should be higher than 100. This protection capacitor bank will produce reactive power Q as calculated by (2-7) for a steady state. The topology of modular surge capacitor protection for transmission system transformers is illustrated in Fig. 2.26.

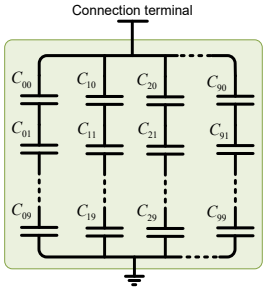


Fig. 2.26. Configuration of a 200 kV surge capacitor

For a steady state, the capacitor bank will produce reactive power Q as calculated by:

$$Q = \omega C_s V_s^2 \tag{2-7}$$

where ω is the angular system frequency, C_s is the capacitance of the surge capacitor, and V_s is the system voltage. For the described example, the value of consumed reactive power will be 1.25 MVAR.

Furthermore, more capacitors can decrease the device's reliability. The reliability of the capacitor bank will decrease based on the system's harmonic pollution, which increases the consumed reactive power during a steady state. Therefore, the surge capacitor for high-voltage transformer protection is not applicable.

2. Series Inductive protection method evaluation

The FDD and the choke [106], [109] are the two main methods for protecting the transformer against resonance overvoltage. The design is based on the ferromagnetic material shielded power conductor. However, there are some differences between these two schemes. Fig. 2.27 depicts a 2D illustration of an FDD and a choke structure cross-section.

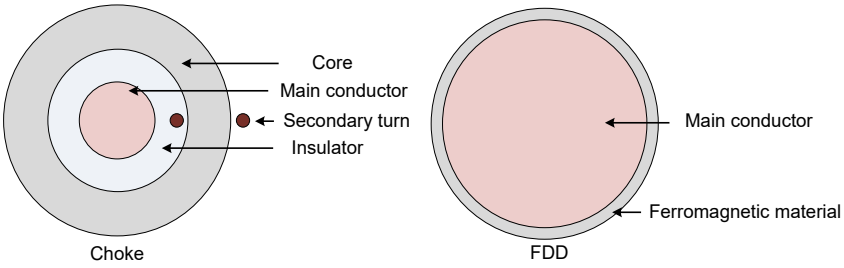


Fig. 2.27. 2D illustration of a choke and an FDD

Namely, the choke contains the core isolated from the main conductor, whereas in the FDD, the ferromagnetic shield is connected electrically to the main conductor. Furthermore, choke has a resistive secondary turn, while FDD does not. FDD is built by winding the extensive length of the illustrated cross-section. However, choke lengths are very short, and FDD's ferromagnetic thickness is much smaller than the choke.

Both structures modeled as a series R-L can protect the transformers against resonance because they are not exposed to a system voltage during a steady state. They can filter the harmonic content and protect transformers.

However, the concerns are the deep saturation of the choke core, high power losses, and thermal desaturation of FDD during steady state. This concern can also affect the correct transient operation of these devices. Besides, the wideband operation of these series filters needs to increase the inductance, which causes reactive power loss in the steady state.

Equations (2-8) and (2-9) show that core saturation depends on the core cross-section and component inductance. The consumed reactive power depends on the inductance value, as seen in equation (2-10). Finally, equation (2-11) shows that the

protection component's imposed impedance should be comparable to the transformer impedance.

$$B << B(\max) \tag{2-8}$$

$$\frac{L.I_t}{A_{core}} << B(\max) \tag{2-9}$$

$$I_T{}^2 \omega L << 10 \quad (kVAR) \tag{2-10}$$

$$Z_{T(\min)}(f) < \omega_T L < Z_{T(\max)}(f) \tag{2-11}$$

Here, B, L, and A_{core} are the protection component's magnetic flux density, inductance, and core cross-section. Z_T, and I_T are the transformer impedance and current, and ω_T is the angular transformer resonance frequency.

It should be mentioned that the consumed active and reactive power can be reduced using the solid-state DC reactor method.

However, the advantages of the presented inductive protection methods are :

- The component is not too large.
- It does not add any electric elements to the power conductor,
- It is a reliable component.

Fig. 2.28 summarizes the advantages and disadvantages of the four key protection components for transformer protection against transient and resonance overvoltages: the SA, the surge capacitors, the FDD, and the chokes.

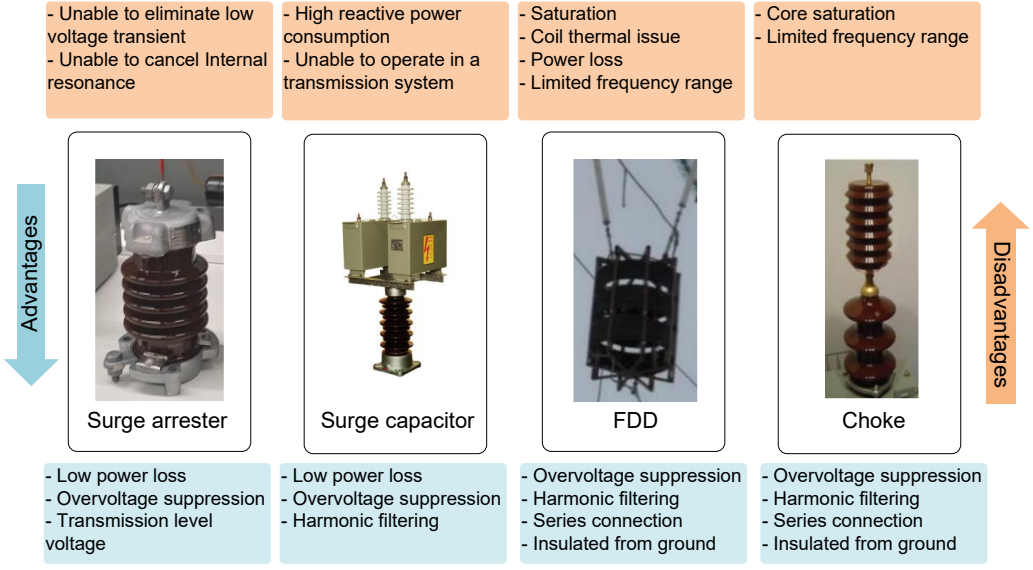


Fig. 2.28. Advantages and disadvantages of protection components

2.7. Conclusion

This chapter comprehensively reviews the causes, modeling techniques, and protection solutions related to transformer resonance in power systems. The key challenges and limitations of existing solutions, particularly for HV applications, have been highlighted by investigating both series and parallel protection methods. While effective to some extent, it is obvious that current protection devices fail to provide full protection against inter-disk and terminal resonance overvoltages for transmission-level transformers. The rest of the thesis focuses on developing robust, multi-functional protection devices capable of addressing these gaps and mitigating the risks associated with transient phenomena and resonance overvoltage in power transformers.

References

[1] E. I. Amoiralis, M. A. Tsili, and A. G. Kladas, "Transformer design and optimization: A literature survey," IEEE Trans. Power Del., vol. 24, no. 4, pp. 1999–2024, Oct. 2009.

[2] F. de Leon, "Discussion of 'Transformer modeling for low- and mid-frequency transients - a review'," IEEE Trans. Power Del., vol. 23, no. 3, pp. 1696–1697, Jul. 2008.

[3] W. Yuanfang and C. Zhou, "Experimental studies on the use of MOV in transformer windings inner protection," IEEE Trans. Power Del., vol. 20, no. 2, pp. 1441, 2005.

[4] R. J. Musil, G. Preininger, E. Schopper, and S. Wenger, "The resonance effect of oscillating system overvoltages on transformer windings," IEEE Trans. Power Appar. Syst., vol. PAS-101, no. 10, pp. 3703–3711, Oct. 1982.

[5] A. M. Miri and C. Sihler, "Damping of resonances at energization of transformers serving large pulse-type loads," IEEE Trans. Ind. Appl., vol. 40, no. 6, pp. 1694–1699, Nov.–Dec. 2004.

[6] S. U. Khayam and Suwarno, "Evaluating the inter-resonance characteristics of various power transformer winding designs," IEEE Access, vol. 9, pp. 54649–54656, 2021.

[7] A. H. Soloot, H. K. Høidalen, and B. Gustavsen, "Influence of the winding design of wind turbine transformers for resonant overvoltage vulnerability," IEEE Trans. Dielectr. Electr. Insul., vol. 22, no. 2, pp. 1250–1257, Apr. 2015.

[8] P. Mitra, A. De, and A. Chakrabarti, "Response of EHV grid transformers to system-originated oscillatory switching transients," IEEE Trans. Power Del., vol. 27, no. 1, pp. 224–235, Jan. 2012.

[9] Y. Liu, S. A. Sebo, R. Caldecott, D. G. Kasten, and S. E. Wright, "Power transformer resonance—measurements and prediction," IEEE Trans. Power Del., vol. 7, no. 1, pp. 245–253, Jan. 1992.

[10] T. Abdulahović and T. Thiringer, "Voltage stress in a transformer winding during very fast transients caused by breaker closing event," IEEE Trans. Power Del., vol. 29, no. 4, pp. 1946–1954, Aug. 2014.

[11] D. Smugała, W. Piasecki, M. Ostrogorska, M. Florkowski, M. Fulczyk, P. Kłys, "Distribution transformers protection against high frequency switching transients," Przegl. Elektrotech. (Electrical Review), vol. 88, no. 5a, 2012.

[12] Y. Zhang, Q. Yang, S. Xie, and C. Zhang, "Mechanism and application of arrester block voltage division to lightning transient voltage monitoring in substation transformers," IEEE Trans. Electromagn. Compat., vol. 61, no. 3, pp. 689–696, Jun. 2019.

[13] W. Piasecki, M. Ostrogórska, M. Florkowski, M. Fulczyk, P. Kłys, "dU/dt protection for distribution transformers," in Proc. Int. Conf. Power Syst. Transients (IPST), Kyoto, Japan, Jun. 2009.

[14] A. Heidary, H. Radmanesh, A. Bakhshi, S. Samandarpour, K. Rouzbehi, N. Shariati, "Compound ferroresonance overvoltage and fault current limiter for power system protection," IET Energy Syst. Integr., vol. 2, no. 4, pp. 325–330, Dec. 2020.

[15] H. Wei, T. Peng, W. Yongkang, and X. Liangle, "Experimental study on consistency of surge test between using gas arrestors and capacitors," in 2018 China Int. Conf. Electricity Distrib. (CICED), 2018, pp. 897–900.

[16] D. Smugała, W. Piasecki, M. Ostrogórska, M. Florkowski, M. Fulczyk, O. Granhaug Prz. Elektrotech, "New approach to protecting transformers against high frequency transients wind turbine case study," Przegl. Elektrotechniczny, Oct. 2013.

[17] S. M. Korobeynikov and N. Y. Ilyushov, "High-current testing of frequency-dependent device," in 2016 11th Int. Forum on Strategic Technology (IFOST), 2016, pp. 326–328.

[18] H. Radmanesh, A. Heidary, SH. Fathi, G. Babamalek Gharehpetian, "Dual function ferroresonance and fault current limiter based on DC reactor," IET Gener. Transm. Distrib., vol. 10, no. 9, pp. 2058–2065, 2016.

[19] A. Heidary, H. Radmanesh, "Smart solid-state ferroresonance limiter for voltage transformers application: Principle and test results," IET Power Electron., vol. 11, no. 15, pp. 2545–2552, 2018.

[20] P. Akiki, A. Xémard, C. Trouilloud, and J.-L. Chanelière, “Study of high frequency transient overvoltage caused by cable-transformer quarter-wave resonance,” Electric Power Systems Research, vol. 197, p. 107287, 2021.

[21] A. H. Soloot, H. K. Høidalen, and B. Gustavsen, "Resonant overvoltage assessment in offshore wind farms via a parametric black-box wind turbine transformer model," Wind Energy, vol. 18, no. 6, pp. 1061–1074, Jun. 2015.

[22] B. Liu, Y. Tong, X.-P. Deng, and X.-X. Feng, "Measuring very fast transient overvoltage and very fast transient current generated by disconnector operating," in 2014 Int. Conf. Power Syst. Technol., 2014, pp. 1349–1354.

[23] E. O. Hassan, E. A. Badran, and F. M. H. Youssef, "Effect of lightning impulses on the resonance stresses in the high voltage power transformers," in 2017 19th Int. Middle East Power Syst. Conf. (MEPCON), 2017, pp. 496–502.

[24] V. A. Rakov and F. Rachidi, "Overview of recent progress in lightning research and lightning protection," IEEE Trans. Electromagn. Compat., vol. 51, no. 3, pp. 428–442, Aug. 2009.

[25] H. K. Høidalen, "Calculation of lightning-induced voltages in models including lossy ground effects," in Int. Conf. Power Syst. Transients (IPST), New Orleans, USA, 2003.

[26] X. Liu and T. Ge, "An effective method for calculating the lightning electromagnetic field over perfectly conducting ground," Appl. Sci., vol. 10, p. 4263, 2020.

[27] A. Andreotti, A. Pierno, and V. A. Rakov, "A new tool for calculation of lightning-induced voltages in power systems—Part I: Development of circuit model," IEEE Trans. Power Del., vol. 30, no. 1, pp. 326–333, Feb. 2015.

[28] W. L. M. de Azevedo, W. C. da Silva, A. R. J. de Araújo, and J. P. Filho, "Computation of transient voltages on wind turbines on frequency-dependent soil caused by lightning strikes," in 2021 Workshop on Communication Networks and Power Systems (WCNPS), 2021, pp. 1–6.

[29] S. Visacro, "Recent advances in lightning research and their impact on the protection of electric systems," in 2018 34th Int. Conf. Lightning Protection (ICLP), 2018, pp. 1–4.

[30] M. Hori, M. Nishioka, Y. Ikeda, K. Noguchi, K. Kajimura, H. Motoyama, and T. Kawamura, “Internal winding failure due to resonance overvoltage in distribution transformer caused by winter lightning,” IEEE Trans. Power Del., vol. 21, no. 3, pp. 1600–1606, Jul. 2006.

[31] X. Zhang, M. Shi, C. He, and J. Li, "On-site oscillating lightning impulse test and insulation diagnosis for power transformers," IEEE Trans. Power Del., vol. 35, no. 5, pp. 2548–2550, Oct. 2020. [32] "IEEE Guide for Direct Lightning Stroke Shielding of Substations," IEEE Std 998-2012 , vol., no., pp.1-227, 30 April 2013.

[32] "IEEE Guide for Direct Lightning Stroke Shielding of Substations," IEEE Std 998-2012 (Revision of IEEE Std 998-1996), pp. 1–227, 30 Apr. 2013.

[33] J. Chang, A. J. Kelly, and J. M. Crowley, Handbook of Electrostatic Processes, 1st ed. New York: Wiley, 1995.

[34] F. Nematollahi and B. Vahidi, "Investigating the effect of lightning channel inclination on the induced voltage in overhead lines in the presence of horizontally stratified ground," Electr. Power Syst. Res., vol. 208, 107919, 2022.

[35] M. Popov, R. P. P. Smeets, L. van der Sluis, H. de Herdt, and J. Declercq, "Experimental and theoretical analysis of vacuum circuit breaker prestrike effect on a transformer," IEEE Trans. Power Del., vol. 24, no. 3, pp. 1266–1274, Jul. 2009.

[36] M. Popov and E. Acha, "Overvoltages due to switching off an unloaded transformer with a vacuum circuit breaker," IEEE Trans. Power Del., vol. 14, no. 4, pp. 1317, 1999.

[37] M. Popov, L. van der Sluis, and G. C. Paap, "Investigation of the circuit breaker reignition overvoltages caused by no-load transformer switching surges," Eur. Trans. Electr. Power, vol. 11, pp. 413–422, 2001.

[38] A. Theocharis, M. Popov, R. Seibold, S. Voss, and M. Eiselt, "Analysis of switching effects of vacuum circuit breaker on dry-type foil-winding transformers validated by experiments," IEEE Trans. Power Del., vol. 30, no. 1, pp. 351–359, Feb. 2015.

[39] L. Liljestrand, M. Lindgren, D. Pommeret, and S. Körner, “Vacuum circuit breaker and transformer interaction in a cable system,” in Proc. 22nd Int. Conf. Exhib. Electricity Distrib. (CIRED), Stockholm, Sweden, Jun. 2013, pp. 1–4.

[40] T. Abdulahović and T. Thiringer, "Voltage stress in a transformer winding during very fast transients caused by breaker closing event," IEEE Trans. Power Del., vol. 29, no. 4, pp. 1946–1954, Aug. 2014.

[41] H. Radmanesh, G. B. Gharehpetian, and H. Fathi, "Ferroresonance of power transformers considering nonlinear core losses and metal oxide surge arrester effects," Electr. Power Compon. Syst., vol. 40, no. 5, pp. 463–479, Feb. 2012.

[42] Y. Li, W. Shi, R. Qin, and J. Yang, "A systematical method for suppressing ferroresonance at neutral-grounded substations," IEEE Trans. Power Del., vol. 18, no. 3, pp. 1009–1014, Jul. 2003.

[43] S. J. Kruger and J. A. de Kock, "Ferroresonance: A review of the phenomenon and its effects," in 2021 Southern African Universities Power Eng. Conf./Robotics and

Mechatronics/Pattern Recognition Assoc. South Africa (SAUPEC/RobMech/PRASA), 2021, pp. 1–6.
[44] Q. Su Charles, Electromagnetic Transients in Transformer and Rotating Machine Windings, 1st ed., 2012, ISBN: 9781466619210.
[45] R. Perez Pineda, R. Rodrigues, and A. Aguila Tellez, "Analysis and simulation of ferroresonance in power transformers using Simulink," IEEE Lat. Am. Trans., vol. 16, no. 2, pp. 460–466, Feb. 2018.
[46] A. Heidary, K. Ghorbanyan, H. Radmanesh, and H. R. R. Khamse, “Voltage sag and harmonic analysis in distribution network,” in Proc. 21st Conf. Electr. Power Distrib. Netw. (EPDC), 2016, pp. 102–105.
[47] C. Boonseng, R. Boonseng, and K. Kularbphettong, "Diagnosis of oscillation and vibration of dry-type transformers caused by harmonic resonance," in 2020 Int. Conf. Diagnostics Electr. Eng. (Diagnostika), 2020, pp. 1–4.
[48] "IEEE Recommended Practice for Monitoring Electric Power Quality," IEEE Std 1159-2019 (Revision of IEEE Std 1159-2009), pp. 1–98, 13 Aug. 2019.
[49] "IEEE Guide for Identifying and Improving Voltage Quality in Power Systems," IEEE Std 1250-2018 (Revision of IEEE Std 1250-2011), pp. 1–63, 16 Nov. 2018.
[50] F. Fuchs and A. S. Masoum, Harmonic Models of Transformers, Power Quality in Power Systems and Electrical Machines, Academic Press, 2008, ISBN: 9780123695369.
[51] "IEEE Recommended Practice for Monitoring Electric Power Quality," IEEE Std 1159-1995, pp. 1–80, 30 Nov. 1995.
[52] "IEEE Standard Conformance Test Procedures for Instrument Transformers," IEEE Std C57.13.2-1991, pp. 1–12, 10 Jul. 1992.
[53] Y. Zhang, C. Klabunde, and M. Wolter, “Harmonic resonance analysis for DFIG-based offshore wind farm with VSC-HVDC connection,” in 2019 IEEE Milan PowerTech, Milan, Italy, Jun. 2019, pp. 1–6.
[54] A. Ametani, T. Ohno, and N. Nagaoka, "Cable modeling for transient simulations," in Cable System Transients: Theory, Modeling and Simulation, IEEE, 2015, pp. 163–184.
[55] T. Ohno, A. Ametani, and C. L. Bak, “Derivation of theoretical formulas of sequence currents on underground cable systems,” in Proc. 22nd International Conference on Power Systems Transients (IPST2011), Delft, The Netherlands, Jun. 14–17, 2011.
[56] N. Nagaoka and A. Ametani, "Transient calculations on crossbonded cables," IEEE Trans. Power Appar. Syst., vol. PAS-102, no. 4, pp. 779–787, Apr. 1983.
[57] L. Colla, S. Lauria, and F. M. Gatta, "Temporary overvoltages due to harmonic resonance in long EHV cables," in IPST, 2007.
[58] G. C. Paap, A. A. Alkema, and L. van der Sluis, "Overvoltages in power transformers caused by no-load switching," IEEE Trans. Power Del., vol. 10, no. 1,1995.
[59] A. Morched, B. Gustavsen, and M. Tartibi, "A universal model for accurate calculation of electromagnetic transients on overhead lines and underground cables," IEEE Trans. Power Del., vol. 14, no. 3, pp. 1032–1038, Jul. 1999.
[60] B. Gustavsen, "Study of transformer resonant overvoltages caused by cable-transformer high-frequency interaction," in 2011 IEEE Power & Energy Soc. Gen. Meeting, 2011, pp. 1–1.

[61] S. M. H. Hosseini, M. Vakilian, and G. B. Gharehpetian, "Comparison of transformer detailed models for fast and very fast transient studies," IEEE Trans. Power Del., vol. 23, no. 2, pp. 733–741, Apr. 2008.

[62] P. T. M. Vaessen, "Transformer model for high frequencies," IEEE Trans. Power Del., vol. 3, no. 4, pp. 1761–1768, Oct. 1988.

[63] A. Chrysochos, G. Papagiannis, T. Papadopoulos, and A. Nousdilis, "Simplified measurement-based black-box modeling of distribution transformers using transfer functions," Electric Power Systems Research, vol. 121, pp. 77–88, 2015.

[64] M. F. Horvat, Z. Jurković, B. Jurišić, T. Župan, and B. Ćućić, "Black-box power transformer winding model," in 2022 7th Int. Adv. Res. Workshop Transformers (ARWtr), 2022, pp. 18–23.

[65] A. Morched, L. Marti, and J. Ottevangers, "A high frequency transformer model for the EMTP," IEEE Trans. Power Del., vol. 8, no. 3, pp. 1615–1626, Jul. 1993.

[66] E. Rahimpour and M. Bigdeli, "Simplified transient model of transformer based on geometrical dimensions used in power network analysis and fault detection studies," in 2009 Int. Conf. Power Eng., Energy Electr. Drives, 2009, pp. 375–380.

[67] P. Gomez, F. de Leon, and F. P. Espino-Cortes, "Improvement of a method to compute the inductance matrix of multilayer transformer windings for very fast transients," IEEE Trans. Power Del., vol. 28, no. 2, pp. 1245–1246, Apr. 2013.

[68] M. Ghaffarian Niasar and W. Zhao, "Impulse voltage distribution on disk winding: Calculation of disk series capacitance using analytical method," in 2020 IEEE Int. Conf. High Voltage Eng. Appl. (ICHVE), 2020, pp. 1–4.z

[69] M. García-Gracia, M. Villén, and M. A. Cova, N. El Halabi, "Detailed three-phase circuit model for power transformers over wide frequency range based on design parameters," Electr. Power Syst. Res., vol. 92, pp. 115–122, 2012.

[70] E. Rahimpour, V. Rashtchi, and R. Aghmasheh, "Parameters estimation of transformers gray box model," in 2017 Int. Conf. Modern Electr. Energy Syst. (MEES), 2017, pp. 372–375.

[71] E. Rahimpour, J. Christian, K. Feser, and H. Mohseni, "Transfer function method to diagnose axial displacement and radial deformation of transformer windings," IEEE Trans. Power Del., vol. 18, no. 2, pp. 493–505, Apr. 2003.

[72] R. Aghmasheh, V. Rashtchi, and E. Rahimpour, "Gray box modeling of power transformer windings for transient studies," IEEE Trans. Power Del., vol. 32, no. 5, pp. 2350–2359, Oct. 2017.

[73] S. D. Mitchell and J. S. Welsh, "Initial parameter estimates and constraints to support gray box modeling of power transformers," IEEE Trans. Power Del., vol. 28, no. 4, pp. 2411–2418, Oct. 2013.

[74] E. Rahimpour and M. Bigdeli, "Simplified transient model of transformer based on geometrical dimensions used in power network analysis and fault detection studies," in 2009 Int. Conf. Power Eng., Energy Electr. Drives, 2009, pp. 375–380.

[75] M. Popov, "General approach for accurate resonance analysis in transformer windings," Electr. Power Syst. Res., vol. 161, pp. 45–51, 2018.

[76] Y. Liu, S. A. Sebo, R. Caldecott, D. G. Kasten, and S. E. Wright, "Power transformer resonance—measurements and prediction," IEEE Trans. Power Del., vol. 7, no. 1, pp. 245–253, Jan. 1992.

[77] E. Mombello and K. Möller, "Impedances for the calculation of electromagnetic transient phenomena and resonance in transformer windings," Electr. Power Syst. Res., vol. 54, no. 2, pp. 131–138, 2000.

[78] S. Wei, "Analysis and study of resonance monitoring and suppression strategies of EHV main transformer," in 2016 3rd Int. Conf. Inf. Sci. Control Eng. (ICISCE), 2016.

[79] M. Popov, L. van der Sluis, G. C. Paap, and H. de Herdt, "Computation of very fast transient overvoltages in transformer windings," IEEE Trans. Power Del., vol. 18, no. 4, pp. 1268–1274, Oct. 2003.

[80] T. Abdulahović and T. Thiringer, "Voltage stress in a transformer winding during very fast transients caused by breaker closing event," IEEE Trans. Power Del., vol. 29, no. 4, pp. 1946–1954, Aug. 2014.

[81] Sriyono, U. Khayam, and Suwarno, "Evaluating the inter-resonance characteristics of various power transformer winding designs," IEEE Access, vol. 9, pp. 54649, 2021.

[82] R. K. Senobari, J. Sadeh, and H. Borsi, "Frequency response analysis (FRA) of transformers as a tool for fault detection and location: A review," Electr. Power Syst. Res., vol. 155, pp. 172–183, Feb. 2018.

[83] Sriyono, Suwarno, and U. Khayam, "Investigating the internal winding resonance characteristics of various power transformer winding designs," in 2020 Int. Symp. Electr. Insul. Mater. (ISEIM), 2020, pp. 541–544.

[84] B. Gustavsen, "Wide band modeling of power transformers," IEEE Trans. Power Del., vol. 19, no. 1, pp. 414–422, Jan. 2004.

[85] D. Filipović-Grčić, I. Ugljesic, V. Milardic, A. Xémard, and A. Guerrier, "High-frequency model of the power transformer based on frequency-response measurements," IEEE Trans. Power Del., vol. 30, no. 1, pp. 34–42, Feb. 2015.

[86] E. Al Murawwi, M. K. Abu-Siada, A. M. El-Metwally, and M. A. Eltamaly, "Effects of terminal connections on sweep frequency response analysis of transformers," IEEE Electr. Insul. Mag., vol. 28, no. 3, pp. 8–13, May–Jun. 2012.

[87] V. Nurmanova, M. Bagheri, A. Zollanvari, K. Aliakhmet, Y. Akhmetov, and G. B. Gharehpetian, "A new transformer FRA measurement technique to reach smart interpretation for inter-disk faults," IEEE Trans. Power Del., vol. 34, no. 4, pp. 1508–1519, Aug. 2019.

[88] M. Rädler, S. Uhrig, and J. L. Velásquez Contreras, "Electrical interferences in SFRA measurements: How to overcome undesirable effects," Transformers Magazine, vol. 4, no. 2, pp. 60–70, 2017.

[89] B. Gustavsen, "Removing insertion impedance effects from transformer admittance measurements," IEEE Trans. Power Del., vol. 27, no. 2, pp. 1027–1029, Apr. 2012.

[90] F. Grecki and B. Wunsch, "Validation of power transformer wideband modeling using standard sFRA method with VNA equipment," in 2019 IEEE PES Asia–Pacific Power Energy Eng. Conf. (APPEEC), 2019, pp. 1–5.

[91] D. Smugała, W. Piasecki, M. Ostrogórska, M. Florkowski, M. Fulczyk, and P. Kłys, "Distribution transformers protection against high frequency switching transients," Przegląd Elektrotechniczny (Electrical Review), vol. 88, no. 5a, pp. 297–300, 2012.

[92] M. A. Atefi, M. A. Khalafi, and M. A. Fadaeinedjad, "Preventing transformer energizing resonant overvoltages using surge arrester temperature rise index and controlled closing method," IEEE Transactions on Power Delivery, vol. 28, no. 2, Apr. 2013.

[93] Y. Zhang, Q. Yang, S. Xie, and C. Zhang, "Mechanism and application of arrester block voltage division to lightning transient voltage monitoring in substation transformers," IEEE Trans. Electromagn. Compat., vol. 61, no. 3, pp. 689–696, Jun. 2019.
[94] "High voltage surge arresters," [Online]. Available: https://library.e.abb.com
[95] "Insulation coordination study for lightning overvoltages in 420 kV power substation," [Online]. Available: https://electrical-engineering-portal.com/download-center/books-and-guides/power-substations/insulation-coordination-study
[96] "Surge protection of arc furnace transformers," Qual-Tech Engineers, Inc., [Online]. Available: https://www.qualtecheng.com
[97] "Surge suppressor capacitors VISHAY ESTA," [Online]. Available: https://www.vishay.com
[98] T. Dionise and S. Johnston, "Surge protection for ladle melt furnaces: LMF transformer terminals were equipped with primary surge protection consisting of surge arresters and RC snubbers," IEEE Ind. Appl. Mag., vol. 21, no. 5, pp. 43–52, Sep.–Oct. 2015.
[99] P. E. Sutherland and M. E. Valdes, "Snubber design for transformer protection," in 2014 IEEE Petroleum and Chemical Industry Tech. Conf. (PCIC), 2014, pp. 343–351.
[100] "High frequency transient surge suppressors ZORC," TRIKE TECHNOLOGIES, [Online]. Available: https://strike.co.za/surge-suppressors
[101] "Zinc Oxide RC-Surge Suppressor (ZORC) Capacitors, for HV-Motor and Transformers," [Online]. Available: https://www.vishay.com
[102] K. Munji, J. Horne, and J. Ribecca, "Design and validation of pre-insertion resistor rating for mitigation of zero missing phenomenon," in Proc. Int. Conf. Power Syst. Transients (IPST), Seoul, South Korea, Jun. 26–29, 2017, Paper No. 17IPST129.
[103] H. Heiermeier and R. B. Raysaha, "Power testing of preinsertion resistors: Limitations and solution," IEEE Trans. Power Del., vol. 32, no. 4, pp. 1688–1695, 2017.
[104] "Live tank circuit breakers 72.5–550 kV," GE Grid Solutions, [Online]. Available: https://www.gegridsolutions.com
[105] S. M. Korobeynikov, S. I. Krivosheev, S. G. Magazinov, V. A. Loman, and N. Ya, "High-frequency transients suppression at substation," in Proc. 2018 IEEE Int. Conf. High Voltage Eng. Appl. (ICHVE), 2018, pp. 1–4.
[106] S. M. Korobeynikov, S. I. Krivosheev, S. G. Magazinov, V. A. Loman, and N. Ya, "Suppression of incoming high-frequency overvoltage in transformer coils," IEEE Transactions on Power Delivery, vol. 36, no. 5, pp. 2988–2994, Oct. 2021.
[107] "Skin effect in composite and ferromagnetic wires," Nature, vol. 147, no. 719, pp. 719, 1941.
[108] W. Piasecki, G. Bywalec, M. Florkowski, M. Fulczyk, and J. Furgał, "New approach towards very fast transients suppression," in Proc. Int. Conf. Power Syst. Transients (IPST), Lyon, France, 2007.
[109] D. Smugała, W. Piasecki, M. Ostrogórska, M. Florkowski, M. Fulczyk, and O. Granhaug, "Very fast transient suppressing device," U.S. Patent US 8,929,048 B2, 2015.
[110] A. Heidary, K. Rouzbehi, H. Radmanesh, and J. Pou, "Voltage transformer ferroresonance: An inhibitor device," IEEE Transactions on Power Delivery, vol. 35, no. 6, pp. 2731–2733, Dec. 2020.

3

CHOKE PROTECTION FOR TRANSFORMER WINDINGS

3.1. Abstract

High electric field intensity in transformer windings, caused by transient signals, can lead to resonance and overvoltage issues. The increasing integration of renewable energy sources into power grids has resulted in more frequent transient events, raising the risk of transformer failure. Studying transformer behavior during transients is essential to prevent such failures and ensure reliable power system operation. This requires accurate models capable of simulating electromagnetic transients in transformer windings. Such models help identify harmful frequency ranges and evaluate suitable protection methods.

This chapter presents an analytical model of transformer windings, validated through experimental measurements. Using this model, the chapter investigates the performance of an R-L protection device, known as a choke, during transient events. The choke is designed to impose a series impedance comparable to that of the transformer winding at critical frequencies where voltage surges are most severe. This protection approach reduces high inter-turn voltages caused by transients while ensuring that the grid operates normally under standard conditions.

The chapter is organized as follows:

Section 3.2 defines the transformer overvoltage problem and outlines the protection device.

This chapter of the thesis is published in the article:

1. A. Heidary, B. Behdani, M. G. Niasar and M. Popov, "Transformer Resonance Analysis and Visualization Using Current Distribution Matrix," in IEEE Transactions on Power Delivery, doi: 10.1109/TPWRD.2026.3688104.
2. F. Nasirpour, A. Heidary, M. G. Niasar, A Lekić, M. Popov, “High-frequency transformer winding model with adequate protection”, Electric Power Systems Research,” vol. 223, 109637, 2023.

Section 3.3 addresses the high-frequency modelling of transformer winding
Section 3.4 defines the transformer winding admittance matrix
Section 3.5 presents transformer model verification
Section 3.6 outlines the experimental test procedure of the choke protection device.
Section 3.7 concludes the chapter.

3.2 AN OVERVIEW OF TRANSFORMER MODELING AND PROTECTION BY CHOKE

Transformers are among the most essential and critical components [1]. Any failure in them may result in long interruptions, costly repairs, and replacement, as well as severe injuries [2,3]. Being in continuous service for decades and exposed to different operating conditions, transformers face high risks during their lifetime. Obtaining data regarding the transformer insulation system and its internal behavior is crucial for the system operators. Furthermore, one of the main requirements of smart grids is high system reliability. In this regard, it is necessary to ensure power transformers' safe and reliable performance by using different protective schemes against the phenomena in the present power system [4]. The main reason for the deterioration of transformer lifetime and possible failures is their vulnerability to fast and very fast transients in the system [5]. During these events, high-frequency overvoltages may occur at transformer terminals, which may excite internal and external resonances in the power system. In such a case, the voltage at different points of the transformer winding can be several times of magnitude higher than that at the transformer terminals [6], which can adversely affect the transformer insulation and may lead to failure. In the last decade, several solutions to suppress fast transients and protect transformers against resonances have been proposed [7-10]. The most common method is to use a surge arrester [10]. However, other solutions are to connect the series R-L component as a composite wire to the transformer or to utilize a parallel R-L component in series with the transformer. More about these solutions can be found in [7-9].

This chapter evaluates the effectiveness of a protection scheme against transient events while gaining insight into transformer behavior. To accomplish this, a detailed transformer winding model is developed for a broad frequency range [10], enabling the identification of resonance and anti-resonance frequencies, as well as voltage amplification in the winding. Subsequently, by using this model, safety criteria for the winding are established. The R-L protection device parameters are also adjusted, and its effects in suppressing resonance overvoltage are studied.

High-Frequency Modeling of Transformer Windings

In general, transformers are modeled based on three methods known as black box, white box, and grey box models [11].

- Black box models represent the behavior of transformers at their terminals and are used in cases where the interaction of the transformer with other parts of the grid is of concern. These models do not provide any more detailed information concerning the resonance phenomena occurring in them [12].
- White box models can be built based on the basic circuit elements, the values of which are dependent only on transformer geometry and materials used for transformer production. Using these models, it is possible to obtain voltage and current values at different nodes, and as such, they are suitable for transient studies.
- The gray box modeling approach is a trade-off between white and black box modeling schemes. This means that gray box models may also enable us to study transient phenomena in transformer winding with sufficient detail. However, unlike white box models, model parameters are obtained based on measurement [13].

In this chapter, the white-box modeling approach is adopted. To implement this method, the windings are subdivided into smaller segments, referred to as winding sections. Each section is then represented using circuit elements.

Fig. 3.1 illustrates the overall structure of a reactor, followed by a detailed representation of the winding referring to just the high voltage winding of a transformer, which consists of disks numbered from 1 to m. To develop the winding model, each disk is treated as an individual winding section and is modeled accordingly, as shown in Fig. 3.2.

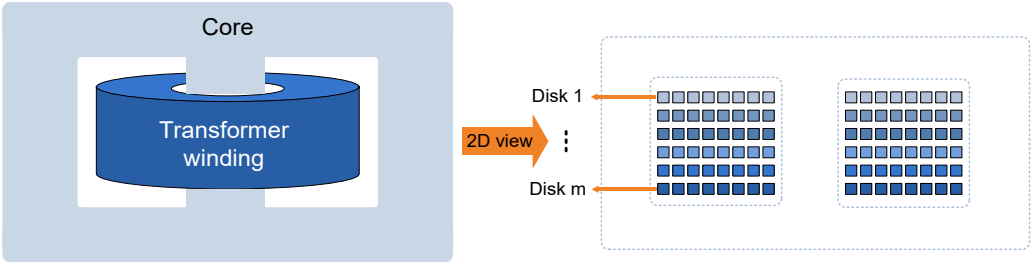


Fig. 3.1. A schematic representation of a transformer winding and a single-wound winding

The circuit model of a single-phase winding section includes the disk inductance, the disk conductor resistance, the disk shunt capacitance, the disk equivalent shunt resistance, as well as the capacitance and resistance to ground associated with each disk. In Fig. 3.2, R_1-R_m are the resistances of each disk, and L_1-L_m refers to the inductances of each disk from disk 1 to disk m. $M_{1\text{-}n}$ shows the mutual inductance

between the first disk and the other disks. C_1-C_m and R_{d1}-R_{dm} are the capacitance associated with each disk and its equivalent parallel resistance. Finally, C_{h1}-C_{hm} and R_{h1}-$R_{h2}$are the capacitance to ground and its equivalent resistance for disk 1 to m.

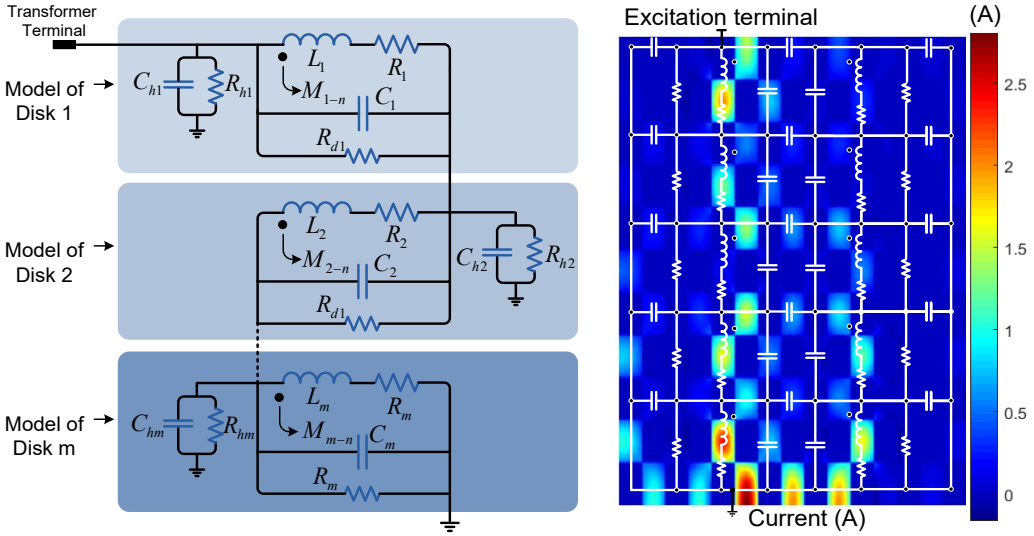


Fig. 3.2. Detailed model of a winding.

Based on the accurate modeling of the transformer winding, the extracted disk model can show the current distribution of the transformer's resonance frequency as an example provided in Figure 3.2 (b), where this overcurrent, causing serious overvoltage, should be protected for transformer safe operation.

The studied single-phase test winding is shown in Fig. 3.3. This winding is a part of a transformer winding typically used for the rated voltage of 345 kV; the winding parameters are presented in Table 3.1.



Fig. 3.3. Laboratory test-winding structure

Table 3.1. Test-winding parameters

Parameter	Value
Number of Disks	22
Number of turns per disk	40
Conductor dimensions	1.8 mm × 8 mm
Conductor insulated dimensions	3.11 mm × 9.31 mm
Radial build	125.5 mm
Inner diameter	750 mm
Outer diameter	1001 mm
Vertical distance between disks	4 mm

Calculation of winding inductances:

As shown in Fig. 3.4, the mutual inductance between the coils can be determined by solving Maxwell's equations or using the vector potential method [14]. It is given by the following expression [14]:

$$M_{12} = \frac{2\mu_0\sqrt{r_1 r_2}}{\sqrt{k'}}\left(K(k') - E(k')\right) \tag{3-1}$$

Where

$$k' = \frac{1-\sqrt{1-k^2}}{1+\sqrt{1-k^2}} \tag{3-2}$$

$$k = \sqrt{\frac{4r_1 r_2}{\sqrt{(r_1+r_2)^2 + d^2}}} \tag{3-3}$$

Here, r_1 and r_2 represent the mean radii of the turns, μ_0 is the permeability of free space, d denotes the vertical distance between the turns, and K and E are the complete elliptic integrals of the first and second kind, respectively.

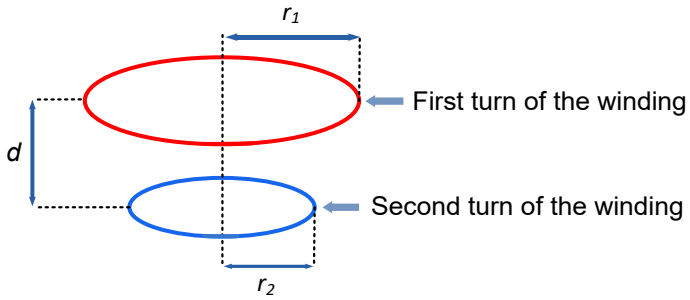


Fig. 3.4. Geometry of two parallel coils

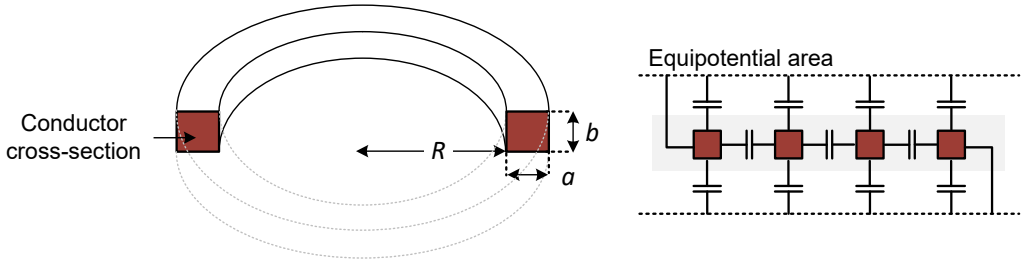
The self-inductance of the turn, as shown in Fig. 3.4, can be determined by treating it as the mutual inductance between two identical turns separated by a vertical distance equal to the geometrical mean distance known as *GMD*, defined in (3-4) as follows:

$$GMD = 0.2235(a+b) \tag{3-4}$$

where *a* and *b* are the width and the height of the coil, as shown in Fig. 3.5.

Winding capacitances calculation:

The capacitance of each disk can be determined using the energy method. Fig. 3.5 (a) and (b) illustrate a high-voltage disk without wound-in shields and the equipotential surfaces between the disks. The capacitance associated with this disk is given by the Stein expression [15]-[16]:



(a) (b)

Fig. 3.5. Geometry of a turn and a winding disk

$$C_h = C_s\left(\left(\frac{\alpha}{2\tanh(\alpha)}\right)+\left(\frac{\alpha}{2\sinh(\alpha)}\right)+\left(\frac{\alpha^2}{4}\right)\right) \tag{3-5}$$

$$C_s = \frac{C_{tt}(N_t-1)}{N_t^2} \tag{3-6}$$

$$\alpha = \sqrt{\frac{4C_{dd}}{C_s}} \tag{3-7}$$

In equations (3-5) to (3-7), C_{tt} and C_{dd} represent the capacitance between two adjacent turns within a disk and the total capacitance between two adjacent disks, respectively. Here, N_t denotes the number of turns in each disk. The values of C_{tt}, and C_{dd} can be determined using equations (3-8) and (3-9):

$$C_{tt} = \frac{\varepsilon_0 \varepsilon_p 2\pi R_{ave}(h + 2\tau_p)}{\tau_p} \tag{3-8}$$

$$C_{dd} = \frac{\varepsilon_0 \pi (R_{out}{}^2 - R_{in}{}^2)}{\left(\frac{\tau_p}{\varepsilon_p} + \tau_a\right)} \tag{3-9}$$

R_{ave}, R_{out}, and R_{in} denote the disks' mean, outer, and inner radii, respectively. h represents the height of the conductor without insulation, while ε_p and ε_0 correspond to the relative permittivity of paper and the permittivity of vacuum, respectively. Additionally, τ_p refers to the double one-sided insulation of the conductor, and τ_a denotes the distance between the disks.

Calculation of winding resistances:

The resistances used in the model represent the conductor's resistances as well as the losses in the insulation. Due to the skin and proximity effects, calculating the AC resistance of the conductors is highly complex, as it requires determining the magnetic flux in the conductors within a complex geometry. Therefore, only the DC resistance of the conductors is considered here.

The relationship between the dissipation factor and frequency for oil-impregnated paper is given by [17]. and is expressed as:

$$\tan\delta = 1.082 \times 10^{-8}\omega + 5 \times 10^{-3} \tag{3-10}$$

Although the paper in this case is not impregnated with oil, expression (3-10) can still be used as a rough estimate for the dissipation factor, as the behavior of the paper in both cases is not expected to differ significantly. As mentioned earlier, due to the high moisture content in the test case, the paper exhibits a higher level of power loss in its dielectric. To account for this effect in the model, expression (3-10) has been modified as follows:

$$\tan\delta = 1.082 \times 10^{-8}\omega + 70 \times 10^{-3} \tag{3-11}$$

Considering the dissipation factor, the equivalent resistance that represents the dielectric losses can be calculated using equation (3-12):

$$R_d = \frac{1}{\tan\delta C_h \omega} \tag{3-12}$$

Here, C_h is the capacitance computed in (3-5), and ω is the angular frequency.

3.3. TRANSFORMER ADMITTANCE MATRIX

Once the values of the elements are known, the admittance matrix of the transformer winding can be constructed. First, the capacitance, resistance, and inductance matrices are calculated, and then the admittance matrix is formed. The procedure for constructing these matrices is outlined below.

Capacitance and dielectric resistance matrices:

The capacitance matrix is a nodal matrix. Since the studied case involves 22 disks, with each disk considered as one section, there are a total of 23 nodes. The diagonal element of the matrix, C_{ii}, represents the sum of all capacitances connected to node *iii*. The off-diagonal element, C_{ij}, represents the capacitance between nodes *i* and *j*, with a negative sign. A similar procedure is applied to construct the dielectric resistance matrix.

Inductance and conductor resistance matrices:

The inductance matrix is a branch matrix. Given the number of sections, the size of the inductance matrix will be 22×22. The diagonal elements of this matrix, L_{ii}, represent the self-inductance of section *i*, while the off-diagonal elements, L_{ij}, represent the mutual inductance between sections *i* and *j*. The conductor resistance matrix is constructed on the same basis, but since mutual resistances are not considered in this study, the off-diagonal elements are set to zero.

Admittance matrix:

The admittance matrix of the transformer can be obtained using (3-13) and (3-14):

$$Y = \Gamma + j\omega C + \frac{1}{R_d} \tag{3-13}$$

$$\Gamma = k(R_d + j\omega L)^{-1} k^T \tag{3-14}$$

Here, C, L, R_d, R_c, and k are the capacitance, inductance, dielectric resistance, conductor resistance, and incidence matrices, respectively, and T denotes matrix transposition. By inverting the admittance matrix, the impedance matrix can be obtained by (3-15):

$$Z = Y^{-1} \tag{3-15}$$

3.4 VERIFICATION OF THE STUDIED WINDING MODEL

The diagonal elements of the impedance matrix, Z_{ii}, represent the impedance seen from node i. To validate the model, the response of the winding for different configurations is measured using the Omicron VNA Bode 100 device, which is capable of determining the sweep frequency characteristics. Fig. 3.6 compares Z_{11}, the harmonic terminal impedance of the winding, obtained from both the analytical model and the measurements.

As shown, there is good agreement between the response from the model and the measured data. The difference in the high-frequency range is attributed to the stray capacitances arising from the connections and cables.

Using equation (3-15), the voltage at node j when node i is excited can be computed using equation (3-16), assuming the end-winding terminal is grounded.

$$V_i = \frac{Z(i,j)}{Z(i,i)} V_i \tag{3-16}$$

Two main outcomes are considered in developing a protection device (choke configuration) based on the modeling method of the studied transformer winding and experimental measurement. The first result, which is illustrated in Fig. 3.6, is the impedance frequency response of the winding terminal. This illustration plots the calculation and experimental test results together, confirming a close match. This plot highlights the overall impedance of the transformer winding in the frequency range between 100 Hz and 1 MHz and points out the resonance frequencies.

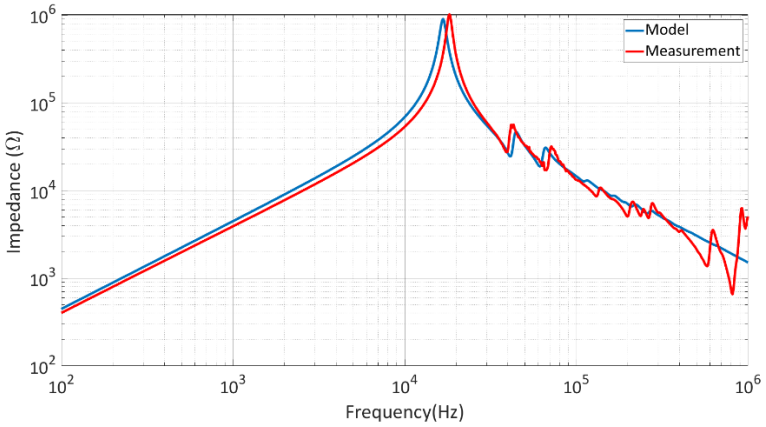


Fig. 3.6. Terminal impedance of the test winding.

Regarding calculating the winding model at the resonance frequency of 37.8 kHz, the voltage between disk 13 and the ground rises to 1.8 p.u where the terminal excited voltage is considered as 1 p.u., due to the external resonance occurrences. This data is illustrated in Fig. 3.7.

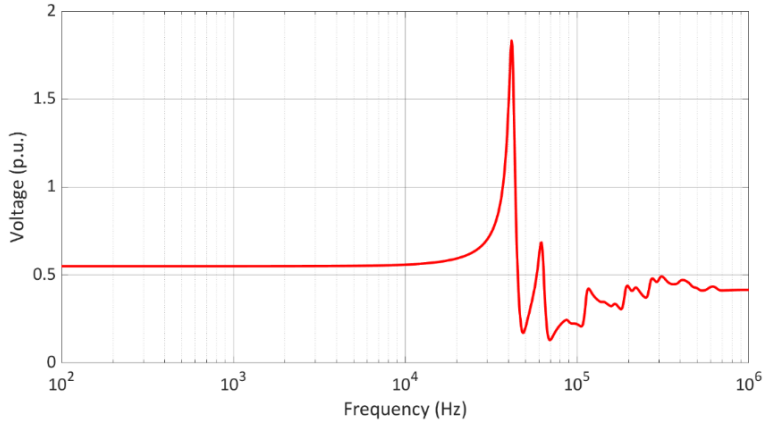


Fig. 3.7. The voltage between disk 13 and ground

As it is obtained from the calculation of the transformer winding model, the resonance frequency around 37-40 kHz is a critical resonance of the studied winding, which causes serious overvoltage on internal disk 13 and might cause insulation failure within the transient phenomena. Therefore, in the next step, the considered frequency for protection device design is 38 kHz. The next step is to suppress the frequency content around this critical frequency by a series suppressor known as a choke.

3.5 PERFORMANCE EVALUATION OF AN R-L PROTECTION CIRCUIT (KNOWN AS A CHOKE)

In this section, an R-L protection device against transients, known as a choke, is developed to suppress the overvoltage occurring in the winding in case of resonance. When high-frequency transients occur, the voltage drop on the choke increases to protect the winding from the resonance overvoltages. Using the data provided by the model of the studied winding, the parameters of the protection device can be adjusted. Here, the critical considerations for the design of the choke are the resonance voltage of the winding, besides its impedance. By applying a suitable series impedance with the transformer, the voltage of the winding at the resonance point will be limited to an acceptable magnitude. This approach is illustrated in Fig. 3.8.

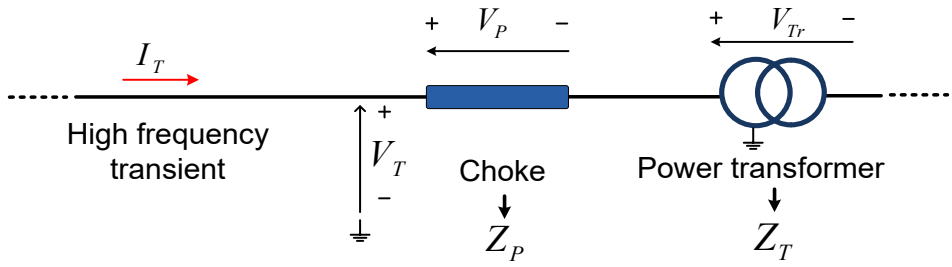


Fig. 3.8. The connection of the choke with the transformer within a network segment

By taking Fig. 8 into account, the expressed conditions in (3-17) to (3-19) are considered when designing the choke, where the protection device is adjusted for the most critical frequency point obtained by the model.

$$V_{Tr} \leq V_{safe} \tag{3-17}$$

$$V_{Tr} = \frac{V_{T(38kHz)}.Z_T}{Z_T + Z_P} \tag{3-18}$$

$$\frac{V_{T(38kHz)}.Z_T}{Z_T + Z_P} \leq V_{safe} \tag{3-19}$$

Here, V_T is the magnitude of the frequency component of the transient voltage, which results in the highest overvoltage on disk 13 of the transformer winding, V_{Tr} is the maximum amplified voltage in the transformer winding, and V_{safe} is the safe operating voltage of the transformer, considering the isolation restriction that should be achieved. Z_T and Z_P are the impedances of the transformer winding and choke at the

resonance frequency, respectively. Therefore, the impedance of the choke in resonance frequency can be adjusted in equation (3-20) as follows:

$$\left(\frac{V_{T(38kHz)}.Z_T}{V_{safe}}\right)-Z_T \le Z_p \qquad (3\text{-}20)$$

Using equation (3-20), the minimum impedance required to be imposed by the choke can be calculated. The structure of the choke is shown in Fig. 3.9, which consists of a ferromagnetic core placed around the transmission line, along with a resistance in its secondary.

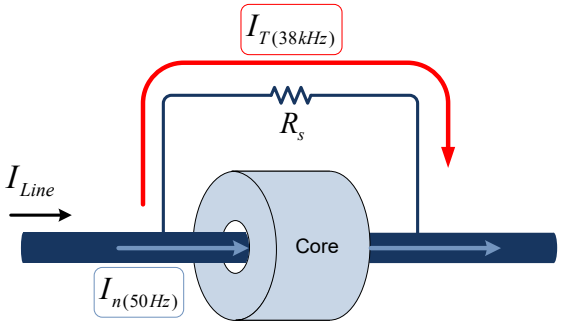


Fig. 3.9. Structure of the designed choke

The purpose of adding a parallel resistance R_s to the protection circuit is to conduct the transient current's high-frequency contents and dissipate the transient signal's energy in the resistive branch. In such a case, the impedance of the inductive branch is much higher, which means it only conducts a small part of the high-frequency current. In contrast, the line current I_{line} is conducted through the inductive branch in the normal condition.

In the laboratory setup, V_{safe} is considered to be 1 p.u. (voltage of insulation part for safe operation). To simulate the higher voltage originated from transient signals, the magnitude of the high-frequency voltage source is adjusted to be 1.5 p.u. It should be noted that this value is considered only for the sake of an explanation of the methodology. The voltage of the transformer winding with and without connecting the choke is examined by implementing the setup as shown schematically in Fig. 3.10 and experimentally in Fig. 3.11 (a). By applying the values of transient voltage and impedance of the transformer winding at the resonance frequency in expression (3-21), choke impedance is calculated as follows:

$$Z_{P(38kHz)} \ge 6\times10^{3}\Omega$$

This impedance is designed basically using equation (3-22).

$$Z_{P(38kHz)} = \frac{R_s.Z_{in}}{R_s + Z_{in}} \geq 6\times10^3$$

Here R_s is the parallel resistor, and Z_{in} is the impedance of the inductive branch. In the first step of the test, the winding is excited by a sinusoidal signal with a frequency of 37.8 kHz, which is the measured critical frequency of the winding. Fig. 3.11 (b) shows the voltage of disk 13 to ground without a choke (considering that the bypass switch is ON). In this case, it is observable that the voltage of disk 13 of winding to ground is 1.8 times higher than the voltage at the terminal and is 3 times higher than the assumed safe voltage, which is calculated by 13 divided by the total number of disks (total number of disks is 22).

Fig. 3.11 (c) shows the same signals by using the choke, where the magnitude of disk 13 is limited to the safe voltage of 1 p.u.. This operation proves the effective protection of the winding against transient resonance. The data of the implemented laboratory setup and measured values are presented in Table 3.2.

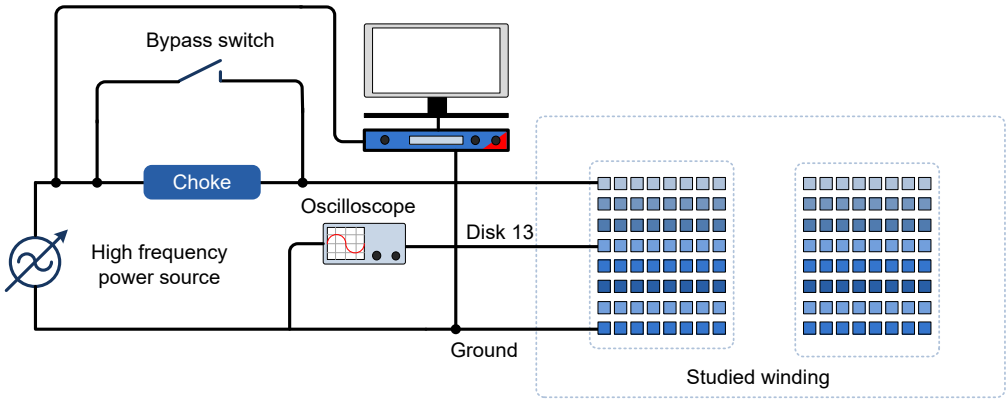
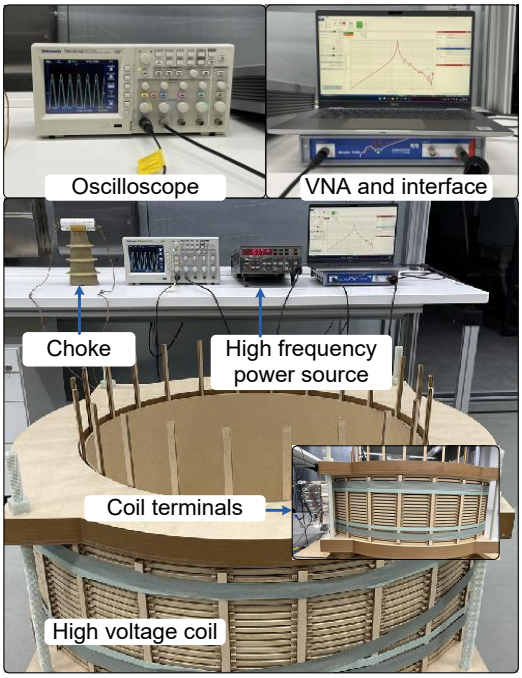
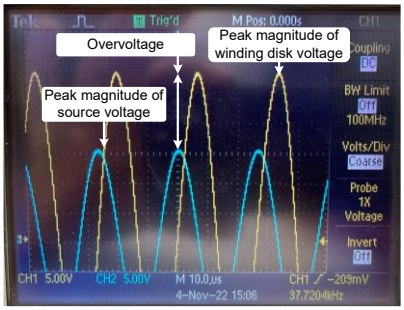


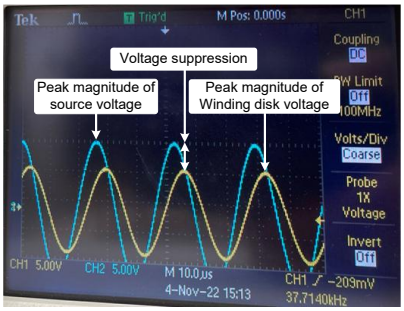
Fig. 3.10. Laboratory setup diagram.



(a)



(b)



(c)

Fig. 3.11 (a) The implemented laboratory setup, b) The voltage at disk 13 without the choke, and c) The voltage at disk 13 with the choke

Table 3.2. Laboratory setup and measurement data

Laboratory equipment data	Detail
High-frequency source	50 Hz - 1 MHz, 0-25V, 50 W
Oscilloscope	Laboratory oscilloscope TDS2014B
impedance analyzer, VNA	Frequency sweep Omicron Bode100
Protection device impedance (50 Hz)	Z=100 mΩ
Protection device impedance (resonance frequency)	Z=10 kΩ
Peak voltage without protection	1.8 p.u
Peak voltage with protection	0.6 p.u

3.6. Conclusion

This chapter presents an analytical model for transformer windings to study their behavior during transient events, particularly focusing on the impact of high-frequency transients and resonance. It is demonstrated that transient overvoltages, which occur at specific resonance frequencies, can significantly damage transformer windings, leading to insulation failure. The critical resonance frequency range is

identified, and its impact on voltage amplification within the transformer winding is analysed using a detailed winding model.

An R-L protection device, known as a choke, was explored to address these challenges as an effective solution for suppressing resonance-induced overvoltages. The choke was designed to match the impedance of the transformer winding at critical frequencies, reducing voltage surges while allowing the system to operate normally under standard conditions. Simulations and experimental validations confirmed the choke's effectiveness in protecting transformer windings during transient events, especially at the critical resonance frequency of around 37-40 kHz.

This chapter of the thesis highlights the importance of accurate transformer modeling and the role of protection schemes in enhancing the reliability and lifespan of power transformers in modern power grids, where the increasing integration of renewable energy sources leads to more frequent transient disturbances. The next chapters explore further improvement of the choke design and investigate additional protective methods for different transformer configurations and operating conditions.

References

[1] Abu-Siada and S. Islam, "A novel online technique to detect power transformer winding faults," IEEE Trans. Power Del., vol. 27, no. 2, pp. 849–857, 2012.

[2] V. Nurmanova, M. Bagheri, A. Zollanvari, K. Aliakhmet, Y. Akhmetov, and G. B. Gharehpetian, "A new transformer FRA measurement technique to reach smart interpretation for inter-disk faults," IEEE Trans. Power Del., vol. 34, no. 4, pp. 1508–1519, 2019.

[3] J. Chong and A. Abu-Siada, "A novel algorithm to detect internal transformer faults," in 2011 IEEE Power Energy Soc. Gen. Meeting, 2011, pp. 1–5.

[4] M. Bagheri, M. S. Naderi, T. Blackburn, and T. Phung, "Practical challenges in online transformer winding deformation diagnostics," in 2011 2nd Int. Conf. Electric Power Energy Conversion Syst. (EPECS), 2011, pp. 1–6.

[5] S. H. Hosseini, M. Vakilian, and G. B. Gharehpetian, "Comparison of transformer detailed models for fast and very fast transient studies," IEEE Trans. Power Del., vol. 23, no. 2, pp. 733–741, 2008.

[6] M. Popov, "General approach for accurate resonance analysis in transformer windings," Electric Power Syst. Res., vol. 161, pp. 45–51, 2018.

[7] D. Smugała, W. Piasecki, G. Bywalec, M. Ostrogorska, O. Granhaug, and P. Skryten, "Very fast transient suppressing device," U.S. Patent US 8,929,048 B2, 2015.

[8] W. Piasecki, G. Bywalec, M. Florkowski, M. Fulczyk, and J. Furgal, "New approach towards very fast transients suppression," in Proc. IPST, 2007.

[9] D. Smugała, W. Piasecki, M. Ostrogórska, M. Florkowski, M. Fulczyk, and O. Granhaug, "New approach to protecting transformers against high frequency transients–wind turbine case study," Prz. Elektrotech., vol. 89, pp. 186–190, 2013.

[10] Y. Zhang, Q. Yang, S. Xie, and C. Zhang, "Mechanism and application of arrester block voltage division to lightning transient voltage monitoring in substation transformers," IEEE Trans. Electromagn. Compat., vol. 61, no. 3, pp. 689–696, 2019.

[11] M. García-Gracia, M. Villén, M. Cova, and N. El Halabi, "Detailed three-phase circuit model for power transformers over wide frequency range based on design parameters," Electric Power Syst. Res., vol. 92, pp. 115–122, 2012.

[12] T. A. Papadopoulos, A. I. Chrysochos, A. I. Nousdilis, and G. K. Papagiannis, "Simplified measurement-based black-box modeling of distribution transformers using transfer functions," Electric Power Syst. Res., vol. 121, pp. 77–88, 2015.

[13] R. Aghmasheh, V. Rashtchi, and E. Rahimpour, "Gray box modeling of power transformer windings for transient studies," IEEE Trans. Power Del., vol. 32, no. 5, pp. 2350–2359, 2017.

[14] E. Rahimpour, J. Christian, K. Feser, and H. Mohseni, "Transfer function method to diagnose axial displacement and radial deformation of transformer windings," IEEE Trans. Power Del., vol. 18, no. 2, pp. 493–505, 2003.

[15] R. M. Del Vecchio, B. Poulin, P. T. Feghali, D. M. Shah, and R. Ahuja, Transformer design principles. CRC Press, 2017.

[16] M. G. Niasar and W. Zhao, "Impulse voltage distribution on disk winding: calculation of disk series capacitance using analytical method," in 2020 IEEE Int. Conf. High Voltage Eng. Appl. (ICHVE), 2020, pp. 1–4.

[17] E. Rahimpour, Hochfrequente Modellierung von Transformatoren zur Berechnung der Übertragungsfunktion [High Frequency Modeling of Transformers using the Transfer Function], Ph.D. dissertation, Univ. of Stuttgart, 2001.

4

TRANSFORMER PROTECTION USING A PARALLEL AIR-CORE REACTOR AND A RESISTOR

4.1. Abstract

Integrating renewable energy resources like wind farms is a growing trend in modern power grids. However, wind generator towers are consistently at risk of lightning strikes, which can damage transformers by allowing lightning transients to travel through the system. The various harmonic components of these transients can excite the transformer's resonance frequencies, leading to both terminal and internal OVs.

To protect transformers from resonance OVs, it is essential to first identify their resonance points. Once these points are known, a protective method can be applied to reduce the harmonic content that contributes to resonance.

This chapter introduces a series-protection device that combines an air-core reactor with suppressor resistance to safeguard transformers. The goal is to offer a solution that protects wind farm transformers from terminal and internal resonance OVs caused by lightning transients. The device's effectiveness is evaluated through analysis, simulation, and experiments conducted in a high-voltage laboratory setting.

The chapter is organized as follows:

This chapter of the thesis is published in the following articles:

1. A. Heidary, M. Ghaffarian Niasar, M. Popov, "Wind farm transformer protection against lightning transients using air core reactor and resistor," Electric Power Systems Research, vol. 249, 2025.
2. A. Heidary, M. Ghaffarian Niasar, M. Popov, "Series Magnetic Coupled Reactor Saturation Considerations for High Voltage AC and DC Power Systems, "International Journal of Electrical Power & Energy Systems, vol. 158, 2024.

Section 4.2 defines the problem and outlines the specifications of the protection device.
Section 4.3 addresses the issue of series reactor core saturation
Section 4.4 introduces a protection model for the transformer.
Section 4.5 examines the effects of the protection device.
Section 4.6 details the experimental test procedure.
Section 4.7 provides a comparison study of the obtained results
Section 4.8 concludes the chapter

4.2. AN OVERVIEW OF THE TRANSFORMER PROTECTION AGAINST TRANSIENT PHENOMENA

Addressing global warming requires major changes in the energy sector, especially through the energy transition [1]. This means shifting from traditional fuel-based power plants to RESs to help solve environmental problems [2]. Wind turbine energy generators are an important part of this transition, as they can provide a large share of the energy needed by industries [3].

However, using wind turbine energy generators increases the risk of lightning strikes because of their tall towers and sharp edges [4]. A lightning strike can damage parts of the power system, such as wind generator insulation, converters, cables, and transformers [5]. Lightning-induced OVs can spread high-frequency currents through the power system [6]. These high voltages and frequencies affect transformers and can trigger resonance frequencies within them [7]. This leads to terminal and internal OVs in transformers, which may cause failures [8]. Therefore, wind farm transformers face a higher risk of resonance OVs and need proper protection against transient signals [9].

Several devices have been suggested to protect transformers from transient components caused by lightning and switching events [10]. The most common is the surge arrester, which is connected directly to transformer terminals to reduce OVs and lower their magnitude [11]. However, surge arresters only protect against terminal OVs, allowing high-frequency transients to pass through and possibly leaving internal resonance OVs unchecked [12]. Other devices include surge capacitors, R-C snubbers, and zinc-oxide snubbers, which use shunt capacitor filters [13]. These solutions, however, face design challenges for transmission voltage levels above 30 kV [14].

Additionally, there are series-connected inductive components [15], such as FDDs and chokes, which also act as protection devices [16]. FDDs usually consist of a coil with a specialized ferromagnetic layer [17], while chokes have a toroidal

ferromagnetic ring core with a resistor in the secondary circuit [18][19]. However, both methods face the challenge of avoiding saturation of the ferromagnetic material [20].

This chapter introduces a new method using a parallel air-core inductor and resistor (PAIR) connected in series with the wind farm transformer. The operation of this protection device is thoroughly analyzed, and the results are validated through EMTP and FEM simulations, followed by tests conducted in a high-voltage laboratory. The analysis shows that the proposed device effectively reduces harmonic components that could cause resonance in lightning transient signals, without the risk of saturation.

4.3. ADDRESSING THE PROBLEM OF SERIES REACTOR SATURATION

SRs are protection devices that add series impedance during fault conditions [21] to limit fault current or overvoltage [22] and protect sensitive power system equipment [23]. Series current-limiting reactors have been widely studied for protecting AC power systems [24] and DC power systems [25] against fault current and transient phenomena. Their role in restoring the point of common coupling voltage in the power grid has also been investigated [26]. To provide effective series impedance, SRs must avoid saturation [27].

In many recent studies on magnetic core series reactors (SRs) used as current limiters or transient suppressors, the critical issue of core saturation during fault conditions has not been adequately addressed [28].

This section of the thesis focuses on identifying two key coefficients that ensure the SR operates outside the saturation region. These coefficients are calculated for various voltage levels. Finally, the inductance of the SR, considering these coefficients, is analyzed through MATLAB Simulink simulations.

To evaluated saturation possibility of SR a worst scenario for overcurrent is considered which can be low impedance short circuit which is presented in Fig. 4.1. The analytical study is conducted for a single-line power system in which a line-to-ground fault occurs as scenario which causes overcurrent, as illustrated in Fig. 4.1. In this system, V_{th} is the Thevenin RMS voltage, I_f is the highest over current, $R_{th,}$ and L_{th} are the Thevenin resistance and inductance computed for the observed system. L_{SR} is the inductance of the SR, R_f is the fault resistance, and ω is the grid frequency.

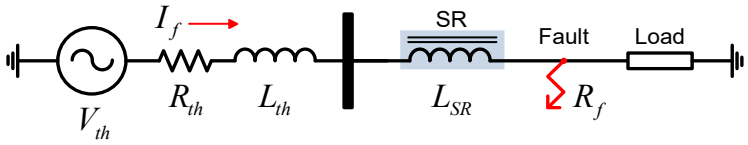


Fig. 4.1. Worst-case SR overcurrent in a power system

Considering that SR saturation is mostly possible for low-impedance faults or transient overcurrents, the analysis is conducted for the highest possible fault current. The steady-state analysis is employed to extract the faulty system coefficients and SR considerations as follows:

$$Z_f = (R_{th} + R_f) + j\omega\left(L_{th} + L_{SR}\right) \tag{4-1}$$

By applying the following assumptions:

$$\omega\left(L_{th} + L_{SR}\right) >> R_{th} + R_f,\ L_{SR} >> L_{th}$$

The faulty system impedance in Fig. 1 is expressed as:

$$\left|Z_f\right| = \omega L_{SR} \tag{4-3}$$

Consequently, the fault current is calculated as:

$$I_f = \frac{V_{th}}{\omega L_{SR}} \tag{4-4}$$

Considering the magnetic flux of SR φ_{SR} in Fig. 4.2, the linking flux equation is written as in (6) by assuming (5).

$$\varphi_{SR} = \varphi_m\ ,\ \varphi_m >> \varphi_l \tag{4-5}$$

$$\varphi_{SR} = \frac{L_{SR}.I_f}{N_{SR}} \tag{4-6}$$

Equation (4-6) states that the value of the magnetic flux φ_m (series reactor main linking flux φ_{SR}) is much higher than that of the leakage flux φ_l. By applying (4) to (6), the following can be derived:

$$\varphi_{SR} = \frac{V_{th}}{\omega}.\frac{1}{N_{SR}} \tag{4-7}$$

$$B_{SR} = \frac{\left(V_{th}/\omega\right)}{\left(N_{SR}.A_{SR}\right)} \tag{4-8}$$

Here N_{SR} and A_{SR} are the number of winding turns and the SR core cross-section, respectively. Furthermore, B_{SR} introduces its magnetic flux density.

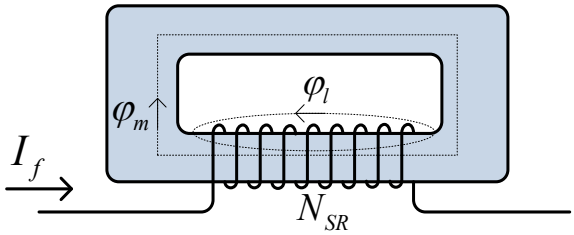


Fig. 4.2. Magnetic flux of the SR

There are two coefficients in (4-8). One of them is G_c, as shown in (4-9), which introduces the coefficient depending on the grid specifications and is called a grid coefficient, and SR coefficient R_c, which we denote as the reactor coefficient expressed by (4-10).

$$G_c = \frac{V_{th}}{\omega} \tag{4-9}$$

$$R_c = N_{SR}.A_{SR} \tag{4-10}$$

Fig. 4.3 depicts an illustration of a B-I characteristic for an SR. Magnetic flux density should be selected before the nonlinear and saturation region is reached, and based on that, the R_c coefficient of SR can be determined (the selected flux density can be varied based on the physics of the SR core). At the same time, the grid coefficient depends on system voltage and angular frequency.

Therefore, boundary equations (11) and (12) can be used to calculate the coefficients for different grids.

$$B_{SR} = \frac{G_c}{R_c} \leq 1.4T \tag{4-11}$$

$$R_c \geq \frac{G_c}{1.4} \tag{4-12}$$

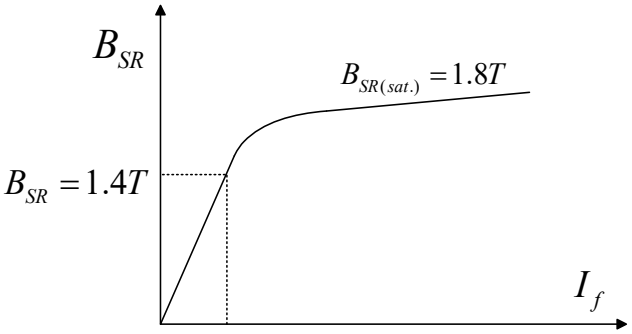


Fig. 4.3. Magnetic flux of the SR with a selected example of the magnetic flux density

Considering the grid and SR coefficient, an AC SR can be designed outside of the saturation region to protect the AC system. The simulation results for core-integrated SR are presented in Fig. 4.4, showing the turns-core cross-section curve for different grid coefficients. If the design of SR takes place above the curve, the saturation in all conditions will be avoided, unless saturation is possible, considering the fault current magnitude.

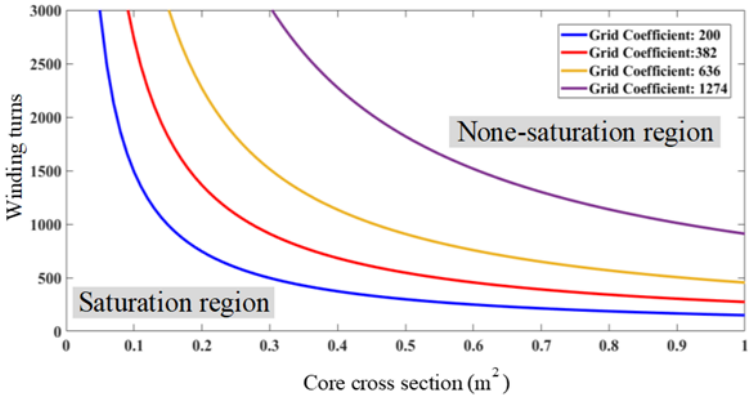


Fig. 4.4. Saturation region of the SR based on the grid coefficient

To conclude this section, saturation for SR as a transient limiter is possible, which can reduce its performance in many cases. Therefore, the following section 4.4 is conducted to evaluate a core-less air core reactor for transient phenomena suppression.

4.4. HIGH-FREQUENCY MODEL OF TRANSFORMER WINDING

The diagram in Fig. 4.5 shows the system under study, which includes a wind energy generator, a cable, a circuit breaker, a series-protection PAIR device, and a transformer. When lightning strikes the wind turbine, the transient signal travels through the generator and enters the power cable. As the electromagnetic wave moves along the cable, it reaches the cable termination, passes through the circuit breaker, and finally arrives at the transformer. This transient signal has two main features: a high magnitude and a wide range of harmonic content. These characteristics make it easy for the transient signal to cause resonance OVs in the transformer, either between the winding disks or at the transformer terminals.

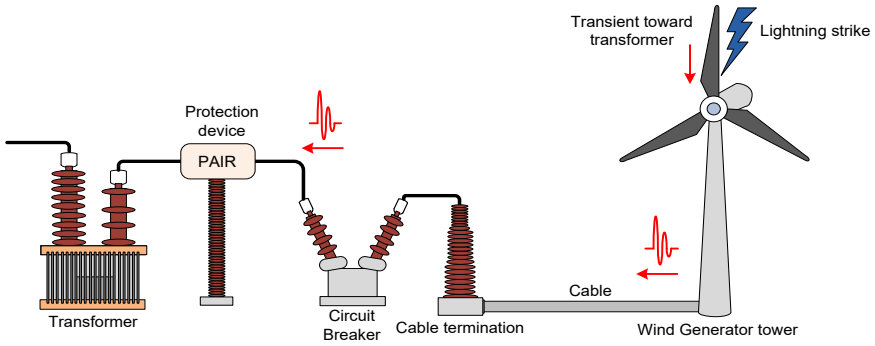


Fig. 4.5. An illustration of the studied power system

To simplify the power system illustrated in Fig. 4.5, the section from the wind generator to the circuit breaker can be replaced with an equivalent circuit. This part of the system is considered the source of transient signals that can excite resonances from the perspective of both the transformer and the protective device. The simplified electrical system is shown in Fig. 4.6 (a). The equivalent circuit consists of a current source representing the lightning (i_l) and an RLC equivalent impedance (Z_{eq}).

Additionally, Fig. 4.6 (b) shows the protection PAIR device. This device consists of an air-core inductor and a parallel resistor connected in series with the transformer. It is isolated from the ground and mounted on an isolation stand. The PAIR device works by reducing the magnitude of high-frequency components of the transient signal through the resistive branch. As a result, the PAIR device operates in two modes: at system frequency and above system frequency.

The PAIR device is modeled as a small inductive impedance in parallel with a relatively large resistor in the system. This design allows power frequency current components to flow mainly through the air-core inductor, which causes minimal voltage drop and power loss in that branch. This operation is shown in Fig. 6 (c).

$$V_p = I_s\left(R_p + j\omega L_p\right) \tag{4-13}$$

$$P_{loss} = \frac{(I_s.j\omega L_p)^2}{R_p} \tag{4-14}$$

Equation (13) defines the PAIR voltage drop V_p during normal operations, depending on the line current I_s and the air-core impedance (R_p+ωL_p). Equation (14) defines the corresponding small power loss P_{loss} during normal operations.

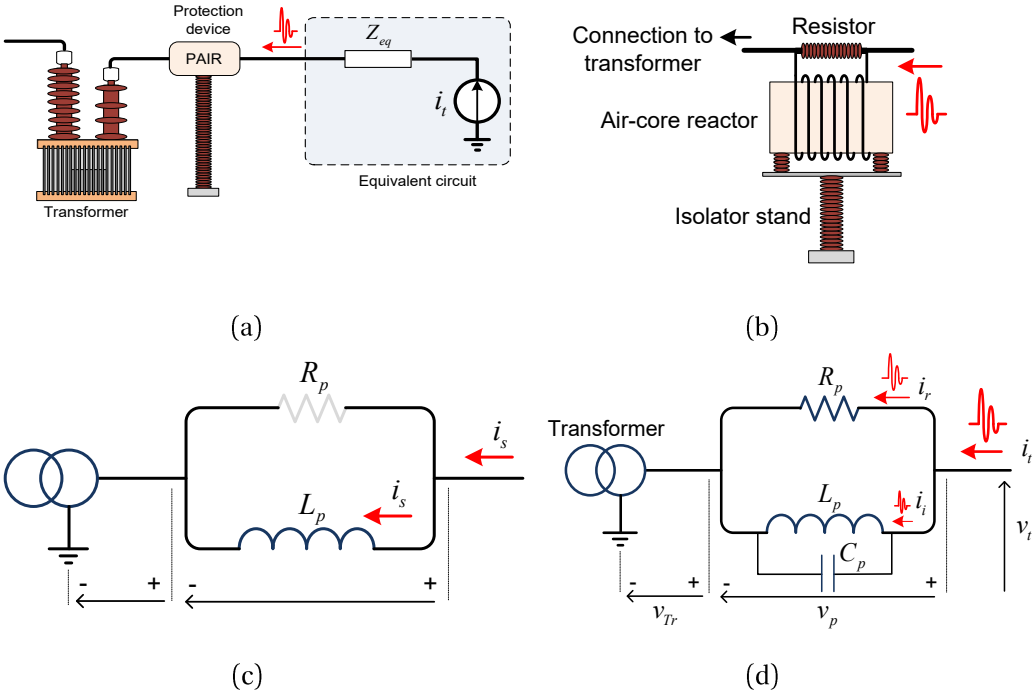


Fig. 4.6. (a) Topology of the series-protection device, (b) configuration of the PAIR (c) circuit model in grid frequency, (d) circuit model against a transient.

The PAIR device behaves as a large impedance in response to transient signals. In this operational mode, the impedance of the air-core inductor increases due to the high-frequency content of the transient signal, causing most of the current to flow into the resistor branch, effectively suppressing the high-frequency transients.

Additionally, the internal capacitance of the inductor C_p or an external tuning capacitance further increases the impedance of the inductor near the resonance point. This operation is depicted in Fig. 4.6 (d). Based on this figure, and applying KCL to the transient signal passing through the PAIR, equations (15) and (16) can be derived as follows:

$$i_t(t) = i_r(t) + i_i(t) \tag{4-15}$$

$$i_t(t) = \left(\frac{v_p(t)}{R_p}\right) + \left(\frac{1}{L_p}\int v_p(t)dt\right) + \left(C_p\frac{dv_p(t)}{dt}\right) \quad (4\text{-}16)$$

In addition, the voltage at the transformer terminals during the transient is computed by equation (4-17).

$$v_{Tr}(t) = v_t(t) - v_p(t) \quad (4\text{-}17)$$

Next, by considering the resonance frequency contents of the transient signal that can potentially cause resonance OVs, the voltage of transformer V_{Tr} is calculated in resonance frequency as (4-18) based on phasor analysis, where ω_r corresponds to the angular frequency of the resonance point.

$$V_{Tr(\omega_r)} = V_{t(\omega_r)} - V_{p(\omega_r)} \quad (4\text{-}18)$$

Following (4-18), the voltage drop of the PAIR, V_p, at the resonance point is calculated by (4-19).

$$V_{p(\omega_r)} = I_{r(\omega_r)}.R_p = I_{i(\omega_r)}.\left(\frac{j(L_p/C_p)}{1-\omega^2 L_p C_p}\right) \quad (4\text{-}19)$$

4.5. TRANSFORMER MODEL FOR PROTECTION STUDIES

The operational principle of the proposed PAIR-based OV protection strategy is to mitigate transient surges entering the transformer at its terminals. Achieving this requires a comprehensive model that accurately captures the transformer's frequency-dependent behaviour from the PAIR device's perspective. A black-box model is constructed for an actual power transformer in this context. This modelling serves two main purposes. First, implementing a high-voltage impulse test in the laboratory poses a risk to the real transformer due to potential OV and resonances. The obtained model is used to create a simplified protection laboratory circuit for the transformer to avoid these risks. Second, accurately tuning the PAIR device to provide maximum impedance at the transformer's resonance point requires an accurate transformer model. The specifications of the test transformer are provided in Table 4.1.

Table 4.1. Test transformer model parameters

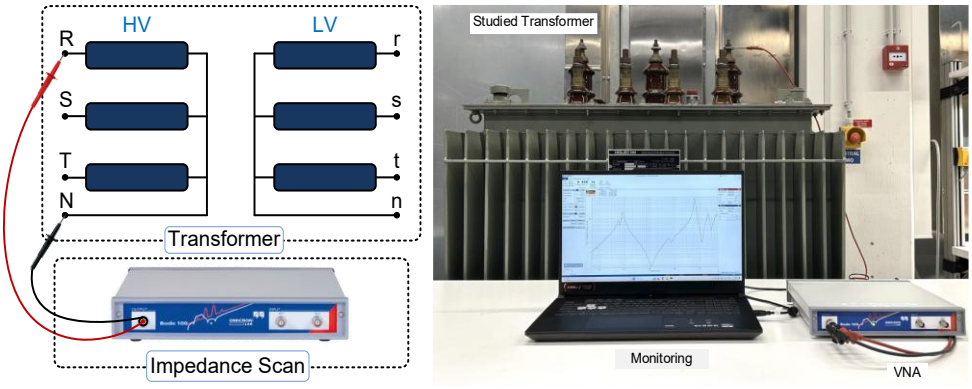
Parameter	Value
Ratio	10 kV / 0.4 kV
Vector Group	YNyn0
Nominal Power	315 kVA
Nominal Frequency	50 Hz

To begin, the harmonic impedance characteristic of the transformer is measured at its terminal using a VNA, as illustrated in Fig. 4.7. In Fig. 4.7 (a), the transformer impedance (Z) is measured at the HV terminal while the remaining terminals are left in an open-circuit condition. Fig. 4.7 (b) shows the laboratory setup used to measure the transformer's terminal impedance.

In the next step, the vector-fitting technique [29] is applied to calculate a rational approximation of $Y(s) = Z^{-1}(s)$ as the corresponding admittance of the terminal under test with respect to the neutral terminal, given by (20):

$$Y(s) = d + e \cdot s + \sum_{i=1}^{n+m} \frac{c_i}{s - p_i} \tag{4-20}$$

where d and e are constants c_i and p_i, respectively, denote residues and poles, considering a number of n real- and m complex poles, while ($s = j2\pi f$) is the Laplace variable at frequency f. It is worth noting that the passivity of the approximated rational function is ensured according to the method proposed in [30]. Based on the calculated vector-fitting coefficients in (8), an equivalent circuit model can be realized, according to Fig. 4.8 [31]. The parameter values of the equivalent circuit are obtained by equations (4-21)-(4-27).



(a) (b)

Fig. 4.7. Transformer terminal impedance measurement: (a) Schematic representation of the setup, (b) Laboratory setup.

Constants d and e in (21) characterize R_0 and C_0 by:

$$R_0 = \frac{1}{d}, \quad C_0 = e \tag{4-21}$$

The real poles characterize the number of n RL branches with $k=1,\ldots,n$, as:

$$R_k = \frac{-p_k}{c_k}, \qquad L_k = \frac{1}{c_k} \tag{4-22}$$

Finally, the complex conjugate pairs with poles $p_k' \pm j p_k''$ and corresponding residues $c_k' \pm j c_k''$ characterise the number of m RLCG branches with $k=n+1,\ldots,m$, yielded by:

$$Y(s) = d + e \cdot s + \sum_{i=1}^{n+m} \frac{c_i}{s - p_i} \tag{4-23}$$

$$L_k = 1/2c_k' \tag{4-24}$$

$$R_k = \left(-2p_k' + 2(c_k' p_k' + c_k'' p_k'')L_k\right)L_k \tag{4-25}$$

$$C_k^{-1} = \left(p_k'^{\,2} + p_k''^{\,2} + 2(c_k' p_k' + c_k'' p_k'')R_k\right)L_k \tag{4-26}$$

$$G_k = -2(c_k' p_k' + c_k'' p_k'')C_k L_k \tag{4-27}$$

Table 4.2 summarizes the parameters of the synthesized circuit model shown in Fig. 4.8, derived from the measured characteristics of the transformer. This circuit model is implemented in EMTP. Fig. 4.9 compares the measured and simulated transformer terminal impedance characteristics. The simulation is performed for two scenarios: (1) considering all obtained circuit model parameters (including both positive and negative values) and (2) eliminating unimportant parameters to simplify the model. As illustrated, the transformer demonstrates susceptibility to series resonance conditions around 11 kHz.

Given that the primary goal of this study is to propose adequate protection for the transformer against transient surges at its terminals, particular attention is focused on the transformer's resonance frequency. From a surge protection perspective, the equivalent circuit in Fig. 4.5 can be simplified by retaining only the branches that contribute to resonance while omitting the others. A laboratory circuit can be constructed to replicate the transformer's behaviour around its resonance frequency, allowing for experimental testing of the proposed PAIR device. This experimental setup is demonstrated in Fig. 4.10 (a).

To ensure that the behaviour of the implemented circuit closely matches that of the studied transformer, a frequency scan is performed using a VNA device, with the results illustrated in Fig. 10 (b).

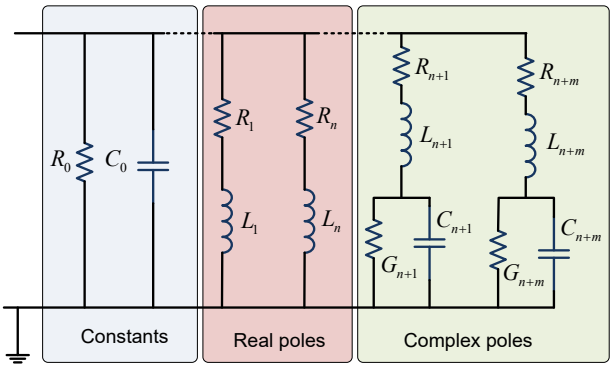


Fig. 4.8. Synthesized equivalent circuit model.

From the impedance character of the laboratory model synthesized for the transformer, it is evident that the critical resonance of the circuit is at approximately 11 kHz, and its impedance is around 1 kΩ. Accordingly, the synthesized circuit has almost the same character as the studied transformer around the critical resonance point. This circuit will be utilized to evaluate the PAIR in the next step.

Table 4.2. parameters of the test transformer model

Branch k	R_k [Ω]	L_k [mH]	C_k [nF]	$1/G_k$ [Ω]
0	1×10^{6}	-	-	-
1	341.35	11.34×10^{3}	-	-
2	1×10^{5}	107.7	-	-
3	1.6×10^{5}	210×10^{3}	2.97×10^{-1}	-2.63×10^{-7}
4	1.22×10^{3}	53.5	3.25	-8.97×10^{4}
5	-1.41×10^{4}	282.88	1.91×10^{-2}	3.63×10^{5}
6	4.1×10^{3}	4.5	2.44×10^{-3}	-1.12×10^{6}

Implementing a high-voltage impulse test in the laboratory carries risks to a real transformer due to potential OV and resonances. To mitigate these risks, parameters obtained from the real transformer are used to develop a high-voltage laboratory transformer model prototype. This model is designed to closely replicate the behaviour of the actual transformer. As can be seen in Table 4.2, using the vector fitting method, several circuit parameters have been obtained with negative values. Auxiliary optimization algorithms have been proposed in the literature to ensure the physical correctness of the equivalent circuit models by calculating non-negative parameters [32]. However, to prevent overcomplicating the analysis, a trial-and-error approach is used. It was determined that adequate model accuracy around the resonance frequency can be achieved by simply eliminating certain elements from the parameters in Table 4.2. The eliminated elements include all elements in Branch 3, series resistance R5 in Branch 5, and parallel conductance G6 in Branch 6. By comparing the responses of the simplified model with the actual measurements in Fig.

4.9, it is evident that the corrected model accurately replicates the resonance behavior of the power transformer under study.

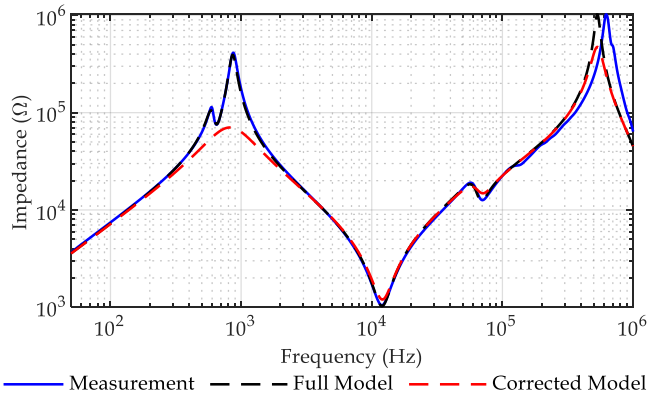
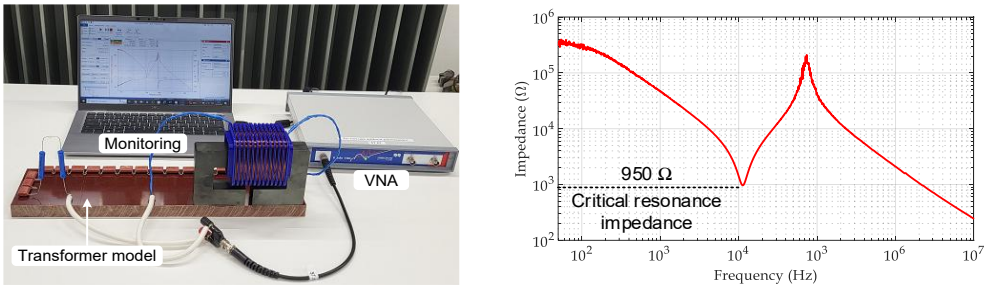


Fig. 4.9. Transformer terminal impedance characteristic.



(a) (b)

Fig. 4.10. (a) Laboratory setup for transformer modeling, (b) Measured transformer impedance sweep characteristic

To further elaborate on resonance frequency detection and modeling for the development of a protection PAIR, a cable-transformer combination presents another critical concern in modern power systems [33]. Similar to standalone transformers, the resonance frequency of a cable-transformer system can be identified through a frequency scan of the cable-integrated transformer. Once the resonance frequency is identified, an air-core reactor with two tuning capacitors can be designed to counteract the critical resonance frequencies in 11 kHz.

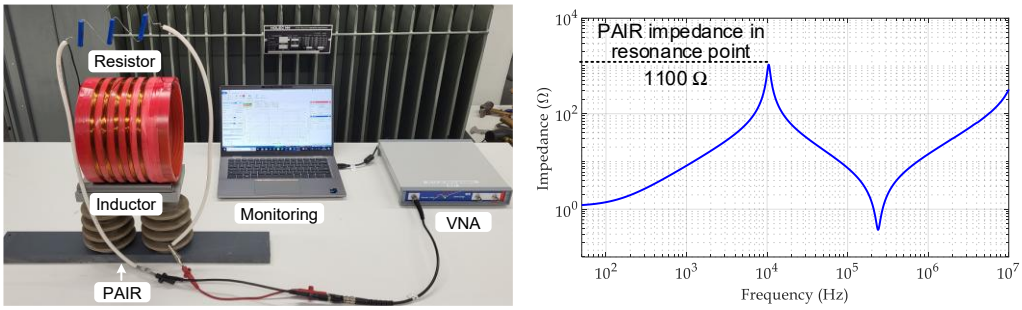
4.6. PROTECTION DEVICE EVALUATION

In this section, the performance of the proposed PAIR is evaluated in three stages. Firstly, the impedance characteristics of the PAIR are analysed using frequency sweep measurements conducted with a VNA device to understand its behaviour in the frequency domain. Next, the configuration shown in Fig. 4.6 (a) is modelled in EMTP software to determine the transformer's voltage response to a lightning impulse at its terminal. Finally, the PAIR's performance is validated in a high-voltage laboratory setup, where its effectiveness in protecting the transformer circuit is assessed. The results of the EMTP simulations and high-voltage laboratory tests are then compared to ensure robust validation. The laboratory PAIR data are presented in Table 4.3.

Table 4.3. Specifications of the designed PAIR

Inductance L_p (mH)	Resistor R_p (Ω)	Coil capacitance C_p (nF)	Tunning capacitance C_t (nF)	Voltage test level V_t (kV)
2	1400	2	8	35

The parameters of the proposed PAIR device are presented in Table 4.3. These specifications ensure that the PAIR introduces significant series impedance at the transformer's resonance point, effectively increasing the transformer's minimal impedance at this frequency to prevent resonance OVs. The designed PAIR, depicted in Fig. 4.11 (a), is based on this approach.



(a) (b)

Fig. 4.11. (a) PAIR protection device frequency sweep test setup, (b) The PAIR impedance sweep

In the initial test, a frequency scan of the PAIR is performed to confirm its impedance behavior at the transformer resonance point (11 kHz in this case). As shown in Fig. 4.11 (b), the PAIR exhibits an impedance of approximately 1.1 kΩ at 11 kHz, which slightly exceeds the transformer's impedance at its resonance frequency. According to (4-18), the PAIR will suppress more than half of the transformer voltage at this frequency.

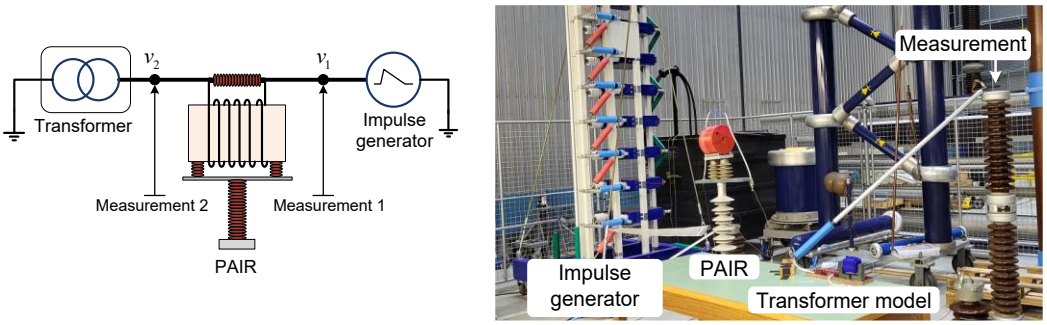
Subsequently, the transformer model connected in series with the PAIR is simulated using the EMTP to assess the transformer's voltage response during impulse testing. The time-domain test, illustrated in Fig. 4.12 and experimental results, validates the PAIR's effectiveness against impulse signals. The simulation results indicate that nearly 1% of the impulse voltage magnitude is mitigated at the transformer terminal, primarily due to the suppression of the frequency content around 11 kHz. Consequently, the transformer experiences no overvoltage during impulse excitation, confirming the PAIR's effectiveness.

4.7. EXPERIMENTAL VALIDATION

This section elaborates on the high-voltage laboratory setup used to test the proposed PAIR device. The test circuit configuration is illustrated in Fig. 4.12 (a). In this setup, the output terminal of the impulse generator is connected to one terminal of the PAIR, with the other terminal linked to the protection-modelled circuit of the transformer. The remaining terminal of the transformer is grounded. Additionally, voltage divider measurement devices are connected to the terminals of both the impulse generator and the transformer.

For the test run, the impulse generator is charged to 33 kV, a level considered safe given the insulation's withstand voltage. The impulse is then applied to the test setup, and the resulting voltages, shown in Fig. 4.12 (b), are recorded using a high-speed oscilloscope. These recorded results are presented in Fig. 13, together with the results from EMTP simulations.

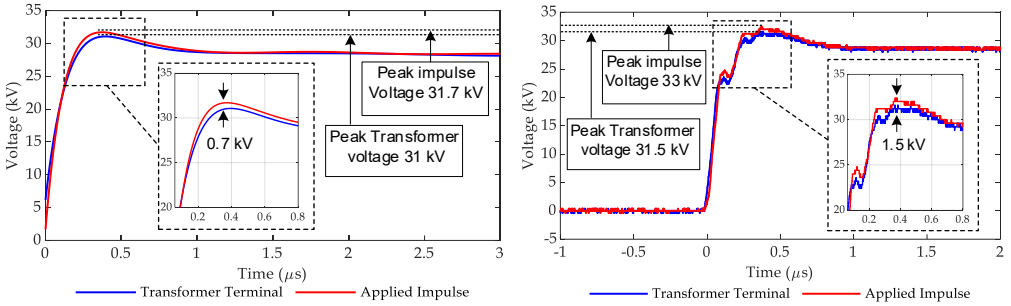
As shown in Fig. 4.13, the voltage at the transformer terminal is lower than that of the impulse generator. Specifically, Fig. 4.13 (a) illustrates that during the high-voltage laboratory test, while the impulse generator reaches a peak magnitude of 33 kV, the peak voltage at the transformer terminal remains at 31.5 kV. This observation closely aligns with the results from the EMTP simulations shown in Fig. 4.13 (b), confirming the accuracy of the transformer terminal voltage prediction.



(a) (b)

Fig. 4.12. (a) Transformer protection model circuit, (b) Transformer circuit-impedance sweep characteristic

In summary, the use of the PAIR reduces the voltage at the transformer terminal during impulse testing by 4.5% and effectively prevents overvoltage occurrences due to the transformer's critical resonance point.



(a) (b)

Fig. 4.13. Voltage measurement of a PAIR impulse test: (a) High-voltage laboratory experimental test, (b) EMTP simulation

Considering the impedance characteristics of the studied transformer, as shown in Fig. 4.11 (b), the critical resonance frequency is 11 kHz, which results in a resonance within the transformer. At this frequency, the transformer impedance is minimal (less than 1 kΩ), indicating that harmonics around this frequency can be detrimental. The PAIR is designed to mitigate this by providing high impedance against these harmful harmonics. Consequently, the experimental test focuses on the harmonics received by the transformer within the 9-12 kHz range, both with and without the operation of the PAIR. The results, presented in Fig. 4.14, provide a clear comparison.

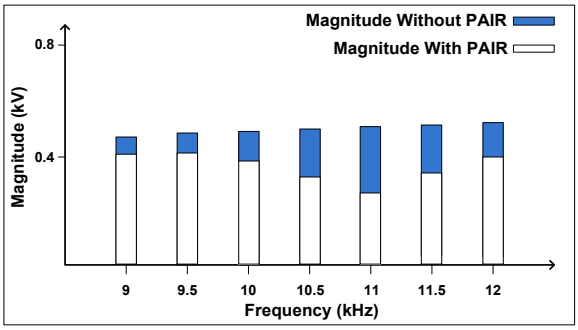


Fig. 4.14. Transformer voltage frequency content (9 kHz<f<12 kHz)

As shown in Fig. 4.14, the magnitude of the frequency content in the transformer voltage is significantly suppressed, indicating that the PAIR effectively limits resonance and overvoltage. Specifically, the frequency content at 11 kHz is reduced by half, demonstrating successful mitigation of resonance at this critical frequency. Additionally, the frequency content in the range close to 11 kHz is also suppressed, further confirming the PAIR's effectiveness in managing harmful harmonics.

4.8. Comparison analysis

Table 4.4 presents the most significant criteria to highlight the specification of the PAIR over the closest protection concept (choke). These criteria refer to: i) the operation frequency range of each device, ii) the provided impedance against the main frequency of the transient signal at the resonance point, the magnetic saturation possibility, and iii) the voltage level.

Table 4.4. Comparison of the PAIR and choke

Features	PAIR	Choke [17]
Connection type	series	Series
Operation frequency range	Tunable in a frequency range	Above 1 MHz
Provided impedance	Above 1 kΩ	Less than 1 kΩ
Saturation possibility	No saturation possibility	Mostly possible
Voltage level	Both the distribution and transmission systems	Distribution system

The reasoning behind this claim is that the design of the air-core reactor is applicable across all voltage levels, as presented in Table 4.4. Therefore, this method is viable for protecting transmission-level transformers that are susceptible to damage from transient phenomena. Additionally, the tuning parallel capacitor and resistor in this method have relatively small values, making them practically implementable.

Based on the data in Table 4.4, the operating frequency of PAIR is tunable to align with the resonance frequency of the protected transformer, whereas the choke is not tunable, as its operating frequency is determined by the fixed R-L circuit components.

Moreover, PAIR's air-core design eliminates concerns about core saturation, a significant issue for core-based series reactors like the choke. In terms of operating voltage levels, PAIR also has an advantage. Its air-core design allows for greater adaptability at higher voltage levels, while the choke, with its compact magnetic core, is typically limited to distribution transformers.

In summary, this comparison demonstrates that PAIR offers several advantages over the traditional choke as a protection method. PAIR not only improves resilience at higher voltage levels but also provides reliable protection against resonance overvoltages in transformers.

4.9. Conclusion

This chapter focuses on developing a protective device designed to shield wind farm transformers from transient signals that can trigger resonance OVs. The proposed protection device, referred to as PAIR (Parallel Air-core Inductor Resistor), consists of an air-core inductor and a parallel resistor connected in series with the transformer. A comprehensive analysis, including PAIR design, EMTP simulations, frequency sweep measurements, and high-voltage impulse tests, demonstrates that the PAIR effectively safeguards transformers against resonance overvoltages without encountering saturation issues in its inductor. The simulated results and high-voltage impulse tests reveal that not only does the transformer coil avoid reaching overvoltage levels, but its voltage magnitude also decreases by 4.5% during impulse testing. Furthermore, the measurements of the harmonic content around the transformer's resonance point (11 kHz) show a 50% reduction in the magnitude of these harmonics. This successful operation of the PAIR mitigates overvoltage risks and ensures the stable performance of transformer systems in wind farms. Furthermore, this protection method is applicable to all types of transformers, with the only variation being the critical resonance frequency, which determines the specific tuning of the PAIR device.

References

[1] D. Bogdanov, J. Farfan, K. Sadovskaia, A. Aghahosseini, M. Child, A. Gulagi, O. Sadovskaia, M. de Oliveira, T. Breyer, and C. Breyer, "Radical transformation pathway towards sustainable electricity via evolutionary steps," Nature Commun., vol. 10, no. 1, pp. 1–16, Dec. 2019.

[2] M. Child, D. Bogdanov, A. Aghahosseini, and C. Breyer, "The role of energy prosumers in the transition of the Finnish energy system towards 100% renewable energy by 2050," Futures, vol. 124, Dec. 2020.

[3] V. Yaramasu, B. Wu, P. C. Sen, S. Kouro, and M. Narimani, "High-power wind energy conversion systems: State-of-the-art and emerging technologies," Proc. IEEE, vol. 103, no. 5, pp. 740–788, May 2015.
[4] A. Candela Garolera, K. L. Cummins, S. F. Madsen, J. Holboell, and J. D. Myers, "Multiple lightning discharges in wind turbines associated with nearby cloud-to-ground lightning," IEEE Trans. Sustain. Energy, vol. 6, no. 2, pp. 526–533, Apr. 2015.
[5] A. Candela Garolera, S. F. Madsen, M. Nissim, J. D. Myers, and J. Holboell, "Lightning damage to wind turbine blades from wind farms in the U.S.," IEEE Trans. Power Del., vol. 31, no. 3, pp. 1043–1049, Jun. 2016.
[6] A. Andreotti, A. Pierno, and V. A. Rakov, "A new tool for calculation of lightning-induced voltages in power systems—Part I: Development of circuit model," IEEE Trans. Power Del., vol. 30, no. 1, pp. 326–333, Feb. 2015.
[7] S. Visacro, "Recent advances in lightning research and their impact on the protection of electric systems," in 2018 34th Int. Conf. Lightning Protection (ICLP), Rzeszow, Poland, 2018, pp. 1–4.
[8] W. Yuanfang and C. Zhou, "Experimental studies on the use of MOV in transformer windings inner protection," IEEE Trans. Power Del., vol. 20, no. 2, pp. 1441–1446, Apr. 2005.
[9] M. Hori, M. Nishioka, Y. Ikeda, K. Noguchi, K. Kajimura, H. Motoyama, and T. Kawamura, "Internal winding failure due to resonance overvoltage in distribution transformer caused by winter lightning," IEEE Trans. Power Del., vol. 21, no. 3, pp. 1600–1606, Jul. 2006.
[10] S. Ghasemi, M. Allahbakhshi, B. Behdani, M. Tajdinian, and M. Popov, "Probabilistic analysis of switching transients due to vacuum circuit breaker operation on wind turbine step-up transformers," Electric Power Syst. Res., vol. 182, p. 106204, 2020.
[11] A. Heidary, M. G. Niasar, M. Popov, and A. Lekić, "Transformer resonance: Reasons, modeling approaches, solutions," IEEE Access, vol. 11, pp. 58692–58704, 2023.
[12] M. Hori, M. Nishioka, Y. Ikeda, K. Noguchi, K. Kajimura, and T. Kawamura, "Internal winding failure due to resonance overvoltage in distribution transformer caused by winter lightning," IEEE Trans. Power Del., vol. 21, no. 3, pp. 1600–1606, Jul. 2006.
[13] M. A. Atefi, M. Sanaye-Pasand, and S. Bahari, "Preventing transformer energizing resonant overvoltages using surge arrester temperature rise index and controlled closing method," IEEE Trans. Power Del., vol. 28, no. 2, pp. 998–1006, Apr. 2013.
[14] P. E. Sutherland, "Snubber circuit design for transformers in an urban high rise office building," IEEE Trans. Ind. Appl., vol. 51, no. 6, pp. 4347–4356, Nov.–Dec. 2015.
[15] A. Heidary, M. Ghaffarian Niasar, and M. Popov, "The principle of magnetic flux switch," Scientific Reports, vol. 14, no. 1, p. 8990, 2024.
[16] F. Nasirpour, A. Heidary, and M. G. Niasar, "High-frequency transformer winding model with adequate protection," Electric Power Syst. Res., vol. 223, 2023.
[17] S. M. Korobeynikov, S. I. Krivosheev, S. G. Magazinov, V. A. Loman, and N. Ya, "Suppression of incoming high-frequency overvoltage in transformer coils," IEEE Trans. Power Del., vol. 36, no. 5, pp. 2988–2994, Oct. 2021.
[18] D. Smugała, W. Piasecki, M. Ostrogórska, M. Florkowski, M. Fulczyk, and O. Granhaug, "New approach to protecting transformers against high-frequency transients–wind turbine case study," Prz. Elektrotech., vol. 89, pp. 186–190, 2013.

[19] A. Heidary, M. G. Niasar, and M. Popov, "Comprehensive evaluation of toroid ring core parallel inductor and resistor as a transformer protection device," IEEE Trans. Circuits Syst. I: Reg. Papers, 2024.

[20] A. Heidary, M. G. Niasar, and M. Popov, "Series magnetic coupled reactor saturation considerations for high voltage AC and DC power systems," Int. J. Electr. Power Energy Syst., vol. 158, 2024.

[21] A. Heidary, H. Radmanesh, K. Rouzbehi, A. Mehrizi-Sani, and G. B. Gharehpetian, "Inductive fault current limiters: A review," Electric Power Syst. Res., vol. 187, 2020.

[22] S. M. Korobeynikov, S. I. Krivosheev, S. G. Magazinov, V. A. Loman, and N. Ya, "Suppression of incoming high-frequency overvoltage in transformer coils," IEEE Trans. Power Del., vol. 36, no. 5, pp. 2988–2994, 2021.

[23] S. Wang, J. Zhou, J. Shu, J. Ma, K. Qin, and T. Liu, "A bidirectional active DC fault current limiter based on coupled inductor," IEEE Trans. Power Del., vol. 37, no. 5, pp. 4427–4437, 2022.

[24] B. I. Kang and J. D. Park, "Application of thyristor-controlled series reactor for fault current limitation and power system stability enhancement," Int. J. Electr. Power Energy Syst., vol. 63, pp. 236–245, 2014.

[25] H. S. Kartijkolaie, M. Radmehr, and M. Firouzi, "LVRT capability enhancement of DFIG-based wind farms by using capacitive DC reactor-type fault current limiter," Int. J. Electr. Power Energy Syst., vol. 102, pp. 287–295, 2018.

[26] M. Firouzi, G. B. Gharehpetian, and M. Pishvaei, "A dual-functional bridge type FCL to restore PCC voltage," Int. J. Electr. Power Energy Syst., vol. 46, pp. 49–55, 2013.

[27] A. Heidary, M. Popov, A. Moghim, M. G. Niasar, and A. Lekić, "The principles of controlled DC reactor fault current limiter for battery energy storage protection," IEEE Trans. Ind. Electron., vol. 71, no. 2, pp. 1525–1534, 2023.

[28] V. Naphade, V. Ghate, and G. Dhole, "Experimental analysis of saturated core fault current limiter performance at different fault inception angles with varying DC bias," Int. J. Electr. Power Energy Syst., vol. 130, p. 106943, 2021.

[29] B. Gustavsen and A. Semlyen, "Rational approximation of frequency domain responses by vector fitting," IEEE Trans. Power Del., vol. 14, no. 3, pp. 1052–1061, Jul. 1999.

[30] B. Gustavsen, "Passivity enforcement of rational models via modal perturbation," IEEE Trans. Power Del., vol. 23, no. 2, pp. 768–775, Apr. 2008.

[31] G. Antonini, "SPICE equivalent circuits of frequency-domain responses," IEEE Trans. Electromagn. Compat., vol. 45, no. 3, pp. 502–512, Aug. 2003.

[32] P. Rahimi Pordanjani, C. Y. Chung, H. Erfanian Mazin, and W. Xu, "A method to construct equivalent circuit model from frequency responses with guaranteed passivity," IEEE Trans. Power Del., vol. 26, no. 1, pp. 400–409, Jan. 2011.

[33] M. Behdani, M. Ghaffarian, and M. Popov, "Analysis of cable-transformer resonant interactions due to CB prestriking transients," in 2024 IEEE Int. Conf. Environ. Electr. Eng. & 2024 IEEE Ind. & Commercial Power Syst. Europe (EEEIC/ICPSEurope), Rome, Italy, 2024, pp. 1–6.

5

RING-CORE PARALLEL INDUCTOR AND RESISTOR FOR TRANSFORMER PROTECTION AGAINST TRANSIENT

5.1. Abstract

The transition to modern energy systems requires integrating various pieces of equipment that undergo frequent switching and are vulnerable to lightning strikes. As a result, power systems experience fast transient switching and lightning surges, making advanced protection solutions essential for power equipment. In the past decade, a ring-core R-PIR has emerged as an effective solution for mitigating fast transients and protecting medium-voltage transformers. However, a comprehensive model is still needed for this component, particularly to expand its applications.

This chapter presents a detailed model of the R-PIR as a protective device, validated through electromagnetic transient simulations, finite element methods, and laboratory experiments. The research aims to analyze the performance and design characteristics of the R-PIR and demonstrate its effectiveness in protecting transformers from fast transients. Experimental results confirm that designing the R-PIR within an appropriate frequency range significantly reduces transient overvoltages affecting transformers.

This chapter of the thesis is published in the article:
A. Heidary, M. Ghaffarian Niasar, and M. Popov, "Comprehensive Evaluation of Toroid Ring Core Parallel Inductor and Resistor as a Transformer Protection Device," IEEE Transactions on Circuits and Systems I: Regular Papers, vol. 71, no. 9, pp. 4298-4308, Sept. 2024.

The chapter is organized as follows:

Section 5.2 defines the goal of the work and explains the role of the R-PIR.
Section 5.3 describes the structure and configuration of the R-PIR.
Section 5.4 focuses on R-PIR modeling.
Section 5.5 analyzes the R-PIR using FEM software.
Section 5.6 examines the frequency response of the R-PIR in EMTP software.
Section 5.7 presents the experimental test setup.
Section 5.8 discusses the key features of the R-PIR.
Section 5.9 summarizes the findings and conclusions.

5.2. AN OVERVIEW OF TRANSFORMER PROTECTION DEVICES AGAINST TRANSIENT OVERVOLTAGE

Fast transient phenomena in power systems occur due to lightning strikes or circuit breaker switching [1], [2]. The increasing integration of renewable generators leads to more switching actions and a higher likelihood of lightning strikes on transmission towers, resulting in more frequent FTs [3]. Although power grids experience various transient waveforms, this chapter focuses on FT analysis based on the standard lightning impulse defined in IEC 61000, which represents a voltage transient with multiple harmonic components [4].

FTs affect power equipment, particularly transformers, by causing resonance and overvoltages [5]. Due to their harmonic content, FTs can induce resonance and potentially damage transformer insulation [6].

Several protection devices have been developed to safeguard high-power transformers against FTs [6], including surge arresters [7], surge capacitors and RC snubbers [8], ZnO arrester RC known as ZORC circuits [9], PIRs [10], [11], and ring core suppressors [12]. While these devices effectively mitigate transient overvoltages, the ring-core parallel inductor and resistor circuit (R-PIR) stands out as a series-connected protection device tested in power grids. It offers advantages such as filtering transient harmonics and operating without requiring a ground connection [13], [14]. The R-PIR has a simple structure comprising a ferromagnetic core, a conductor, and a resistive secondary suppressor [15]. It is connected in series with the transformer, such as those used in wind farms [16], and effectively suppresses FTs, as demonstrated in [17], [18]. Additionally, ring magnetic cores have been applied to cables, overhead lines, and gas-insulated cables to mitigate lightning transients [20], [21].

The concept of a parallel RL circuit in series with an overhead line or cable is a well-known method for suppressing transient oscillations [22], [23]. Similarly, chokes have

been proposed as RL circuits in [24], [25], however, their effectiveness has not been thoroughly studied.

This thesis chapter develops a detailed R-PIR model using FEM simulations and EMT analysis. These simulations are validated through laboratory experiments, followed by high-voltage impulse testing to assess the R-PIR's performance in protecting a low-power HV transformer and suppressing transient oscillations.

The main contributions of this chapter include:

- A comprehensive evaluation of the R-PIR, including FEM and EMTP analysis, frequency-domain analysis, and high-voltage testing.
- Detailed parameter determination for designing different R-PIR configurations.
- Performance analysis based on the R-PIR's magnetic and electric field distribution.
- Black-box frequency sweep circuit modeling and validation.
- High-voltage testing to examine the R-PIR's impact on transient oscillation suppression.

5.3. R-PIR CONFIGURATION AND OPERATION

As an FT suppressor, the R-PIR is a two-winding component connected in series with the transformer to protect it from overvoltages and resonance caused by fast transients. It consists of a core, a primary conductor, secondary windings, and a resistor. Fig. 5.1 illustrates the structure of the R-PIR and its connection to the transformer.

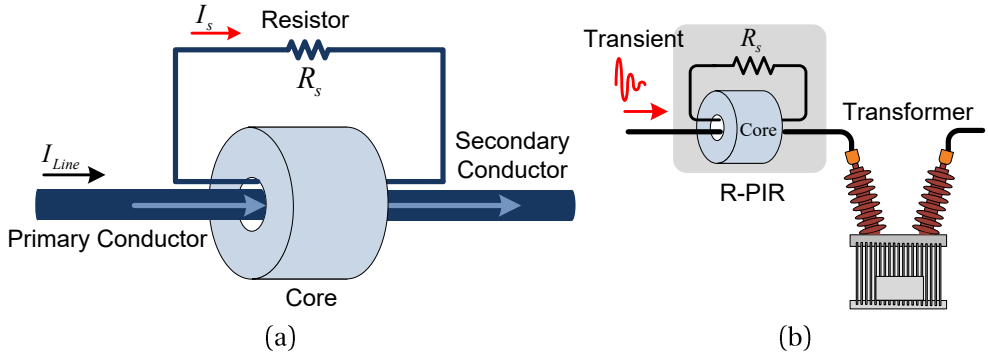


Fig. 5. 1. a) R-PIR structure, b) the series connection of an R-PIR with a transformer

As shown in Fig. 5.1(a), a part of the line conductor passes through the core, serving as the R-PIR's primary turn, while the secondary winding is wrapped around the core, forming the suppression section. A resistor (R_s) is connected to the secondary winding to suppress transient signals induced by the secondary current. Fig. 5.1(b) illustrates the R-PIR's connection to the transformer for FT protection.

The R-PIR operates in two modes. In the first mode, when no FT signal is present during normal power system operation, the R-PIR's impedance remains negligible. In the second mode, when FTs occur, the device attenuates the high-frequency components of the transient through its voltage drop, preventing transformer resonance and overvoltages.

5.4. R-PIR MODELING

The R-PIR can be viewed as a series transformer with a resistor in its secondary circuit. However, at higher frequencies, a more detailed circuit model is required to account for the capacitive effects of the conductors. Therefore, the analysis begins with the R-PIR's low-frequency model, considering its operation at power system frequency. Next, the high-frequency model is examined, focusing on the interaction between the R-PIR and fast transients.

The primary objective of this section is to derive equations for calculating all R-PIR parameters. These parameters will then be used for the simulations to evaluate the R-PIR's performance.

A. R-PIR power system frequency analysis

The turn ratio of the R-PIR is one and can be represented using a transformer equivalent circuit to accurately describe its behavior at power system frequency. In this model, only resistances and inductances are considered, while insulation and capacitive effects are neglected due to their high impedance at low frequencies.

Fig. 5.2 illustrates the power system frequency model of the R-PIR, which can be used to analyze power losses during steady-state operation.

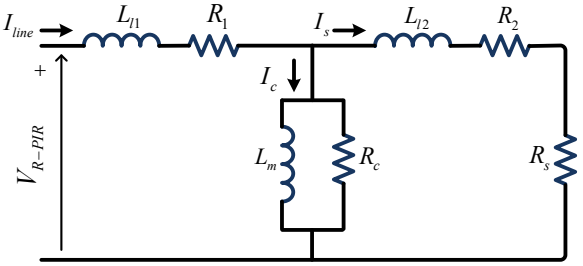


Fig. 5.2. Low-frequency equivalent circuit of the R-PIR

In the illustrated circuit of Fig. 5.2, L_{l1} and L_{l2} are the leakage inductances of the R-PIR for the primary and the secondary side, while R_1 and R_2 are the primary and secondary resistance, respectively. L_m is the R-PIR's magnetizing inductance, and R_c is the modeled resistance of the core where the turns ratio is 1:1.

The total impedance of the R-PIR, Z_c, and R-PIR voltage drop, $V_{R\text{-}PIR}$ can be computed by (5-1) and (5-2).

$$Z_c = R_1 + j\omega L_{l1} + \left(R_c \parallel j\omega L_m \parallel \left(R_2 + R_s + j\omega L_{l2}\right)\right) \tag{5-1}$$

$$V_{R-PIR} = I_{line}\left(R_1 + j\omega L_{l1} + \left(R_c \parallel j\omega L_m \parallel \left(R_2 + R_s + j\omega L_{l2}\right)\right)\right) \tag{5-2}$$

By applying Kirchhoff's Current Law (KCL), the current in each branch can be computed as follows:

$$I_{line} = I_c + I_s \tag{5-3}$$

$$I_c = \frac{V_{R-PIR} - \left(I_{line}(R_1 + j\omega L_{l1})\right)}{\left(\frac{R_c . j\omega L_m}{R_c + j\omega L_m}\right)} \tag{5-4}$$

$$I_s = \frac{V_{R-PIR} - \left(I_{line}(R_1 + j\omega L_{l1})\right)}{R_2 + R_s + j\omega L_{l2}} \tag{5-5}$$

Here, I_{line}, I_c, I_s are the currents of the power line, core branch, and secondary side, respectively. Considering the current of each branch, the power loss P_{loss} of R-PIR for a power system frequency can be determined as follows:

$$P_{loss} = P_p + P_c + P_s \tag{5-6}$$

$$P_p = {I_{line}}^2 R_1 \tag{5-7}$$

$$P_c = \frac{\left(V_{R-PIR} - \left(I_{line}(R_1 + j\omega L_{l1})\right)\right)^2}{R_c} \tag{5-8}$$

$$P_s = \left(R_2 + R_s\right)\left(\frac{V_{R-PIR} - \left(I_{line}(R_1 + j\omega L_{l1})\right)}{R_2 + R_s + j\omega L_{l2}}\right)^2 \tag{5-9}$$

The cross-section of the conductors and core should be increased to decrease the power loss of the R-PIR during steady-state operation. Moreover, power loss can be decreased by decreasing the resistance R_s.

Reactive power consumption Q of the R-PIR for a power frequency can be determined as follows:

$$Q = Q_p + Q_c + Q_s \tag{5-10}$$

$$Q_p = I_{line}{}^2 j\omega L_{l1} \tag{5-11}$$

$$Q_c = \frac{\left(V_{R-PIR} - \left(I_{line}(R_1 + j\omega L_{l1})\right)\right)^2}{j\omega L_m} \tag{5-12}$$

$$Q_s = \left(j\omega L_{l2}\right)\left(\frac{V_{R-PIR} - \left(I_{line}(R_1 + j\omega L_{l1})\right)}{R_2 + R_s + j\omega L_{l2}}\right)^2 \tag{5-13}$$

To decrease the reactive power consumption, the cross-section of the core should be decreased accordingly, considering that the leakage inductance value is much smaller than the magnetizing inductance.

Applying the following condition to the equivalent circuit of the R-PIR simplifies its equivalent circuit.

$$R_2 + j\omega L_{l2} << R_s \tag{5-14}$$

$$R_1 + j\omega L_{l1} << j\omega L_m \,||\, R_c \,||\, R_s \tag{5-15}$$

According to (5.14) and (5.15), L_{l1}, R_1, L_{l2}, and R_2 can be ignored from the equivalent circuit, and the final R-PIR model for power frequency analysis can be represented by an R-L shunt circuit, as illustrated in Fig.5.3.

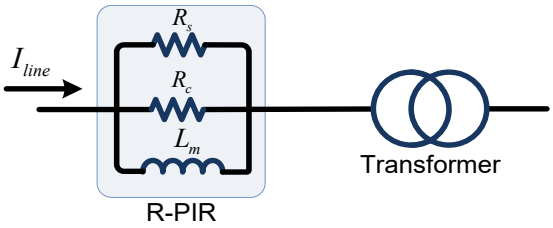


Fig. 5.3. Simplified equivalent circuit of the R-PIR (for power frequency analysis)

B. R-PIR high-frequency analysis

Various harmonic components are generated during the fast transient state, and the R-PIR protects the transformer by suppressing these harmonics. Therefore,

developing a high-frequency model of the R-PIR is crucial for designing an effective protection device. To ensure accuracy, all electrical elements of the R-PIR must be considered in the high-frequency model. Concerning the high-frequency model, the capacitive terms of the R-PIR are the capacitances of primary terminal C_1, secondary terminal C_2, and primary to secondary conductor C_{12}. These capacitances are shown in Fig. 5.4.

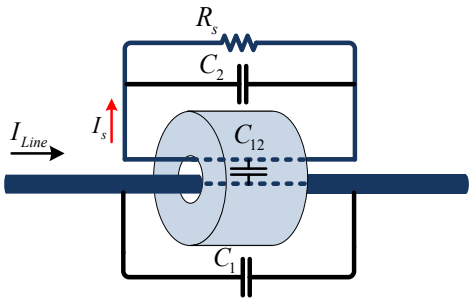


Fig. 5.4. Considered capacitance in R-PIR structure

This model assumes that the capacitances of the conductors to the ground are very low because of the large distance between the conductors and the ground.

The resistances of the primary and secondary conductors are also essential for the high-frequency model. These resistances include two terms, DC resistances R_{dc1} and R_{dc2}, and frequency-dependent resistances $R_1(f)$ and $R_2(f)$. Besides, the resistance of the core is also a function of the frequency. The high-frequency model of the R-PIR is depicted in Fig. 5.5. Furthermore, regarding the operation frequency range of R-PIR (mostly around 10 kHz to 1 MHz) and the length of R-PIR (around 200 mm), the wavelength is much larger than the R-PIR length. Consequently, the amount of magnetic field emission is negligible, so the lumped-parameter representation of R-PIR is suitable.

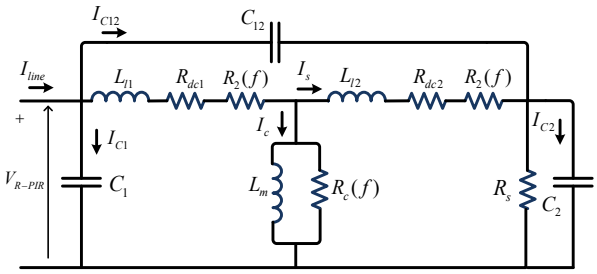


Fig. 5.5. High-frequency equivalent circuit of R-PIR

The impedance of the R-PIR and its voltage drop depending on the frequency, according to the equivalent circuit shown in Fig. 5.5, can be determined by the following expressions:

$$Z_1 = R_{dc1} + R_1(f) + j\omega L_{l1} \tag{5-16}$$

$$Z_2 = R_{dc2} + R_2(f) + j\omega L_{l2} \tag{5-17}$$

$$Z_{core} = R_c \parallel j\omega L_m \tag{5-18}$$

$$Z_{AB} = \frac{Z_1.Z_2 + Z_2.Z_{core} + Z_{core}.Z_1}{Z_{core}} \tag{5-19}$$

$$Z_{BC} = \frac{Z_1.Z_2 + Z_2.Z_{core} + Z_{core}.Z_1}{Z_1} \tag{5-20}$$

$$Z_{CA} = \frac{Z_1.Z_2 + Z_2.Z_{core} + Z_{core}.Z_1}{Z_2} \tag{5-21}$$

$$Z_c = \left(Z_{CA} \parallel \frac{1}{j\omega C_1}\right) \parallel \left(\left(Z_{AB} \parallel \frac{1}{j\omega C_{12}}\right) + \left(Z_{BC} \parallel \frac{1}{j\omega C_2}\right)\right) \tag{5-22}$$

$$V_{R-PIR} = I_{line}\left(\left(Z_{CA} \parallel \frac{1}{j\omega C_1}\right) \parallel \left(\left(Z_{AB} \parallel \frac{1}{j\omega C_{12}}\right) + \left(Z_{BC} \parallel \frac{1}{j\omega C_2}\right)\right)\right) \tag{5-23}$$

To calculate the R-PIR's impedance, Z_1, Z_2, and Z_{core} are first computed to simplify the circuit components, and then Z_{AB}, Z_{BC}, and Z_{CA} are applied to compute star-connected impedances to delta impedances. By taking into account (5.22), the R-PIR can provide a remarkable impedance against the high-frequency content of the FTs. Consequently, the magnitude of the high-frequency signal can be suppressed by its voltage drop, as shown in (5.23), and the transformer will be protected against FT accordingly.

C. R-PIR R-L-C elements calculation

Coke resistance and secondary energy calculation

In the R-PIR design, the DC resistances of the primary and secondary conductors (frequency-independent resistance) depend on the conductors' conductance, length, and cross-section. Therefore, the expression for DC resistance computation can be written as follows:

$$R_{dc1} = \frac{l_p}{\sigma S_p} \tag{5-24}$$

$$R_{dc2} = \frac{l_s}{\sigma S_s} \tag{5-25}$$

In this equation, the conductance of both primary and secondary σ is considered the same. l_p and l_s refer to the lengths of the primary and secondary conductors passing through the core, respectively. It is taken into account the fringing field effect at the edges of the R-PIR (as per the FEM model); this includes an additional length of $b/4$, where b is the core radius. S_p and S_s are the cross-sections of the primary and secondary conductors.

References [16] and [17] represent the R-PIR's frequency-dependent resistance related to the skin effect depth and proximity effect. The resistances $R_1(f)$ and $R_2(f)$ can be computed according to (5-26):

$$R_{1,2}(f) = R_{dc1,2}\left(\mathrm{Re}\left\{\sqrt{j2\pi f\mu_0\sigma}\frac{d_{1,2}}{t}\sqrt{\frac{\pi}{4}}.d\coth(d)\right\}+\mathrm{Re}\left\{2\sqrt{j2\pi f\mu_0\sigma}\frac{d_{1,2}}{t}\sqrt{\frac{\pi}{4}}.d\tanh(d/2)\right\}\right) \tag{5-26}$$

Where f is the transient oscillation frequency, μ_0 is the magnetic permeability of the conductor, $d_{1,2}$ is the diameter of the primary or secondary conductor, and t is the distance between the conductors' centers. Moreover, in this equation, "Re" refers to the real part of the complex expression provided in the brackets.

W_D is the transferred energy to the R-PIR's secondary resistor and is computed by (5-27). This energy must be dissipated by the appropriate design of the secondary resistor's size and material. Here, the transient voltage oscillation $v(t)$ is assumed to be linear and consists of two regions (rising and falling). t_0 is the time when the transient oscillation occurs, and t_1 is the end of the rising trend of the transient oscillation. t_1 is also the time when the transient oscillation starts decreasing, and t_2 is the end of the transient oscillation. Furthermore, m_r and m_f are the rates of the rising and decreasing of the transient oscillation, respectively, and R_s is the resistance of the secondary winding.

$$W_D = \int_{t0}^{t1}\frac{m_r v^2_{(t)}}{R_s}dt + \int_{t1}^{t2}\frac{m_f v^2_{(t)}}{R_s}dt \tag{5-27}$$

D. R-PIR inductance calculation

Considering the R-PIR as a linear device, the component's leakage and magnetizing inductance can be computed by (5-28)-(5-30). By taking into account that the number

of primary and secondary turns (N_1 and N_2) of the R-PIR is one, the inductances L_{l1}, L_{l2}, and L_m are only functions of associated reluctances.

$$L_{l1} = \frac{N_1^2}{R_{l1}} = \frac{1}{R_{l1}} \tag{5.28}$$

$$L_m = \frac{N_1.N_2}{R_m} = \frac{1}{R_m} \tag{5.29}$$

$$L_{l2} = \frac{N_2^2}{R_{l2}} = \frac{1}{R_{l2}} \tag{5.30}$$

These equations are derived by using the equivalent magnetic circuit of the R-PIR shown in Fig. 5.6, where R_{l1}, R_{l2}, are the leakage air and core reluctances, respectively.

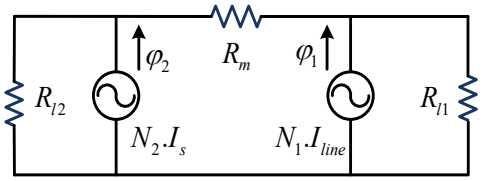


Fig. 5.6. The R-PIR magnetic equivalent circuit

In this circuit, the reluctance of the only core R_m is frequency-dependent. However, ferrite cores are particularly affected at frequencies above 100 kHz. This means that the R-PIR inductances can be considered frequency-independent over the 10-100 kHz range, which is the main operating frequency range of the R-PIR. These reluctances can be computed as follows:

$$R_{l1} = \frac{l_{a1}}{A_{a1}.\mu_0} \tag{5.31}$$

$$R_m = \frac{l_c}{A_c.\mu_c} \tag{5.32}$$

$$R_{l2} = \frac{l_{a2}}{A_{a2}.\mu_0} \tag{5.33}$$

Here, l_{a1} and l_{a2} are the average lengths of the leakage flux paths in the air, and A_{a1} and A_{a2} are the average cross-sections of the leakage flux direction. l_c is the average length of the core, and, μ_0 and μ_c are the air and core permeability, respectively.

E. R-PIR capacitance calculation

It is possible to model various capacitances between conductors in the R-PIR structure. However, most parallel capacitors have negligible values and can be ignored. Therefore, overall capacitance is determined by considering the largest one

in the R-PIR model. Regarding this assumption, the capacitance between the primary and secondary conductors and the primary and secondary terminals can be calculated.

The capacitance calculation between the primary and secondary conductors

This subsection deals with the determination of the capacitances of the primary and secondary conductors of the R-PIR. The assumption here is that the core as an equipotential surface is ignored because of its distance from the conductors ($b>>d-(a1+a2)$). To calculate the capacitance between the primary and secondary conductors, the geometry shown in Fig. 5.7 is used. These two conductors are considered parallel cylinders inside the core, and the capacitance can be calculated by (5-34).

Where $a1$ and $a2$ are the radii of the primary and secondary conductors, and d is the distance between their centres.

$$C_{12} = \frac{2\pi\varepsilon_0 d}{(\ln(a_1/d) - \ln(a_2/d))} \tag{5-34}$$

Here, ε_0 is the permittivity of the conductor, which is roughly equal to the permittivity of the air. C_{12} is obtained in F/m.

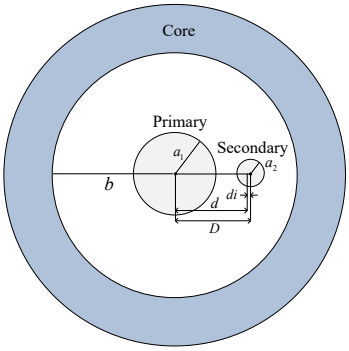


Fig. 5.7. Geometry of primary and secondary conductors inside the core

The next step is to determine the terminal capacitance of the primary and secondary turns of the R-PIR. The capacitance of the primary terminal is calculated according to Fig. 5.8.

To calculate the capacitance of the primary terminal, it is assumed that the core is an equipotential surface where the voltage V_c to ground is half of the R-PIR primary conductor voltage drop V_1, and the secondary conductor has a negligible impact. V is the voltage distribution along the primary conductor, which varies from V_1 to V_0.

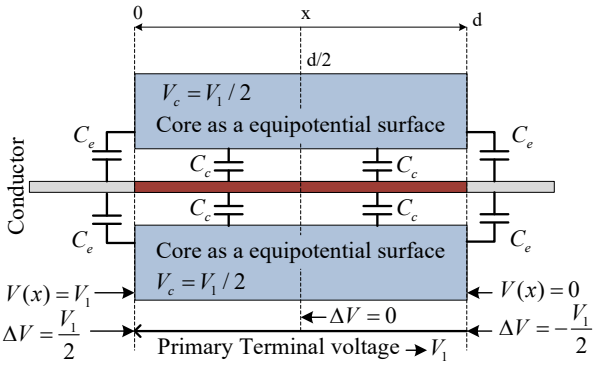


Fig. 5.8. R-PIR capacitances

As illustrated in Fig. 5.8, the capacitance value between the piece of conductor covered by the core C_c is larger than the edge capacitance C_e. This assumption is given by (5-35) and (5-36).

$$\sum C_c >> \sum C_e \tag{5-35}$$

$$V_c = \frac{V_1}{2} \tag{5-36}$$

Voltage differences between the core and each point of the conductor are defined as ΔV and expressed by (5-37). The voltage distribution $V(x)$ along the conductor to the ground is a function of distance x (which varies between 0 and d) and is represented by (5-38).

$$\Delta V(x) = V(x) - V_c \tag{5-37}$$

$$V(x) = V_1 - x \tag{5-38}$$

In the first step, the capacitance of the primary terminal is calculated to determine the capacitance of the cylindrical conductor and the core that shields the conductor. This capacitance is calculated by (5-39) assuming a uniform electric field in space between the conductor and core.

$$C_c = \frac{2\pi\varepsilon_0 d}{\ln(b/a)} \tag{5-39}$$

In (5.39), it is assumed that the voltage differences between the conductor and core ΔV are equal at each point, which shows that the electric field between the inner and outer cylinders is homogeneous. However, this is not the case in the R-PIR, and the voltage is distributed between the conductor and core. This condition is considered for the calculation of the terminal capacitance by using the stored electrical energy equation as expressed by (5-40).

$$W_e = \frac{1}{2}\int_0^d C_c \left(\Delta V(x)\right)^2 dx \tag{5-40}$$

By solving (5.40), considering that d is the length of the core, the stored energy in the capacitances of the R-PIR will be calculated by the presented equation in (5-41).

$$2W_e = \frac{C_c}{3} \tag{5-41}$$

In the next step, by focusing on the polarity of the voltage between the primary conductor and core, it is clear that the capacitance of half of the horizontal length of the R-PIR (*d/2*) is connected in series with the other half of the R-PIR. Therefore, the capacitance of the R-PIR for the primary terminal can be expressed by (5-42).

$$C_1 = \frac{\pi\varepsilon_0 d}{6\ln\left(b/a\right)} + C_e/2 \tag{5-42}$$

This equation can be derived by taking into account the equivalent circuit, which is illustrated in Fig. 5.9.

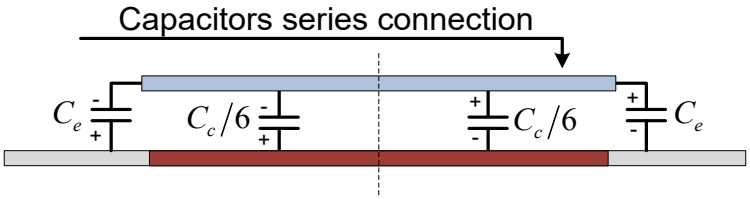


Fig. 5.9. Equivalent circuit for R-PIR primary capacitance calculation.

The capacitance of the secondary terminal of the R-PIR is calculated by taking into account that the distance between the primary and secondary conductors is shorter than the distance between the secondary conductor and the core. The capacitance between the primary and secondary conductors is calculated by (5-39), and then the energy method with a series connection of the capacitors along the conductor is applied. The secondary terminal capacitance can be determined as:

$$C_2 = \frac{\pi\varepsilon_0 d}{6\left(\ln\frac{a_1}{d} - \ln\frac{a_2}{d}\right)} + C_e/2 \tag{5-43}$$

5.5. FEM ANALYSIS OF R-PIR

The Fem simulation of the proposed R-PIR is prepared by two sections, considering the magnetic field and the electric field analysis as follows:

A. Design of the studied R-PIR in the FEM platform

To evaluate the R-PIR's specifications, the geometry of the R-PIR is constructed in an FEM environment. The geometric size of the R-PIR is based on the analytical studies reported in section 5.2. Two constraints should be taken into account when designing R-PIR. First, there is a minimal impact in steady-state operation (very low voltage drop), and second, there is an acceptable impedance during transient oscillation to suppress its magnitude. Accordingly, Table 5.1 presents the parameters of the R-PIR used for the FEM analysis, including geometric data and material properties.

The FEM analysis confirms the following performances of R-PIR:

- Magnetic flux density in the core and core saturation aspects
- R-PIR's inductance and resistance
- Voltage distribution in the R-PIR structure and critical insulation regions
- The capacitance between the primary and secondary conductors of the R-PIR

Table 5.1. Parameters of simulated R-PIR

Parameter	value
Core length	200 mm
Core radius	34 mm
Core thickness	10 mm
Primary conductor radius	1 mm
Secondary conductor radius	0.2 mm
Core permeability	2000
Core material	VITROPERM
Core Electrical conductivity	0.4 m/Ωmm2
Secondary turn resistance	3 kΩ
Core material	Ferrite
Conductor material	Copper
Core maximum saturation flux density	1200 mT
Applied voltage to the primary 60 Kv a unit voltage	1 p.u.
Applied current to primary (normal state)	100 A
Applied current to primary (transient oscillation state)	100 A

Fig. 5.10 shows the 3D design of the studied tuned choke and the applied mesh in the FEM software environment.

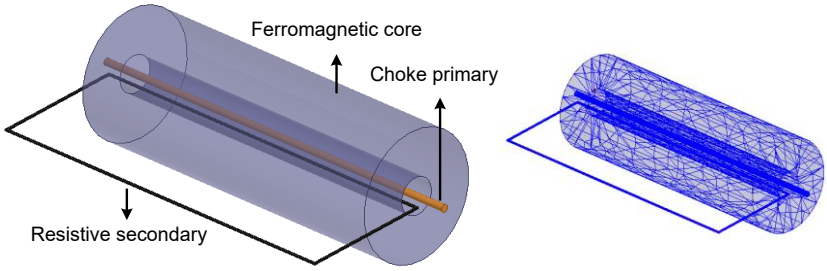


Fig. 5.10. a) 3D geometric design of R-PIR, b) mesh plot of R-PIR

Firstly, the performance of the core (considering magnetic flux density) is studied by exciting the primary side with a steady-state and high-frequency current. Here, the magnetic flux density distribution in the core presents the flux density value for each core section. Secondly, the voltage distribution of the R-PIR is presented to evaluate the capacitive model of the R-PIR and the critical points, considering the insulation effects.

B. Magnetic flux density and R-PIR's inductance for steady-state and transient oscillation operation

For the steady-state case, a 10 kV source, including its equivalent impedance, is connected in series to the primary terminal of the R-PIR. This case demonstrates that the R-PIR is connected to the power line where the steady-state peak current is 100 A. Hence, the performance of the R-PIR can be evaluated in a steady state. All FEM simulations are carried out by the transient solver supported by the FEM software tool.

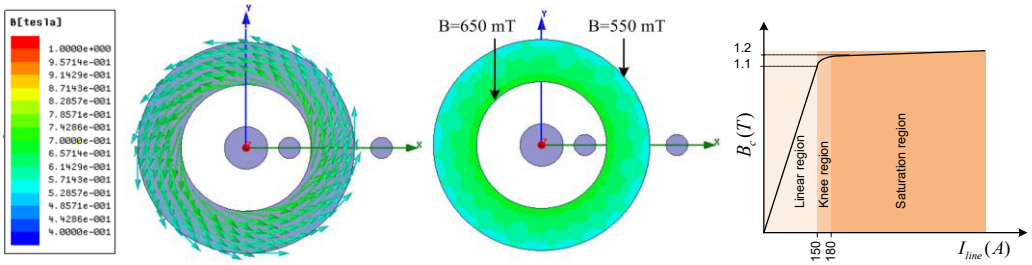
Fig. 5.11 (a) shows the magnetic behavior of the studied core, and Fig. 5.11 (b) depicts the magnetic maximum flux density of the core for both 2D vector and magnitude plots. This simulation shows that the maximum magnetic flux density during steady-state in the R-PIR reaches 650 mT, while the average is 600 mT. The critical result is that during steady-state, the core is far from being saturated and is capable of suppressing fast transient oscillations during the faulty period.

In the next case, a high-frequency source is applied with a crest voltage, which is twice as high as the steady-state system voltage at a frequency of 100 kHz. This simulation case demonstrates the core magnetic flux density in the R-PIR as the transient oscillation passes through it. This high-frequency source excites the primary turn of the R-PIR by 100 A. Fig. 5.12(a) shows the core's maximum magnetic flux density distribution. It can be observed that the magnetic flux density in the layer of the core closest to the primary conductor is 230 mT, while the outer layer's magnetic flux density is 20 mT. The huge difference in magnetic flux density in the core layers is due

to the induced eddy currents during the high-frequency period. The average magnetic flux density in this state is 125 mT.

Fig. 5.12(b) shows the distribution of the maximum magnetic flux density in the core, which shows the effects of the transient oscillation and steady-state line current on the R-PIR core, considering the current peak magnitude. It is found that the maximum magnetic flux density reaches 880 mT in the layer closest to the conductor, while the average magnetic flux density in the core cross-section is 725 mT.

Based on the FEM analysis, the R-PIR inductance of the primary terminal is 280 μH for the steady-state case and 259 μH for the transient oscillation case (excited at 100 kHz). Additionally, for the steady-state analysis, the conductor's leakage inductances for both the primary and secondary sides are 0.8 μH, and the resistances are 14 mΩ and 66 mΩ, respectively. When DC excitation is applied, the resistances are 12 mΩ and 65 mΩ. For a frequency of 100 kHz, the resistances of the primary and secondary sides increase to 27 mΩ and 98 mΩ, respectively. Moreover, by superimposing the values of the average flux density for the two frequencies (50 Hz and 100 kHz), the maximum average flux density is 725 mT, which is in the linear region of the saturation characteristic.



(a) (b)

Fig. 11. a) B-I curve of the studied core, b) R-PIR magnetic flux density for a power frequency (50 Hz)

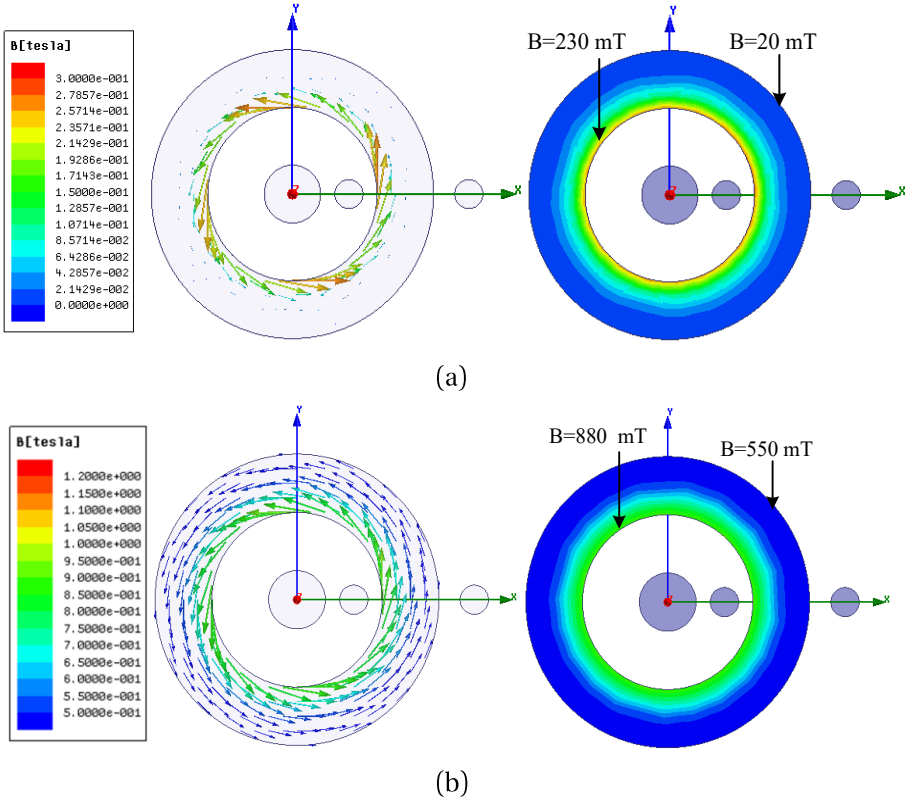


Fig. 5.12. R-PIR magnetic flux density for a frequency of 100 kHz

C. Voltage distribution in the R-PIR

This case study considers the effect of the primary and secondary conductors, for which the voltage is (approximately) 1 V. Fig. 5.13 shows the voltage distribution in the R-PIR. By using the energy calculation method, the primary terminal capacitance of the R-PIR is determined as 60 pF.

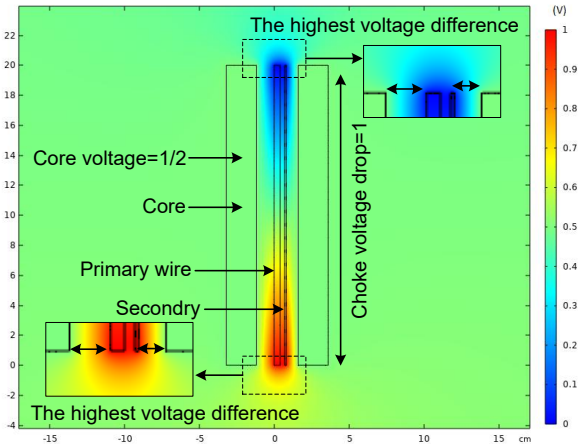


Fig. 5.13. R-PIR primary voltage distribution.

The other obtained result from the simulation is that the external edge of the core and conductors experiences the highest electric potential, which should be taken into account for the insulation design. Moreover, the secondary terminal capacitance and the capacitance between the primary and secondary conductors are 80 pF and 68 pF, respectively.

5.6. EMTP SIMULATION OF R-PIR

This section deals with the R-PIR's characteristics simulated by EMTP. Here, the presented equivalent circuit of the R-PIR, which is shown in Fig. 5.5, is used, and the parameters of the circuit elements are determined by applying the FEM analysis.

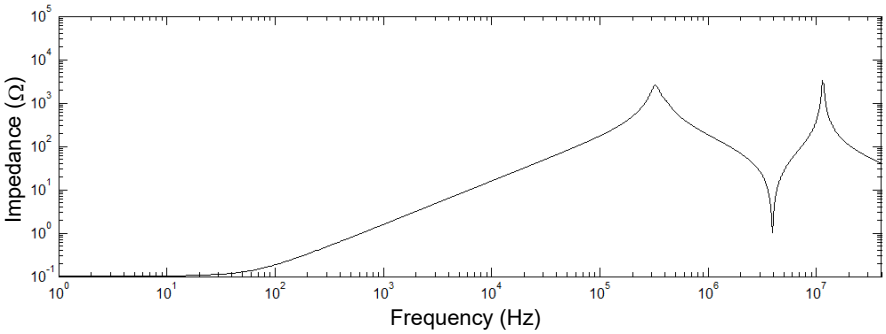


Fig. 5.14. R-PIR EMTP frequency-dependent impedance.

The primary terminal frequency-dependent impedance of the R-PIR is obtained using this equivalent circuit. Fig. 5.14 shows that the R-PIR impedance for low frequencies is very low, and it increases with the frequency increase, reaching approximately 1.3 kΩ around the first resonance frequency (220 kHz). It decreases to its minimum (12

Ω) at the next resonance point (30 MHz). This frequency-dependent characteristic shows that the R-PIR can provide an acceptable impedance within the range of 0.1MHz to 2 MHz to successfully protect the transformer against resonances. Moreover, this resonance frequency can be changed based on the design of the R-PIR (considering the value of the capacitances and inductances).

5.7. EXPERIMENTAL EVALUATION OF R-PIR

According to the performed analysis, an experimental test setup, shown in Fig. 5.15, is designed to study the R-PIR. The analysis is conducted by applying three types of tests. For the first test, the secondary R-PIR is open. The second test is carried out by having the secondary side of the R-PIR short-circuited, and the third test is carried out when the R-PIR operates for an actual case.

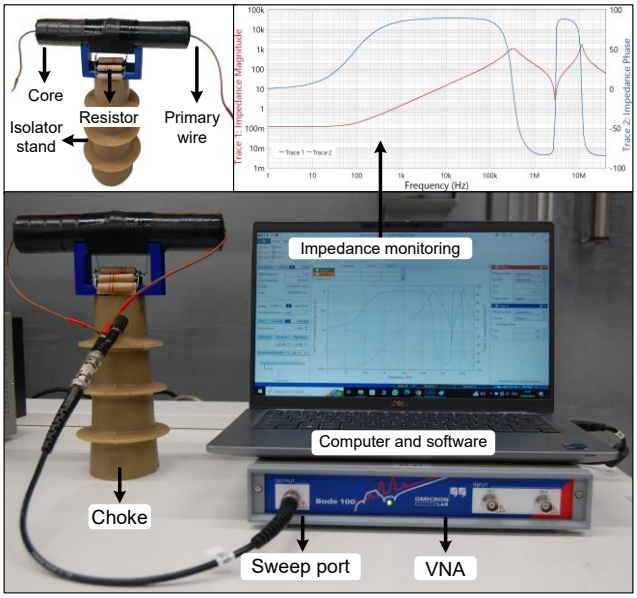


Fig. 5.15. Laboratory measurement setup

The FS terminal impedance measurement is performed by using a VNA Bode 100 with a frequency range of up to 40 MHz. This device measures the R-PIR's frequency response by applying a current in the milliamperes range. Therefore, its measurement is more valid when the R-PIR works in linear regions.

The geometric data of the R-PIR for the laboratory test setup are presented in Table 5.1. Impedance measurements are conducted using the VNA device to measure the R-

PIR impedance, resistance, inductance, and capacitance within the 1 Hz to 40 MHz frequency range. The values of the circuit parameters can be obtained by selecting appropriate frequencies for each test. The obtained results are presented in Fig. 5.16 and Fig. 5.17.

A. R-PIR open-circuit test

The secondary of the R-PIR (suppressor resistor circuit) is open for the open-circuit test. The impedance of the primary terminal is measured in an FS mode. The effect of the secondary RLC circuit is negligible, and therefore, the remaining elements are the leakage and magnetizing inductance (L_{l1}+L_m), resistances (R_{dc1} and R_f), and capacitance (C_1) of the R-PIR primary side. Fig. 5.16 (a), (b), (c), and (d) show the impedance, resistance, inductance, and capacitance of the primary R-PIR circuit. Overall, its impedance rises from 70 mΩ to 1500 Ω within the range of 20 Hz to 1 MHz (as a resonance point). Afterward, its impedance decreases till the next resonance point. The obtained data from this test are summarized in Table 5.2.

Table 5.2. R-PIR parameters for the open-circuit test

Open-circuit FS measurement						
Measured parameter	L_m+L_{l1}	R_{dc1}	R_f(10kHz)	R_f(100kHz)	C_1	Z_c (max)
parameter value	250 µH	70 mΩ	0.2 Ω	10 Ω	56 pF	1.5 kΩ

As shown in Fig. 16 and Table II, by applying the open-circuit test, one can obtain the leakage and magnetizing inductance of the R-PIR primary side, DC resistance, frequency-dependent resistance, capacitance of the R-PIR primary terminal, and the maximum impedance values of R-PIR's primary terminal. Fig. 5.17 presents the FS measurement of the R-PIR's capacitance between the primary and secondary terminals for the open-circuit state.

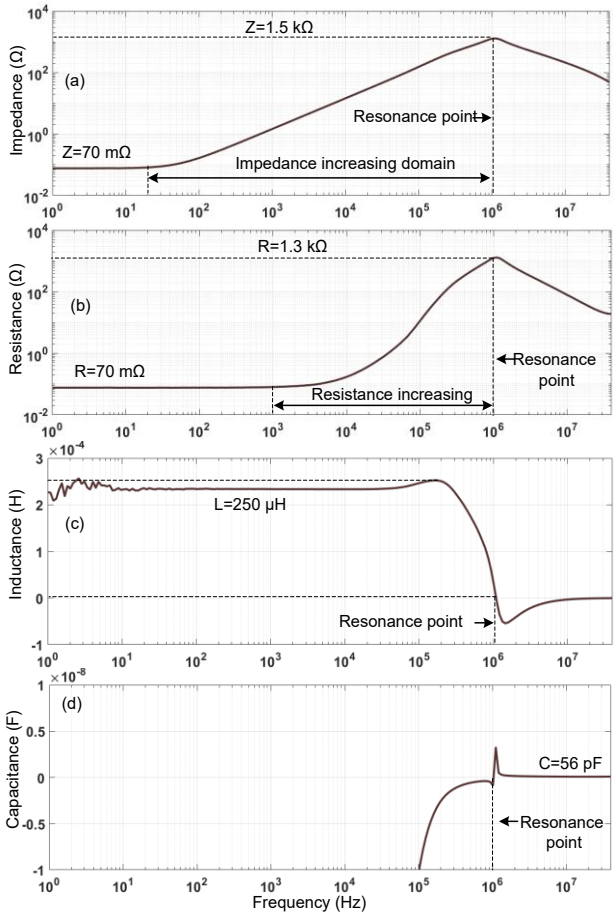


Fig. 5.16. R-PIR open-circuit FS a) terminal impedance, b) terminal resistance, c) terminal inductance, and d) terminal capacitance measurement

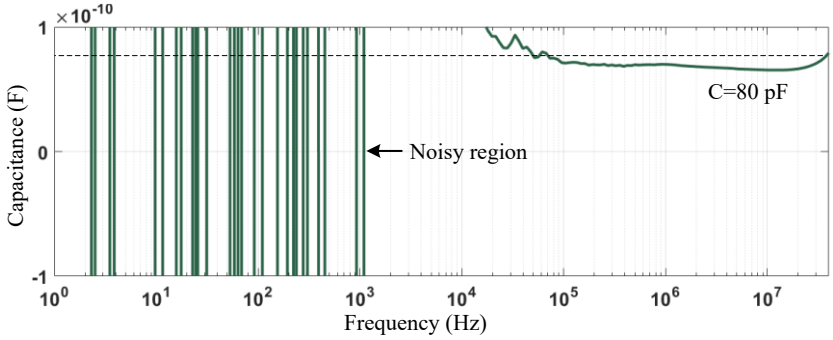


Fig. 5.17. R-PIR open-circuit FS capacitance measurement between primary and secondary terminals

B. *R-PIR short-circuit test*

For this test scenario, the secondary of the R-PIR is short-circuited. This configuration removes the magnetization and secondary capacitance of the R-PIR; the remaining elements are the leakage inductances (L_{l1}+L_{l2}), resistances (R_{dc1} and R_{dc2}), and primary capacitance (C_l).

As can be seen in Fig. 5.18, the resonance point is shifted to almost 20 MHz because of the decreased value of R-PIR inductance. The results of this test are presented in Table 5.3.

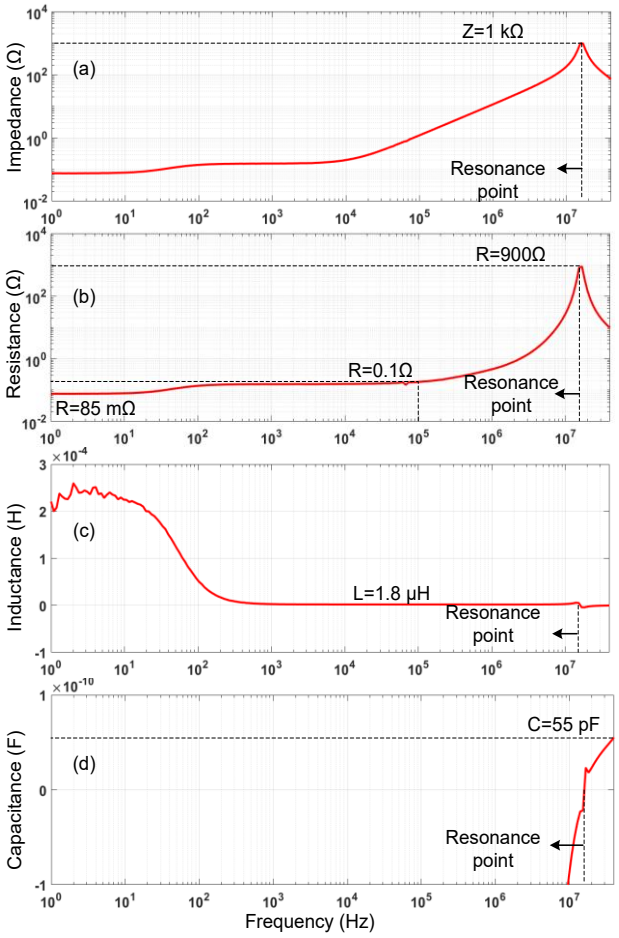


Fig. 5.18. The R-PIR short-circuit FS a) terminal impedance, b) terminal resistance, c) terminal inductance, and d) terminal capacitance measurement

Table 5.3. R-PIR parameters for the short-circuit test

Short-circuit FS measurement						
Measured parameter	L_{l1}+L_{l2}	R_{dc1}+R_{dc2}	R (10kHz)	R_f (100kHz)	C_l	Z_c (max)
parameter value	1.8 μH	85 mΩ	0.095 Ω	0.1 Ω	55 pF	1 kΩ

Considering the measured data, it can be concluded that the frequency-dependent resistor does not increase significantly in the high-frequency region.

C. R-PIR operating mode test

For the final experimental test, defined as R-PIR operating mode, where the secondary is connected to a suppressing resistor, FS measurements of the primary terminal are performed with the secondary side connected to a resistor. The measured results are shown in Fig. 5.19.

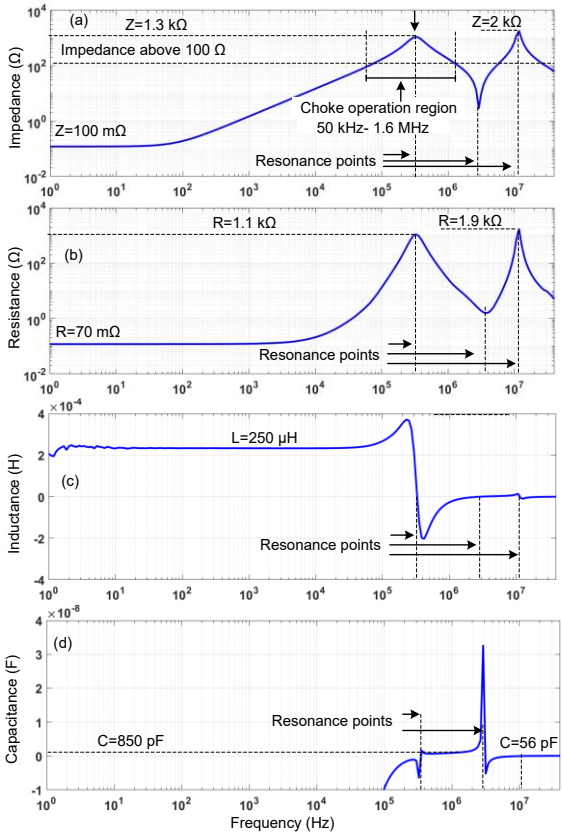


Fig. 5.19. R-PIR operation state: a) terminal impedance, b) terminal resistance, c) terminal inductance, and d) terminal capacitance measurement

According to Fig. 5.19(a), the operating range of the R-PIR is from 50 kHz to 1.8 MHz, where its total impedance remains above 100 Ω. The measured data are also summarized in Table 5.4.

Table 5.4. R-PIR parameters for the operating mode test

Operating mode FS measurement						
Measured parameter	L_m	C_1	C_2	R	R(100 kHz)	Z_c(max)
parameter value	250 µH	56pF	78pF	100 mΩ	20 Ω	2 kΩ

D. Validation of the R-PIR parameters

Based on the measurements performed in previous part, all the parameters of the R-PIR can be accurately determined and compared to those obtained by FEM analysis and analytical formulas derived in Section 5.3. Table 5.5 summarizes these results.

Table 5.5. Validation of the R-PIR parameters

Parameter	L_m	L_{l1}	L_{l2}	C_1	C_2	C_{12}	R_{dc1}	R_{dc2}	R_f
Measurement	255 µH	0.9 µH	0.9 µH	56 pF	78 pF	60 pF	70 mΩ	15 mΩ	30 mΩ
FEM	259 µH	0.8 µH	0.8 µH	56 pF	80 pF	68 pF	65 mΩ	12 mΩ	27 mΩ
Calculation	260 µH	0.8 µH	0.8 µH	55 pF	79 pF	67 pF	65 mΩ	14 mΩ	28 mΩ

E. Impulse test of the R-PIR prototype

To validate the operation of the R-PIR and its performance in reducing the magnitude of the transient voltage oscillation, an impulse test is carried out where the R-PIR prototype is connected in series with a 10 kV, 200 VA transformer. The peak value of the impulse voltage is 10 kV. Fig. 5.20 shows the test setup, which is configured similarly to Fig. 5.1(b). Fig. 5.21 shows the applied impulse voltage (blue curve), the voltage on the transformer terminal (red curve), and the voltage drop across the R-PIR (purple curve). It is clearly shown that the R-PIR contributes to a considerable decrease in the transformer voltage.

It can also be seen that the peak value of the transformer terminal voltage decreases by 20% (from 10 kV to 8 kV), and its rate of rise drops from 25 kV/µs to 20 kV/µs. Moreover, considering the R-PIR voltage drop during the impulse test, the R-PIR suppresses almost 40% of the average voltage, which is measured by the oscilloscope.

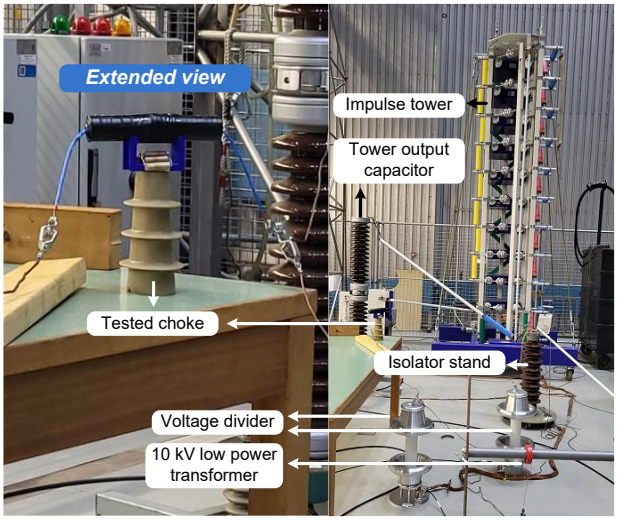


Fig. 5.20. High-voltage test setup to study the R-PIR performance

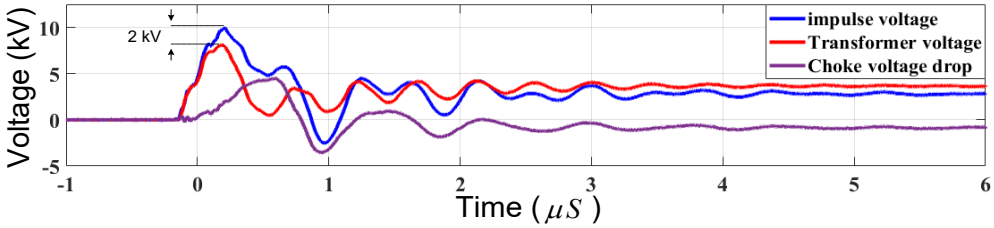


Fig. 5.21. Measured transient oscillation for the R-PIR test

The performed analysis of the R-PIR shows the main advantages of the R-PIR compared to the mature state-of-the-art solutions, such as the surge arrester [7], the snubber [8], and the serial ring core [16]. Apart from transient overvoltage suppression, other advantages are in terms of power consumption during steady-state operation introduced as PCSS, the effects on transient oscillation introduced as EOTO, the voltage level during the steady-state operation introduced as VLSS, the grounding requirement introduced as GR, and tuneable frequency response introduced as TFR. These advantages are summarized in Table 5.6.

Table 5.6. R-PIR advantages compared to other solutions

Features	Arrester [7]	Surge capacitor [8]	Series rings [19]	R-PIR
PCSS	High active power loss in the transmission voltage level	High reactive power consumption at the transmission voltage level	High reactive power consumption in high-current lines	Low active and reactive power consumption
EOTO	Chopping overvoltages	Filtering transient oscillations	Filtering transient oscillations	Filtering transient oscillations
VLSS	Grid voltage	Grid voltage	Almost zero	Almost zero
GR	Required grounding	Required grounding	Does not require grounding	Does not require grounding
TFR	No tuning possibility	No tuning possibility	No tuning possibility	Tuning possibility

Comparative analysis presented in Table 5.6 shows the good performance of R-PIR, as a new protection device against fast transient oscillations. The effect during steady-state operation is negligible, and during fast transient oscillations, R-PIR behaves as a filter that successfully suppresses a large amount of the transient signal without specific grounding requirements. Another advantage is that R-PIR can be tuned and designed for different system configurations and voltage levels.

Compared to surge arresters, the R-PIR provides critical resonance frequency filtering, protecting the wind farm transformer from both terminal and internal resonance, which can lead to overvoltage conditions. In contrast, surge arresters allow the transformer to experience resonance-induced overvoltage before mitigating it by diverting a large current to the ground.

5.8. Conclusion

This chapter presented a detailed study of the R-PIR as a protection device against fast transients. A comprehensive model was developed, considering both low- and high-frequency characteristics. The finite element method and electromagnetic transient simulations were used to analyze its performance, and the results were validated through experimental tests.

The findings confirm that the R-PIR effectively suppresses transient overvoltages and mitigates resonance effects in transformers. The device can operate efficiently over a wide frequency range by carefully designing its parameters. The experimental results

demonstrated that the R-PIR significantly reduces the impact of fast transients, improving the protection and reliability of power transformers.

This research highlights the importance of considering both electrical and magnetic properties when designing R-PIRs. Future work can explore further optimization techniques to enhance performance and expand applications in modern power grids.

References

[1] M. Popov and E. Acha, "Overvoltages due to switching off an unloaded transformer with a vacuum circuit breaker," IEEE Trans. Power Del., vol. 14, no. 4, pp. 1317–1326, Oct. 1999.

[2] M. Hori, M. Nishioka, Y. Ikeda, K. Noguchi, K. Kajimura, H. Motoyama, and T. Kawamura, "Internal winding failure due to resonance overvoltage in distribution transformer caused by winter lightning," IEEE Trans. Power Del., vol. 21, no. 3, pp. 1600–1606, Jul. 2006.

[3] A. H. Soloot, H. K. Høidalen, and B. Gustavsen, "Influence of the winding design of wind turbine transformers for resonant overvoltage vulnerability," IEEE Trans. Dielectr. Electr. Insul., vol. 22, no. 2.

[4] IEC 61000-4-5:2014+AMD1:2017 CSV Consolidated version – Electromagnetic compatibility (EMC) – Part 4-5: Testing and measurement techniques – Surge immunity test.

[5] T. Abdulahović and T. Thiringer, "Voltage stress in a transformer winding during very fast transients caused by breaker closing event," IEEE Trans. Power Del., vol. 29, no. 4, pp. 1946–1954, Aug. 2014.

[6] P. Akiki, A. Xémard, C. Trouilloud, and J. Chanelière, "Study of high frequency transient overvoltage caused by cable-transformer quarter-wave resonance," Electric Power Syst. Res., vol. 197, 2021.

[7] M. A. Atefi, M. Sanaye-Pasand, and S. Bahari, "Preventing transformer energizing resonant overvoltages using surge arrester temperature rise index and controlled closing method," IEEE Trans. Power Del., vol. 28, no. 2, pp. 998–1006, Apr. 2013.

[8] T. Dionise and S. Johnston, "Surge protection for ladle melt furnaces: LMF transformer terminals were equipped with primary surge protection consisting of surge arresters and RC snubbers," IEEE Ind. Appl. Mag., vol. 21, no. 5, pp. 43–52, Sept.–Oct. 2015.

[9] Zinc oxide RC-Surge Suppressor (ZORC) capacitors, for HV-Motor and Transformers, [Online]. Available: https://www.vishay.com

[10] K. Munji, J. Horne, and J. Ribecca, "Design and validation of pre-insertion resistor rating for mitigation of zero missing phenomenon," in Proc. Int. Conf. Power Syst. Transients (IPST), Seoul, South Korea, Jun. 26–29, 2017.

[11] H. Heiermeier and R. B. Raysaha, "Power testing of preinsertion resistors: Limitations and solution," IEEE Trans. Power Del., vol. 32, no. 4, pp. 1688–1695, Aug. 2017.

[12] L. Zhou, L. Huang, R. Wei, and D. Wang, "A novel lightning overvoltage protection scheme using magnetic rings for transmission line systems," IEEE Trans. Ind. Electron., vol. 70, no. 12, pp. 12872–12882, Dec. 2023.

[13] S. M. Korobeynikov, V. V. Shishkin, A. V. Ponomarev, A. V. Shishkin, and V. V. Zubov, "Suppression of incoming high-frequency overvoltage in transformer coils," IEEE Trans. Power Del., vol. 36, no. 5, pp. 2988–2994, Oct. 2021.

[14] D. Smugała, W. Piasecki, M. Ostrogórska, M. Florkowski, M. Fulczyk, and P. Kłys, "Distribution transformers protection against high frequency switching transients," Przegląd Elektrotechniczny, vol. 88, no. 5a, pp. 296–300, 2012.

[15] D. Smugała, W. Piasecki, M. Ostrogórska, M. Florkowski, M. Fulczyk, and O. Granhaug, "New approach to protecting transformers against high frequency transients – wind turbine case study," Przegląd Elektrotechniczny, vol. 89, no. 10, pp. 186–190, 2013.

[16] D. Smugała, W. Piasecki, M. Ostrogórska, M. Florkowski, M. Fulczyk, and O. Granhaug, "Wind turbine transformers protection method against high-frequency transients," IEEE Trans. Power Del., vol. 30, no. 2, pp. 853–860, 2015.

[17] F. Nasirpour, A. Heidary, M. Ghaffarian Niasar, A. Lekić, and M. Popov, "High-frequency transformer winding model with adequate protection," Electric Power Systems Research, vol. 223, p. 109637, Oct. 2023.

[18] S. Ghasemi, M. Allahbakhshi, B. Behdani, M. Tajdinian, and M. Popov, "Probabilistic analysis of switching transients due to vacuum circuit breaker operation on wind turbine step-up transformers," Electric Power Systems Research, vol. 182, p. 106204, May 2020.

[19] A. Heidary, M. Ghaffarian Niasar, F. Nasirpour, A. Lekić, and M. Popov, "Transformer resonance: Reasons, modeling approaches, solutions," IEEE Access, vol. 11, pp. 58692–58704, 2023.

[20] L. Zhou, L. Huang, R. Wei, and D. Wang, "A novel lightning overvoltage protection scheme using magnetic rings for transmission line systems," IEEE Trans. Ind. Electron., vol. 70, no. 12, pp. 12872–12882, Dec. 2023.

[21] S. Burow, W. Köhler, S. Tenbohlen, and U. Straumann, "Damping of VFTO by RF resonator and nanocrystalline materials," in 2013 IEEE Electrical Insulation Conf. (EIC), Ottawa, ON, Canada, 2013, pp. 439–443.

[22] L. V. Bewley, Travelling Waves on Transmission Lines. Dover, 1963.

[23] E. O. Taylor, Ed., Power System Transients, 1954.

[24] W. Piasecki, G. Bywalec, M. Florkowski, M. Fulczyk, and J. Furgal, "New approach towards very fast transients suppression," in Proc. Int. Conf. Power Syst. Transients (IPST), 2007.

[25] D. Smugała, W. Piasecki, M. Ostrogórska, M. Florkowski, M. Fulczyk, and O. Granhaug, "Very fast transient suppressing device," United States patent US 8,929,048 B2, 2015.

6

MULTI-MODULE SERIES SUPPRESSOR FOR TRANSFORMER RESONANCE OVERVOLTAGE PROTECTION

6.1. Abstract

The large-scale integration of RESs presents significant challenges for modern power grids, particularly with wind farms playing a crucial role in energy generation. However, frequent switching operations during wind farms' (dis)connection and lightning strikes on wind turbines can induce severe transient overvoltages. These FTs pose a serious risk to wind farm substations, potentially compromising the reliability of renewable energy generation. In particular, protecting wind farm transformers from FTs, resonances, and resulting overvoltages is essential for ensuring stable operation. This chapter of the thesis proposes a modular series transient suppressor (MSTS) designed to enhance the protection of wind farm transformers against FTs, thereby improving system reliability. The MSTS consists of multiple resonant circuit modules, including a core, a low-voltage capacitor, and a resistor, connected in series with the transformer. Its operational behaviour is analyzed using analytical methods and validated through simulation studies. Furthermore, experimental testing on a developed MSTS prototype confirms its effectiveness in mitigating transient

This chapter of the thesis is published in the article:
A. Heidary, M. Ghaffarian Niasar and M. Popov, "Multi-module series suppressor for the protection of wind farm transformers against resonance overvoltages," International Journal of Electrical Power & Energy Systems, vol. 172, 2025.

overvoltages in a wind farm transformer model circuit at a 60 kV transient voltage level.

The chapter is structured as follows:

Section 6.2 defines the problem, explains the state-of-the-art solutions, and the research gap
Section 6.3 describes the MSTS configuration, design, and analysis
Section 6.4 focuses on the MSTS simulation in the EMTP platform
Section 6.5 analyzes the MSTS using FEM software.
Section 6.6 examines the features of the MSTS based on a comprehensive experimental test
Section 6.7 discusses the MSTS advantages based on a comparison
Section 6.8 summarizes the findings and conclusions.

6.2. AN OVERVIEW OF TRANSFORMER RESONANCE OVERVOLTAGE AND PROTECTION

Lightning strikes in power systems create FTs that travel through the network, posing risks to power equipment [1]. The increasing use of RESs like wind farms, compact substations, and switching operations in power grids further contributes to frequent FTs [2], [3]. These transients can severely affect wind farm transformers, causing resonance and overvoltage conditions [4], which can damage transformer windings and wind generators. The harmonic content of FTs may resonate with transformer windings, weakening insulation, and increasing failure risks [5].

Protecting wind farm transformers is essential for system reliability [6]. Various protection methods exist, including surge arresters [7], surge capacitors, RC snubbers [8], ZORC devices [9], PIR [10], FDD [11], [12], and chokes [13], [14]. However, these methods have limitations such as voltage constraints, operational delays, and ineffective harmonic filtering. Most solutions do not fully address internal resonance overvoltages, particularly in wind farm transformers [15].

Recent studies have introduced new protection strategies. One approach adds a series suppressor to the transformer coil model, showing promising results [16]. Another method uses a tuned choke with a resonance capacitor on the secondary winding [17]. Research has also explored placing multiple toroid cores on the guard wire of transmission lines, which improved protection [18].

Despite these advancements, an effective device is still needed to provide high impedance over a wide frequency range while withstanding high voltage stress [19].

This chapter proposes a modular series transient suppressor (MSTS) to protect wind farm transformers from fast transients. The MSTS offers:

- Wide frequency coverage,
- High voltage endurance,
- Modular design for scalability,
- Resonance frequency shifting in each module,
- Multilayer core design to prevent saturation.

The MSTS is analyzed using FEM and EMTP simulations. Its effectiveness is further validated through experimental testing.

6.3. MSTS CONFIGURATION, DESCRIPTION, AND ANALYSIS

The MSTS is a protection device installed in series with the wind farm transformer, as shown in Fig. 6.1. Its primary function is to mitigate resonance overvoltages. Acting as a series filter, the MSTS reduces the impact of transient events such as wind generator switching and lightning strikes by attenuating critical frequency components within an acceptable range. The structure and configuration of the MSTS are illustrated in Fig. 6.2.

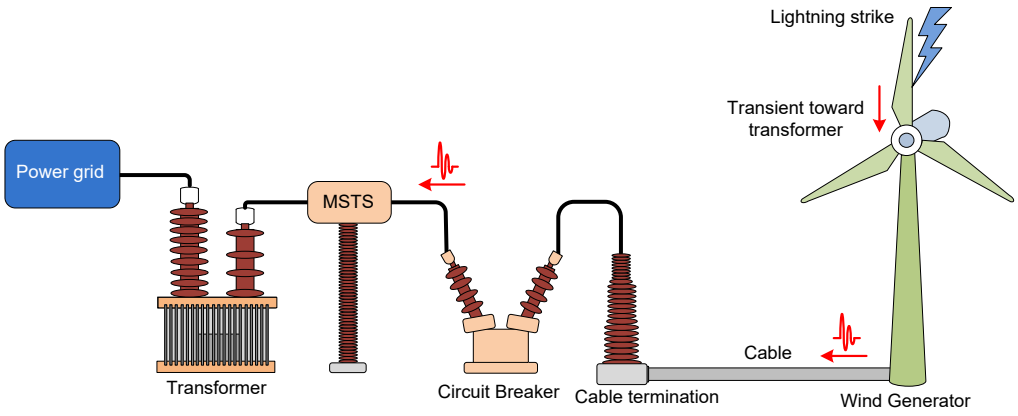


Fig. 6.1. MSTS integration with wind farm transformer substation

As shown in Fig. 6.2(a), the MSTS is a modular device, with each module consisting of:

- A toroid core around a power line cable (acting as a one-turn primary),

- A one-turn secondary winding,
- A resistor (R_s),
- A capacitor (C_s),
- An arrester (Ar).

The key difference between the modules is the capacitance (C_s) on the secondary side, which is adjusted within a specific range to modify the impedance characteristics of each module. In this design, the toroid core is placed around the main conductor of the power line, which serves as the primary turn of the series protection device. The secondary turn connects to a parallel suppressor resistor, resonance capacitor, and arrester for enhanced transient suppression.

1. Fig. 6.2(b) illustrates the overall MSTS circuit installed in series at the wind farm transformer terminal.

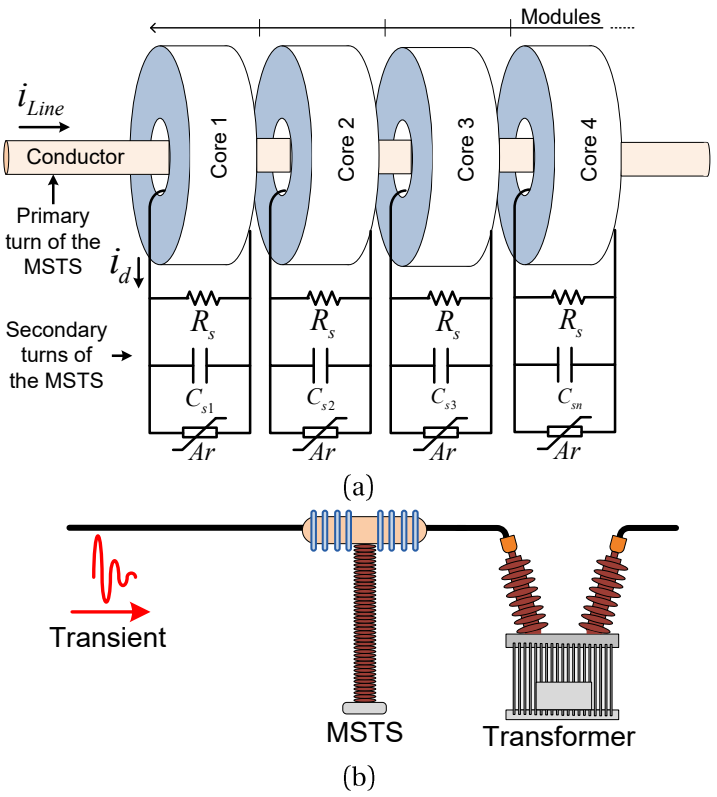


Fig. 6.2. a) MSTS structure, b) configuration in series with a wind farm transformer

The MSTS operation is analyzed in two scenarios:

1. Nominal frequency operation,
2. Response to transient signals

A. MSTS operation in the power grid's normal operation

During nominal power grid operation, no transient signals are present. Therefore, the low-frequency equivalent of the coupled inductor can be used to analyze the MSTS operation. An equivalent circuit is shown in Fig. 6.3.

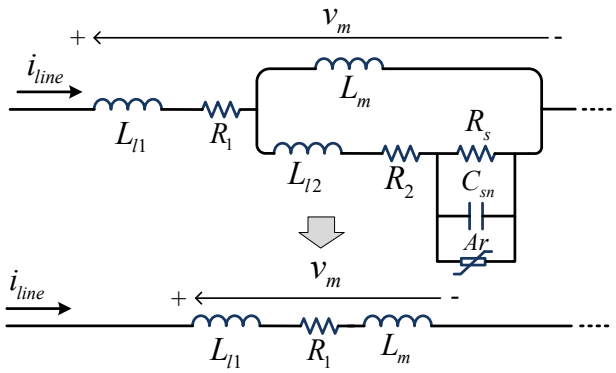


Fig. 6.3. Equivalent circuit of an MSTS module for nominal frequencies

The impedance value of the secondary circuit (including the resistor in the range of kilohms and the capacitor in the range of nanofarads) is much larger than the magnetization inductance L_m. Therefore, the equivalent circuit is simplified, encompassing the leakage inductance of a short piece of power cable or line that passes through the core, the MSTS module's magnetization inductance, and the cable section's resistance that passes through the cores. By assuming (6-1), the impedance of the MSTS in series with a line can be expressed by equation (6-2), where n refers to the number of modules.

$$j\omega L_m << R_2 + j\omega L_{l2} + \left(R_s \parallel \frac{1}{j\omega C_s} \parallel R_{Ar} \right) \tag{6-1}$$

$$Z_m = n\left(R_1 + j\omega(L_{l1} + L_m)\right) \tag{6-2}$$

The impedance Z_m of the MSTS, as obtained by (6-2), is a small value at power frequency. Therefore, the voltage drop computed by (6-3) can be ignored. The impedance is roughly similar to the cable impedance (here, the impedance is likely to be the impedance of several meters of the line), and the voltage drop is nearly zero.

$$V_m = I_{line}.n\left(R_1 + j\omega(L_{l1} + L_m)\right) \tag{6-3}$$

In addition, the power loss of the MSTS Ploss is negligible during normal operations, as computed by (6-4).

$$P_{loss} = nR_1\left(I_{line}\right)^2 \tag{6-4}$$

B. MSTS operation during transient oscillations

In this section, it is assumed that the transient signal contains high-frequency oscillations passing through the MSTS. Therefore, the high-frequency equivalent circuit of a module of the MSTS is considered. This equivalent circuit is illustrated in Fig. 6.4.

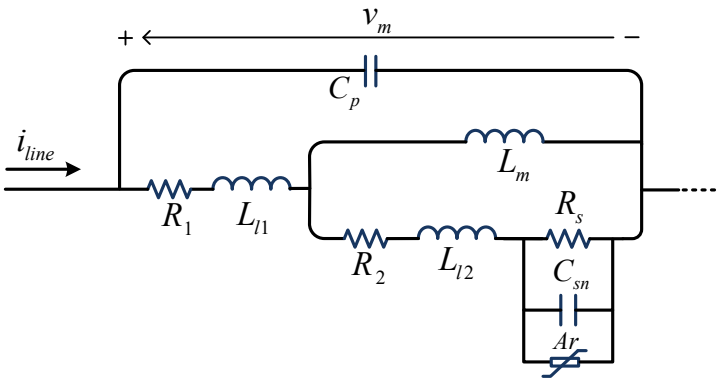


Fig. 6.4. MSTS High-frequency equivalent model

The circuit has several resonance frequencies depending on the value of the connected capacitor (C_{sn}) to the secondary side of each module of MSTS. The equivalent circuit of one module of MSTS is illustrated in Fig. 6.4. The notable feature of the MSTS is its ability to provide significant overall impedance against critical harmonics of transient signals, where its impedance is the sum of the module's impedance around its resonance point. This resonance frequency, which provides exceptionally high impedance in series with the wind farm transformer, is due to the resonance occurring between the magnetizing inductance L_m of each module and the capacitances (C_{sn}) of the secondary side of each module of the MSTS. This resonance frequency is tunable by changing the value of the external capacitance in the secondary circuit. The impedance of the MSTS is computed as presented in (6-5), where m refers to the number of modules needed to develop the MSTS.

$$Z_m = \sum_{m=1}^{n} \left(\frac{1}{\omega C_p} \right) \| \left(R_1 + j\omega L_{l1} + \left(j\omega L_m \| \left(R_2 + j\omega L_{l1} + \left(\frac{1}{\omega C_{sn}} \| R_s \right) \right) \right) \right) \quad (6\text{-}5)$$

By carrying out the frequency sweep calculation for $\omega=2\pi f$ between the nominal frequency (f=50 Hz) and the maximum studied frequency in (6-5), the frequency response of MSTS can be obtained during the frequency sweep domain. Furthermore,

the power loss of the connected resistors at the secondary side of MSTS modules can be computed by (6-6), and the total dissipated energy W_m in the resistor by (6.7).

$$P_{loss} = \frac{n\left(v_s(t)\right)^2}{R_s} \tag{6-6}$$

$$W_m = n\int_0^t \frac{\left(v_s(t)\right)^2}{R_s} dt \tag{6-7}$$

where t refers to the duration of the transient signal and v_s is the secondary-side voltage, which is the sum of the secondary voltage of each mode as shown in (6-8).

$$v_s = v_{m1} + v_{m2} + \ldots + v_n \tag{6-8}$$

C. *Parameters calculation of MSTS*

The most critical data for designing the parameters of the MSTS is the wind farm transformer's critical resonance frequency range and its impedance around the resonance frequency. The main point is that the impedance of MSTS in this frequency range should be comparable to the wind farm transformer impedance, suppressing the voltage magnitude at the wind farm transformer terminal. The algorithm of the MSTS is designed in Fig. 6.5.

In this algorithm, the first step is to perform a wind farm transformer impedance sweep measurement starting from the grid frequency. This sweep identifies the resonance point and the wind farm transformer impedance (Z_{tr}) at the critical resonance frequency. The character of the wind farm transformer model is illustrated in Fig. 6.5. This simplified model reflects the wind farm transformer's critical resonance based on the wind farm transformer RLC disk model, which is elaborated on in [16]. Then, by considering the resonance capacitor (C_{sn}) specifications based on the constraints of sizing and voltage, the core cross-section is computed to satisfy the requirement $Z_m \geq Z_{tr}$. In the next step, the core cross-section is recalculated based on the nominal current of the power line to ensure that it operates well below the core saturation region.

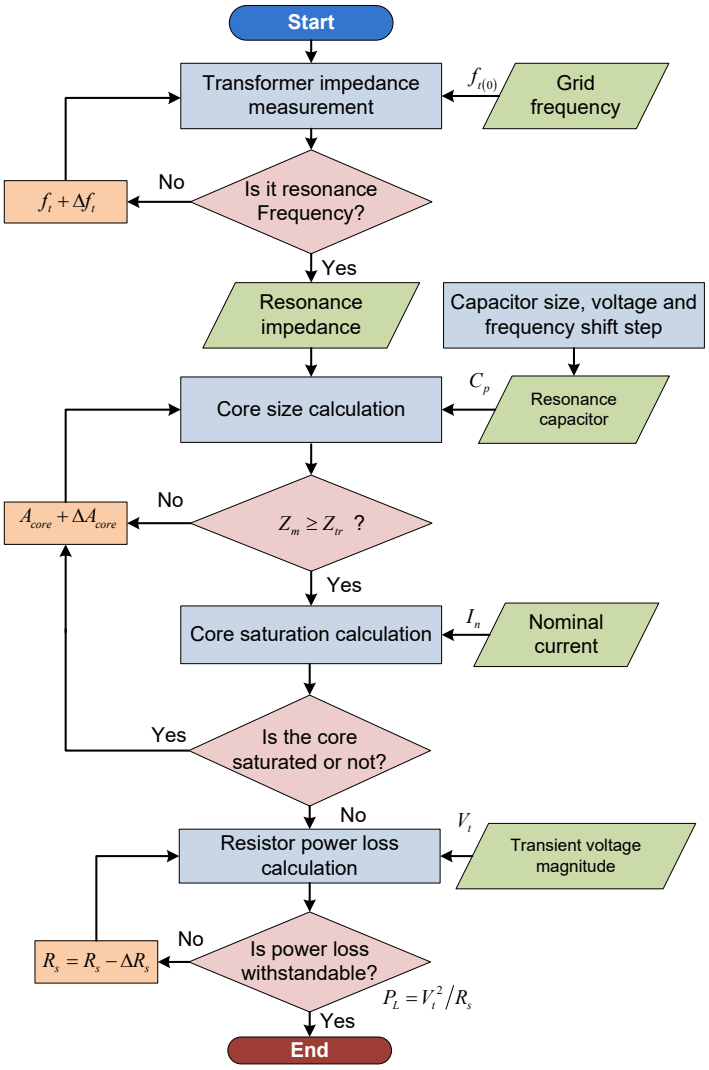


Fig. 6.5. The MSTS design algorithm

Ultimately, the secondary-connected resistor R_2, acting as a damper, is selected by considering the maximum possible power dissipation $p_{loss}(max)$. The arrester in the secondary circuit does not engage during normal operation; its primary function is to protect the resonance capacitor from overvoltage, with its operating voltage set equal to the capacitor's maximum voltage.

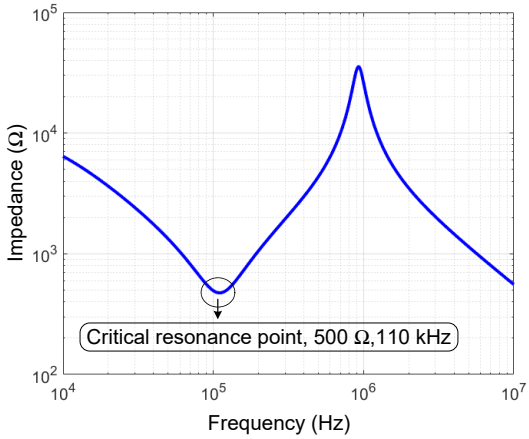


Fig. 6.6. Harmonic impedance of the considered equivalent circuit of the transformer

6.4. MSTS SIMULATION IN EMT SOFTWARE

Once the values are met, the model of the designed MSTS, as shown in Fig. 6.4, is implemented in EMTP for further evaluation. The simulated MSTS consists of 10 modules, with the characteristics of each module group as shown in Table 6.1. The main parameters are calculated based on the algorithm depicted in Fig. 6.5. The wind farm transformer's resonance frequency spans from 100 to 120 kHz, with a resonance impedance (Z_{tr}) of approximately 500 Ω. The selected resonance capacitor of the MSTS secondary side (C_{sn}) varies from 10 to 60 nF at 5 kV. The magnetization inductance (L_m) and secondary resistor (R_s) can be determined based on the equivalent circuit to satisfy the constraint, which is $Z_m \geq Z_{tr}$. The remaining parameters are functions of the module geometry, calculated using the method described in [18].

Table 6.1. Parameters and features of the simulated MSTS

Module	L_m	L_{l1}	L_{l2}	R_1	R_2	R_S	C_{sn}	C_p
1,2	72 µH	0.25 µH	0.2 µH	4 mΩ	8 mΩ	98 Ω	15 nF	18 pF
3,4,5	72 µH	0.25 µH	0.2 µH	4 mΩ	8 mΩ	98 Ω	22 nF	18 pF
6,7,8	72 µH	0.25 µH	0.2 µH	4 mΩ	8 mΩ	98 Ω	33 nF	18 pF
9,10	72 µH	0.25 µH	0.2 µH	4 mΩ	8 mΩ	98 Ω	50 nF	18 pF

As shown in Table 6.1, the studied MSTS consists of ten modules, with some modules sharing identical parameters to enhance the overall impedance of the MSTS near the resonance frequencies of the modules. The geometry data of the MSTS is presented in Table 6.2, and the associated parameters are provided in Fig. 6.7.

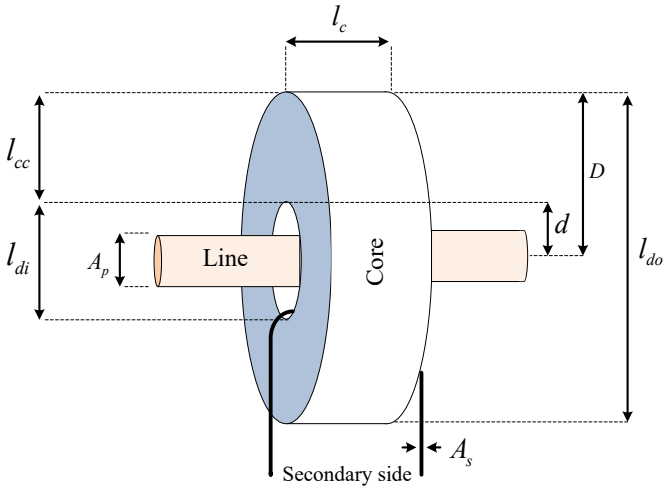


Fig. 6.7. MSTS module geometry

Table 6.2. Parameters of the core MSTS module

Parameter	description	Value
l_c	Length of the core	25 mm
l_{cc}	Length of the core side	110 mm
l_{di}	The inner diameter of the core	20 mm
l_{do}	The outer diameter of the core	130 mm
D	The outer radius of the core	65 mm
d	The inner radius of the core	10 mm
A_p	Primary wire cross-section	2 mm^2
A_s	Secondary wire cross-section	1 mm^2
μ_c	Magnetic permeability	4000
B_m	Maximum magnetic flux density	1.2 T

A. Frequency sweep simulation of MSTS

The simulation is carried out for the frequency response of the MSTS over the studied frequency range. This simulation aims to extract the characteristics of the MSTS across a wide range of frequencies (50 Hz to 10 MHz) to assess its impact on the wind farm transformer's critical resonance frequency (100- 120 kHz). The resulting impedance sweep curves are presented in Fig. 6.8.

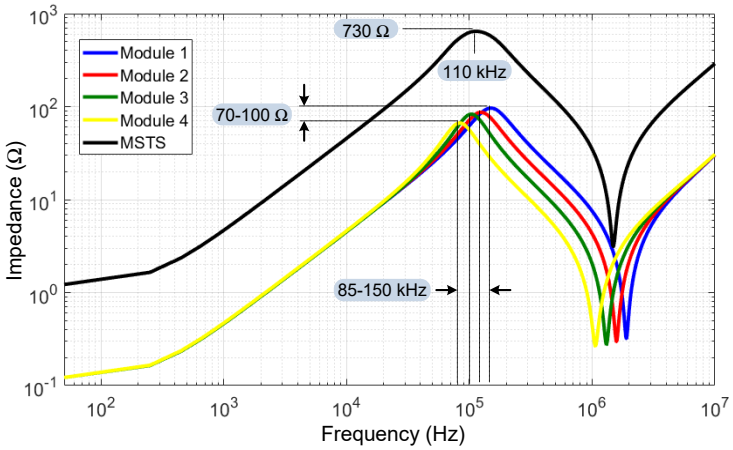


Fig. 6.8. Impedance character of MSTS simulated model

The MSTS terminal FS shows that the impedance of the MSTS exceeds 500 Ω within the 80-180 kHz range, peaking at nearly 800 Ω (black curve, Fig. 8). This peak results from the combined effects of each module within the MSTS. The system's overall resonance occurs around 110 kHz, while the individual resonance frequencies of modules 1, 2, 3, and 4 are 85 kHz, 101 kHz, 120 kHz, and 150 kHz, respectively. At these resonance points, the impedance of each module ranges between 70 and 100 Ω. Based on the MSTS design specifications, the second resonance point, where the impedance is minimized, occurs above 1 MHz. This frequency is far from the resonance point of the wind farm transformer and does not affect its operational frequency range. The designed MSTS matches the resonance frequency of the wind farm transformer well.

B. Impulse time domain simulation of MSTS

The simulation test setup consists of an MSTS connected in series to an equivalent circuit of a transformer (the character is shown in Fig. 6.6) with a resonance frequency of 105 kHz and a resonance impedance of 500 Ω , as shown in Fig. 6.2(b). The simulation evaluates the MSTS's performance in limiting the transient voltage's frequency content at the operating frequency and suppressing the overall magnitude of the transient signal. The excitation source is a lightning transient signal, with its specifications shown in Fig. 6.9 as the blue curve. Following the excitation, the black curve illustrates the voltage drop across the MSTS, while the red curve shows the voltage at the wind farm transformer terminal.

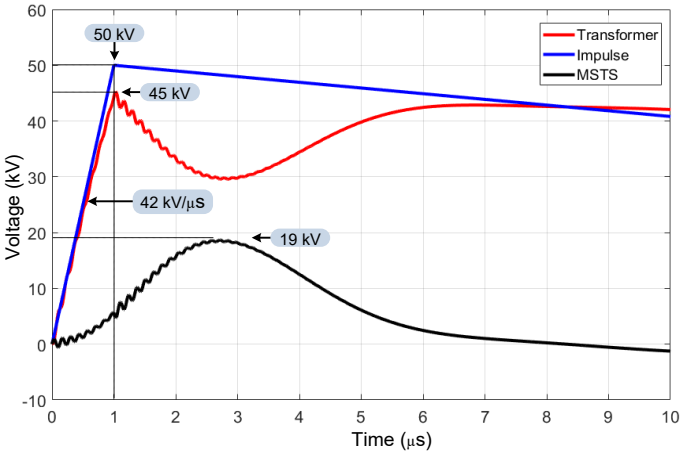


Fig. 6.9. Impulse time domain simulation of protected wind farm transformer with MSTS

As shown in Fig. 6.9, the MSTS demonstrates a significant voltage drop in response to the impulse transient. The effects are evident in the reduced peak voltage and overall voltage magnitude at the wind farm transformer terminal and in the rate of RRV. Specifically, the peak voltage at the wind farm transformer terminal is 45 kV, which is 5 kV lower than the 50 kV peak of the impulse source, while the RRV is reduced to 42 kV/μs from the original value, which is 50 kV/μs. The peak voltage across the MSTS, acting as a suppressor, also reaches 19 kV. This simulation confirms that the designed MSTS effectively reduces the magnitude and RRV of the transient signal at the wind farm transformer terminal, thereby eliminating the magnitude of the harmonic content.

6.5. MSTS MAGNETIC FLUX FIELD STUDY

This section discusses the distribution of the magnetic flux density in the MSTS core. The saturation effect is addressed, which is a critical concern for series-connected inductors [20]. The primary challenge lies in the non-uniform distribution of the magnetic flux density in the toroidal core, causing saturation in areas near the primary winding; as such, the performance of the MSTS core is reduced. A new solution to mitigate this phenomenon is to utilize a multilayer core instead of a unified toroid core. This multilayer design constrains the magnetic flux distribution, ensuring uniformity and preventing core saturation.

The effectiveness of this solution is demonstrated through simulations by using FEM analysis. The redesigned MSTS's inductance is also evaluated to confirm the improvements. In the first step, the geometry of the MSTS module is modeled by FEM, with meshing applied accordingly. Next, the mathematical constraints governing each

core layer's characteristics are discussed. Finally, the magnetic flux distribution and saturation status are analyzed, as illustrated in Fig. 6.10.

Geometry design and constraints of MSTS:
The maximum flux density of the core is a key constraint for ensuring the proper operation of the designed MSTS. Typically, commercially available cores operate within a range of 0.1 T to over 2 T. For the MSTS design, the maximum magnetic flux density of the cores is set at 1.2 T. Additionally, the required magnetization inductance for each module, with one turn as the primary winding, is 72 μH, as shown in Table 6.1. Consequently, the overall core cross-section can be determined based on the magnetic permeability. The core specification in the linear state is calculated as follows (where L_{uc} represents the inductance of the module when the core is uniform).

$$L_{uc} = \frac{\mu_{uc} l_c}{\pi}\left(\frac{D-d}{D+d}\right) \tag{6-9}$$

In (6.9), μ_{uc} represents the magnetic permeability of the unified core, and other geometrical parameters are defined in Fig. 6.5 and Table 6.2. To improve the magnetic distribution in the unified core module, the inductance of the multilayer scheme module should match that of the unified core module. However, the geometry, number of layers, and magnetic permeability of the cores should be adjusted. The next constraint is presented in (6.10), which shows that the inductance of the unified core module is equal to the summation of inductances generated with each core layer (L_{c1}, L_{c2}, and L_{c3}). Here, the number of layers is considered to be three.

$$L_{uc} = L_{c1} + L_{c3} + L_{c3} \tag{6.10}$$

The geometry of the multilayer modules is depicted in Fig. 6.10.

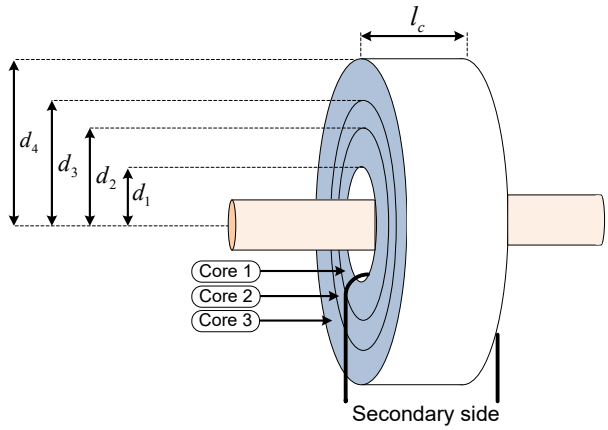


Fig. 6.10. Geometry of a multilayer core module

By considering the geometry parameters, the inductance of each core is calculated by (6-11), (6-12), and (6-13), ensuring that all three inductances are equal, as shown by (6-14).

$$L_{c1} = \frac{\mu_{c1} l_c}{\pi}\left(\frac{d_2 - d_1}{d_2 + d_1}\right) \tag{6-11}$$

$$L_{c2} = \frac{\mu_{c2} l_c}{\pi}\left(\frac{d_3 - d_2}{d_3 + d_2}\right) \tag{6-12}$$

$$L_{c3} = \frac{\mu_{c3} l_c}{\pi}\left(\frac{d_4 - d_3}{d_4 + d_3}\right) \tag{6-13}$$

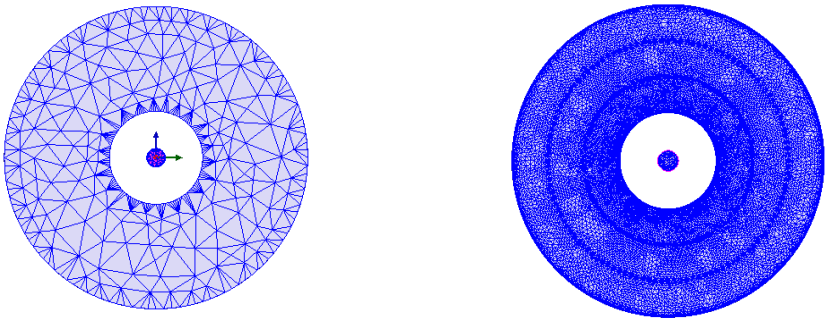
$$L_{c1} = L_{c2} = L_{c3} \tag{6-14}$$

To satisfy equation (6-14), condition (6-15) must be met, while for the geometry, the constraint expressed by (6-16) should hold, where the length of each module core is (l_c) the same.

$$\mu_{c1} < \mu_{c2} < \mu_{c3} \tag{6-15}$$

$$\left(\frac{d_2 - d_1}{d_2 + d_1}\right) > \left(\frac{d_2 - d_1}{d_2 + d_1}\right) > \left(\frac{d_2 - d_1}{d_2 + d_1}\right) \tag{6-16}$$

With constraints (6.9), (6.14), and (6.15), geometries of unified and multilayer cores are designed and meshed in a FEM model, as illustrated in Fig. 6.11 (a) and (b). The primary objective is to compare the unified core and the multilayer core modules in terms of magnetic flux density distribution and saturation behavior.



(a) (b)

Fig. 6.11. Applied FEM meshes for module geometry, a) unified core, b) multilayer core

In this part, the magnetic flux analysis focuses on the two described configurations: the unified core and the multilayer core. Both concepts for magnetic flux density are plotted and presented in Fig. 6.12 (a) and (b). Table 6.2 presents the unified core concept features, and the multilayer simulated concept data is given in Table 6.3.

Table 6.3. Magnetic and geometric parameters of the multilayer MSTS module

Parameter	description	Value
l_c	Length of the core	25 mm
d_1	The inner radius of the core 1	10 mm
d_2	The outer radius of the core 1	25 mm
d_3	The outer radius of the core 2	50 mm
d_4	The outer radius of the core 3	65 mm
μ_{c1}	Magnetic permeability (core 1)	2500
μ_{c2}	Magnetic permeability (core 2)	4000
μ_{c3}	Magnetic permeability (core 3)	5000
B_m	Maximum magnetic flux density	1.2 T

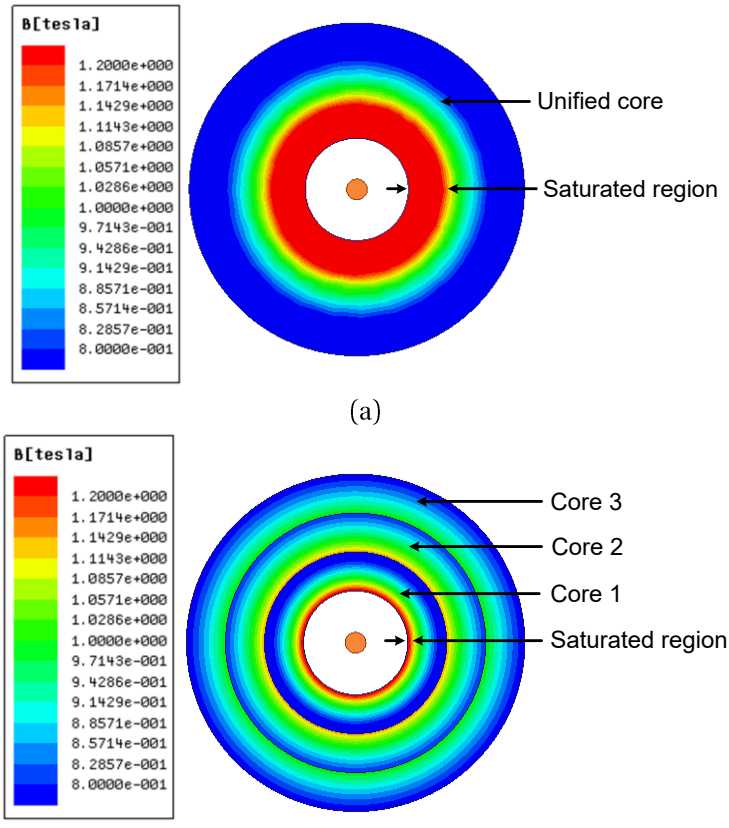


Fig. 6.12 a) Magnetic flux density in unified core, b) Magnetic flux density in multilayer core

As shown in Fig. 6.12(a), when the primary conductor of the single core module is excited with 100 A current (consistent with the designed scale of the prototype), a significant portion of the toroidal core near the wire becomes saturated. This saturation affects approximately 25 mm of the core, significantly reducing each module's performance in the MSTS system. The inductance of the module before being saturated is approximately 72 μH, and it drops to 42 μH after saturation.

A multilayer scheme was implemented to address this issue, utilizing three layers to distribute the magnetic flux density. The data for each layer is presented in Table 6.3. As shown in Fig. 6.12 (b), the thickness of the saturation region near the wire is reduced to approximately 1 mm. The inductance of each module before saturation remains around 72 μH, and after saturation, it only decreases slightly to 71 μH. Therefore, the multilayer design of the MSTS modules significantly improves the device's performance and effectively manages saturation concerns in this protection device.

6.6. MSTS EXPERIMENTAL VALIDATION

This section aims to comprehensively evaluate the technical performance of the MSTS device for the frequency and time domains. The results of the designed MSTS closely align with those of the simulated model, with the data used from Tables 6.1 and 6.3, respectively. The laboratory test results are divided into two scenarios, as follows.

A. Frequency sweep evaluation

In the first test scenario, the impedance of the designed MSTS is measured using the frequency sweep method. A VNA, model Omicron Bode 100, is employed for the measurements, covering a frequency range from 50 Hz to 10 MHz. The test setup, illustrated in Fig. 6.13, is designed to take into account the frequency response impedance of the MSTS.

In the laboratory test, the impedance of each module and the MSTS terminal is measured, with the results shown in Fig. 6.14. It can be seen that the maximum impedance of the MSTS reaches 700 Ω near the resonance frequency of 110 kHz. Additionally, the first resonance of each module occurs between 85 and 150 kHz, with peak impedance values ranging from 70 to 100 Ω. These experimental results are in line with the simulated results obtained using the EMTP MSTS model, as presented in Fig. 6.8.

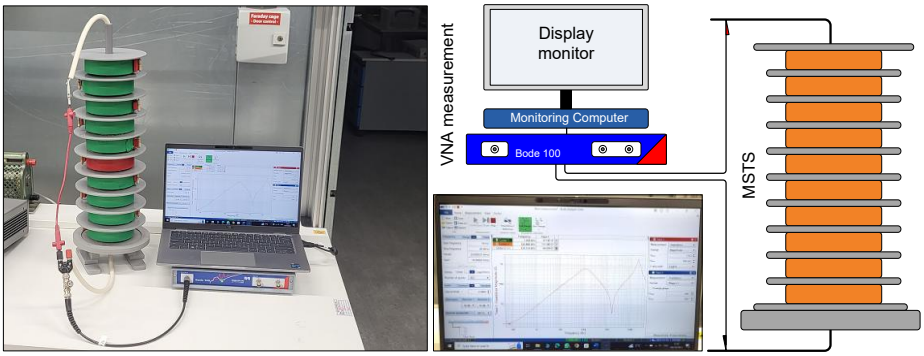


Fig. 6.13. Impedance frequency response measurement setup of MSTS

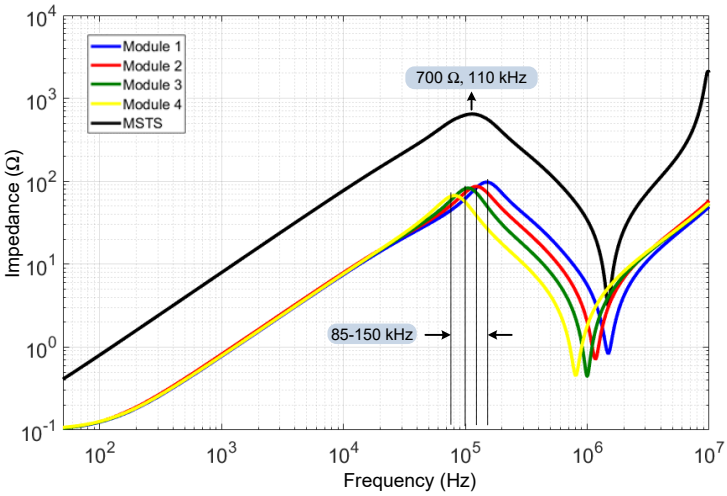


Fig. 6.14. Harmonic impedance measurement results of MSTS

B. High voltage impulse test evaluation

The MSTS impulse evaluation test setup is presented in Fig. 6.15. The designed MSTS is connected in series to the wind farm transformer terminal (which is represented by an RLC circuit) and an impulse generator. The resonance frequency of the wind farm transformer model is considered to be 110 kHz.

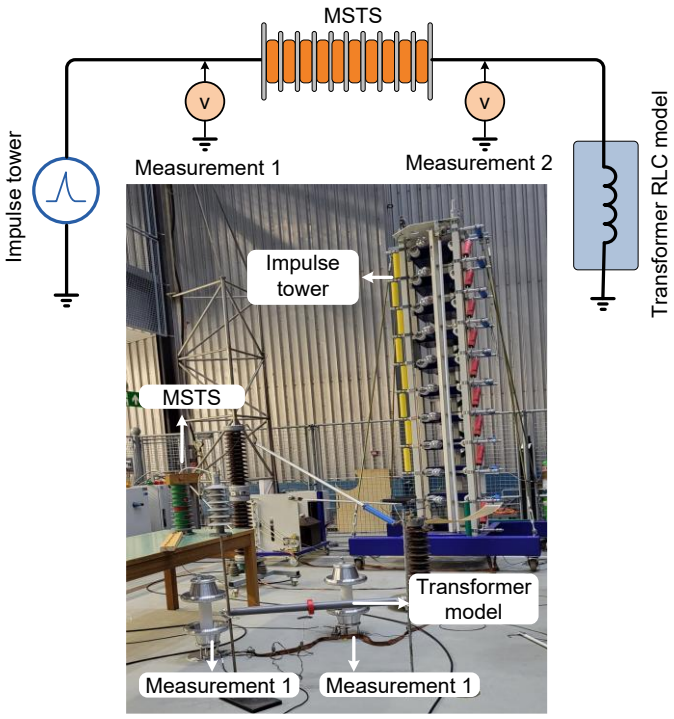


Fig. 6.15. Impulse HV test setup of MSTS

Furthermore, the maximum voltage of the impulse tower is 60 kV, while reaching this maximum magnitude within 1.2 µs declines to 50% of the maximum magnitude of the transient peak magnitude in 50 µs. This setup consists of two fast measurement high-voltage probes (50 MHz) based on RC voltage division. The first probe is connected to an impulse generator terminal, and the second probe is connected to the wind farm transformer terminal. Hence, by subtracting the measured voltages, the voltage drop of the MSTS can be determined.

The results of the laboratory test setup are shown in Fig. 6.16. This plot includes the impulse generator voltage (blue curve), wind farm transformer terminal voltage (red curve), and the voltage drop across the MSTS (black curve). Based on the obtained results, the peak voltage at the wind farm transformer decreases from 60 kV to 42 kV, with a voltage decline rate of 40 kV/µs. This reduction is due to the voltage drop across the MSTS, which reaches a peak value of 20 kV. The experimental results are validated by EMTP simulation, as shown in Fig. 6.9.

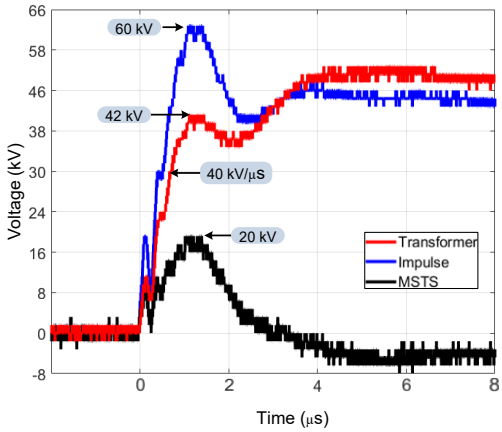


Fig. 6.16. Impulse test result of MSTS

From the perspective of the voltage drop across the MSTS structure, it provides adequate wind farm transformer protection at transmission voltage levels. Despite the MSTS being a prototype design, it can withstand a voltage drop of 60 kV, considering its modular design. This voltage is distributed across the ten modules of the MSTS, and by assuming a nearly linear distribution, each module experiences approximately 6 kV. For this, if the voltage level is suitable, it is straightforward to design the necessary insulation. Additionally, increasing the number of modules for higher voltage levels is possible, which is convenient for tuning the MSTS for different protection levels.

By applying FFT to both the impulse generator signal and the wind farm transformer voltage at its resonance frequency, it is evident that the MSTS effectively suppresses transient signals near the transformer's critical resonance frequency. As shown in Fig. 6.17, the frequency content around this resonance point, within the MSTS's operating range, is reduced by approximately 70%. This corresponds to the frequency where the MSTS provides its highest impedance, demonstrating its effectiveness in mitigating harmful transients. This frequency-based analysis confirms the MSTS's role as a reliable protection device for wind farm transformers.

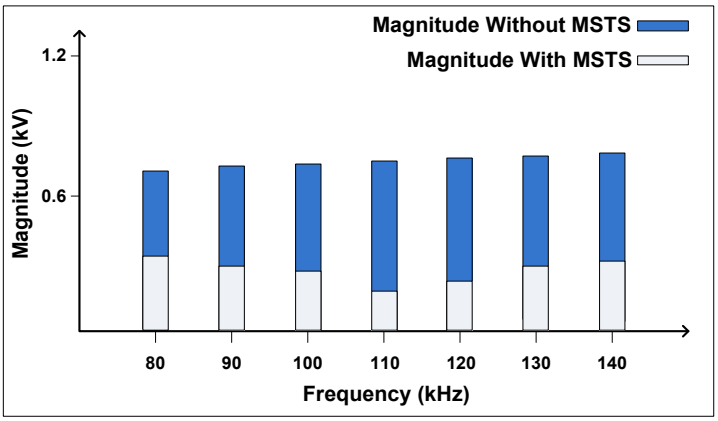


Fig. 6.17. Harmonic content of wind farm transformer voltage with and without the MSTS operation

6.7. MSTS ADVANTAGES DISCUSSION BASED ON COMPARISON

To briefly discuss the overall features provided by the MSTS, the following points should be highlighted:

- The MSTS is a viable solution for protecting wind farm transformers against transient voltage signals. This issue is resolved because of its modular design, which makes it straightforward to withstand higher voltage by distributing it across the series modules.
- The MSTS can be tuned within a wide frequency range to protect the wind farm transformer around the critical resonance frequency. This feature is provided by using a frequency shift for each MSTS module by using secondary resonance capacitors.
- The advantage of MSTS is the multilayer design of the MSTS core; the magnetic flux is distributed and unified on the core, resulting in better performance of the MSTS, which is far from the saturation condition on the core.

The discussed features have been proven throughout this study. To clarify the advantages of the designed MSTS, Table 6.4 compares the features provided by the MSTS and the well-known protective choke [13], [14] and surge arrester specifications [21], which are used as a wind farm transformer series protection device against transients.

Table 6.4. Comparison of MSTS features

Features	MSTS	Choke [13]-[14]	Arrester [21]
Connection type	Series	Series	Parallel
Operation frequency range	Tunable in a wide range	Above 1 MHz	No frequency dependency
Provided impedance	This can be adjusted by the number of modules	Less than 1 kΩ	Low shunt impedance only in the case of overvoltage
Saturation possibility	This can be avoided by the multilayer design of the core	Mostly possible	No ferromagnetic component
Voltage level	Both the distribution and transmission systems	Distribution system	Both the distribution and transmission systems
Wind farm transformer internal resonance protection	Yes	Yes	No
Need for grounding	No	No	Yes

As shown in Table 6.4, the MSTS operates over a wider frequency range and withstands higher voltage levels than traditional protective chokes. Its adjustable impedance and modular multilayer core design prevent saturation features not typically found in conventional chokes, giving it a significant operational advantage.

Compared to surge arresters, the MSTS offers critical resonance frequency filtering, protecting the wind farm transformer from both terminal and internal resonance, which can cause overvoltages. In contrast, surge arresters allow resonance-induced overvoltages to occur before mitigating them by diverting large currents to the ground.

6.8. Conclusion

This chapter introduces the MSTS as an advanced protection device for wind farm transformers in modern power grids. Designed to mitigate transient overvoltages, the MSTS features a modular architecture, adjustable resonance-shifting capacitors, and multilayer cores, significantly enhancing its ability to suppress harmful transient signals.

Simulation and experimental results confirm the MSTS's effectiveness, demonstrating:

- A 30% reduction in peak transient signals,

- A 34% decrease in voltage rise rate,
- A 70% suppression of harmonic content at critical resonance frequencies.

The modular design enables high-voltage endurance and simplifies installation and maintenance. Additionally, the multilayer core structure prevents magnetic saturation, ensuring stable performance across a wide range of operating conditions. Unlike conventional protection methods, such as surge arresters and chokes, the MSTS provides targeted resonance frequency filtering, addressing both terminal and internal resonance effects before they lead to severe overvoltages.

Its ability to integrate with renewable energy-based grids makes it a promising solution for future smart power networks, where transient disturbances pose increasing challenges. By offering a scalable, efficient, and high-performance approach to transient suppression, the MSTS represents a step forward in enhancing the reliability and resilience of modern wind power systems.

References

[1] G. C. Paap, A. A. Alkema, and L. Van der Sluis, "Overvoltages in power transformers caused by no-load switching," IEEE Trans. Power Del., vol. 10, no. 1, pp. 301–307, Jan. 1995.

[2] Y. Yasuda, N. Uno, H. Kobayashi, and T. Funabashi, "Surge analysis on wind farm when winter lightning strikes," IEEE Trans. Energy Convers., vol. 23, no. 1, pp. 257–262, Mar. 2008, doi: 10.1109/TEC.2007.905361.

[3] A. H. Soloot, H. K. Høidalen, and B. Gustavsen, "Influence of the winding design of wind turbine transformers for resonant overvoltage vulnerability," IEEE Trans. Dielectr. Electr. Insul., vol. 22, no. 2, pp. 1250–1257, Apr. 2015.

[4] T. Abdulahović and T. Thiringer, "Voltage stress in a transformer winding during very fast transients caused by breaker closing event," IEEE Trans. Power Del., vol. 29, no. 4, pp. 1946–1954, Aug. 2014.

[5] P. Akiki, A. Xémard, C. Trouilloud, and J. Chanelière, "Study of high frequency transient overvoltage caused by cable-transformer quarter-wave resonance," Electric Power Syst. Res., vol. 197, 2021.

[6] M. Firouzi and G. B. Gharehpetian, "Improving fault ride-through capability of fixed-speed wind turbine by using bridge-type fault current limiter," IEEE Trans. Energy Convers., vol. 28, no. 2, pp. 361–369, Jun. 2013.

[7] A. Heidary, M. G. Niasar, M. Popov, and A. Lekić, "Transformer resonance: Reasons, modeling approaches, solutions," IEEE Access, vol. 11, pp. 58692–58704, 2023.

[8] T. Dionise and S. Johnston, "Surge protection for ladle melt furnaces: LMF transformer terminals were equipped with primary surge protection consisting of surge arresters and RC snubbers," IEEE Ind. Appl. Mag., vol. 21, no. 5, pp. 43–52, Sept.–Oct. 2015.

[9] Zinc oxide RC-surge suppressor (ZORC) capacitors, for HV-motor and transformers. [Online]. Available: https://www.vishay.com
[10] K. Munji, "Design and validation of pre-insertion resistor rating for mitigation of zero missing phenomenon," in Proc. Int. Conf. Power Syst. Transients (IPST2017), 2017, pp. 26–29.
[11] H. Heiermeier and R. B. Raysaha, "Power testing of preinsertion resistors: Limitations and solution," IEEE Trans. Power Del., vol. 32, no. 4, pp. 1688–1695, Aug. 2017.
[12] S. M. Korobeynikov, S. I. Krivosheev, S. G. Magazinov, V. A. Loman, and N. Ya, "Suppression of incoming high-frequency overvoltage in transformer coils," IEEE Trans. Power Del., vol. 36, no. 5, pp. 2988–2994, Oct. 2021.
[13] D. Smugała, "Distribution transformers protection against high frequency switching transients," Przegląd Elektrotech. (Electrical Review), vol. 88, no. 5a, 2012.
[14] D. Smugała, W. Piasecki, M. Ostrogórska, M. Florkowski, M. Fulczyk, and O. Granhaug, "New approach to protecting transformers against high frequency transients – wind turbine case study," Przegląd Elektrotechniczny, vol. 89, no. 10, pp. 186–190, 2013.
[15] D. Smugała, W. Piasecki, M. Ostrogórska, M. Florkowski, M. Fulczyk, and O. Granhaug, "Very fast transient suppressing device," U.S. Patent 8,929,048 B2, Jan. 6, 2015.
[16] F. Nasirpour, A. Heidary, M. G. Niasar, and M. Popov, "High-frequency transformer winding model with adequate protection," Electric Power Syst. Res., vol. 223, pp. 109637, 2023.
[17] A. Heidary, M. Ghaffarian Niasar, and M. Popov, "Comprehensive evaluation of toroid ring core parallel inductor and resistor as a transformer protection device," IEEE Trans. Circuits Syst. I: Regul. Pap., vol. 71, no. 9, pp. 4298–4308, Sep. 2024.
[18] L. Zhou, L. Huang, R. Wei, and D. Wang, "A novel lightning overvoltage protection scheme using magnetic rings for transmission line systems," IEEE Trans. Ind. Electron., vol. 70, no. 12, pp. 12872–12882, 2023.
[19] W. Piasecki, G. Bywalec, M. Florkowski, M. Fulczyk, and J. Furgal, "New approach towards very fast transients suppression," in Proc. IPST, 2007.
[20] A. Heidary, M. G. Niasar, and M. Popov, "Series magnetic coupled reactor saturation considerations for high voltage AC and DC power systems," Int. J. Electr. Power Energy Syst., vol. 158, pp. 109909, 2024.
[21] Y. Zhang, Q. Yang, S. Xie, and C. Zhang, "Mechanism and application of arrester block voltage division to lightning transient voltage monitoring in substation transformers," IEEE Trans. Electromagn. Compat., vol. 61, no. 3, pp. 689–696, Jun. 2019.

7

INTRODUCTION OF FUTURE GRIDS' TRANSFORMER PROTECTION TRANSIENT SUPPRESSORS

7.1. ABSTRACT ON FUTURE PROTECTION DEVICES

Various transient phenomena regularly affect power system equipment, resulting in resonance effects and overvoltages. Transient phenomena will increase by extending the power systems and integrating modern electronic-based converters and renewable generators. Transients pollute the power system with numerous harmonics, causing transformer resonance, which may damage them by causing severe overvoltages. Indeed, the connection of the transformer with cables and renewable generators exacerbates the overvoltage threat.

Some conventional protection methods, such as surge arresters or chokes, can safeguard transformers against transient overvoltages. Several novel protection approaches, such as PAIR, R-PIR, and MSTS, were introduced and comprehensively analyzed in the previous chapter. This chapter advances further by presenting additional protection methods for transformers against transient overvoltages, focusing on innovative concepts with a potential application in future power systems. The proposed novel protection concepts are as follows:

- The cable shield-connected grounding reactor
- Series-parallel connected transient suppressor
- Permanent magnet-based reactor transient suppressor

The first protection device, the shield-connected grounding reactor (SCGR), is a reactor designed to safeguard cable-integrated transformers against transient and resonance overvoltages. The device is based on a ferrite core and incorporates an air-gap reactor connected between the cable shield and ground at the transformer terminal. The design aims to establish a series resonance from the cable core to ground by appropriately selecting the shield capacitance and reactor inductance to target the critical transformer resonance frequency. In this way, the device suppresses high-frequency components propagating along the cable core and redirects them to ground, effectively preventing resonance excitation in the transformer.

The second protection scheme, series parallel connected transient suppressor (SPTS), consists of a toroidal ring core with two conductors passing through it, forming the primary and secondary turns. The primary turn corresponds to the main line conductor, while the secondary turn is the cable shield, which forms an RC circuit grounded at one end. This arrangement produces a counteracting voltage against the transient signal, thereby reducing its magnitude and limiting its impact on the transformer.

The third protection method, permanent magnet transient suppressor (PMTS), is based on a series of reactors incorporating permanent magnets. Connected in series with the transformer, each reactor integrates a permanent magnet within its core. This configuration allows the device to selectively suppress either the positive or negative polarity of transient signals. By attenuating a substantial portion of the transient energy, the PMTS effectively shields the transformer from resonance overvoltage and enhances its operational reliability.

Overall, this chapter briefly studies the concept of protection introduced for future power systems. The study consists of a protection schemes conceptualizing, an analytical study, and a case simulation.

The chapter is organized as follows:

Section 7.2 defines the problem and outlines the future power system used technologies
Section 7.3 defines the design rationale and analysis of the SCGR
Section 7.4 simulation results of the SCGR
Section 7.5 defines the design rationale and analysis of the SPTS
Section 7.6 simulation results of the SPTS
Section 7.7 defines the design rationale and analysis of the PMTS
Section 7.8 simulation results of the PMTS
Section 7.9 provides a comparison study of the obtained results
Section 7.10 concludes the chapter

7.2. AN OVERVIEW OF THE CABLE-INTEGRATED TRANSFORMER PROTECTION AGAINST TRANSIENT PHENOMENA AND FUTURE POWER SYSTEM PROTECTION DEVICES

Addressing global warming requires major changes in the energy sector, especially through the energy transition [1]. This means shifting from traditional fuel-based power plants to RESs to help solve environmental problems [2]. Wind energy generators are important devices for the energy transition, as they can provide a large share of the energy needed by industries [3].

However, the use of wind energy generators increases the risk of lightning strikes because of their tall towers and sharp edges [4]. A lightning strike can cause damage to the power system, such as wind generator insulation, converters, cables, and transformers [5]. Lightning-induced OVs can spread high-frequency currents through the power system [6]. These high voltages and frequencies affect transformers and can trigger resonance frequencies within them [7]. This leads to terminal and internal OVs in transformers, which may cause failures [8]. Therefore, wind farm transformers face a higher risk of resonance OVs and need proper protection against transient signals [9].

Several devices have been suggested to protect transformers from transient components caused by lightning and switching events [10]. The most common is the surge arrester, which is connected directly to transformer terminals to reduce OV magnitudes [11]. However, surge arresters only protect against terminal OVs, allowing high-frequency transients to pass through and possibly unchecked internal resonance OVs [12]. Other devices include surge capacitors, R-C snubbers, and zinc-oxide snubbers, which use shunt capacitor filters [13]. These solutions, however, face design challenges for transmission voltage levels above 30 kV [14].

Additionally, there are series-connected inductive components [15], such as FDDs and chokes, which also act as protection devices [16]. FDDs usually consist of a coil with a specialized ferromagnetic layer [17], while chokes have a toroidal ferromagnetic ring core with a resistor in the secondary circuit [18][19]. However, both methods face the challenge of avoiding saturation of the ferromagnetic material [20].

This chapter introduces a new method considering future power system technologies using SCGR, SPTS, and PMTS. These three protection concepts are designed by using a ferrite core, permanent magnet, and superconducting technologies, which in the future power system will be more comment. The analysis of these components can be

more insightful for use in future grids to provide more advanced solutions for protecting transformers against transient phenomena.

7.3. CABLE SHIELD CONNECTED GROUNDING FERRITE CORE REACTOR FOR PROTECTION OF CABLE-CONNECTED TRANSFORMERS AGAINST TRANSIENT OVERVOLTAGE

In modern power systems, transformers connected to RESs via underground cables are increasingly vulnerable to transient overvoltages caused by switching operations and lightning strikes. The integration of cables introduces multiple resonance points, which heighten the risk of damaging overvoltages at transformer terminals. This chapter addresses the protection of cable-connected transformers against harmonic-rich transient conditions. A novel shielding cable–ground reactor (SCGR) is proposed to eliminate resonances and suppress overvoltages. The approach is validated through analytical studies, detailed simulations, and experimental results, confirming its reliability for future power systems [1]-[3].

The primary role of a power system cable is to interconnect different components within the power network. A typical cable consists of three main parts: the core conductor, the shield (normally grounded), and the insulating layer between the conductor and the shield. The equivalent model of the cable includes distributed inductances and resistances representing the conductor, along with capacitances between the conductor and the grounded shield. When this cable model is connected to the complex RLC representation of a transformer, multiple resonance points may arise. These resonances can significantly amplify transient responses, potentially leading to severe overvoltages across the transformer [21]-[25].

The primary cause of damage to cable-connected transformers under transient conditions is the resonance between the transformer and the connected cable circuit, which interacts with the transient signal frequencies [26]. Resonance can lead to overvoltages in the primary, secondary, or internal windings, resulting in partial or complete insulation breakdown and, ultimately, transformer failure [27].

Considering the crucial role of cable-connected transformers in the power system, implementing a feasible and practical protection device is essential to safeguard the power system [27]. Section 7.4 presents a new protection method for cable-connected transformers against transient overvoltage by using an SCGR.

7.4. SCGR CONFIGURATION AND OPERATION RATIONALE

An SCGR is a protection device connected to the cable shield and the ground. This configuration is illustrated in Fig. 7.1, where a transformer is connected to the cable. Applying an inductor between the cable shield and the ground creates an L-C circuit between the cable core and the ground. This idea enhances the protection of the cable-connected transformers at the critical resonance point and also in the higher-frequency resonances. The operation principle for normal and fault conditions is presented in the subsection as follows:

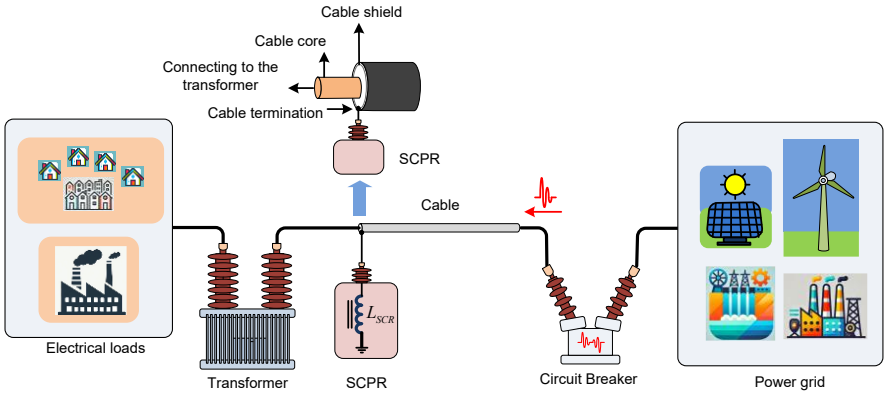


Fig. 7.1. SCGR integration with cable-connected transformer

A. SCGR effects in the steady state condition

In this condition, it is assumed that the only frequency component passing through the cable toward the transformer is the nominal system frequency, which is 50 Hz. Since the inductance of the designed SCGR is minimal at this frequency, it behaves like a grounding wire with very low impedance. Therefore, under normal operating conditions, when the voltage at the SCGR connection point is stable and free from high-frequency transients, the cable shield is effectively grounded through the SCGR's low impedance. The impedance of the SCGR in the steady-state condition is calculated by equation (7.1).

$$Z_{GR} = R_{GR} + j\omega L_{GR} = R_{GR} + \frac{j\omega N_{GR}^{2}}{\frac{l_{core}}{A_{core}\mu_{core}} + \frac{l_{ag}}{A_{ag}\mu_{0}}} \tag{7-1}$$

In this equation, Z_{GR} refers to the impedance of the SCGR in the steady state condition, which consists of very small resistance R_{GR} and inductance L_{GR}. The SCGR Inductance is an airgap-type core integrated reactor. In this SCGR structure, N_{GR} refers to winding turns. l_{core}, A_{core}, and μ_{core} are the length, cross-section, and permeability of the SCGR

core, while l_{ag}, A_{ag}, and μ_0 are the length, cross-section, and permeability of the SCGR air gap.

B. SCGR effects in the transient condition

During a transient event, when high-frequency components travel through the cable toward the transformer, resonance at the transformer terminal, or internal resonance, can result in overvoltage. By connecting the SCGR and tuning its inductance to the critical resonance frequency, the combined impedance of the cable shield capacitance and the SCGR becomes very low. This means that the high-frequency content responsible for transformer resonance is diverted and grounded through the series LC circuit formed by the cable shield capacitance and SCGR inductance. This operation is illustrated in Fig. 7.2.

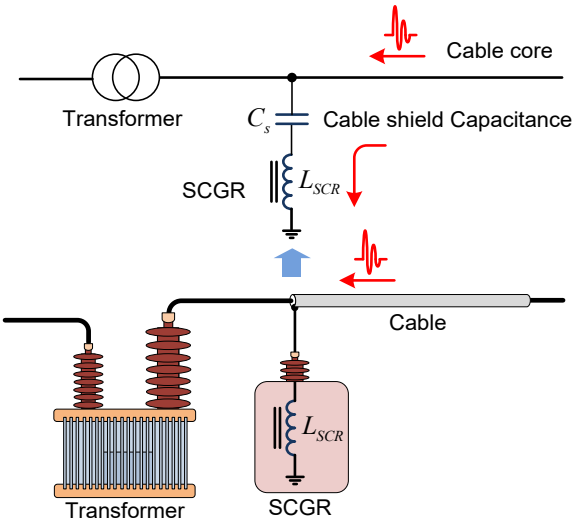


Fig. 7.2. LC model formed by SCGR and the cable shield

Therefore, the frequency content conducted by the cable core, responsible for dangerous resonance, is grounded by the cable shield and SCGR with impedance close to zero.

C. Analysis and design procedure of SCGR

To design the SCGR, the following procedure is considered:

- Measurement of the cable-connected transformer's critical resonance point causes overvoltage at the transformer terminal and significant voltage

magnification from the primary to the secondary winding, potentially damaging the transformer and connected electrical equipment.

- Measurement of the effective cable capacitance at the resonance frequency observed at the grounding terminal.
- Calculate the SCGR value by considering the resonance between the cable shield capacitance and the SCGR inductance at the first critical resonance.
- Validate the calculated SCGR performance under nominal frequency operation.
- Validate the SCGR response at the next higher critical resonance frequency.

This procedure is illustrated as a flowchart in Fig. 7.3, as follows:

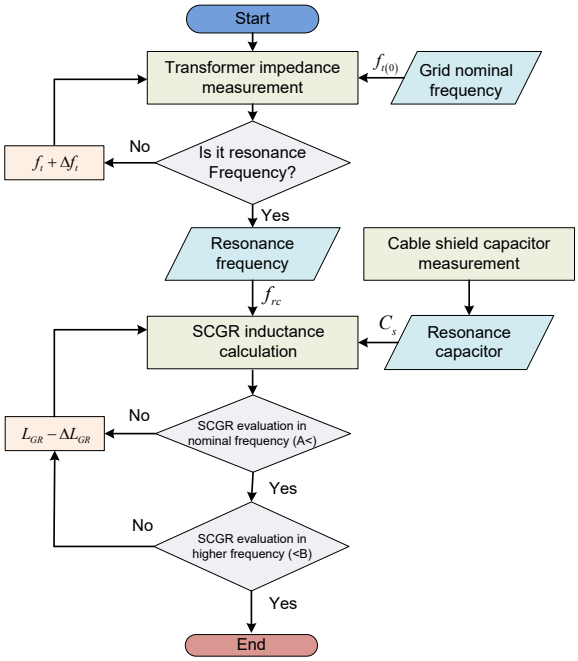


Fig. 7.3. SCGR design algorithm

The results of the SCGR design procedure include negligible impact during steady state nominal frequency of the cable-connected transformer, optimal performance at the first and most critical resonance point, and substantial protective effects at higher-frequency critical resonances. The ultimate goal is to suppress and effectively reduce transformer overvoltage.

During steady state nominal frequency, the preference is to minimize the impedance of the SCGR. It can be considered that the maximum constraint is *A* and the minimum constraint is *B*, and the resistance of the SCGR is ignored. Equation (7.2) refers to the SCGR inductance, which should be considered.

$$A < \left(\frac{N_{GR}^{\ 2}}{\frac{l_{core}}{A_{core}\mu_{core}} + \frac{l_{ag}}{A_{ag}\mu_0}} \right) < B \tag{7-2}$$

In equation (7-2), the minimum value of parameter A is determined under steady-state conditions, considering the following criteria:

- The preferred fault current magnitude in the cable shield,
- The acceptable voltage magnitude in the cable shield,
- The maximum withstandable voltage magnitude of the SCGR under steady-state operation.

The upper boundary of the SCGR inductance is determined considering:

- Critical resonance frequency of the transformer
- The effective equivalent capacitance of the cable C_s in the transformer terminal, where the SCGR is connected

Considering these two factors, the inductance of the SCGR creates a resonance with cable shield capacitance to make a low-impedance branch to conduct the transient harmful content from the cable core to the ground. This behaviour satisfies the protection effects of the SCGR. This impedance can be calculated based on (7.3). The important point about B is that the inductance of the SCGR should be close to constraint B obtained by the resonance frequency of the SCGR and cable equivalent capacitance (C_s).

$$B = \left(\frac{1}{4\pi^2 C_s} \right) \tag{7-3}$$

7.5. EMTP SIMULATION SCGR IN A CASE STUDY

A cable connected to a transformer is considered to evaluate the protective effects of the SCGR. Two key parameters obtained from this case are the critical resonance frequency of the cable-integrated transformer and the cable capacitance at that frequency. Based on this information, the inductance of the SCGR is calculated using the circuit model shown in Fig. 7.2, aiming to form a series resonance with the cable shield capacitance. The SCGR is expected to ground the first critical resonance current, which travels through the cable core toward the transformer, while also reducing the influence of the cable shield at higher frequencies to suppress overvoltages on the transformer side.

A. *Transformer critical resonance frequency*

To simulate and determine the critical resonance frequency of the transformer, a simplified model of the studied transformer is developed in EMT software, following the simulation diagram in Fig. 7.4 (a), where a frequency sweep test is conducted to evaluate the frequency-dependent impedance characteristics. As shown in Fig. 7.4 (b), the first critical resonance frequency appears at approximately 200 kHz. At this frequency, the transformer impedance drops to nearly 1 Ω, which is considerably low and may cause severe transient overcurrents as well as harsh overvoltages in the windings.

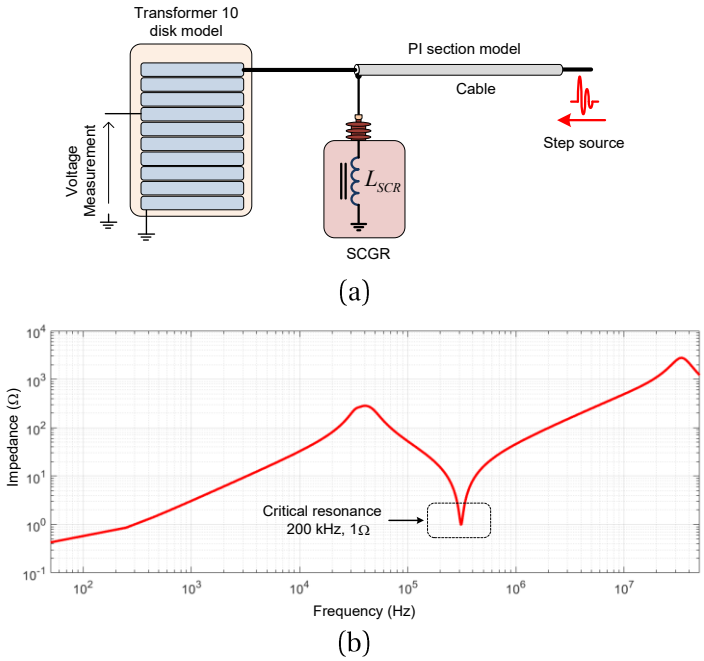


Fig. 7.4. a) Simulation diagram, b) Frequency sweep impedance simulation of the studied transformer

Furthermore, the capacitance of the studied cable at this frequency, measured at the termination terminal, is extracted from the model and found to be approximately 14 pF. The calculated and applied parameters used in the EMT model are summarized in Table 7.1, serving as the basis for the subsequent EMT simulations.

Table 7.1. Data for EMTP simulation

Parameter	Description	Value
f_{rc}	First critical resonance frequency	200 kHz
C_s	Cable shield capacitance	5 nF
L_{SCR}	Inductance of SCGR	500 µH
Vs	Electric system voltage level	8 kV
P_n	Nominal power	500 kW

B. *Transformer overvoltage simulation without SCGR connection*

In this section, the simulation is performed with the cable integrated into the transformer, and the circuit is excited by an ideal step voltage source to observe the distributed voltage across the transformer disks. A key consideration is that the voltage is measured on the primary winding at 70% of the disks from the grounded terminal of the transformer which face overvoltage due to internal resonance, while no protection device is applied at the transformer terminal.

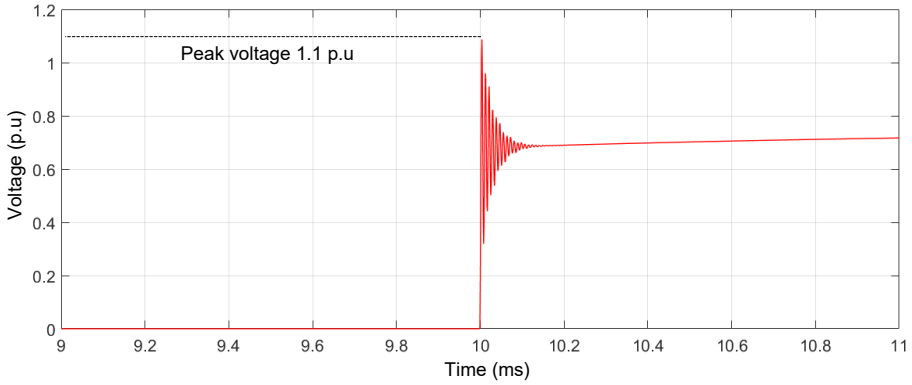


Fig. 7.5. Voltage of 70% of the studied transformer primary winding

As obtained from the simulation, the voltage across 70% of the disks to ground in the transformer primary winding, illustrated in Fig. 7.5, reaches 1.1 p.u., which is 0.4 p.u. Higher than the normal operating voltage. Such an overvoltage may cause insulation damage in this portion of the winding. This overvoltage will be mitigated in the next step using the designed SCGR protection device.

C. *Transformer voltage simulation with SCGR protection effect*

In the next part of the simulation, the voltage at the same transformer terminal is illustrated in Fig. 7.6, where the SCGR protection device is connected to the cable termination. The simulation is carried out considering the illustrated diagram in Fig

7.2. This result demonstrates the influence of the SCGR on suppressing internal resonance and mitigating overvoltage within the transformer.

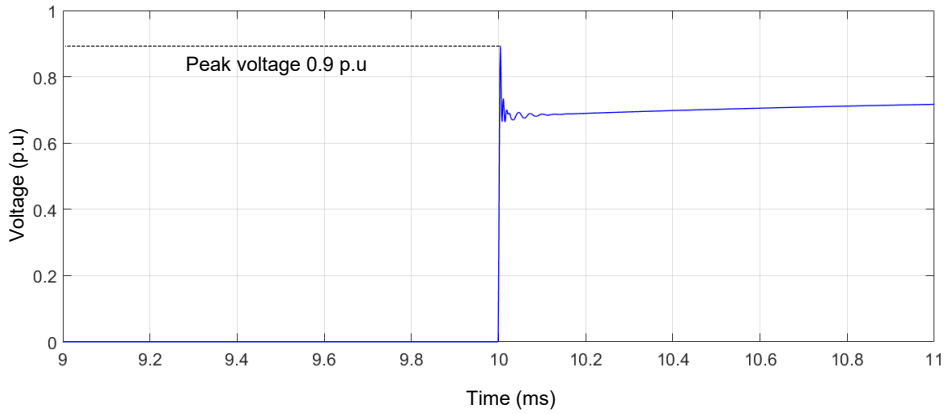


Fig. 7.6. Voltage of 70% of the studied transformer primary winding

As shown in the simulation results presented in Fig. 7.6, the voltage across 70% of the transformer disk to ground decreases from 1.1 p.u. (without the protection device) to 0.9 p.u. When the SCGR is applied, this clearly verifies the effectiveness of the proposed SCGR as a transient suppressor for the cable-integrated transformer.

7.6. Definition and design of a series-parallel transient suppressor

In this section, the proposed SPTS is designed based on the electrical system's ferromagnetic core and cable shield capacitor specifications. The rationale behind the design is to use a series of ring toroid cores with a cable and a parallel branch, including cable shield capacitance and inductance of the toroid core. A combination of the series inductance and parallel branch creates a coupling in the core, resulting in a reverse voltage against the transformer's critical resonance frequency, suppressing the transient signal effects and protecting the transformer from resonance overvoltage.

A. SPTS structure and configuration

The designed SPTS consists of a toroid core coupling the cable's core wire to the cable shield's LC grounding circuit. From the configuration aspect, the SPTS is connected in series with a transformer where the cable core conductor passes through the toroid core, and the cable shield is grounded by the core inductance. Fig. 7.7 illustrates the structure and configuration of the SPTS.

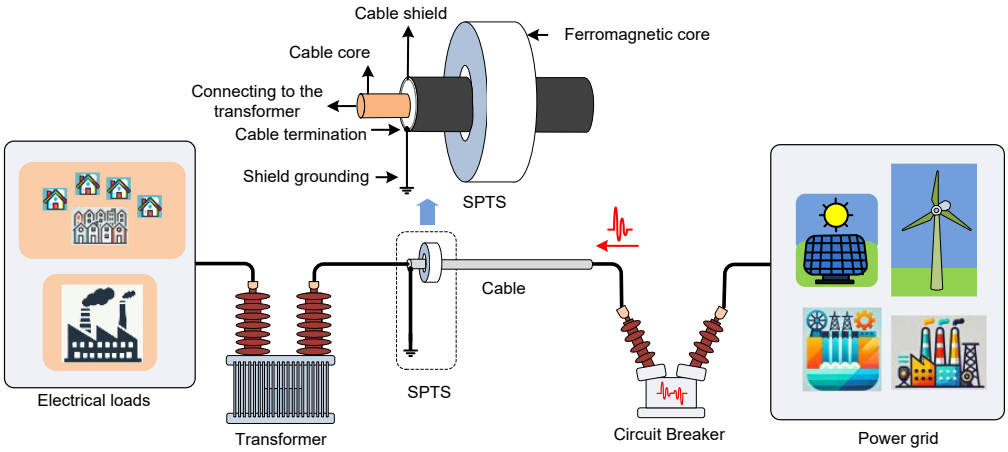


Fig.7.7. Configuration and topology of the SPTS

Considering the configuration of the SPTS, Fig. 7.8 illustrates the detailed model of the proposed device. As shown in Fig. 7.8 (a), which provides an expanded view of Fig. 7.8 (b), the toroidal core placed around the cable establishes magnetic coupling between the cable conductor and the shield. In this arrangement, the toroidal core functions as a transformer: the cable conductor acts as a primary winding (L_{SPTS}), and the shield serves as a secondary winding, with both forming a single turn, and thus a 1:1 turns ratio. The shield at the transformer terminal is grounded after passing through the core. Consequently, the secondary circuit, consisting of the secondary inductance (denoted as L_{sc}) in series with the shield capacitance, effectively connects the cable conductor to ground.

Based on this model, the SPTS is configured in a series–parallel connection with respect to the transformer. The parallel branch exhibits a resonance frequency determined by the series LC circuit, which should be tuned to match the critical resonance frequency of the protected transformer. Furthermore, the series inductance provided by the SPTS must be sufficient to attenuate the critical harmonic components of the transient signal, thereby protecting the transformer from resonance overvoltages.

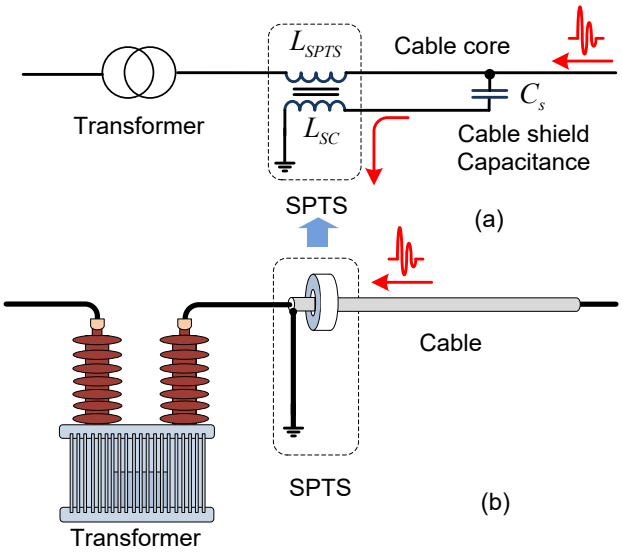


Fig. 7.8. LC model formed by SCGR and the cable shield

The operating principle of the proposed SPTS is discussed separately for normal steady state operating conditions and transient conditions.

B. SPTS effects on the steady state operation

During steady-state conditions, when the electric system frequency is a nominal frequency of 50 Hz, the series impedance of the SPTS is very small, which can be neglected. Furthermore, the shield of the cable is connected to ground in the cable termination through the inductance of the SPTS, which is negligible and has no effect on the shielded connection to ground. Inductances and impedance of the SPTS by ignoring the coupling effect can be calculated using equations (7-4) and (7-5).

$$L_{SPTS} = \left(\frac{A_{core} \cdot \mu_{core}}{2\pi (r_{in} + r_{out})} \right) \tag{7-4}$$

$$Z_{SPTS} = f_s \left(\frac{A_{core} \cdot \mu_{core}}{(r_{in} + r_{out})} \right) \tag{7-5}$$

Here, L_{SPTS}, as inductance of SPTS, is a function of core cross-section (A_{core}), core permeability (μ_{core}), and core inner and outer radius (r_{in} and r_{out}). Therefore, impedance of the SPTS (Z_{SPTS}) is calculated in (7-4) considering the power system frequency (f_s).

C. SPTS operation in the transient condition

In the transient state, a variety of harmonic components of the disturbance signal attempt to propagate through the SPTS. Among these components, the most critical is the transformer resonance frequency. To address this, the LC secondary branch of the SPTS must be tuned to the transformer's critical resonance frequency. This tuning is achieved by adjusting the impedance of the SPTS secondary inductance (L_{SPTS}) in relation to the cable capacitance at the termination point. The dimensions of the toroidal core determine the inductance value. By neglecting the steady-state current in the primary turn, the resonance frequency and corresponding core geometry can be calculated using (7-6).

$$\left(\frac{A_{core}.\mu_{core}}{(r_{in}+r_{out})}\right)=\frac{1}{2\pi f_c^{\,2}C_s} \tag{7-6}$$

Here f_c is the critical resonance frequency. After tuning the secondary circuit, the critical resonance current flows through the secondary branch of the SPTS, inducing a counteracting voltage in the primary that opposes the transient signal. This operation is illustrated in Fig. 7.9. The SPTS (v_{SPTS}) reverse induced voltage can be calculated using equation (7-7).

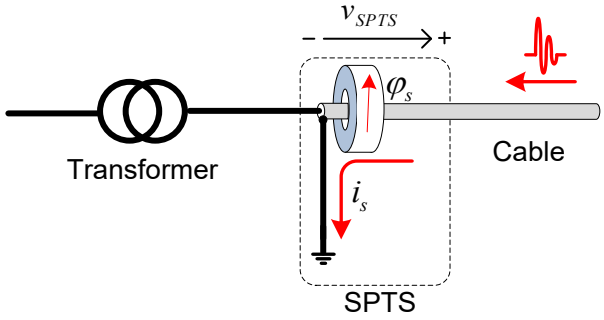


Fig. 7.9. LC model formed by SCGR and the cable shield

$$v_{SPST}(t)=\left(\frac{A_{core}.\mu_{core}}{2\pi(r_{in}+r_{out})}\right)\frac{di_s}{dt} \tag{7-7}$$

Here, i_s is the current of the secondary of the SPTS, where it generates flux of the φ_s in the SPTS's core.

7.7. SIMULATION OF THE DESIGNED SPTS

In this simulation, the transformer and electrical system are considered in the same configuration as in Sections 7.4 (a) and (b). Accordingly, the simulation diagram is the same as Fig. 7.4 (a), and the critical resonance frequency of the transformer, obtained from Fig. 7.4 (b), is 200 kHz, and the voltage across 70% of the disks from the grounded terminal reaches 1.1 p.u. When tested with a square waveform. In the next step, the EMT platform is used to apply the SPTS model to the cable to evaluate the impact of the SPTS on the system response.

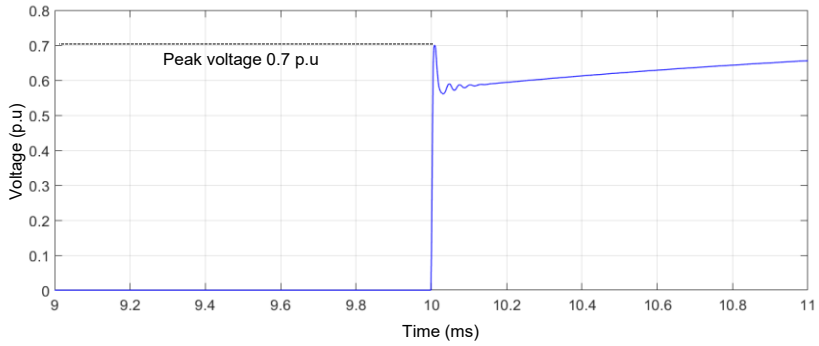


Fig. 7.10. Effects of the SPTS on the transformer disk voltage (70% of total transformer disks to ground)

As shown in the simulation results in Fig. 7.10, after applying the SPTS to the cable, the winding 70% disk voltage to ground is suppressed from 1.1 p.u. to 0.7 p.u. This demonstrates the effective operation of the SPTS in safeguarding the transformer against resonance-induced overvoltages.

7.8. DESIGN, CONFIGURATION, AND ANALYSIS OF THE PMTS

A. Design and configuration of the PMTS

The integration of PMs with ferromagnetic cores can enhance the performance of DC-biased reactors. This technique can further improve series transient suppressors in future power systems. Embedding PMs within ferromagnetic cores leads to partial core saturation during steady-state operation, allowing the core to become active once transient phenomena are applied to the suppressor. The configuration of the proposed permanent magnet-based suppressor, PMTS, and its design rationale are as follows:

The transient suppressor consists of two toroidal ferromagnetic cores. In each core, pieces of neodymium PMs (type N52) are embedded. The power line passes through the cores and is connected to the transformer. The configuration is illustrated in Fig. 7.11.

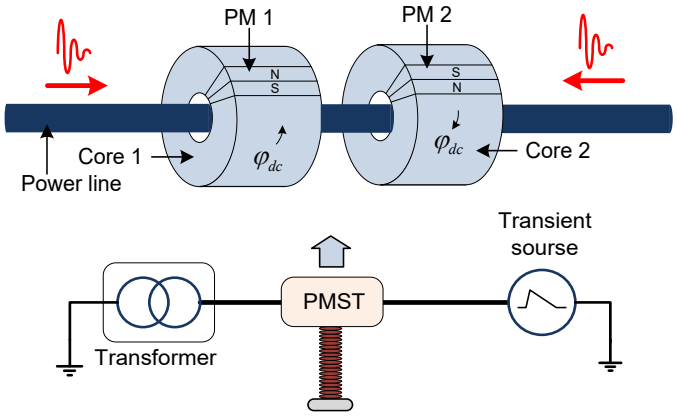


Fig. 7.11. PMTS structure and configuration

The design rationale of the PMTS is based on core saturation during steady-state operation. In this condition, no transient occurs, and the PMTS does not affect the power system. The PM fully saturates both cores, not influencing the power line.

When a transient passes through the cores, depending on the polarity of the transient current, one core exits the saturation region and becomes active. This suppresses the transient signal by introducing considerable impedance in series with the transformer. This principle enables the PMTS to protect the transformer from overvoltage. The operational region of the PMTS, considering the magnetic flux density in the core, is illustrated in Fig. 7.12.

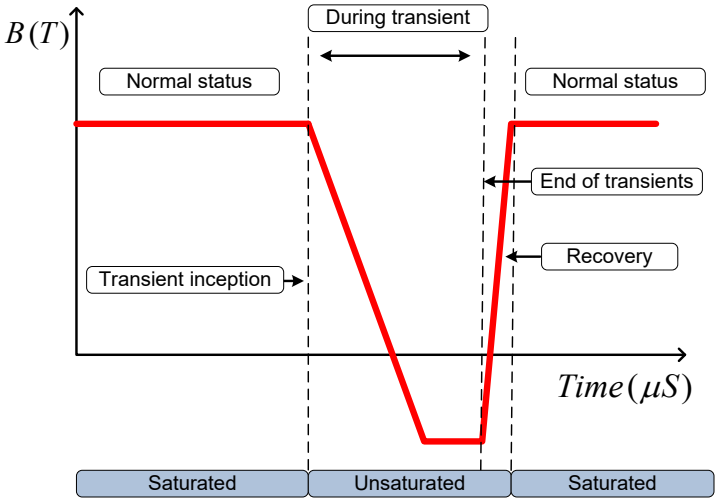


Fig. 7.12. PMTS operational region, considering the core magnetic flux density

As shown in Fig. 7.12, the PMTS cores are fully saturated before a transient's inception. During a transient, the core whose DC flux is in the opposite direction of the transient current flux exits the saturation region. In this state, the PMTS is activated and imposes a series impedance to suppress the transient signal and protect the transformer. After the transient current is interrupted, the PMTS recovers from the unsaturated region to saturation and resumes steady-state operation.

B. Operational analysis of the PMTS

In this subsection, the operation of the PMTS is analyzed under steady-state and transient conditions. To simplify the calculations, the core behavior is assumed to be linear, operating either in deep saturation or in the linear region. This assumption is reasonably accurate, as the core flux is not fully coupled due to the presence of the permanent magnet.

Steady-state condition

In the steady-state condition, the cores of the PMTS are deeply saturated by the DC magnetic flux produced by the permanent magnets. Under this condition, the flux generated by the alternating current of the power line is significantly smaller than the DC flux and, therefore, cannot drive the saturated core out of the saturation region. Equations (7-4) and (7-5) are the magnetic flux density of cores B_{core1} and B_{core2} of PMTS, and the flux of the cores φ_{core1} and φ_{core2}.

$$B_{core1} = B_{core2} = B_{DS} \tag{7-4}$$

$$\varphi_{core1} = \varphi_{core2} = \frac{B_{DS}}{A_{core}} \tag{7-5}$$

Here, B_{DS} refers to the magnetic flux density in the deep saturation condition, and A_{core} is the cross-section of each core. Considering (7-6), the voltage drop of PMTS (v_{PMTS}) during normal conditions is calculated by (7-6).

$$v_{PMST} = \frac{1}{A_{core}} . \frac{dB_{DS}}{dt} \approx 0 \tag{7-6}$$

Transient condition

In the transient condition, the magnitude of the transient current rises swiftly, leading the PMTS cores to go out of the saturation region. The magnetic flux of the PMTS is

calculated in (7-7) and (7-8) while the nonlinear behavior of the core is ignored, assuming it has reached the linear stage swiftly.

$$\varphi_{core1} = \varphi_{core2} = \varphi_{dc} - \varphi_{Tr} \tag{7-7}$$

$$\varphi_{Tr} = \frac{i_{Tr}}{R_{core}} \tag{7-8}$$

In the (7-8), the transient current can be considered the first rising ramp of the transient signal, which is a significant part of the transient current. The linear rising current is defined in (7-9).

$$i_{Tr}(t) = At \tag{7-9}$$

Where t is time and A is a coefficient referring to the rate of rise of the transient signal. Also, the reluctance of the core is determined by the sum of the reluctance of the PM (R_{PM})and the reluctance of the ferromagnetic core (R_F). The reluctance of the PMTS and ferromagnetic part of the core is calculated in (7-10) and (7-11).

$$R_{core} = R_{PM} + R_F \tag{7-10}$$

$$R_F = \frac{l_F}{A_{core} + \mu_{core}} \tag{7-11}$$

The PMTS's voltage drop in the transient condition is defined by applying derivation to the core flux, following equation (7-12).

$$v_{PMST} = \frac{d\left(\varphi_{dc} - \varphi_{Tr}\right)}{dt} = \frac{d\left(\varphi_{dc} - \dfrac{At}{\dfrac{l_F}{A_{core} + \mu_{core}} + R_{PM}}\right)}{dt} \tag{7-12}$$

Therefore, PMTS reflects the transient signal by generating the voltage in (7-12), which causes suppression of the transient voltage toward the transformer.

7.9. FEM SIMULATION OF THE PMTS DURING NORMAL AND TRANSIENT CONDITIONS

In this section, a geometry of the PMTS is designed in the FEM platform, and its operation is studied throughout normal conditions and transient fault by considering inductance and magnetic flux calculation during the three operation states. The data of the designed PMTS is provided in Table 7.2, aligned with Fig.7.11.

Table 7.2. PMTS design data used for FEM simulation

Parameter	Description	Value
A_{core}	Core cross-section	60*100 mm^2
D_u	Toroid core outer diameter	400 mm
D_i	Toroid core inner diameter	280 mm
B_{sat}	Core saturation flux density	1.2 T
PM	Permanent magnet type	Nd 52
S_{PM}	Permanent magnet size	60*100*40 mm^3

A. FEM simulation of the PMTS in the steady-state condition

In this condition, the current passing through the line conductor corresponds to the steady-state current with a normal magnitude, while the permanent magnet saturates the ferromagnetic core of the PMTS with DC magnetic flux. Fig. 7.13 shows the 3D design of the proposed PMTS and its mesh configuration.

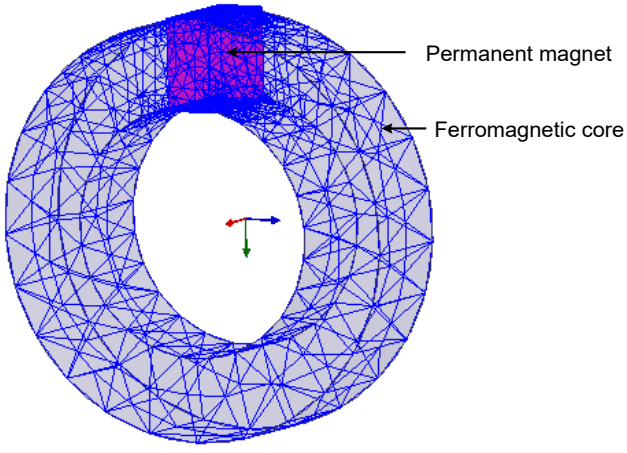


Fig. 7.13. PMTS 3D geometry and mesh plot

The simulation result for one core of the PMTS is illustrated in Fig. 7.14, where the saturation region of the core begins at 1.2 T. The simulation results show that the core

is saturated by the permanent magnet under steady-state operating conditions, and the PMTS voltage drop is zero.

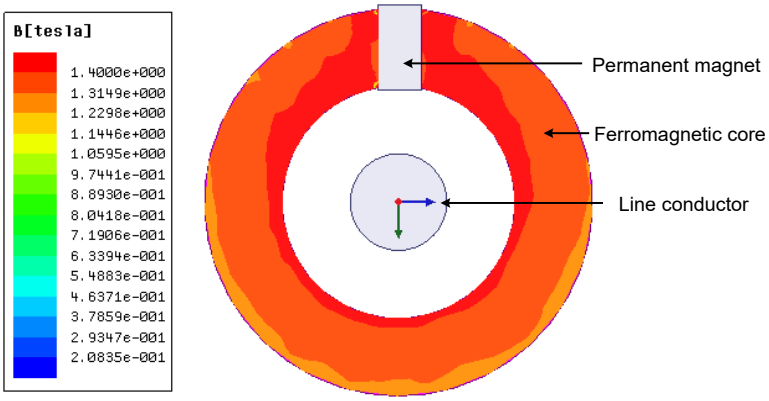


Fig. 7.14. PMTS FEM simulation in the steady-state condition

B. FEM simulation of the PMTS in the transient condition

In the transient condition, the line conductor, modeled as a coil in the FEM platform, is excited by a surge impulse. Based on this simulation, the magnetic flux density of the core and its variation, corresponding to the voltage drop across the PMTS, are illustrated in Fig. 7.15 over the time sequence.

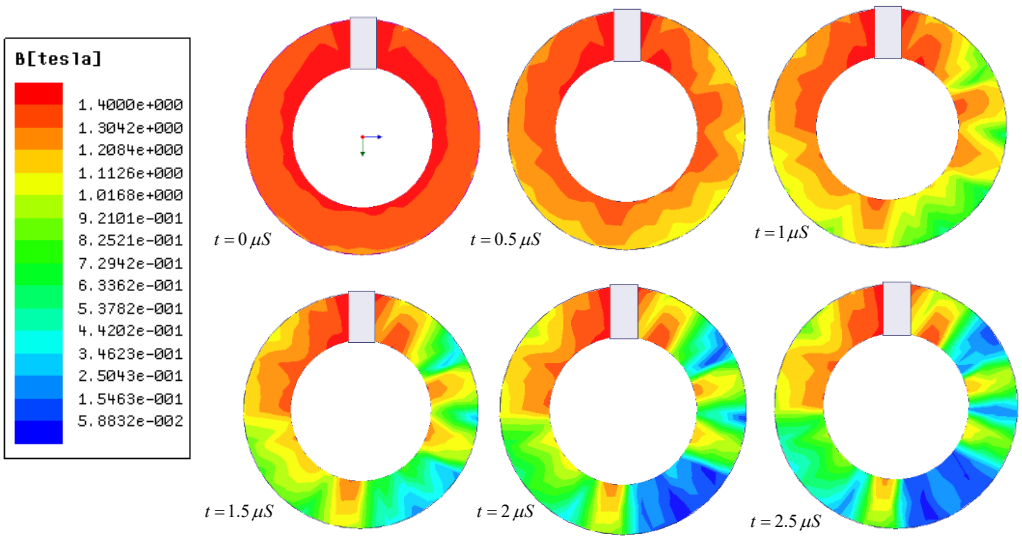


Fig. 7.15. PMTS FEM simulation in the transient condition

In this simulation, the peak magnitude of the transient signal reaches 100 kV, considered as 1 p.u with a rise time of 1.2 μs, where the peak magnitude of the current reaches 500 A. The results indicate that the PMTS can reduce the surge peak voltage in the transformer disk to 0.54 p.u introducing considerable series impedance in the power line. As illustrated in Fig. 7.15, when the magnitude of the transient current in the system increases, the PMTS responds by exiting the saturation region and imposing additional series impedance, thereby suppressing the transient phenomenon. The voltage of 70% of the transformer disk to ground is illustrated in Fig. 7.16.

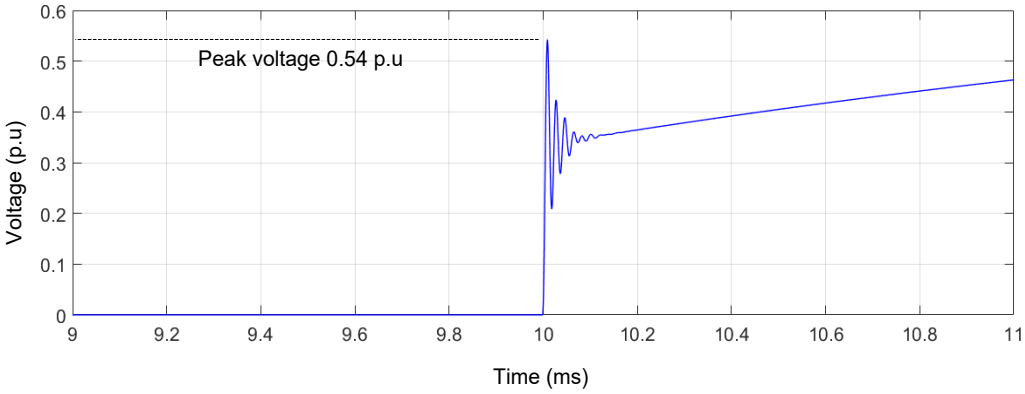


Fig. 7.16. Effects of the PMST on the transformer disk voltage (70% of total transformer disks to ground)

7.10. Comparison of designed transient suppressor protection devices

In this section, three different protection devices are conceptually designed for future power system applications against transient phenomena. Each device possesses its own characteristics, including both advantages and limitations. To illustrate these aspects, a rough comparison of their main features is presented in Table 7.3.

The highlighted advantages of each concept are as follows:

SCGR: A shunt device connected to the cable shield, which conducts no current during steady-state operation.

SPTS: Its working principle is based on reverse voltage generation, which can substantially suppress the magnitude of transient signals.

PMTS: A permanent magnet–based structure that, under steady-state conditions, has no effect due to deep core saturation, while imposing high impedance during transient occurrences.

Table 7.3. Comparison of designed protection devices against transient phenomena

Features	SCGR	SPTS	PMTS
Installation type	Parallel with the cable shield	Series-parallel with cable	Series with transformer
Resonance frequency filtering	Yes	Yes	Yes
Operation against the transient	Shunt impedance less than 50 Ω	Reverse voltage generation	Temporally high impedance, higher than 2 kΩ at 200 kHz
Saturation possibility	No	No	No
Voltage level	Both the distribution and transmission systems	Distribution system	Distribution system
Need for grounding	Yes	Yes	No

The disadvantages of each concept are as follows:

SCGR: It operates effectively only within a limited frequency range due to the cable shield's small capacitance (in the range of several nano Farad).

SPTS: Its parallel–series configuration makes the structure more complex compared to other protection schemes.

PMTS: Relies on permanent magnets, making it more vulnerable to reverse magnetic flux, which may lead to degradation over time.

7.11. Conclusion

This chapter presents the conceptual design of three different protection devices against transients, with the primary objective of safeguarding transformers from resonance-induced overvoltages. These devices, SCGR, SPTS, and PMTS, are proposed as potential candidates for future power systems, where cable integration is expected to become increasingly dominant.

To introduce these concepts, the analytical design procedure of each device was first discussed, followed by numerical simulations carried out in EMT and FEM platforms. The simulation results verify the effectiveness of the proposed protection schemes under transient conditions, demonstrating their capability to suppress resonance overvoltages and mitigate insulation stress in transformer windings.

The obtained results highlight several promising benefits of the designed protection devices, including effective overvoltage suppression, improved transformer reliability, and potential applicability in advanced cable-integrated grids. Nevertheless, these schemes' feasibility and large-scale implementation present challenges that require further investigation. In future research, issues such as practical design constraints, long-term reliability, material limitations, experimental validation, and integration with existing protection systems must be carefully addressed to move these concepts toward real-world applications.

References

[1] G. C. Paap, A. A. Alkema, and L. Van der Sluis, "Overvoltages in power transformers caused by no-load switching," IEEE Trans. Power Del., vol. 10, no. 1, pp. 301–307, Jan. 1995.

[2] Y. Yasuda, N. Uno, H. Kobayashi, and T. Funabashi, "Surge analysis on wind farm when winter lightning strikes," IEEE Trans. Energy Convers., vol. 23, no. 1, pp. 257–262, Mar. 2008, doi: 10.1109/TEC.2007.905361.

[3] A. H. Soloot, H. K. Høidalen, and B. Gustavsen, "Influence of the winding design of wind turbine transformers for resonant overvoltage vulnerability," IEEE Trans. Dielectr. Electr. Insul., vol. 22, no. 2, pp. 1250–1257, Apr. 2015.

[4] T. Abdulahović and T. Thiringer, "Voltage stress in a transformer winding during very fast transients caused by breaker closing event," IEEE Trans. Power Del., vol. 29, no. 4, pp. 1946–1954, Aug. 2014.

[5] P. Akiki, A. Xémard, C. Trouilloud, and J. Chanelière, "Study of high frequency transient overvoltage caused by cable-transformer quarter-wave resonance," Electric Power Syst. Res., vol. 197, 2021.

[6] M. Firouzi and G. B. Gharehpetian, "Improving fault ride-through capability of fixed-speed wind turbine by using bridge-type fault current limiter," IEEE Trans. Energy Convers., vol. 28, no. 2, pp. 361–369, Jun. 2013.

[7] A. Heidary, M. G. Niasar, M. Popov, and A. Lekić, "Transformer resonance: Reasons, modeling approaches, solutions," IEEE Access, vol. 11, pp. 58692–58704, 2023.

[8] T. Dionise and S. Johnston, "Surge protection for ladle melt furnaces: LMF transformer terminals were equipped with primary surge protection consisting of surge arresters and RC snubbers," IEEE Ind. Appl. Mag., vol. 21, no. 5, pp. 43–52, Sept.–Oct. 2015.

[9] Zinc oxide RC-surge suppressor (ZORC) capacitors, for HV-motor and transformers. [Online]. Available: https://www.vishay.com

[10] K. Munji, "Design and validation of pre-insertion resistor rating for mitigation of zero missing phenomenon," in Proc. Int. Conf. Power Syst. Transients (IPST2017), 2017, pp. 26–29.

[11] H. Heiermeier and R. B. Raysaha, "Power testing of preinsertion resistors: Limitations and solution," IEEE Trans. Power Del., vol. 32, no. 4, pp. 1688–1695, Aug. 2017.

[12] S. M. Korobeynikov, S. I. Krivosheev, S. G. Magazinov, V. A. Loman, and N. Ya, "Suppression of incoming high-frequency overvoltage in transformer coils," IEEE Trans. Power Del., vol. 36, no. 5, pp. 2988–2994, Oct. 2021.
[13] D. Smugała, "Distribution transformers protection against high frequency switching transients," Przegląd Elektrotech. (Electrical Review), vol. 88, no. 5a, 2012.
[14] D. Smugała, W. Piasecki, M. Ostrogórska, M. Florkowski, M. Fulczyk, and O. Granhaug, "New approach to protecting transformers against high frequency transients – wind turbine case study," Przegląd Elektrotechniczny, vol. 89, no. 10, pp. 186–190, 2013.
[15] D. Smugała, W. Piasecki, M. Ostrogórska, M. Florkowski, M. Fulczyk, and O. Granhaug, "Very fast transient suppressing device," U.S. Patent 8,929,048 B2, Jan. 6, 2015.
[16] F. Nasirpour, A. Heidary, M. Ghaffarian Niasar, and M. Popov, "High-frequency transformer winding model with adequate protection," Electric Power Syst. Res., vol. 223, pp. 109637, 2023.
[17] A. Heidary, M. Ghaffarian Niasar, and M. Popov, "Comprehensive evaluation of toroid ring core parallel inductor and resistor as a transformer protection device," IEEE Trans. Circuits Syst. I: Regul. Pap., vol. 71, no. 9, pp. 4298–4308, Sep. 2024.
[18] L. Zhou, L. Huang, R. Wei, and D. Wang, "A novel lightning overvoltage protection scheme using magnetic rings for transmission line systems," IEEE Trans. Ind. Electron., vol. 70, no. 12, pp. 12872–12882, 2023.
[19] W. Piasecki, G. Bywalec, M. Florkowski, M. Fulczyk, and J. Furgal, "New approach towards very fast transients suppression," in Proc. IPST, 2007.
[20] A. Heidary, M. G. Niasar, and M. Popov, "Series magnetic coupled reactor saturation considerations for high voltage AC and DC power systems," Int. J. Electr. Power Energy Syst., vol. 158, pp. 109909, 2024.
[21] Y. Zhang, Q. Yang, S. Xie, and C. Zhang, "Mechanism and application of arrester block voltage division to lightning transient voltage monitoring in substation transformers," IEEE Trans. Electromagn. Compat., vol. 61, no. 3, pp. 689–696, Jun. 2019.
[22] IEEE Draft Guide for Field-Testing of Shielded Power Cable Systems Rated 5 kV and Above with Damped Alternating Current Voltage (DAC), IEEE P400.4/D8, Sept. 2014, pp. 1–47.
[23] M. Popov, L. Grcev, H. K. Hoidalen, B. Gustavsen, and V. Terzija, "Investigation of the overvoltage and fast transient phenomena on transformer terminals by taking into account the grounding effects," IEEE Trans. Ind. Appl., vol. 51, no. 6, pp. 5218–5227, Nov.–Dec. 2015.
[24] A. Morched, B. Gustavsen, and M. Tartibi, "A universal model for accurate calculation of electromagnetic transients on overhead lines and underground cables," IEEE Trans. Power Del., vol. 14, no. 3, pp. 1032–1038, Jul. 1999.
[25] I. Lafaia, J. Mahseredjian, A. Ametani, M. T. Correia de Barros, I. Koçar, and Y. Fillion, "Frequency and time domain responses of cross-bonded cables," IEEE Trans. Power Del., vol. 33, no. 2, pp. 640–648, Apr. 2018.
[26] B. Behdani, M. Ghaffarian Niasar, and M. Popov, "Effect of cable sheath termination on transient overvoltages due to high-frequency cable-transformer resonance," Electric Power Syst. Res., vol. 250, 2026.

8

DISCUSSION OF THE RESULTS AND CONCLUSION

8.1. THESIS SUMMARY

This thesis has addressed the crucial problem of protecting power transformers in modern and future power systems against transient phenomena and resonance overvoltages. Transformers, being the backbone of the transmission and distribution grid, are increasingly exposed to fast transients originating from lightning strikes, switching operations, and interactions with cables, power electronic devices, and nonlinear loads. These transients excite internal and external resonances in transformer windings, which lead to severe overvoltages that can compromise insulation integrity and ultimately cause transformer failure.

The research systematically investigated the challenge of transformer protection against resonance overvoltage through analytical studies, frequency-domain modeling, time-domain simulations, scaled-down prototyping, and high-voltage laboratory experiments. The work identified the limitations of existing protection methods, such as surge arresters, RC snubbers, and standard filters, which fail to provide comprehensive suppression of resonances and harmonic interactions in high-voltage transformers.

To overcome these challenges, the thesis developed and validated several novel protection devices that target resonance overvoltages and transient suppression with higher precision and effectiveness. The innovations include:

- Parallel RL Circuits: Designed to mitigate resonance by absorbing harmonic energy and limiting overvoltages in low- to medium-voltage test environments.
- Air-Core Reactor with Parallel Resistor: A series suppressor capable of suppressing high-frequency transients without introducing significant power losses at fundamental frequency.

- Tuned Chokes: A frequency-selective solution that can be adapted to specific resonance points in transformers, thereby preventing the amplification of critical harmonics.
- Modular Series Transient Suppressor: A scalable device combining resistors and inductors in a modular form, providing robust suppression of a wide spectrum of resonance-induced overvoltages.
- Cable Shield-Connected Grounding Reactor: A protection scheme designed for cable, transformer interactions, suppressing traveling waves entering transformer terminals.
- Series-parallel connected transient suppressor: this protection device is also designed for a cable-integrated transformer to safeguard it against transient and resonance overvoltage by generating reverse voltage against the transient signal.
- Permanent Magnet-Based Transient Suppressor: An innovative concept using magnetic materials to interact with transient fields and provide non-linear damping.

Each of these devices was carefully analyzed, modeled, simulated, and experimentally validated where feasible, resulting in a comprehensive evaluation of their capabilities and applicability in modern transmission systems. The work also produced a black-box and gray-box transformer modeling framework for resonance studies, which successfully identified resonance frequencies and guided the design of protection devices.

8.2. Comparison of the studied protection solutions

A key outcome of this thesis is the systematic comparison of the studied solutions across multiple dimensions, including effectiveness in suppressing overvoltages, harmonic filtering capability, implementation feasibility, and compatibility with transmission-level transformers.

1. Parallel RL Circuit:

Strengths: Simple, cost-effective, and effective for damping harmonics in experimental setups.

Limitations: Limited scalability to transmission levels and less effective against very fast transients.

The PAIR protection topology and structure are illustrated in Fig. 8.1:

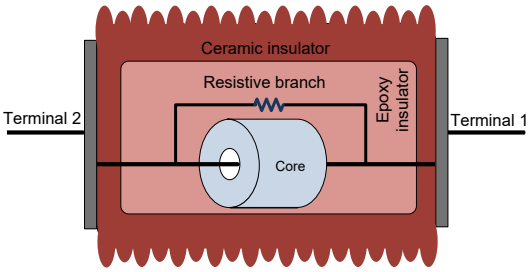


Fig. 8.1. PAIR protection topology implementation scheme

2. Air-Core Reactor with Parallel Resistor:

Strengths: Robust performance at high frequencies, experimentally validated at high-voltage impulse tests.

Limitations: Increased size and cost for higher voltage levels, requiring careful design to minimize fundamental power losses.

The R-PIR protection overall implementation scheme is illustrated in Fig. 8.2:

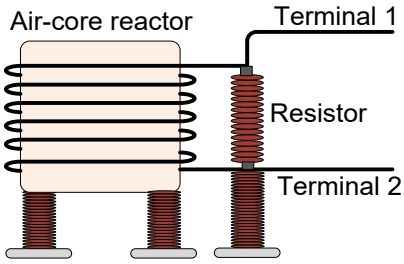


Fig. 8.2. R-PIR protection implementation scheme

3. Tuned Choke:

Strengths: Provides selective suppression at resonance frequencies, tunable design, validated by FEM simulations and high-voltage tests.

Limitations: Sensitive to parameter variations, requires accurate identification of transformer resonance frequencies.

The tuned choke protection overall topology and implementation scheme is illustrated in Fig. 8.3:

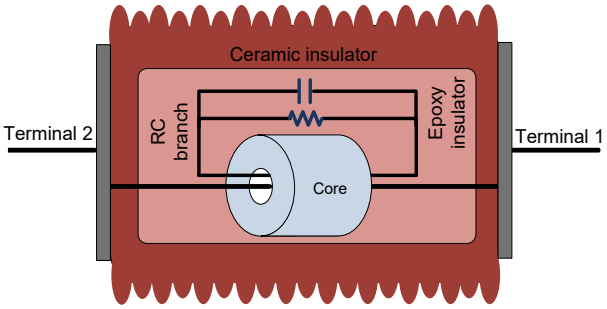


Fig. 8.3. Tuned chock protection implementation scheme

4. Modular Series Transient Suppressor:

Strengths: Highly effective for a broad frequency range, scalable architecture, and experimentally verified at multiple voltage levels.

Limitations: Increased complexity compared to simple suppressors, requiring careful modular arrangement for high-voltage applications.

The MSTS protection overall topology and implementation scheme is illustrated in Fig. 8.4 as follows:

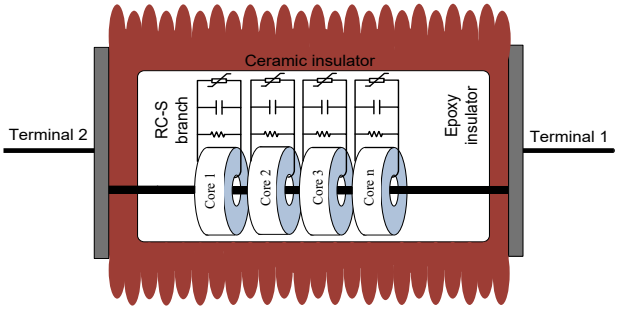


Fig. 8.4. MSTS protection implementation scheme

5. Cable Shield-Connected Grounding Reactor (SCGR):

Strengths: Specifically addresses traveling waves from cables, effective for modern grids with extended underground connections.

Limitations: Application-specific, requires integration with transformer grounding design.

The SCGR protection overall topology and implementation scheme is illustrated in Fig. 8.5:

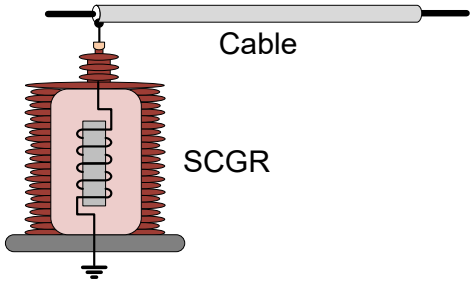


Fig. 8.5. SCGR protection implementation scheme

6. Series parallel transient suppressor:

Strengths: Specifically addresses traveling waves from cables, effective for modern grids with extended underground cable connections. This scheme can completely interrupt the critical frequency content by generating reverse voltage.

Limitations: Application-specific, requires integration with cable and cable termination grounding design.

The SPTS protection device topology and implementation scheme are illustrated in Fig. 8.6:

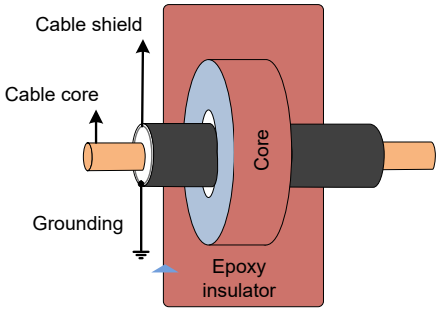


Fig. 8.6. SPTS protection implementation scheme

7. Permanent Magnet-Based Transient Suppressor:

Strengths: Innovative concept with a potentially compact design, which, for the suppression, uses nonlinear characteristics of magnetic materials.

Limitations: Technology readiness level is still low; further investigation for thermal and long-term is required.

The PMTS protection device topology and overall implementation scheme are illustrated in Fig. 8.7:

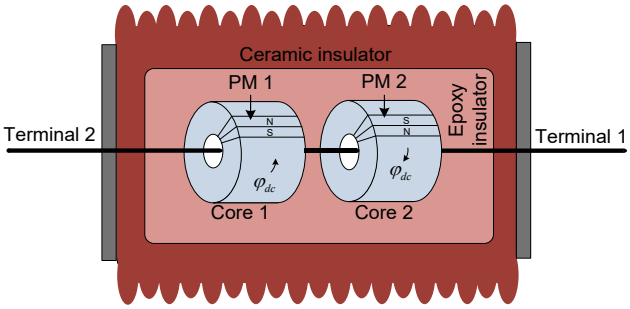


Fig. 8.7. PAIR protection implementation scheme

This part introduces a comparison table listing the main features of the studied protection schemas. The details are listed in Table 8.1.

Table 8.1. Comparison of designed protection devices effects

Features	PAIR	R-PIR	Tuned choke	MSTS	SCGR	SPTS	PMTS
Connection type	Series with transforme r	Series with transformer	Series with transformer	Series with transformer	Parallel with the cable shield	Series-parallel with cable	Series with transforme r
Operation frequency range	Above 1 MHz	limited frequency band	Tunable 80-500 kHz	Tunable in a wide range	Above 200 kHz	limited frequency band	Wide frequency range
Provided impedance against transient	Less than 1 kΩ	Less than 1 kΩ	Less than 1 kΩ	This can be adjusted by the number of modules	Shunt impedance less than 50 Ω	Reverse voltage generation	Temporall y high impedance , higher than 5 kΩ
Saturation possibility	Yes	No	Yes	This can be avoided by the multilay er design of the core	No	No	No
Voltage level	Distributio n system	Both the distribution and transmissio n systems	Both the distribution and transmissio n systems	Both the distribution and transmission systems	Both the distribution and transmissio n systems	Distributio n system	Distributio n system
Transforme r internal resonance protection	Yes	Yes	Yes	Yes	Yes	Yes	Yes
Need for grounding	No	No	No	No	Yes	Yes	No

The MSTS and tuned choke devices emerge as the most promising near-term solutions for protecting transmission transformers. At the same time, PMTS, SCGR, and SPTS represent long-term innovative directions that may reshape transformer protection in the era of advanced materials.

8.3. KEY ACHIEVED RESULTS

The research presented in this thesis has yielded several significant results that advance the understanding and practice of transformer protection against transient phenomena:

1. Identification of Resonance Conditions

- The resonance frequencies of high-voltage transformers were identified through analytical models, frequency-domain analysis, and experimental validation.
- Both "internal resonance" (between winding disks) and "external resonance" (transformer–cable interaction) were characterized, providing a clear map of vulnerable frequencies for representative transformer designs.

2. Black-Box and Gray-Box Modeling Frameworks

- The development of black-box and gray-box transformer models enabled accurate resonance studies without requiring full internal design data.
- The models proved effective in both simulation platforms (MATLAB/Simulink, EMTP-RV, ANSYS Maxwell) and experimental frequency sweep tests, bridging the gap between theoretical analysis and practical measurement.

3. Validation of Protection Devices

- Laboratory tests confirmed the capability of the "parallel RL circuit" and "air-core reactor with parallel resistor" to suppress resonance overvoltages in scaled-down prototypes.
- The "tuned choke" demonstrated frequency-selective protection, validated through FEM analysis and impulse testing, showing strong mitigation at identified resonance frequencies.
- The "MSTS" was validated as a robust suppressor across a broad frequency range, capable of handling fast transients and providing scalable protection for transmission-level transformers.

4. High-Voltage Experimental validation

- Impulse tests ranging from 10 kV to 60 kV were performed, confirming some of the designed devices' effectiveness under realistic stress conditions.
- Frequency sweep measurements (using VNA and SFRA) validated the suppression characteristics of the prototypes, ensuring that simulation results matched physical behavior.

5. Innovative Device Proposals

- New concepts such as the PMTS, SCGR, and SPTS were introduced, analyzed, and simulated.
- These solutions demonstrated strong potential for future grids with extended underground cables, high penetration of power electronics, and advanced materials.

6. System-Level Insights

- The interaction between transformers, cables, grounding grids, and suppressor devices was systematically studied, showing that device effectiveness depends strongly on system configuration.
- These insights underline the importance of integrated protection design, rather than considering transformer technology improvement.

In summary, the thesis established a comprehensive portfolio of protection strategies, validated them through multiple approaches, and demonstrated their practical feasibility for the reliable operation of future power systems.

8.4. Practical guidelines and methodological insights

Beyond theoretical contributions, this thesis provides actionable guidelines for engineers, researchers, and industry stakeholders dealing with transformer protection:

1. Resonance Identification and Monitoring

- Wideband frequency-domain measurements (SFRA, VNA) should be routinely applied to detect resonance frequencies in new transformer designs.
- Early detection of critical frequencies allows proposed protective measures to be implemented before transformers are deployed in the field.

2. Device Selection Based on Application Context

- For medium-voltage systems or laboratory-scale setups, parallel RL circuits provide a simple, effective solution.
- MSTS and tuned choke are more suitable for transmission-level transformers due to their scalability and robust performance.
- The SCGR offers a targeted solution against traveling-wave-induced resonances in systems with long underground cables.

3. Integration into Cable Integrated Transformer Systems

- Protection devices should be designed as part of the transformer–cable–grounding system, not as isolated components.

- For instance, the effectiveness of SCGR strongly depends on cable length and grounding design, emphasizing the need for co-engineered solutions.

4. Prototyping and Experimental Validation

- Simulation alone is insufficient; prototyping and high-voltage impulse tests are essential to capture nonlinearities and parasitic effects not present in theoretical models.
- When carefully designed, the thesis demonstrated that scaled-down prototypes provide reliable indicators of full-scale behavior.

5. Design Considerations

- Protection devices must balance voltage suppression, harmonic filtering, and minimal losses at fundamental frequency.
- Device scalability is supposed to account for the physical size, cost, and thermal performance, especially for transmission applications.

6. Industrial Implementation

- For near-term adoption, devices such as MSTS and tuned chokes can be incorporated into substation designs with minimal disruption to existing layouts.
- Emerging technologies like PMTS and SPTS should be monitored as long-term candidates for integration in future smart grids with advanced materials.
- The installation of the protection schemes is a guideline suggested in three categories: installation around the cable, cable termination, or next to the transformer around the overhead connection. These installations are illustrated in Fig. 8.8.

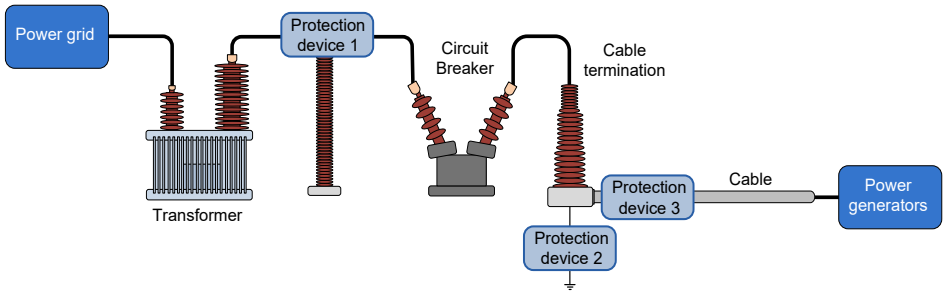


Fig. 8.8. Installation suggestion of the protection schemes

7. Standardization Pathways

- The findings suggest that there is a need for new international guidelines for transformer protection against resonant overvoltages, to complement existing standards for lightning and switching surges.
- These guidelines should encourage utilities to adopt resonance-aware protection strategies during both design and operation.

By following these methodological insights, utilities, manufacturers, and system operators can systematically enhance transformer resilience, reducing the risk of costly failures and ensuring reliable operation in increasingly complex power systems.

8.5. Scientific and industrial contributions

This thesis provides several original contributions to the scientific research and industrial practice in the domain of transformer protection. These contributions can be grouped into four main categories:

1. Advancement of Scientific Understanding

- Resonance Phenomena in Transformers: The thesis provides a comprehensive analysis of internal and external resonance conditions, linking them directly to transformer design, cable connections, and system configurations.
- Modeling Approaches: The development of black-box and gray-box models represents a methodological advancement, offering reliable techniques to study transformer resonance without requiring full manufacturer design data.
- Integrated Protection Perspective: By analyzing the transformer as a part of a transformer–cable–grounding system, the conducted research advances the scientific framework for studying transient interactions in power systems.

2. Development of Innovative Protection Devices

Seven novel devices were designed, analyzed, and some of them were prototyped and tested. These include:

- Parallel RL Circuit
- Air-Core Reactor with Parallel Resistor
- Tuned Choke
- Modular Series Transient Suppressor
- Cable Shield-Connected Grounding Reactor
- Series parallel transient suppressor
- Permanent Magnet-Based Transient Suppressor

This systematic exploration of series and parallel suppressors broadens the toolbox available for addressing resonance-induced overvoltages, marking a significant leap beyond conventional surge arresters and RC filters.

3. Experimental and Validation Contributions

- The thesis bridges the gap between simulation and reality through small-scale prototyping and high-voltage testing(10–60 kV impulse tests).
- By validating simulation results with the actual measurements, the work provides robust evidence for the feasibility of the proposed devices.
- This validation path provides a reproducible methodology for other researchers and engineers developing advanced equipment for electrical system protection.

4. Industrial and Societal Impact

- The research is directly relevant to TSOs, DSOs, and transformer manufacturers, addressing the growing risk of transformer failures due to transient phenomena in modern grids.
- By protecting transformers more effectively, the proposed solutions enhance grid reliability, asset lifetime, and operational safety, thereby reducing economic losses and increasing public trust in the electricity supply.
- The industrial collaboration in the PRoteuS project (with TenneT, Alliander, Royal Smit Transformers, and National Grid UK) ensures that the contributions are not purely academic, but they are strongly aligned with the practical needs.

In summary, the scientific contributions lie in advancing modeling and understanding of resonance, while the industrial contributions focus on developing implementable protection solutions that directly support the resilience of future power systems.

8.6. Limitations and Challenges

While this thesis has introduced several promising protection devices and modeling approaches, it is equally important to acknowledge the limitations and challenges encountered during the research:

1. Scalability of Prototypes

The majority of experimental validations were conducted on scaled-down prototypes. Although results provide strong indicators of full-scale performance, scaling laws may introduce challenges related to size, cost, and material behavior in practical high-voltage environments.

2. Material and Thermal Considerations

- Devices such as the PMTS rely on permanent magnet materials whose performance under prolonged thermal stress and aging remains uncertain.
- Similarly, ferromagnetic materials operate with lower performance under saturation conditions, and their effectiveness is also influenced by thermal effects.

3. Parameter Sensitivity

- Frequency-selective devices, such as tuned chokes, depend heavily on accurate knowledge of transformer resonance frequencies.
- Variations in transformer manufacturing, aging, or changes in system configuration (cable length modifications) can shift resonance points, potentially reducing effectiveness.

4. Integration with Existing Infrastructure

- Some devices require non-trivial modifications to substation layouts (SCGR integration with cable shielding systems).
- Large-scale deployment would necessitate design adjustments and standardization, which may slow down industrial adoption.

5. Focus on Resonance and Transients

- The thesis primarily focuses on resonance-induced overvoltages from lightning, switching, and harmonic content.
- Broader challenges, such as thermal faults, aging-related failures, or cyber-physical vulnerabilities in smart grids, are not in the scope of this work.

6. Standardization Gap

- Current international standards (IEC, IEEE) provide guidelines for surge arresters and insulation coordination, but lack comprehensive frameworks for resonance-aware transformer protection.
- Utilities may hesitate to adopt advanced devices without standardization until their effectiveness is fully codified in industry practice.

These limitations highlight the areas where further research and industrial collaboration are necessary. They also demonstrate that while the proposed solutions significantly advance transformer protection, ongoing work is essential to transition them from research prototypes to field-ready technologies.

8.7. RESPONSE TO THE RESEARCH QUESTIONS

The main research questions of this thesis and the responses to them, based on the research carried out in this thesis, are presented as follows:

1. Which transient signal frequencies cause transformer resonances?

According to the analytical studies, electromagnetic transient (EMT) simulations, and experimental tests conducted in this research, transformer resonances occur at frequencies where the transformer impedance reaches its extremum values. These frequencies correspond to the resonance points of the transformer. At these resonance frequencies, the phase characteristic of the circuit changes from inductive to capacitive.

2. What types of transformer resonances lead to overvoltage, and how does the cable connected to the transformer influence the resonances and associated overvoltages?

Transformer resonances can be classified into two main types:

• **Internal resonance:** This occurs when the internal components of the transformer reach resonance. In this case, the internal inductances and capacitances of the transformer interact and create resonance conditions that may lead to overvoltages across the winding disks. For example, the voltage on some disks with respect to ground may increase significantly, leading to insulation failure. In this condition, however, the voltage at the transformer terminal generally remains within a normal and safe range.

• **Terminal resonance:** This occurs when the transformer impedance interacts with the capacitive or inductive components of the connected cable or power line. In this case, the voltage at the transformer terminal can increase significantly and reach unsafe levels.

3. What is the most viable solution for protecting transformers against fast transients, considering the high-frequency model of the transformer connected to the grounding and cable system?

Since the primary cause of transformer resonance in systems connected to grounding and cables is the harmonic content of transient voltages, which excites both internal and terminal resonances, implementing a series protection device that suppresses a significant portion of the transient harmonic content is a viable, practically applicable solution. Such a device prevents the excitation of resonance and consequently avoids the formation of resonance-induced overvoltages in the transformer.

4. How does the innovative protection component operate to suppress fast transients and their effects on transformers?

The innovative protection devices proposed in this thesis are primarily series components that are tuned to the critical resonance frequencies of the transformer. These devices reduce the magnitude of the resonance-exciting frequency components by introducing considerable impedance at the targeted frequencies.

5. Why does the innovative protection component outperform existing solutions?

The proposed protection devices not only reduce the magnitude of the transient voltage applied to the transformer but also filter the critical frequency components that may excite transformer resonance. Furthermore, due to their modular structure, the proposed series devices are scalable and can be adapted for application in higher voltage levels.

8.8. Future work and next steps

The findings of this thesis open several promising directions for future research and development in transformer protection:

1. Scaling to Transmission-Level Applications

- While prototypes and scaled-down experiments demonstrated clear effectiveness, further work is needed to design, manufacture, and test full-scale devices for high-voltage applications (≥400 kV).
- Large-scale pilot projects in collaboration with utilities would validate the devices' performance under real-world grid conditions.

2. Advanced Materials and Technologies

- Continued research into novel magnetic materials and new configurations like SCGR, SPTS, and PMTS could make the protection devices more practical and cost-effective.
- Investigations into nano-composites, amorphous alloys, and high-temperature superconductors may enable compact, efficient, and reliable devices in diverse operating conditions.

3. Integration with Digital Protection Systems

- The next generation of power systems will rely on digital substations, wide-area monitoring, and IEDs.
- Protection devices should be integrated with these digital platforms, enabling adaptive operation where suppressors are tuned or activated based on real-time grid conditions

4. Field Deployment and Long-Term Testing

- Future research must focus on long-duration tests of prototype devices under realistic environmental and loading conditions.
- These studies would clarify aging, thermal stability, and reliability issues, which are critical for industrial acceptance.

5. Standardization and Guidelines Development

- Collaboration with IEEE, IEC, and CIGRÉ working groups is essential to develop international standards that explicitly address resonance-aware transformer protection.
- The results of this thesis provide a scientific foundation for drafting such guidelines, but broader consensus-building and field validation will be required.

6. Extension to Other Equipment

- The concepts developed for transformers could be extended to other vulnerable power system components such as cables, circuit breakers, and instrument voltage transformers.
- This would create a holistic protection framework, ensuring resilience of the entire transmission and distribution network against transient phenomena.

7. Application in Renewable-Rich Grids

- With the rapid expansion of renewable energy integration and the increasing role of power electronics, resonance and harmonic issues are expected to intensify.
- Tailoring protection devices for offshore wind farms, solar plants, and hybrid AC/DC grids is a logical next step, ensuring compatibility with future grid architectures.

In summary, future research should focus on refining, conducting more experimental validation tests, reliability studies, and AI-based optimization of the devices introduced in this thesis and embedding them within the broader ecosystem of advanced materials, digital protection, and renewable-dominated networks.

8.9. Concluding remarks

This thesis addresses one of the most pressing challenges in modern power systems: safeguarding transformers against transient phenomena and resonance overvoltages. Through a combination of theoretical modeling, simulation, prototyping, and experimental validation, the performed work:

- Identifies the resonance mechanisms that make transformers vulnerable to fast transients.
- Evaluates existing protection methods, exposing their limitations in addressing complex resonance conditions.
- Develops, analyzes, and validates seven novel protection devices that significantly expand the options available for transformer protection.
- Demonstrates the feasibility of these devices through simulations and laboratory tests, establishing a solid foundation for industrial implementation.

The research that was conducted contributes to the scientific understanding of the resonance phenomenon and the practical development of protection technologies that the industry can adopt. While some devices, such as the MSTS and tuned choke, are ready for near-term implementation, others, notably SCGR, SPTS, and PMTS, represent long-term innovations that may define the next generation of transformer protection using mature materials and technologies.

On a broader level, this work emphasizes that transformer protection must evolve from isolated solutions to system-integrated strategies. The interaction between transformers, cables, grounding systems, and transient suppressors must be addressed holistically to ensure the resilience of the entire grid.

As power systems transition toward renewable energy integration, digitalization, and decentralization, the solutions developed in this thesis will contribute to a more reliable, sustainable, and future-proof grid. The journey from conceptual design to industrial deployment is ongoing; however, the presented results in this thesis provide a cornerstone toward a new era of transformer protection.

LIST OF THE PUBLICATIONS

A

PEER-REVIEWED PUBLISHED JOURNAL REVIEW ARTICLES

1. **A. Heidary**, M. G. Niasar, M. Popov, and A. Lekić, "Transformer Resonance: Reasons, Modeling Approaches, Solutions," ***IEEE Access***, vol. 11, pp. 58692-58704, 2023.

PEER-REVIEWED JOURNAL ARTICLES

1. **A. Heidary**, M. Ghaffarian Niasar, and M. Popov, "Comprehensive Evaluation of Toroid Ring Core Parallel Inductor and Resistor as a Transformer Protection Device," ***IEEE Transactions on Circuits and Systems*** I: Regular Papers, vol. 71, no. 9, pp. 4298-4308, Sept. 2024.
2. **A. Heidary**, M. Ghaffarian Niasar, and M. Popov, "Transformer Resonance Analysis and Visualization Using Current Heat Map Matrix," ***IEEE Transactions on Power Delivery***, April 2026, doi: 10.1109/TPWRD.2026.3688104
3. **A. Heidary**, M. Ghaffarian Niasar, F. D. Marvasti, and M. Popov, "Superconducting Magnetic Energy Storage-Based DC Circuit Breaker for HVDC Applications," ***IEEE Transactions on Power Electronics***, vol. 39, no. 10, pp. 13890-13899, Oct. 2024.
4. **A. Heidary**, M. Popov, A. Moghim, M. Ghaffarian Niasar, and A. Lekić, "The Principles of Controlled DC-Reactor Fault Current Limiter for Battery Energy Storage Protection," ***IEEE Transactions on Industrial Electronics***, vol. 71, no. 2, pp. 1525-1534, Feb. 2024.
5. **A. Heidary**, B. Behdani, M. Ghaffarian Niasar, M. Popov, "Wide-Frequency Transient and Resonance Behavior of Superconducting Transformers," ***IEEE Transactions on Applied Superconductivity***, Submitted, 2026.
6. **A. Heidary**, M. Ghaffarian Niasar, and M. Popov, "The principle of magnetic flux switch," ***Nature Scientific Reports***, vol. 14, no. 1, 8990, 2024.
7. **A. Heidary**, B. Behdani, M. Ghaffarian Niasar, M. Popov, "Wind farm transformer protection against lightning transients using air core reactor and resistor," ***Electric Power Systems Research***, vol. 249, 2025.
8. **A. Heidary**, M. Ghaffarian Niasar, M. Popov, "Multi-module series suppressor for the protection of wind farm transformers against resonance overvoltages," ***International Journal of Electrical Power & Energy Systems***, vol. 172, 2025.

9. **A. Heidary**, M. Ghaffarian Niasar, M. Popov, Series magnetic coupled reactor saturation considerations for high voltage AC and DC power systems, ***International Journal of Electrical Power & Energy Systems***, vol. 158, 2024.
10. F. Nasirpour, **A. Heidary**, M. Ghaffarian Niasar, A. Lekić, M. Popov, "High-frequency transformer winding model with adequate protection," ***Electric Power Systems Research***, vol. 223, 2023.

PUBLISHED BOOK

1. **A. Heidary**, M. Popov, and M. Ghaffarian Niasar, "Advanced Fault Current Limiters: Definition, Design, and Future Trends," ***Wiley-IEEE Press***, ISBN: 978-1-394-35915-8, September 2026.

PEER-REVIEWED PUBLISHED CONFERENCE ARTICLES

1. **A. Heidary**, B. Behdani, M. Ghaffarian Niasar, M. Popov, "Wind farm transformer protection against lightning transients using air core reactor and resistor," IPST 2025.
2. F. Nasirpour, **A. Heidary**, M. Ghaffarian Niasar, A. Lekić, M. Popov, "High-frequency transformer winding model with adequate protection," IPST 2023.
3. F. Nasirpour, B. Behdani, **A. Heidary**, M. G. Niasar, F. Ghassemi, K. Velitsikakis, ... & M. Popov, "Enhancing Power Transformer Reliability: High-Frequency Modeling, Transient Interactions, and Overvoltage Protection Scheme," In Cigre 2024. Cigré, Paris.

THESIS SUPERVISION, PRESENTED COURSE, AND LABORATORY DEMO PRESENTATION

1. Supervising a group of Bachelor's students' theses entitled "Design & Reliability Assessment of AEA Propulsion Grid".
2. Supervising a group of Bachelor's students' theses entitled "DC Solid State Circuit Breaker for AEA".
3. Provided a lecture on the application of DC circuit breakers for protection in solar power plants.
4. Preparation of a demonstration and analysis of transient measurements involving AC breakers, fast breakers, and fuses, supporting students in understanding dynamic protection behavior in modern photovoltaic systems.

ACKNOWLEDGMENT

This thesis marks the culmination of a long research, learning, and personal growth journey. It would not have been possible without the invaluable support, guidance, and encouragement of many people and institutions to whom I wish to express my deepest gratitude.

First and foremost, I owe my heartfelt thanks to my wife, **Soraia**, and to my family. Their patience, love, and constant encouragement sustained me through every challenge. Without their unwavering support, this work would not have been possible.

I would like to express my sincere gratitude to my promotors and supervisors, Prof. dr. ir. Marjan Popov, and Dr. ir. Mohamad Ghaffarian Niasar, for their invaluable guidance, critical insights, and encouragement throughout my Ph.D. journey. Their expertise and advice have profoundly shaped my academic work and professional outlook.

My appreciation also goes to the members of the Intelligent Electrical Power Grids (IEPG) group at TU Delft. I am grateful for the stimulating discussions, technical support, and collegial atmosphere that made my time in the group both productive and enjoyable. I am especially thankful to my colleagues Behzad Behdani and Farzad Nasirpour for their friendship, collaboration, and continuous encouragement throughout this journey.

Special thanks are extended to the Graduate School of TU Delft staff, who supported me in navigating the doctoral process, and to the university staff who assisted in academic and administrative matters.

I am indebted to the High Voltage Laboratory staff and TU Delft High Voltage group, whose expertise, assistance, and collaboration were essential for this thesis's experimental work. Their dedication made the demanding laboratory studies both feasible and successful.

I also gratefully acknowledge the contributions of the project partners in the PRoteuS project, including TenneT TSO B.V., Alliander N.V., Royal SMIT Transformers, and National Grid UK, and also the consortium members: Forooz Ghassemi, Kostas Velitsikakis, Maarten van Riet, Mark Wilkinson, Mart van der Meijden, Sjoerd Nauta, Imre Tannemaat, Jos Veens, Afshin Pashaei, and Luc Dorpmanns. Their collaboration,

insights, and support provided a strong industrial context that enriched the outcomes of this research.

Furthermore, I wish to thank the Dutch Research Council (NWO) for its financial support for this research within the framework of the TTW project "Protection of Future Power System Crucial Components (PRoteuS)." Their support made this work possible.

Mr. Hossein Adib, my Experimental Science teacher, deserves my sincere appreciation for his kindness, dedication, and hard work. His supportive and friendly approach inspired me to become engaged and deeply interested in exploring the world of science.

Finally, I would like to thank Delft University of Technology for providing an excellent academic environment and the resources necessary to pursue my research. I am proud to have carried out this work in such an inspiring institution.

Amir Heidary
Delft, June 2026

BIOGRAPHY



Amir Heidary was born in Tabriz, Iran, in 1987. He received the B.Sc. degree in Power Electrical Engineering from the Technical and Vocational University of Zanjan (TVU) and Islamic Azad University (IAU), Abhar, Iran, in 2009, and the M.Sc. degree in Power System Engineering from IAU, Zanjan, Iran, in 2021. He is currently pursuing a Ph.D. in Power System Engineering at Delft University of Technology (TU Delft), Delft, The Netherlands, with an expected completion in 2026.

His doctoral research focuses on transformer protection against resonance overvoltages in Power Systems. During his research, he has published several high-quality articles in IEEE Transactions, multiple Q1 Elsevier journal papers, an IEEE Access review article, a Nature paper, and a book accepted by Wiley-IEEE Press.

From 2009 to 2019, he worked at Eleprotect (APOG Co.) in Iran, where he served as Technical Director and led industrial R&D projects on fault-current limiters, HVDC breakers, superconducting protection devices, and renewable energy prototypes. His applied research has resulted in 11 patents.

Mr. Heidary is a Senior Member of IEEE and has served as an Associate Editor on the IEEE Transactions on Power Delivery Editorial Board. He has also served as a reviewer for many high-quality journals. His research interests include transient protection, modern fault current limiters, superconducting devices, HVDC protection systems, smart grids, and magnetic-based switching technologies.

